

LMSC-4-05-69-7 • OCTOBER 1969

LMSC-4-05-69-7

ELASTIC AND PLASTIC STRESSES AT WELD SINKAGES AND OTHER DISCONTINUITIES IN PRESSURE VESSELS

J. SKOGH and A. M. C. HOLMES

N70-15637

FACILITY FORM 002

(ACCESSION NUMBER)

(THRU)

240

(CODE)

(PAGES)

OR-102071

(CATEGORY)

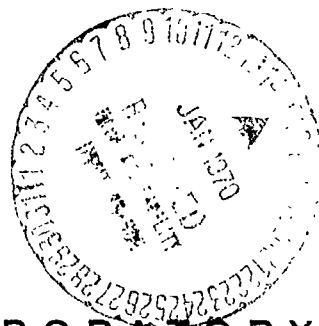
(NASA CR OR TX OR AD NUMBER)

CONTRACT NAS9-8303

Lockheed

PALO ALTO RESEARCH LABORATORY

**LOCKHEED MISSILES & SPACE COMPANY • A GROUP DIVISION OF LOCKHEED AIRCRAFT CORPORATION
PALO ALTO, CALIFORNIA**



CR 102071

NAS 9-8303

ELASTIC AND PLASTIC STRESSES AT WELD
SINKAGES AND OTHER DISCONTINUITIES
IN PRESSURE VESSELS

By
J. Skogh and A.M.C. Holmes

LMSC/4-05-69-7

October 1969

Lockheed Palo Alto Research Laboratory
Palo Alto, California

FOREWORD

The research described in the present report was performed under Contract NAS9-8303 with the NASA/Manned Spacecraft Center, Houston, Texas, with Mr. H. C. Kavanaugh as Contract Monitor.

The following persons made significant contributions to the work:

Mr. J. Skogh	-	Project Leader
Mr. A.M.C. Holmes	-	Experimental Program
Dr. C. R. Steele	-	Consultant, Asymptotic Solutions
Mr. P. Stern	-	Consultant, Elastic-Plastic Computer Programs
Mr. M. Kural	-	Methods
Mr. S. Jensen	-	Programming

ABSTRACT

Two problems of geometric discontinuities in pressure vessels are treated in detail: mismatch and weld sinkage. Design graphs are given for elastic stresses in such discontinuities for arbitrary materials and a wide range of geometries. Nonlinear pressure coupling effects are accounted for. Design graphs for plastic stresses, including residual stress, are given for cylinders and spheres with weld sinkage type discontinuities. These graphs are applicable to materials with stress-strain curves resembling that of titanium 6Al-4V. Failure criteria for static and cyclic loadings are discussed.

The methods employed in generating the data required for the design graphs consisted of a synthesis of asymptotic, closed form solutions and parametric computer studies. The theoretical results were checked with a test program using cylinders and spheres with weld sinkage type discontinuities. Excellent correlation between theory and test was achieved.

In addition to the solutions of mismatch and weld sinkage problems, recommended engineering solutions for a large number of discontinuity problems are given in a matrix with systematically classified discontinuities.

CONTENTS

Section		Page
	FOREWORD	ii
	ABSTRACT	iii
	NOMENCLATURE	vi
1	INTRODUCTION	1-1
2	ELASTIC ANALYSIS	2-1
	2.1 Stress Factors	2-3
	2.2 Mismatch and Abrupt Thickness Change	2-6
	2.3 Weld Sinkage	2-16
3	PLASTICITY ANALYSIS OF WELD SINKAGE	3-1
	3.1 Stress-Strain Relations	3-4
	3.2 Preliminary Analyses	3-5
	3.3 Details of Plasticity Effects - Cylinders and Spheres	3-8
	3.4 Design Graphs for Cylinders and Spheres	3-14
4	FAILURE CRITERIA	4-1
	4.1 Static Failure	4-1
	4.2 Repeated Loading	4-3
5	APPLICATION	5-1
	5.1 Design Graphs: Elastic Stresses	5-2
	5.1.1 Mismatch and Abrupt Thickness Change	5-2
	5.1.2 Weld Sinkage	5-30
	5.2 Design Graphs: Plastic Stresses	5-39
	5.2.1 Weld Sinkage	5-39

Section		Page
6	EXPERIMENTAL PROGRAM	6-1
	6.1 Introduction	6-1
	6.2 Description of the Specimens and their Manufacture	6-3
	6.3 Instrumentation and Test Details	6-15
	6.4 Data Processing and Presentation	6-29
7	CORRELATION BETWEEN THEORY AND TEST	7-1
8	REFERENCES	8-1
APPENDIX		
A	Systematic Classification of Solutions to Dis- continuity Problems in Pressure Vessels	A-1
B	Derivation of Shell Equations in Complex Form	B-1
C	Derivation of Analytical Expressions for a Cylinder with Weld Sinkage	C-1
D	Elastic-Plastic Behavior of Cylinder with Small Slope Discontinuity	D-1
E	Experimental Results (Bound in Separate Volume)	E-1

NOMENCLATURE

a, b	Nondimensional Constants defined by Eqs. 4.2, 4.3
A, B	Nondimensional Constants defined by Eq. 2.18
c	$t\sqrt{12(1-\nu^2)}$
C_e	Constant defined by Eq. 4.2
C_p	Constant defined by Eq. 4.3
E	Modulus of Elasticity - lb/in ²
F_{tu}	Ultimate Strength - lb/in ²
F_{ty}	Yield Strength - lb/in ²
G	Shear Modulus - lb/in ²
h	Horizontal (perpendicular to shell centerline) Deformation - inch
H	Horizontal (perpendicular to shell centerline) Force - lb/in
$\left. \begin{array}{l} \tilde{H} \\ H^* \end{array} \right\}$	Defined by Eq. (B9.8)
Im	Imaginary part
k	Ect
K	Nondimensional Constant defined by Eq. 2.10
K_f	Material Constant defined by Eq. 4.6

l	Length of Plastic Zone - inch
L	Sinkage Length - inch
L_c	Critical Length (Fig. 5-3) - inch
m	Mismatch $m = 2 \frac{R_b - R_a}{t_a + t_b}$
\bar{m}	$6M/Et^2 \epsilon_y$
m_1, m_2	Nondimensional Constants defined by Eq. 2.18
M	Moment - inlb/in
M_e	Elastic Moment - inlb/in
M_y	Yield Moment - inlb/in
M_ϕ	Meridional Moment - inlb/in
M_{ϕ_c}	Meridional Moment, complementary solution - inlb/in
M_{ϕ_m}	Meridional Moment, particular solution - inlb/in
M_θ	Hoop Moment - inlb/in
M_{θ_c}	Hoop Moment, complementary solution - inlb/in
M_{θ_m}	Hoop Moment, particular solution - inlb/in
\bar{n}	$N/(Et \epsilon_y)$
n_1, n_2	Nondimensional Constants
N	Stress Resultant - inlb/in

N_f	Number of Cycles to Failure
N_φ	Meridional Stress Resultant - lb/in
N_{φ_c}	Meridional Stress Resultant, complementary solution - lb/in
N_{φ_m}	Meridional Stress Resultant, particular solution - lb/in
N_θ	Hoop Stress Resultant - lb/in
N_{θ_c}	Hoop Stress Resultant, complementary solution - lb/in
N_{θ_m}	Hoop Stress Resultant, particular solution - lb/in
p	Internal Pressure - lb/in ²
p_m	Normalizing Pressure - lb/in ²
	$p_m = 2 \frac{t}{R} F_{tu} \quad (\text{sphere})$
	$p_m = \frac{2}{\sqrt{3}} \frac{t}{R} F_{tu} \quad (\text{cylinder})$
P_H	Horizontal Force/Unit Area - lb/in ²
P_V	Vertical Force/Unit Area - lb/in ²
P_z	Normal Force/Unit Area - lb/in ²
Q	Shear Force - lb/in
$r(s)$	Radius Perpendicular to Center Line of Shell - inch
r_1	Meridional Radius of Curvature - inch

r_2	Hoop Radius of Curvature - inch
R	Cylinder Radius, Sphere Radius - inch
R_2	Hoop Radius - inch
R_a, R_b	Cylinder Radii Corresponding to Thickness t_a, t_b - inch
R_p	Polar Radius - inch
R_T	Toroidal Meridional Radius - inch
Re	Real Part
s	Meridional Surface Coordinate - inch
t	Shell Thickness - inch
t_a, t_b	Cylinder Thicknesses Corresponding to Radii R_a, R_b - inch
u	Tangential Deformation - inch
v	Vertical Deformation - inch
V	Vertical Force - lb/in
w	Normal Deformation - inch
x, y, z	Cartesian Coordinates
$\alpha = \frac{r_2}{2R_m}$	Reduced Stress Factor
$\bar{\alpha}_m$	Equivalent Stress Factor in Membrane Region
α_θ	Hoop Stress Factor

α_{φ}	Meridional Stress Factor
$\Delta = \epsilon R$	Total Weld Sinkage - inch
$\Delta\omega$	Sinkage Angle - radians
ϵ	Shape Factor
ϵ_0	Strain at Middle Surface - in/in
$\epsilon_1, \epsilon_2, \epsilon_3$	Strains in Directions 1, 2, 3 - in/in
ϵ_{θ}	Hoop Strain - in/in
ϵ_{φ}	Meridional Strain - in/in
$\bar{\epsilon}$	Effective Strain (Eq. 3.2) - in/in
$\bar{\epsilon}_e$	Effective Elastic Strain - in/in
$\bar{\epsilon}_f$	Effective Failure Strain - in/in
$\bar{\epsilon}_p$	Effective Plastic Strain - in/in
$\bar{\epsilon}_R$	Effective Residual Strain - in/in
$\bar{\epsilon}_t$	Effective Total Strain - in/in
$\bar{\epsilon}_y = 0.867 F_{tu}/E$	Normalizing Strain - in/in
$\bar{\epsilon}_1, \bar{\epsilon}_2$	Defined by Eq. B12.4 - in/in
θ	Hoop Angle - radians
κ_{θ}	Change in Hoop Curvature - in ⁻¹
κ_{φ}	Change in Meridional Curvature - in ⁻¹

μ	Geometric Factor (Eq. 2.15c, 2.19)
ν	Poisson's Ratio
ρ	$= \frac{p}{\frac{2}{\sqrt{3(1-\nu^2)}} E \left(\frac{t}{R_2}\right)^2}$ Pressure (Nonlinearity) Parameter
ρ_1	Meridional Radius of Curvature at Weld Sinkage Crease - in ⁻¹
$\sigma_1, \sigma_2, \sigma_3$	Stresses in Directions 1, 2, 3 - lb/in
σ_θ	Hoop Stress - lb/in ²
σ_ϕ	Meridional Stress - lb/in ²
$\bar{\sigma}$	Effective Stress (Eq. 3.1) - lb/in ²
$\bar{\sigma}_R$	Effective Residual Stress - lb/in ²
ϕ	Meridional Angle - radians
ϕ_1, ϕ_2	Meridional Angles Defining Weld Sinkage Geometry - radians
ϕ_d	Sinkage length (see Fig. 3-1) - radians
χ	Rotation - radians
χ_l	Rotation in Plastic Zone - radians

Section 1
INTRODUCTION

The present work is an effort to apply state-of-the-art knowledge to the solution of certain problems relating to discontinuities in rotationally symmetric shells subjected to internal pressure. While, of course, an elementary aspect of the design of a pressure vessel is to avoid discontinuities in thickness, radius, and slope, such discontinuities are the rule in the manufactured product. A typical example is weld sinkage, another is mismatch. Both these problems are being considered in this work, and design curves are given, as follows

- Elastic stresses in undercut and/or mismatched shells for arbitrary shell configurations
- Elastic stresses in weld sinkage type discontinuities for arbitrary shell configurations
- Plasticity effects, including residual stresses and strains, in cylindrical and spherical pressure vessels with weld sinkage type discontinuities. Material: Titanium 6Al-4V, or similar.

In addition, a method for the approximate determination of low-cycle fatigue is given.

The discontinuity problem is here treated from the theory of thin shells point of view. Thus, local stress concentrations in the sense of the theory of elasticity are not being considered. This is in keeping with current praxis and does not introduce any limitations on the results given, except for high-cycle fatigue, where the elastic stress concentrations can be important. However, this latter problem is not part of the present study.

While one of the discontinuities treated here in detail is referred to as "weld sinkage", and another is "mismatch and/or undercut", this nomenclature should not be construed as to imply that the complete problem, including stresses introduced during the fabrication process, has been solved. Rather, only the geometric aspects are being considered; the discontinuities are assumed to be free of residual stresses and strain at the application of the first pressure load. However, residual stresses and strains which result from this (and subsequent) load cycles can be determined from the information contained here.

The results given in this report have been obtained by the application of both analytical and direct numerical methods. The numerical methods used consists of two computer programs, BOSOR [1]^{*} for elastic, and EPSOR [2] for elastic/plastic analyses. While the direct numerical methods can be used to very good advantage for the analysis of virtually any geometric shape, the disadvantage of the numerical analysis is that the proper grouping of the many physical variables of the problem into a few significant parameters is very difficult to discover. On the other hand, the simplified analytical methods of asymptotic integration give such groupings directly. In the present investigation the two approaches proved most complementary, and rather than a duplication of effort an interaction of discovery was evident at several points of the investigation. The asymptotic results would give the significant parameters, which were confirmed by numerical results. On several occasions the numerical results would suggest a simple general behavior, thus motivating an analytical effort in that direction. Where analytical investigations would appear to be too cumbersome, or difficult, corrections to a simpler analytical result would be generated by the numerical methods. Examples of this is the nonlinear behavior in the elastic region and the discovery of identical behavior for cylinders and spheres with weld sinkage^{**}. Another example is the considerable

* Numbers in square brackets indicate references in Section 8.

** However, both these problems have since been dealt with in considerable analytical detail by the consultant, C. R. Steele.

difficulty in treating the elastic/plastic problem analytically.

A small experimental program, consisting of measurements on titanium spheres and cylinders with carefully machined-in weld sinkage type discontinuities was also a part of the present work. While the experimental study of shells with discontinuities is made very difficult by the rapidly varying stress distributions, and the virtual impossibility of making measurements at the point of maximum stress, the results of the tests do verify the analytic and numerical results, both elastically and plastically. During the tests care was taken not to collapse the test specimen, the reason for this being the possibility of using the same specimens for low-cycle fatigue experimentation at a future date.

The main goal in the present investigation has been the establishment of the design curves in Section 5. Typical uses of these graphs would be

- Determination of acceptable drawing tolerances for weld sinkage and/or mismatch for pressure vessels
- Determination of internal pressure capabilities for shells with manufacturing defects in the form of weld sinkage

While the design curves have been derived specifically for two types of discontinuities (meridional slope discontinuity, and mismatch/undercut) for two shell types (spherical and cylindrical) they should be applicable, at least approximately, to shells with arbitrary discontinuities. This statement is warranted by the high degree of uniformity of shell behavior found in the present study, which indicates that the significant aspect about a discontinuity is not its shape, or geometry, but only the degree to which induced forces are added to the basic membrane forces. Thus, a discontinuity can be characterized solely, or practically so, by the moments and shears which are induced by it.

Section 2
ELASTIC ANALYSIS

Determination of discontinuity stresses is an important problem in the design of pressure vessels. Discontinuity stress can arise from three basic sources:

- Geometric discontinuity. (Abrupt change in radius of curvature and/or thickness of the shell.)
- Material discontinuity. (Abrupt change in mechanical properties.)
- Load discontinuity. (Abrupt change in load intensity of static loading - "line load".)

In an actual structure these causes may, of course, appear singly or in any combination.

The linear elastic analysis of thin shells of revolution is at the present well founded and prediction of stresses in such structures can be made with relatively high accuracy. For simple shell geometries, solutions to the discontinuity problem have been obtained in closed form. For more complex geometries, numerical techniques have been employed, and a number of computer programs are available.

At the start of the present investigation a survey of existing methods of analysis was made. As a result of that survey the matrix of Appendix A was developed. This matrix lists available methods (other than computer programs) for a number of systematically classified discontinuities. Most of these may be thought of as intentional discontinuities, necessitated by design. Accidental discontinuities arising from the manufacture process are poorly represented - actually only methods for elastic analysis of cylinders with mismatch and undercut are available. Consequently, the

present investigation has been directed to fill this gap: the discontinuities treated here are mismatch/undercut and weld sinkage in cylinders and spheres (and, by extension, in arbitrary shell configurations).

Both closed form solutions and computer programs were used to develop the methods of analysis presented in Section 5. The derivation of closed form solutions for the linear elastic problem are shown in detail in Appendices B and C. The solutions given there, and used throughout the present work, are based on the following assumptions:

- a) Normals of the undeformed middle surface are displaced into normals of the deformed middle surface;
- b) Transverse shear strains and stress normal to the shell midsurface are negligible;
- c) The thickness-to-radius ratio is small;
- d) The material is homogeneous and isotropic;
- e) Deformations are small;
- f) Hooke's law applies;

Similar solutions together with numerous results, graphs, charts and tables useful in design situations can be found in references by Timoshenko [3], Flügge [4], Novozhilov [5], and Tsui [6], among others. Asymptotic solutions for the nonsymmetric loading of elastic shells can be found in recent works by Steele [7 & 8].

Most of the closed form solutions suffer from one or more of the following limitations:

- They are applicable to elastic analysis only;
- The range of geometries covered is rather limited;
- With few exceptions only uniform thickness shells may be analyzed;
- They assume implicitly, through the use of the principle of superposition, a linear relationship between load and deformation.

These limitations seriously restrict the applicability of closed form solutions. However most of these limitations have been removed by the use

of numerical methods in conjunction with the use of high speed digital computers.

The importance of nonlinear elasticity appears to be largely unappreciated, even though Nachbar [9] in 1959 showed that stresses computed on the basis of the classical theory may be unconservative, depending on loading and geometrical parameters. Briefly, the deficiency stems from the assumption that the principles of superposition are valid; i.e., the influence coefficients are independent of the pressure acting on the shell. This assumption is implicitly stated in the derivation of these methods by writing the shell equilibrium equations in terms of the undeformed shell. Nachbar's investigation, which takes into account the nonlinear interaction of membrane and discontinuity stresses, shows that as the membrane stresses become "large" there is an appreciable decrease in the influence coefficients; the shell becomes apparently stiffer under pressure. In the present work the nonlinear effects have been determined numerically by application of the computer program BOSOR [1]. This program, being thoroughly checked out in about two years of operation, was also used to check out the nonlinear, elastic, portion of the computer program used for the plasticity analyses (see Section 3).

The BOSOR computer program solves the Reissner nonlinear shell equations [10] for the thin shell of revolution by the method of finite differences: the nonlinear differential equations are reduced to a set of nonlinear simultaneous equations, which are solved by iterating a suitable set of linear equations until the desired convergence has been achieved. Reference [1] contains a detail discussion of this method of solution.

2.1 Stress Factors

In the present report the term stress factor is used to relate the stress at a particular point to an easily determined reference stress, the meridional membrane stress.

The meridional membrane stress in the basic shell is

$$\sigma_{\varphi_m} = \frac{N_{\varphi_m}}{t} = \frac{p R_2}{2t} \quad (2.1)$$

This equation is valid for all axisymmetric, closed, shells with pressure loading. The uniaxial stress factors are defined in terms of the basic meridional stress:

$$\alpha_{\varphi} = \frac{\sigma_{\varphi}}{\sigma_{\varphi_m}} \quad (2.2a, b)$$

$$\alpha_{\theta} = \frac{\sigma_{\theta}}{\sigma_{\varphi_m}}$$

According to the von Mises yield criterion the equivalent stress $\bar{\sigma}$ is related to the uniaxial stresses by the equation

$$\bar{\sigma} = \sqrt{\sigma_{\varphi}^2 + \sigma_{\theta}^2 - \sigma_{\varphi} \sigma_{\theta}} \quad (2.3)$$

An equivalent, or effective, stress factor is defined similarly to the uniaxial stress factors

$$\bar{\alpha} = \frac{\bar{\sigma}}{\sigma_{\varphi_m}}$$

or

$$\bar{\alpha} = \sqrt{\alpha_{\varphi}^2 + \alpha_{\theta}^2 - \alpha_{\varphi} \alpha_{\theta}} \quad (2.4)$$

Further, a reduced stress factor is defined, as follows

$$\alpha = \frac{\bar{\sigma}}{\bar{\alpha}_m} \quad (2.5)$$

where $\bar{\alpha}_m$ is the equivalent stress factor in the membrane region of the shell.

For the sphere the reduced stress factor becomes

$$\alpha = \bar{\alpha} \quad (\text{sphere})$$

and for the cylinder

$$\alpha = \bar{\alpha} / \sqrt{3} \quad (\text{cylinder})$$

The stress factors are, by definition, a function of the particular shell geometry under study. They are also a function of the applied loading, i.e. they are nonlinear. This elastic nonlinearity is a relatively recent development in the theory of shells with discontinuities; the first thorough investigation of the subject was made by Nachbar [9], who found that the influence coefficients of thin shells are a function of a pressure parameter

$$\rho = \frac{p}{\frac{2}{\sqrt{3(1-\nu^2)}} E \left(\frac{t}{R_2}\right)^2} \quad (2.6)$$

Thus, since the stress is a function of the influence coefficients, the stress factors α_φ , α_θ , $\bar{\alpha}$, and α are also function of the pressure parameter ρ

$$\left. \begin{aligned} \alpha_\varphi &= \alpha_\varphi(\rho) \\ \alpha_\theta &= \alpha_\theta(\rho) \\ \bar{\alpha} &= \bar{\alpha}(\rho) \\ \alpha &= \alpha(\rho) \end{aligned} \right\} \quad (2.7)$$

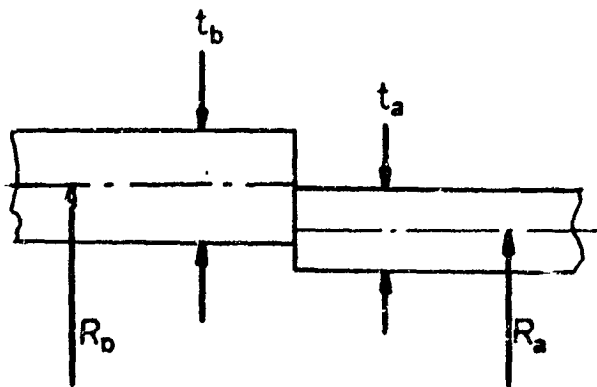
2.2. Mismatch and Abrupt Thickness Change

Bizon [11] has already investigated the elastic stresses in a cylinder with mismatch and/or thickness change for several joint configurations, including lap filleted and unfilleted butt joints. The unfilleted butt joint (see Fig. 2-1) was selected in the present work as a subject for studying the behavior of any shell with such a discontinuity, and if possible, for developing a universal design graph for such shells.

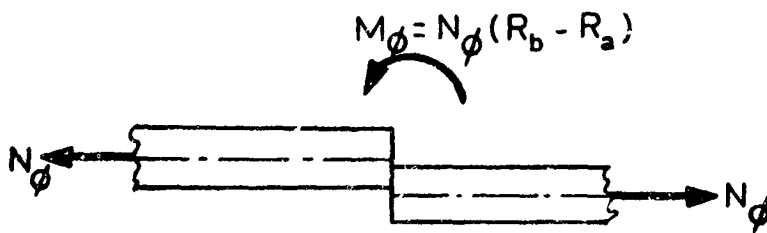
Bizon's results are presented in the form of charts showing an effective, biaxial, stress factor as a function of the geometry and the pressure parameter ρ . For the purposes of the present investigation, however, the individual uniaxial stress factors are required. Consequently, these factors were computed using the BOSOR [1] computer program. Complete design graphs showing the maximum stress are presented in Section 5.1.1.

The primary effect of a mismatch is that a moment equal to $N \Delta R$ is introduced into the shell. If the thickness on either side is the same one half of this moment will be absorbed by the left shell and one half by the right shell, resulting in an antisymmetric stress and deformation situation. The maximum stress occurs at the point of application of the moment. Since this moment is of the nature of an externally applied line load, and not affected by the influence coefficients, no nonlinear effects will occur at the discontinuity, however, the attenuation length will be slightly changed and consequently the lower stresses at some distance from the discontinuity behave in a slightly nonlinear way.

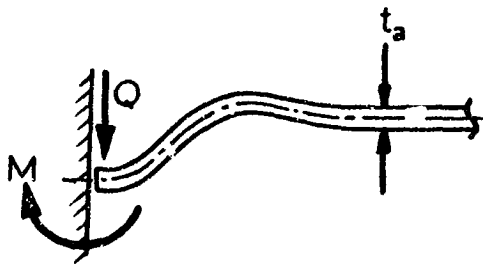
When the thicknesses in the two joined shells are unequal the external discontinuity moment will be distributed between the two shells in proportion to their thicknesses. Secondary forces in the form of shear and moments caused by the restraining effect of the shells on each other are also induced, resulting in stresses at the discontinuity which are highly dependent on the influence coefficients and thus nonlinear. In the extreme case, where the thickness ratio of the shells is zero, the thinner shell becomes fully clamped and is prevented from rotation at and in the vicinity of the



(a) GEOMETRY



(b) PRIMARY FORCES



(c) DISCONTINUITY FORCES,
 $t_a/t_b = 0$

Fig. 2-1 Unfilleted Butt Joint

discontinuity (see Fig. 2-1c). In this case, however, the stress variation at the juncture is linear. The reason for this is the absence of rotation at this point; an examination of the nonlinear equations indicates that the dominant term for nonlinear effects is (rotation) x (axial stress resultant). Figure 2-2 shows results from computer computations for spheres and cylinders with a clamped edge (or $t_a/t_b = 0$). Unexpectedly, the stress factor for the sphere increases as the thickness ratio R/t decreases. The explanation for this probably lies in the fact that the thicker shell has a longer boundary zone, which extends sufficiently for it to be affected by the shell curvature. This explanation seems to be backed up by the curves for the cylinder which is not affected in this way. However, the cylinder shows a slight non-linearity with increasing loads (higher ρ) which probably is accountable to higher-order effects (rotations close to the clamped edge are roughly twice as large for the cylinder as for the sphere).

For cases intermediary to the two extremes a definite nonlinear behavior is evident, as shown by design curves in Section 5.1.1. Further illustrations of this are provided by Figures 2-3 and 2-4 which show deformation and stress resultant curves for cylinders and spheres, respectively. The plots are made for two values of the nonlinearity parameter, 0.5 and 5. The values for the lower load have been multiplied by a factor of 10 so as to offer a direct comparison between the two loads. If nonlinearity effects were present the curves for the two loads would have been identical. The maximum stress always occurs in the thinner shell. The similarity between the cylinder and sphere curves and the well known fact that in the bending analysis of nonshallow shells any shell can be approximated by an equivalent cylinder* suggests the possibility of using the results for cylinders with mismatch for any shell.

Consider any one of the design charts in Section 5.1.1, for example the one on page 5.20. At $m = 1$ the only cause for the bending moment which

* See, for example, Ref. [12], p. 68 ff.

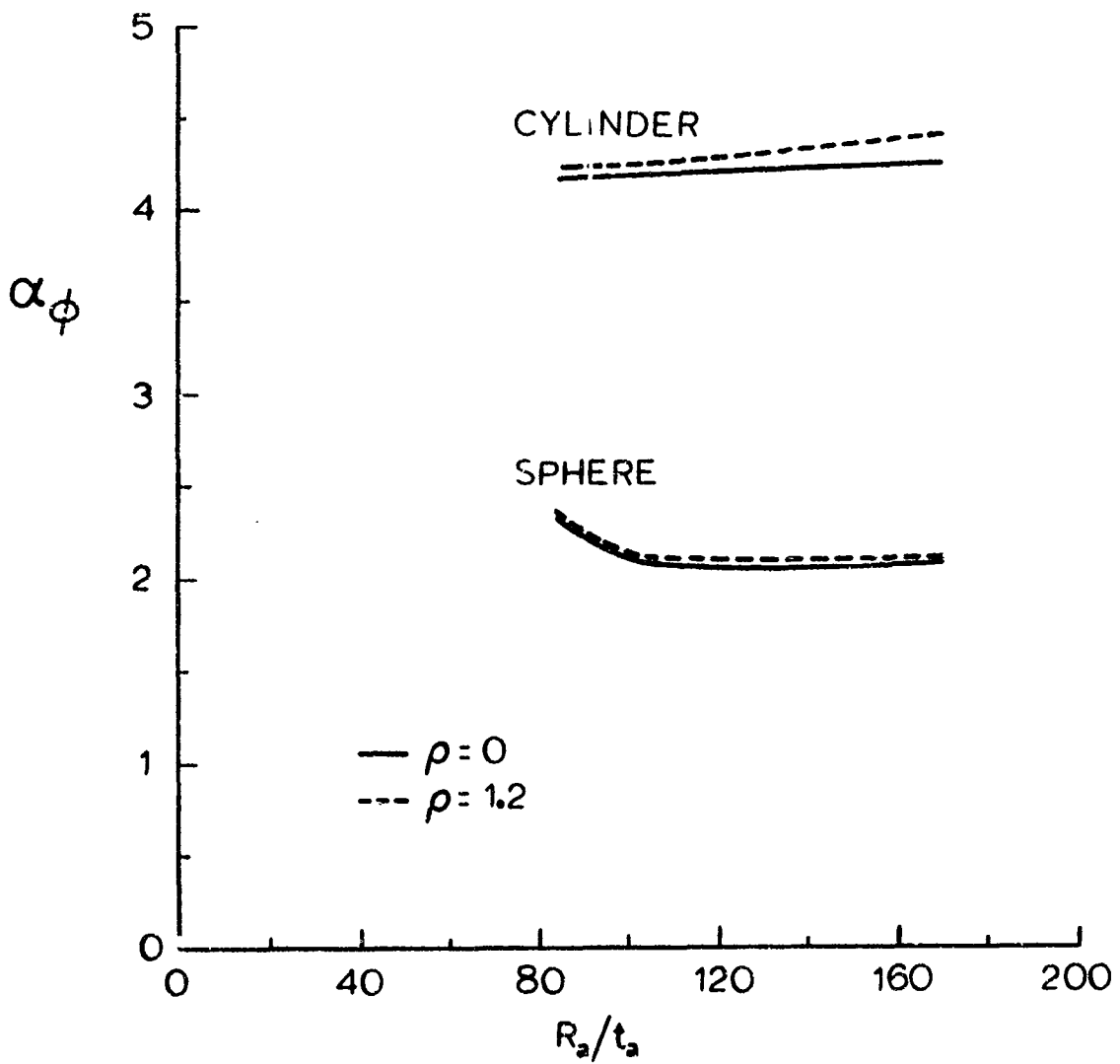


Fig. 2-2 Clamped Spheres and Cylinders: Meridional Stress Factors

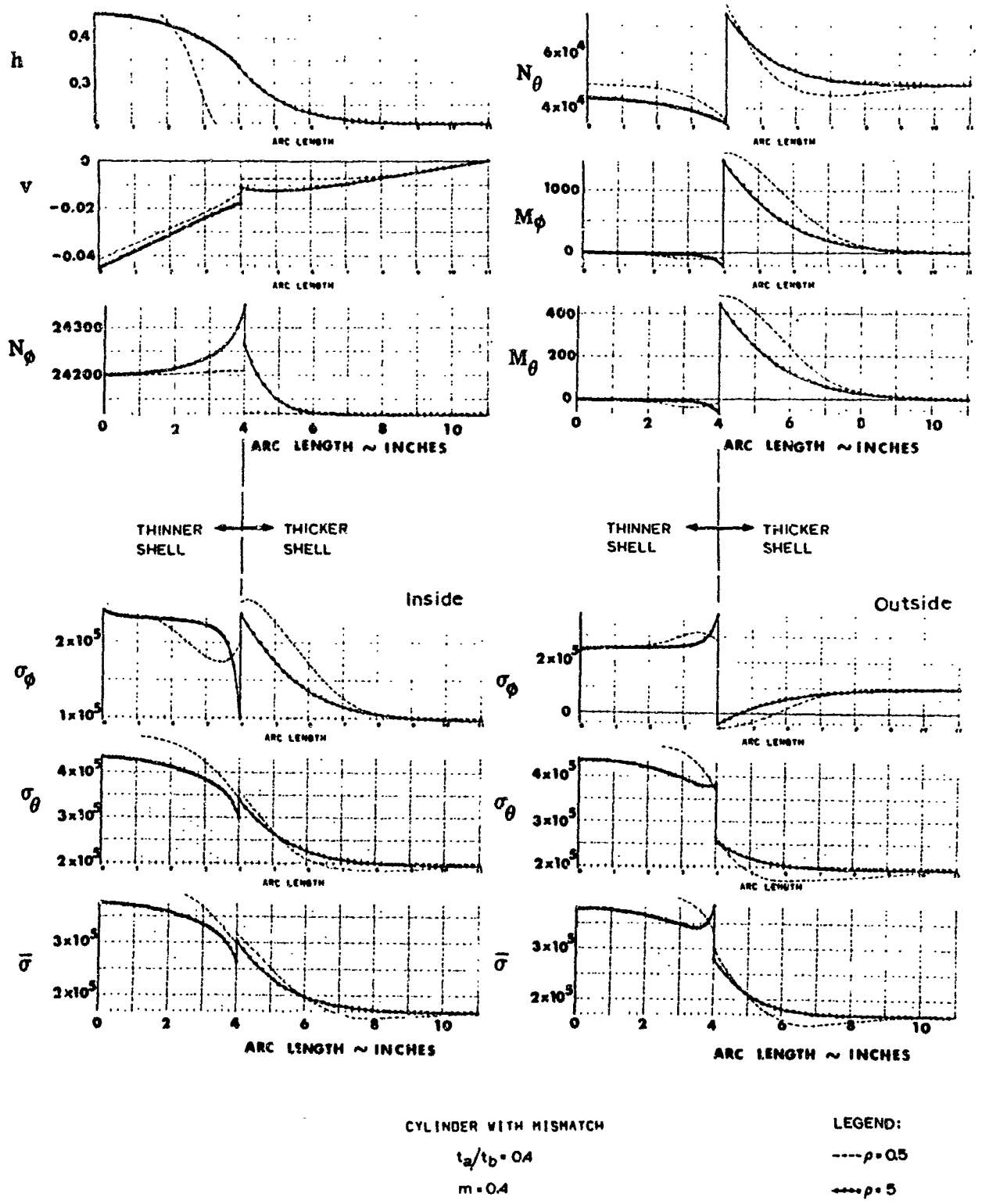
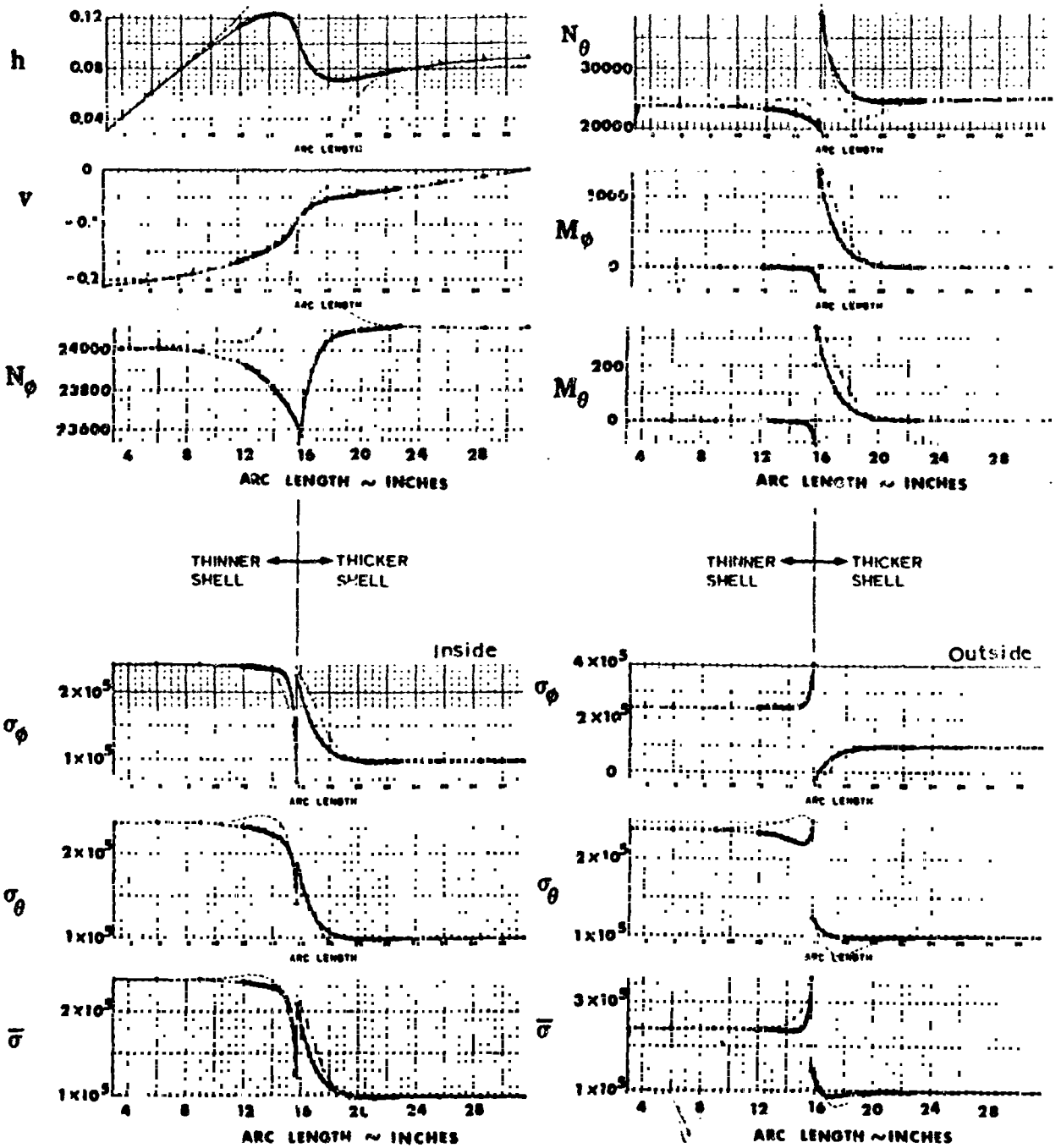


Fig. 2-3 Cylinder with Mismatch and Undercut: Deformations and Stress Resultants



SPHERE WITH MISMATCH
 $t_a/t_b = 0.4$
 $m = 0.4$

LEGEND:
 --- $\rho = 0.5$
 --- $\rho = 5$

Fig. 2-4 Sphere with Mismatch and Undercut: Deformations and Stress Resultants

exists there is the differential radial displacement which occurs in the membrane solution (the thinner shell expands more than the thicker one). If, for any reason, this displacement is changed, the bending moment will change in proportion. Thus,

$$\left. \begin{aligned} M &\propto \Delta \delta \\ \alpha_{\varphi} &= \left(\frac{\alpha_{\varphi_0} - 1}{\Delta \delta} \right)_{\text{CYL}} \Delta \delta + 1 \end{aligned} \right\} \text{at } m = 0$$

or

where $\Delta \delta =$ differential expansion

As a mismatch, m , is introduced, an additional moment is introduced into the structure. This moment is of the nature of an externally applied load, and is not affected by the differential expansion $\Delta \delta$. Thus, by simply moving the family of curves up or down (or displacing the intercept at $m = 0$ in proportion to $\Delta \delta$) the graph should be applicable to any shell geometry that fits the category mentioned in the beginning of this chapter. A conversion formula which describes this parallel displacement is

$$(\alpha_{\varphi})_{\text{SR}} = (\alpha_{\varphi})_{\text{CYL}} - \left(1 - \frac{\delta_{\text{SR}}}{\delta_{\text{CYL}}}\right) (\alpha_{\varphi_0} - 1) \quad (2.8)$$

for meridional stresses. For the hoop stresses the following formula is derived

$$(\alpha_{\theta})_{\text{SR}} = 1 + (\alpha_{\theta})_{\text{CYL}} - (\alpha_{\theta_0}) \left(1 - \frac{\delta_{\text{SR}}}{\delta_{\text{CYL}}}\right) - 2 \frac{\delta_{\text{SR}}}{\delta_{\text{CYL}}} \quad (2.9)$$

where

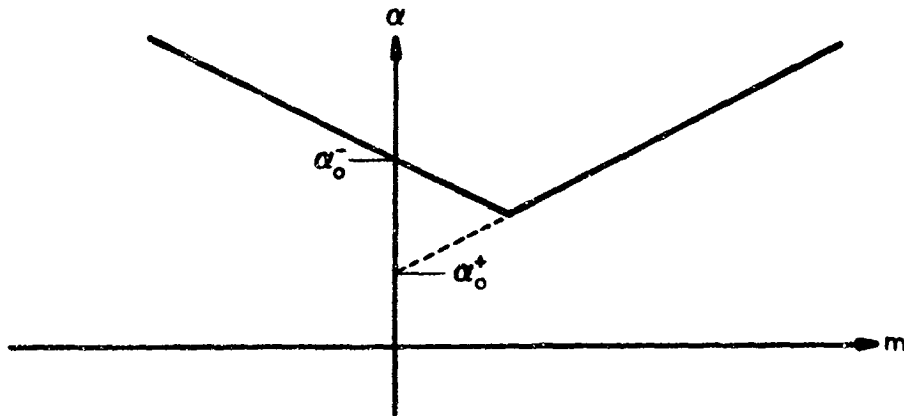
$$\frac{\delta_{\text{SR}}}{\delta_{\text{CYL}}} = \frac{N_{\theta_m} - \nu N_{\varphi_m}}{p R_2 \left(1 - \frac{\nu}{2}\right)}$$

$R_2 =$ Radius at the discontinuity measured normal to the shell meridian (hoop radius)

$N_{\theta_m} =$ Membrane hoop stress resultant

N_{φ_m} = Membrane meridional stress resultant
 α_{φ_0} , α_{θ_0} : Intercepts ($m = 0$)
 Subscripts SR = Shell of Revolution
 CYL = Cylinder

The intercepts α_{φ_0} and α_{θ_0} are taken from the appropriate curves. Note, that in the cases where the curves have the following shape



there are two intercepts, one for the branch of the curve with negative slope (α_0^-), and one for the branch of the curve with positive slope (α_0^+).

Applying the formulas to the sphere, for which $N_{m\theta} = N_{m\varphi} = \frac{\rho R}{2}$, one gets the following conversion formulas:

$$\left. \begin{aligned}
 (\alpha_{\varphi})_{SR} &= (\alpha_{\varphi})_{CYL} - .588 (\alpha_{\varphi_0} - 1) \\
 (\alpha_{\theta})_{SR} &= (\alpha_{\theta})_{CYL} - .588 \alpha_{\theta_0} + .177
 \end{aligned} \right\} \begin{array}{l} \text{Sphere} \\ (v = 0.3) \end{array}$$

These formulas were used to calculate stress factors for a sphere with $t_a/t_b = .4$ for varying mismatch and nonlinearity factors ρ . The results, compared with independent computer solutions, are shown in the table below:

ρ	Meridional Stress Factor, α_φ				Hoop Stress Factor, α_θ			
	m = .4		m = 1		m = .4		m = 1	
	Eq. 2.8	Computer	Eq. 2.8	Computer	Eq. 2.9	Computer	Eq. 2.9	Computer
0	1.49	1.45	2.68	2.62	1.02	1.01	1.64	1.54
1	1.60	1.56	2.83	2.79	1.02	1.02	1.58	1.52
2	1.66	1.61	2.91	2.87	1.02	1.03	1.54	1.50
3	1.69	1.64	2.96	2.91	1.02	1.03	1.52	1.49
4	1.73	1.67	3.00	2.94	1.02	1.03	1.51	1.48
5	1.76	1.68	3.04	2.96	1.02	1.03	1.50	1.47

These results show very good agreement between the two methods.

The unfilleted joint is, of course, an abstraction and in reality there would always be a fillet or a radius between the two mismatched shells. If the fillet is relatively small, say of the order of the shell thickness, the effect on the maximum stress is surprisingly small. In Fig. 2-5 a comparison between the unfilleted joint and a 45° filleted joint* is made for the case where the thicknesses are equal on either side of the shell. The figure shows that the effective stress factor α_e is quite insensitive to the fillet, except for the very high nonlinearity parameter value of $\rho = 10$. (It is doubtful that much higher values than $\rho = 1$ will be experienced for metal pressure vessels.) The geometry selected for Fig. 2-5 shows the largest difference between the filleted and the unfilleted joints. As the thickness ratio t_a/t_b decreases the differences become progressively smaller, and at $t_a/t_b = 0$ the results for filleted and unfilleted joints are identical.

* Data taken from Bizon [11]

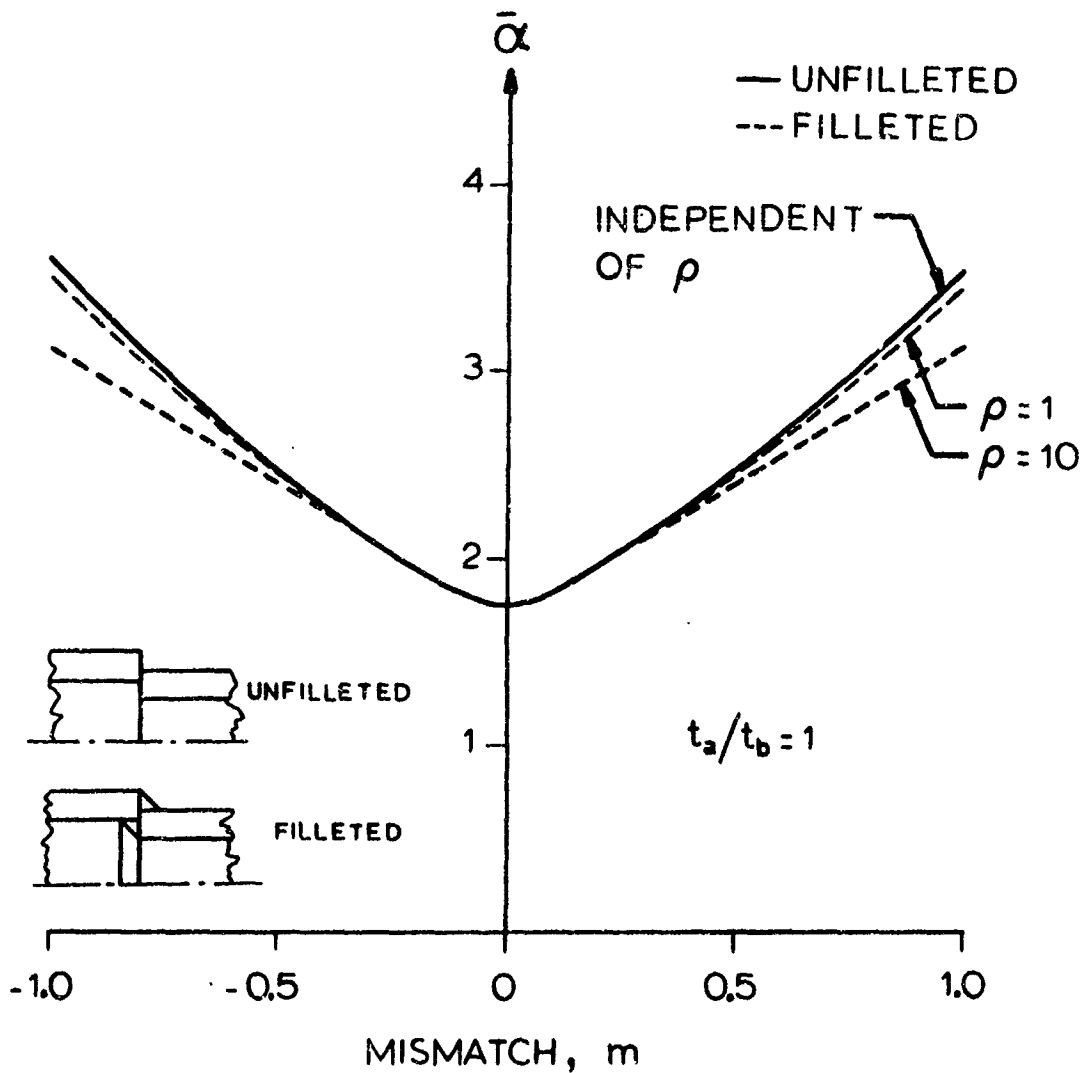


Fig. 2-5 Effective Stress in Filleted and Unfilleted Butt Joints

2.3 Weld Sinkage

The term weld sinkage is here used to describe a meridional slope discontinuity of the general shape indicated by Fig. 2-6. The discontinuity is symmetric around the circumference of the shell and also symmetric with respect to its lowest point. Discontinuities of this type frequently occur during welding. However, in the present report only the geometric effects of the discontinuity are studied; residual stresses which could have been introduced during the welding process are neglected and the shell is considered stress (and strain) free before the application of the first pressure loading.

The geometry of a shell of revolution is fully determined by two quantities: the meridional radius of curvature, r_1 , and the hoop radius of curvature, r_2 . These two quantities, in turn, are functions of the meridional geometry, and are variables within the zone of discontinuity, L . For the purposes of parametric investigations it is convenient to be able to express the radii of curvature analytically. Any number of equations may be used to describe the general shape of the discontinuity zone "L" in Fig. 2-6, however, the equation

$$r(s) = R(1 - \epsilon e^{-K|s|/R}) \quad (2.10)$$

is particularly useful since it, as shown in Appendix C, permits a closed form solution. The main sinkage geometry parameters, length, depth, and angular change become, for this representation

$$\left. \begin{aligned} L &\rightarrow \infty \\ \Delta &= \epsilon R \\ \Delta \varphi &= 2 \arcsin(\epsilon K) \end{aligned} \right\} \quad (2.10a)$$

The fact that the sinkage length is infinite means, simply, that L is not a parameter for this particular geometry*. However, by manipulation of the

*As is shown later, L has no influence on the maximum stress.

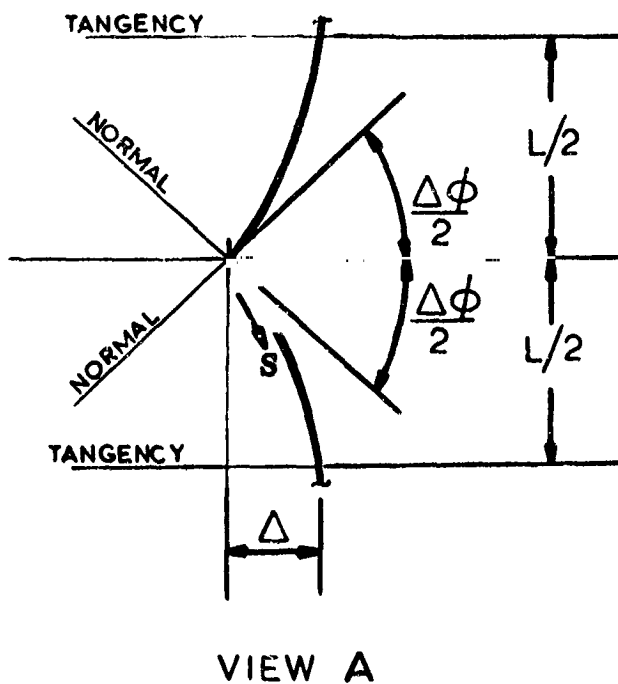
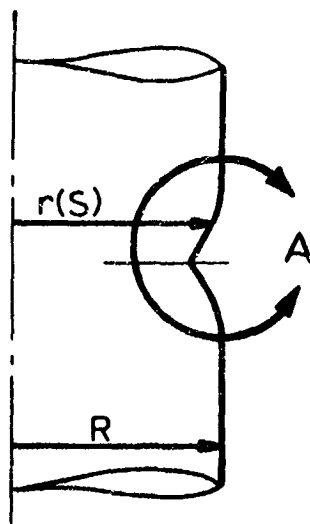


Fig. 2-6 Weld Sinkage (Slope Discontinuity)

arbitrary constants ϵ and K , values of L which for all practical purposes are finite may be simulated. For example, the geometries shown in Fig. 2-7 result from varying K .

Fig. 2-8 shows typical stress and deformation curves for a cylinder with a slope discontinuity defined by Eq. 2.10 as computed by the use of the computer program BOSOR. Nonlinear effects are shown by the difference in the curves for $\rho = 0.5$, and the curves for $\rho = 5$. (The abscissas pertain to the higher load; the curves for $\rho = 0.5$ have been multiplied by a factor of 10.) For the higher load the maximum stresses exceed considerably the strength capabilities of existing metals and this high load is used only to illustrate the trend of the nonlinearity effects.

The stress factors developed in Appendix C for cylinders with discontinuities described by Eq. 2.10 are

$$\alpha_{\phi} = 1 + \left(\frac{3}{1 - \nu^2} \right)^{1/2} \epsilon K \left(\frac{R}{2c} \right)^{1/2} \frac{1 + \sqrt{2} \mu}{1 + \mu^2 + \sqrt{2} \mu} \quad (2.11)$$

$$\alpha_{\theta} = 2 + \epsilon K \left(\frac{R}{2c} \right)^{1/2} \frac{1}{1 + \mu^2 + \sqrt{2} \mu} + \nu(\alpha_{\phi} - 1) \quad (2.12)$$

where

$$\mu = \left(\frac{c K^2}{R} \right)^{1/2} \quad (2.13)$$

$$c = \frac{t}{\sqrt{12(1 - \nu^2)}} \quad (2.14)$$

It is interesting to note that while Eq. (2.11) is derived for small and relatively gentle deviations from the nominal geometry, it still is capable of yielding correct results over a wide range of geometrical variations. Consider the following: When the parameter K approaches infinity the shell becomes a cylinder with radius R everywhere except

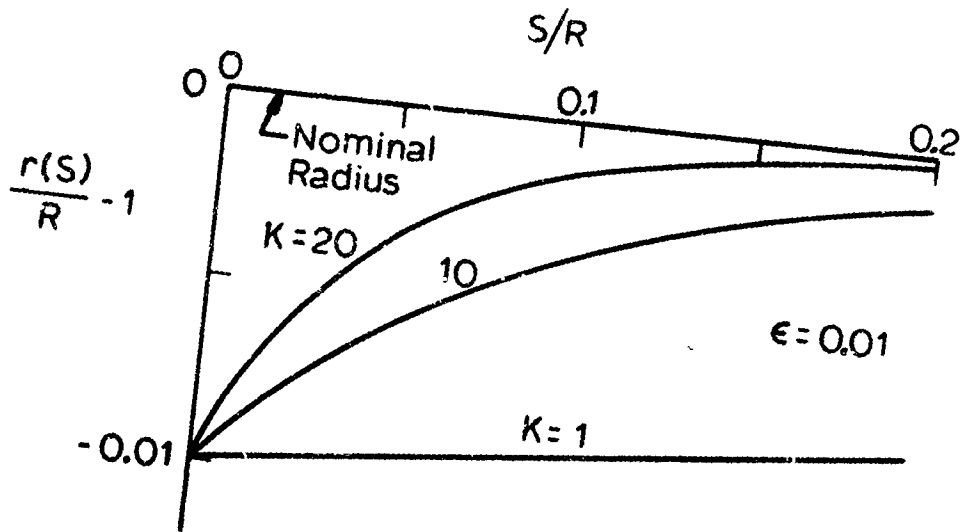


Fig. 2-7 Sinkage Geometry Possibilities According to Eq. 2.10 with $\epsilon = 0.01$

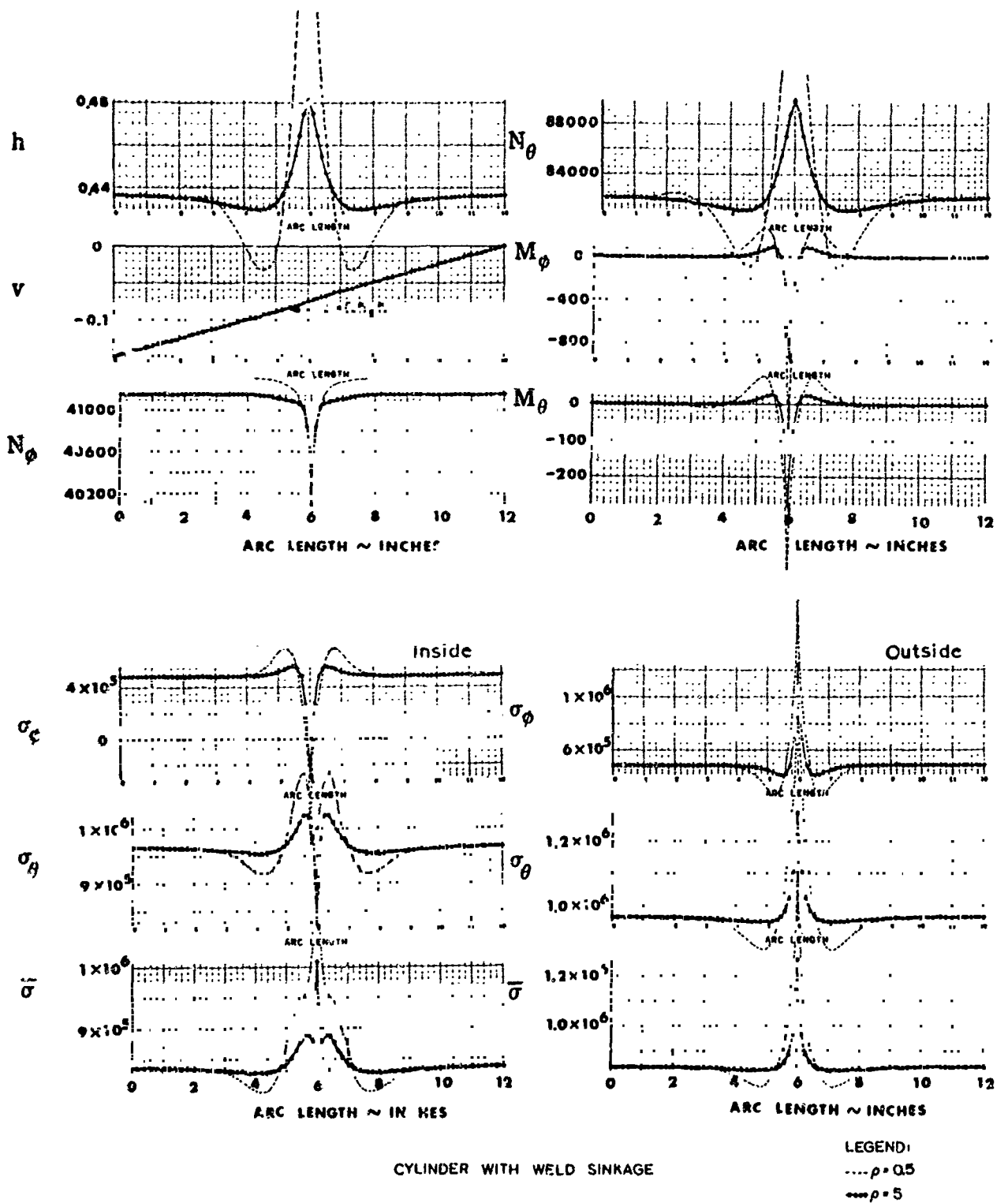


Fig. 2-8 Deformations and Stresses in Cylinder with Weld Sinkage

at the crease, where the radius is $R - R \epsilon$, thus creating a pure eccentricity of the magnitude $R \epsilon$. The eccentricity moment is then $N R \epsilon$ and the resulting bending stress $6 N R \epsilon / t^2$. Thus, the stress factor is $1 + \frac{6 R \epsilon}{t}$. Now, from Eq. 2.11

$$\begin{aligned} \lim_{K \rightarrow \infty} \alpha_{\varphi} &= 1 + \left(\frac{3}{1-\nu^2}\right)^{1/2} \epsilon K^2 \left(\frac{R}{2cK^2}\right)^{1/2} \frac{\sqrt{2} \left(\frac{cK^2}{R}\right)^{1/2}}{\left(\frac{cK^2}{R}\right)} \\ &= 1 + \left(\frac{3}{1-\nu^2}\right)^{1/2} \epsilon R \frac{\sqrt{12(1-\nu^2)}}{t} \\ &= 1 + \frac{6 R \epsilon}{t} \end{aligned}$$

Also

$$\lim_{K \rightarrow 0} \alpha_{\varphi} = 1$$

Thus, the equation gives correct results at both limits ($K \rightarrow 0$ and $K \rightarrow \infty$).

The geometrical variables appearing in the formulas above can easily be expressed in terms of fundamental quantities, as follows

$$\left. \begin{aligned} \epsilon K &= \sin \frac{\Delta \varphi}{2} \\ \epsilon R &= \Delta \\ \mu^2 &= \frac{1}{\sqrt{12(1-\nu^2)}} \frac{t}{R} \left(\frac{R}{\rho_1 \tan \frac{\Delta \varphi}{2}}\right)^2 \end{aligned} \right\} \quad (2.15a-c)$$

where $\Delta \varphi$ and Δ are defined according to Fig. 2-6, and $1/\rho_1$ is the meridional curvature at the crease. Inserting these quantities into Eq. 2.11 and 2.12 one gets

$$\alpha_{\varphi} = \left(\frac{3 \sqrt{3}}{\sqrt{1-\nu^2}}\right)^{1/2} \left(\sin \frac{\Delta \varphi}{2}\right) \sqrt{\frac{R}{t}} \frac{1 + \sqrt{2} \mu}{1 + \mu^2 + \sqrt{2} \mu} \quad (2.16)$$

$$\alpha_{\theta} = 2 + \sqrt[4]{3(1-\nu^2)} \left(\sin \frac{\Delta\phi}{2} \right) \sqrt{\frac{R}{t}} \frac{1}{1 + \mu^2 + \sqrt{2} \mu} + \nu(\alpha_{\phi} - 1) \quad (2.17)$$

In this form the stress factors are expressed only in fundamental quantities of the shell geometry and could thus be applied to any cylindrical shell with a slope discontinuity. That this is not only possible but also permissible will be shown later in this section. It will also be empirically shown that while the above formulas are derived for a cylinder, they also can be applied, with accurate results, to a sphere, if the curvature $1/\rho_1$ is taken to mean the deviation from the nominal curvature, rather than the curvature itself.

Nonlinear pressure effects are not accounted for in the derivation described above. It is, however, evident from the details of the derivation shown in Appendix C that any modifications due to geometrical deviations caused by the pressure should only be applied to the terms containing the μ parameter. Thus, the nonlinear effects should be a function only of the geometric parameter μ , and, of course, the pressure parameter ρ . By applying the computer program BOSOR [1] to a series of shells with systematically varied values of μ and ρ the nonlinear effects were investigated, resulting in the design graphs of Section 5.1.2. In the development of these design graphs a series of checks were made on the validity of the results and the allowable range and combination of individual values of the various parameters. These checks included the following:

Check of Applicability to Relatively Thick Shells

The design graphs are based on computed data for cylinders with a radius-to-thickness ratio of 100. A comparison between stress factors obtained from the design graphs and computed directly, for $R/t = 10$ was made. Results are as follows

μ^2		0.1		5	
$\Delta\phi$		10.4°		65.8°	
		Graph	Computer	Graph	Computer
$\rho = 0$	α_ϕ	1.63	1.49	2.82	2.77
	α_θ	2.43	2.32	2.79	2.81
$\rho = .5$	α_ϕ	1.51	1.41	2.68	2.57
	α_θ	2.33	2.26	2.72	2.71

The agreement is good, especially for the more severe (large $\Delta\phi$) discontinuities. The graphs will, apparently, always give slightly conservative results for the thick shells.

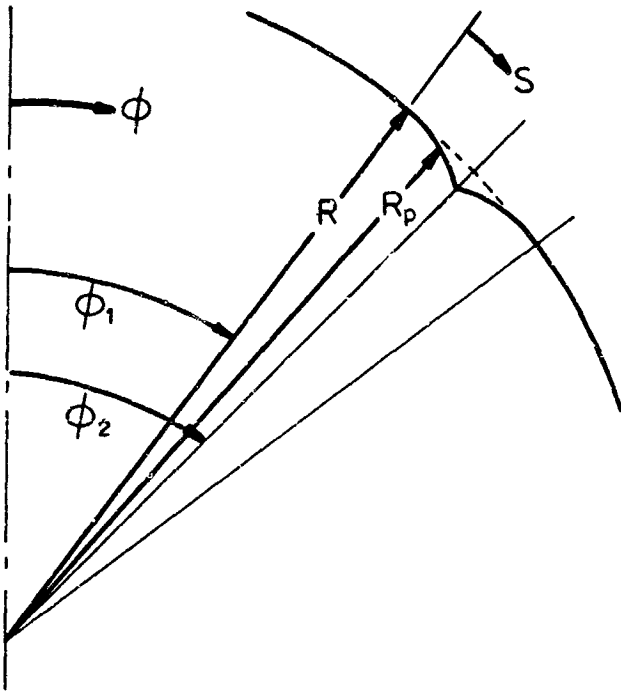
Check of Applicability to Arbitrary Meridians

A series of computer runs were made on a discontinuity configuration in a cylinder, and a series for the same discontinuity configuration in a sphere. In both cases the meridian was represented by an equation of the form

$$R_p = R + A \left(\frac{\phi - \phi_1}{\phi_2 - \phi_1} \right)^{m_1} + B \left(\frac{\phi - \phi_1}{\phi_2 - \phi_1} \right)^{m_2} \quad (2.18)$$

(see Fig. 2-9), rather than the exponential equation (2.10). The total sinkage and the sinkage length were kept constant. The change in meridional curvature, ρ , was identical for the two shell configurations. To accomplish this the meridian for the sphere was represented by

$$R_p = R + A \left(\frac{\phi - \phi_1}{\phi_2 - \phi_1} \right)^{m_1}$$



NOMENCLATURE

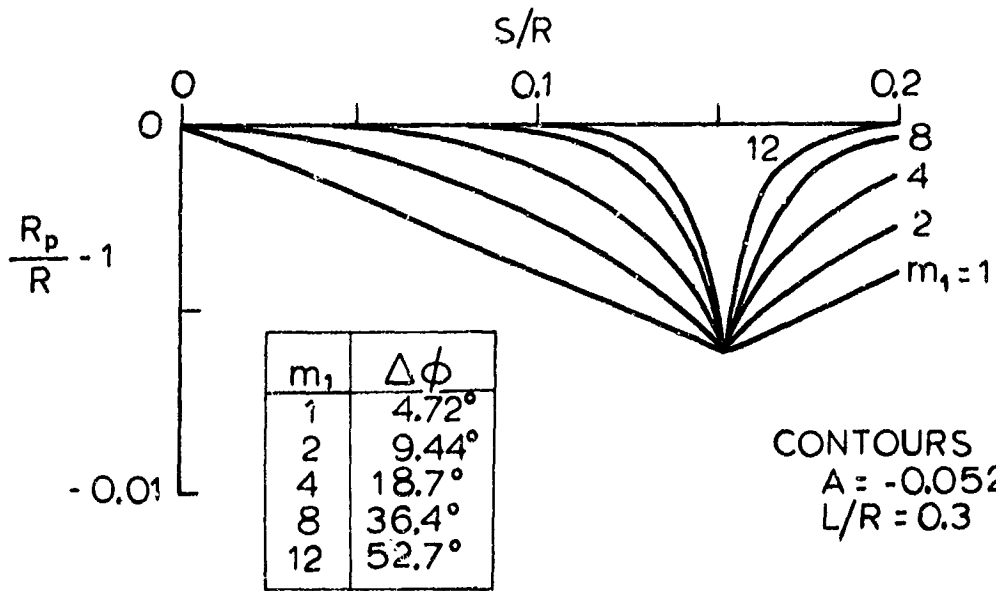


Fig. 2-9 Sinkage as Represented by Eq. 2.18

and for the cylinder by the formula

$$R_p = R + \frac{R}{2} \mu^2 \left(\frac{\varphi - \varphi_1}{\varphi_2 - \varphi_1} \right)^2 + A \left(\frac{\varphi - \varphi_1}{\varphi_2 - \varphi_1} \right)^{m_1}$$

By varying the exponent m_1 the angle $\Delta\varphi$ was varied between about five and fifty degrees. Figure 2-9 shows the discontinuity contours used in both series of runs. The radius-to-thickness ratio was 106.3. Table 1 shows the pertinent data for both the spheres and the cylinders, taken from the computer output. The primary parameters - sinkage angle $\Delta\varphi$ and radius-to-thickness ratio - are identical for the spheres and cylinders. The curvature $1/\rho_1$ should ideally also have been identical; the small differences noted in the table below are due to the fact that these quantities are evaluated numerically, not analytically, in the program. The parameter μ^2 is calculated using the definition according to Eq. (2.15c).

The table below shows very good agreement between the maximum meridional stress in the spheres and the cylinders. Thus the conclusion is made that there is no difference in the stress increase for the two types of shells, regardless of the non-linearity parameter ρ .

Exponent m_1		1	2	3	4	8	12
Angle, $\Delta\varphi$	sphere	4°.72	9°.44	14°.14	18°.7	36°.5	52°.7
	cylinder	4°.72	9°.44	14°.14		36°.5	
Curvature, $\frac{1}{\rho_1}$	sphere	.001613	.06604	.1930	.3775	1.585	3.279
	cylinder	.00372	.06421	.1915		1.714	
μ^2	sphere	.00032	.1325	.507	1.080	4.75	9.08
	cylinder	.00169	.1250	.500		5.56	
$\rho = .0373$	sphere	7237	9536	10940	11900	13900	14790
	cylinder	7216	9530	10920		13900	
$\rho = .615$	sphere	105100	137900	159900	175900	212400	230500
	cylinder	104900	137800	159600		212600	
$\rho = 1.193$	sphere	188800	246000	286500	317100	390900	429700
	cylinder	188600	245800	286000		391400	

Similarly, the change in maximum hoop stress, compared to the undisturbed shell, is remarkably similar for the two types of shells, as shown in the table below

Exponent m			1	2	3	4	8	12
Angle, $\Delta\phi$	sphere		4°.72	9°.44	18°.14	18.7	36°.5	52°.7
	cylinder		4°.72	9°.44	18°.14		36.5	
Curvature, $\frac{1}{\rho_1}$	sphere		.001613	.0660	.1930	.3775	1.585	3.279
	cylinder		.00372	.06421	.1915		1.714	
$\frac{2}{\mu}$	sphere		.00032	.1325	.507	1.0	4.75	9.08
	cylinder		.00169	.1250	.500		5.56	
$\rho=.0373$	N_θ	sphere	401.9	402.8	393.8	383.2	348.5	327.2
	cylinder		673.5	675.5	666.4		621.4	
	$N_\theta - N_{\theta\infty}$	sphere	129.9	130.8	121.8	111.2	76.5	55.2
	cylinder		129.5	131.5	122.4		77.4	
$\rho=.615$	N_θ	sphere	6023	6042	5947	5830	5426	5167
	cylinder		10510	10540	10450		9938	
	$N_\theta - N_{\theta\infty}$	sphere	1535	1554	1459	1342	938	679
	cylinder		1534	1564	1474		962	
$\rho=1.193$	N_θ	sphere	11060	11090	10950	10780	10170	9773
	cylinder		19760	19810	19680		18940	
	$N_\theta - N_{\theta\infty}$	sphere	2354	2384	2244	2074	1464	1067
	cylinder		2342	2398	2268		1528	

N_θ = total hoop stress resultant

$N_{\theta\infty}$ = hoop stress resultant for undisturbed shell

A comparison between stress factors for spheres computed by the BOSOR computer program, and by the graphs in Section 5.1.2 is given below.

m_1		1		4		8		12	
μ^2		.000318		1.080		4.75		9.08	
$\Delta\varphi$		4°.72		18°.7		36°.5		52°.7	
		graph	computer	graph	computer	graph	computer	graph	computer
$\rho=.0373$	α_φ	1.99	2.13	3.72	3.50	4.32	4.08	4.90	4.35
	α_θ	1.83	1.82	2.41	2.71	2.49	2.23	2.65	2.24
$\rho=1.193$	α_φ	1.69	1.73	3.12	2.91	4.10	3.59	4.75	3.95
	α_θ	1.54	1.49	1.96	1.81	2.20	1.96	2.45	2.04

This table shows a reasonably good agreement, considering that the geometrical representation is quite different from that for which the method of Section 5.1.2 is derived. Almost total agreement occurs for values of m_1 in the range 2-3, but even for such extremes as $m_1 = 1$ (juncture of two cones) and $m_1 = 12$ (extreme curl) the results are in fair agreement (maximum deviation is 20% overestimation). Results similar to the above were obtained for other combinations of the parameters $\Delta\varphi$ and μ . Thus, the method may be considered usable for a wide range of geometries outside of the one for which the method is derived. Thus the usage of the fundamental parameters (2.15a-c) is justified for any sinkage configuration for which these quantities can be determined.

The question arises as to how to determine the fundamental parameters. The sinkage Δ and the angle $\Delta\varphi$ can be determined relatively easily by measurements, but the curvature change ρ_1 cannot be measured directly. The value of the curvature does, however, only appear in the parameter μ , which has a rather mild influence on the maximum stress and which, therefore, does not need to be determined with exactness. If it is assumed that the sinkage contour is according to Eq. 2.10, simple algebra gives the following expression for μ

$$\mu = \frac{0.55}{\Delta} \left(\sin \frac{\Delta\varphi}{2} \right) \sqrt{Rt} \quad (2.19)$$

for $\nu = 0.3$

Thus, μ can be determined with sufficient accuracy from measurements of only Δ and $\Delta\varphi$ (and, of course, Rt).

Section 3
PLASTICITY ANALYSIS OF WELD SINKAGE

Due to the difficulty of the problem, the analysis of plasticity effects was made almost entirely by the use of the computer program EPSOR [2]*. This program uses a finite-difference approach where the equilibrium and compatibility equations are solved in an iterative manner. In its original form the program was not suitable for solving discontinuity problems. However, after suitable modifications (introducing the elastic nonlinear effects discussed elsewhere, and providing for a meridional geometric discontinuity) the program was successfully applied to the weld sinkage problem. With these changes the capabilities of the computer program EPSOR are as follows:

Shell Geometry - General shell of revolution, defined by two principal radii of curvature. The thickness is permitted to vary in the meridional direction. Thin-shell theory is used, i.e., the thickness is small in comparison to both radii of curvature.

Stress-Strain Relations - Because of axial symmetry, and the thin-shell assumption, the only non-zero stress components are the principal stresses σ_{ϕ} and σ_{θ} , which coincide with the meridional and hoop directions. The stress-strain relations used pertain to a temperature-dependent work-hardening material with the von Mises yield function. The loading possibilities are:

- o For small initial changes in loads the shell response is elastic, provided that no previous plastic straining has taken place.
- o As the loads are increased, stresses at certain points of the shell reach values corresponding to initial plastic yielding.

* However, a simplified closed form solution is shown in Appendix D.

- o Further increase in load results in the development of specified elastic and plastic regions.
- o At some further time during load history, unloading from a plastic to an elastic state may take place. (Residual stresses upon unloading are computed.)
- o Reloading from an elastic region which had been plastic constitutes the final possibility for formation of elastic and plastic regions.

Equilibrium Equations - The equilibrium equations are written in terms of the deformed shell, thus giving a nonlinear behavior in the elastic range.

Governing Differential Equations - The governing differential equations are analogous to those given in Ref. 3.

Methods of Solution - The governing differential equations and boundary conditions are transformed into a set of algebraic equations by finite difference approximations. At a given time in the load history the solution is advanced an increment in time t by solving these equations in conjunction with the flow rules associated with the loading function to determine the implicit plastic strain increment. This is accomplished by an iterative scheme. Finally, the complete solution for a specific load history is given by an integration with respect to time by a step-by-step procedure.

The program EPSOR was used to develop numerical solutions for a family of sinkage geometries as illustrated in Fig. 3-1. This particular geometry conforms closely to the one represented by Eq. 2.18, and is also the one used (with variations) in the experimental program. Both cylinders and spheres with this sinkage geometry were investigated, elastically and plastically. The elastic solutions were compared with those obtained from the BOSOR [1] program with excellent agreement. Maximum stresses computed

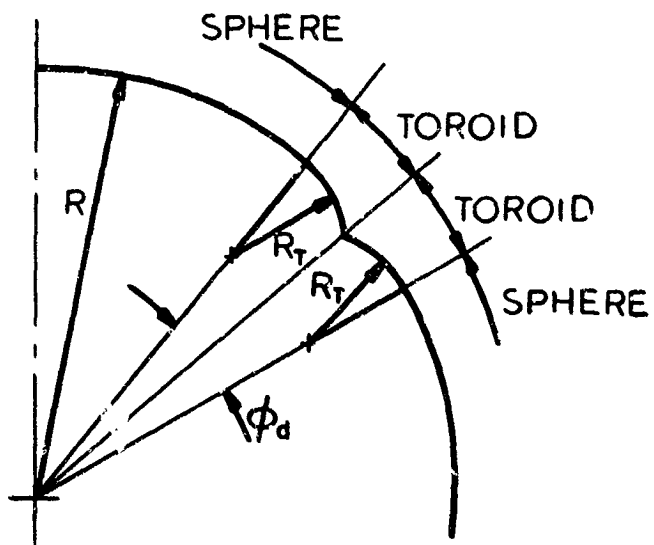
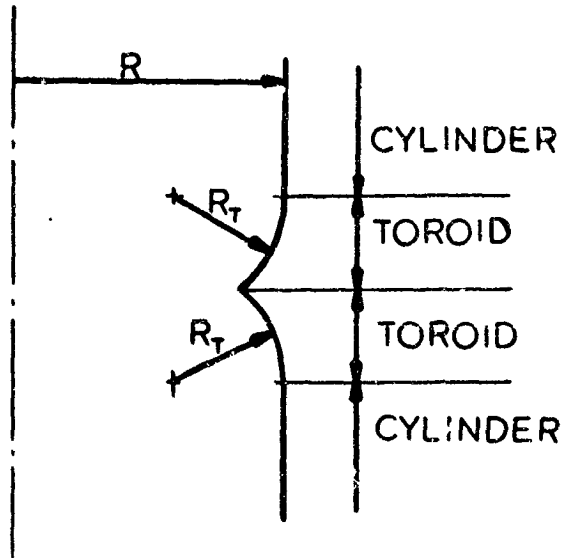


Fig. 3-1 Discontinuity Geometry Used in Plasticity

by the two programs agreed to three or four significant figures.

3.1 Stress-Strain Relations

The use of EPSOR for plastic analysis requires that stress-strain curves in terms of effective stresses and strains are available. The definitions are (see Ref. 13, p. 89)

$$\text{Effective Stress} \quad \bar{\sigma} = \frac{1}{\sqrt{2}} \sqrt{(\sigma_1 - \sigma_2)^2 + (\sigma_1 - \sigma_3)^2 + (\sigma_2 - \sigma_3)^2} \quad (3.1)$$

$$\text{Effective Strain} \quad \bar{\epsilon} = \frac{\sqrt{2}}{3} \sqrt{(\epsilon_1 - \epsilon_2)^2 + (\epsilon_1 - \epsilon_3)^2 + (\epsilon_2 - \epsilon_3)^2} \quad (3.2)$$

where indices 1, 2, and 3 indicate the direction. Applying these equations to a uniaxial stress-strain curve (σ_1 vs. ϵ_1):

$$\left. \begin{aligned} \sigma_2 = \sigma_3 = 0 \\ \epsilon_2 = \epsilon_3 = \nu \epsilon_1 \end{aligned} \right\} \text{Uniaxial}$$

Then

$$\left. \begin{aligned} \bar{\sigma} &= \frac{1}{\sqrt{2}} \sqrt{\sigma_1^2 + \sigma_1^2} = \sigma_1 \\ \bar{\epsilon} &= \frac{\sqrt{2}}{3} \sqrt{\epsilon_1^2(1+\nu)^2 + \epsilon_1^2(1+\nu)^2 + 0} = \frac{2}{3} \epsilon_1(1+\nu) \end{aligned} \right\} \text{Uniaxial} \quad (3.3)$$

Thus, given a uniaxial stress-strain curve (σ_1 vs. ϵ_1), the last two equations define an effective stress-strain curve.

The total effective strain is divided into a plastic and an elastic part (Ref. 13, p. 91)

$$\bar{\epsilon} = \bar{\epsilon}_p + \frac{2(1+\nu)}{3E} \bar{\sigma} \quad (3.4)$$

After some manipulation the following equations for effective strains result

$$\left. \begin{aligned} \bar{\epsilon}_p &= \frac{2}{3} (1 + \nu) \left(\epsilon_1 - \frac{\sigma_1}{E} \right) \\ \bar{\epsilon}_t &= \frac{2}{3} (1 + \nu) \epsilon_1 \\ \bar{\epsilon}_t - \bar{\epsilon}_p &= \frac{2}{3} (1 + \nu) \frac{\sigma_1}{E} \\ &= \frac{\sigma_1}{3G} \end{aligned} \right\} \quad (3.5)$$

where indices p and t stand for plastic and total, respectively. Plots of $\bar{\sigma}/3G$ vs. $\bar{\epsilon}_p$ and $\bar{\epsilon}_t$ vs. $\bar{\epsilon}_p$ for titanium 6Al-4V STA are shown in Fig. 3-2. The curves labeled Tita #4 and Tita #6 were obtained from coupon tests on two test specimens used in the experimental part of the present study (see Section 6), while the curve labeled NASA was obtained from stress-strain curves used in the Apollo program. Due to the similarity of the curves (the only significant difference being the ultimate strength) it was decided to use the NASA curve in the plasticity studies made in the program.

3.2 Preliminary Analyses

The curves of Fig. 3-2 labeled NASA were used to perform an initial plastic analysis of a standard test case (sphere with weld sinkage as in Fig. 3-1). Results from this analysis are shown in Fig. 3-3a where the

* But the analyses made for test result verification used the appropriate, experimental, stress-strain curves.

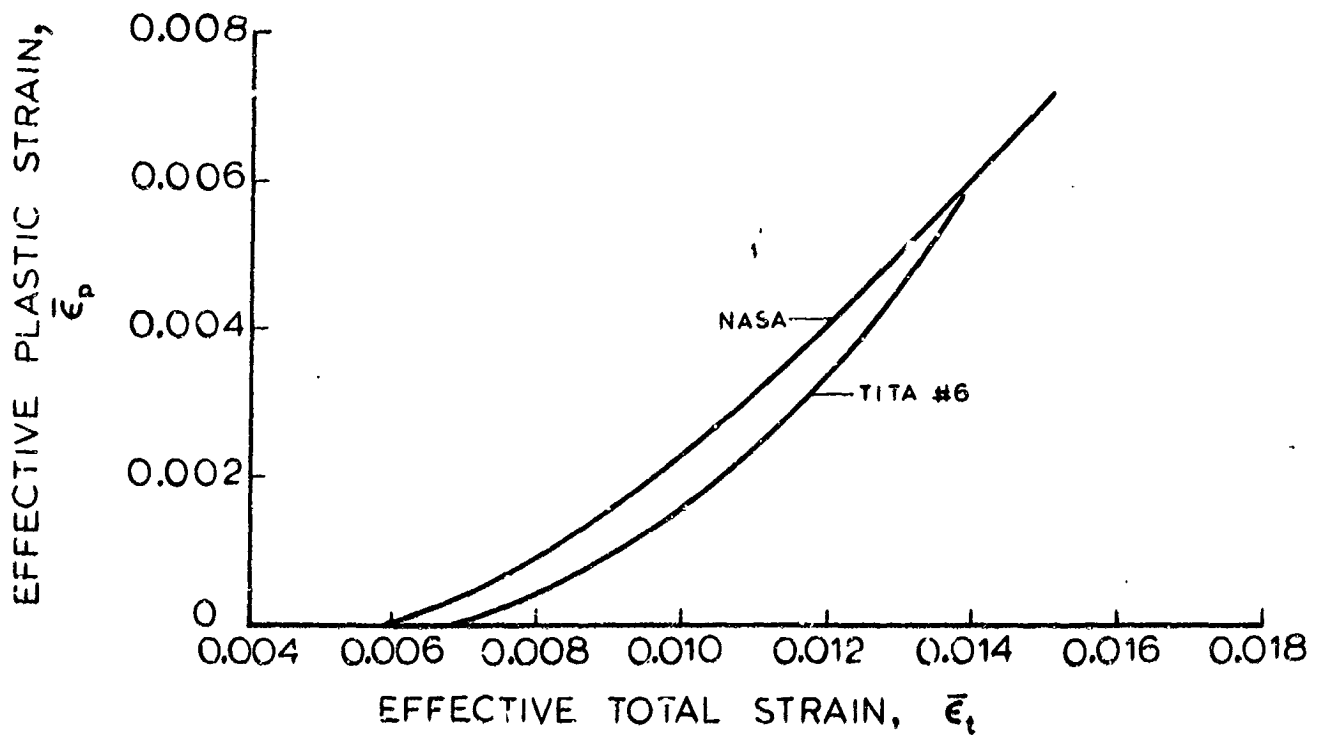
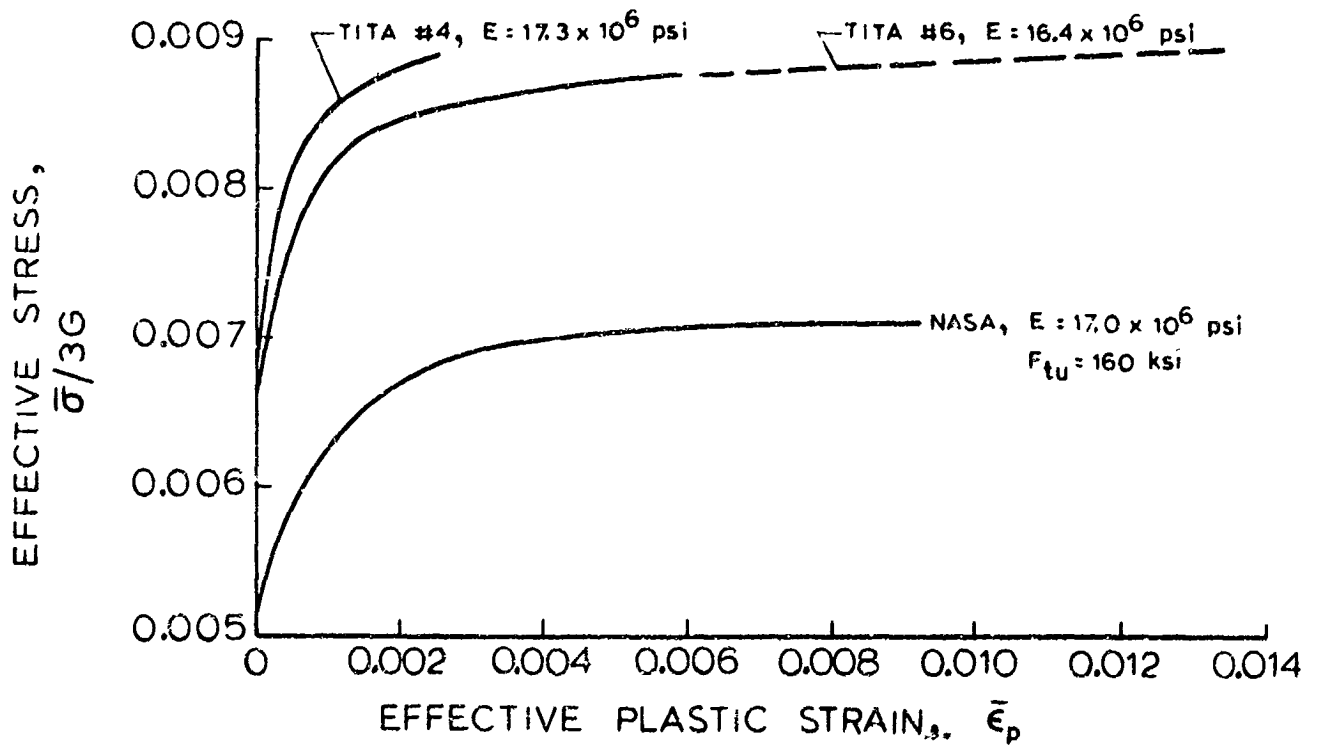
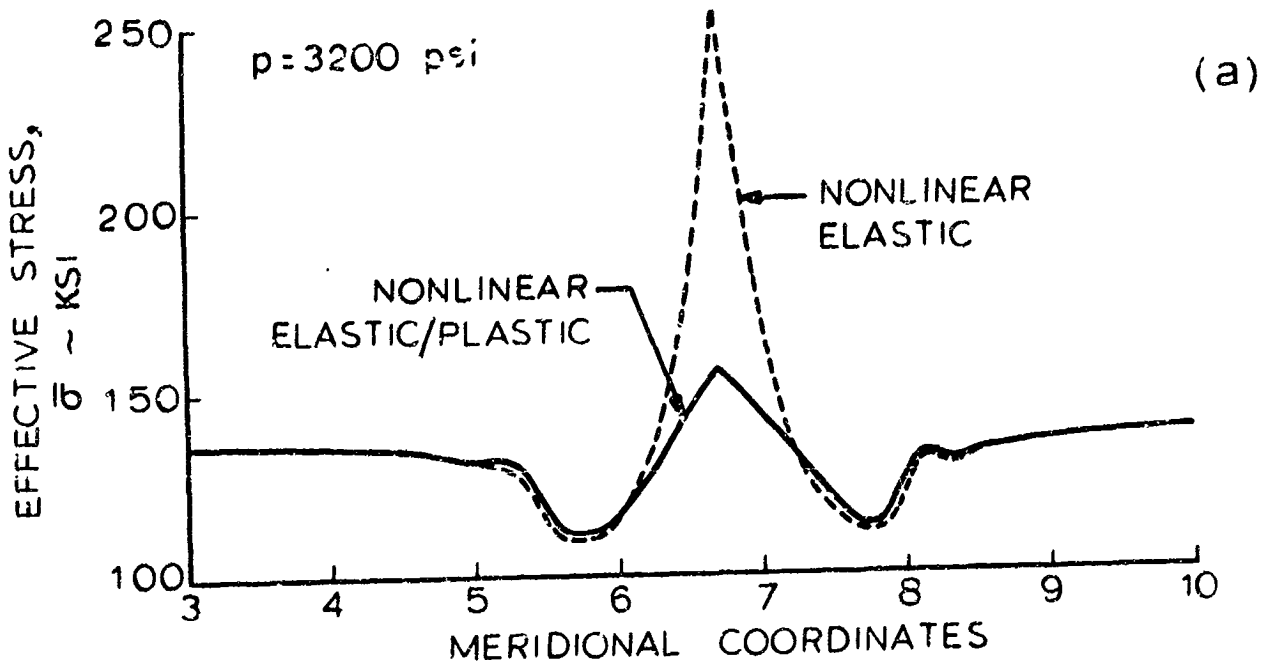


Fig. 3-2 Stress-Strain Curves for Titanium 6Al-4V STA



GEOMETRIC CONFIGURATION: SPHERE, $R = 8.5$
 $t = 0.10$
 $R_t = 5.5$
 $\phi_d = 17.2^\circ$

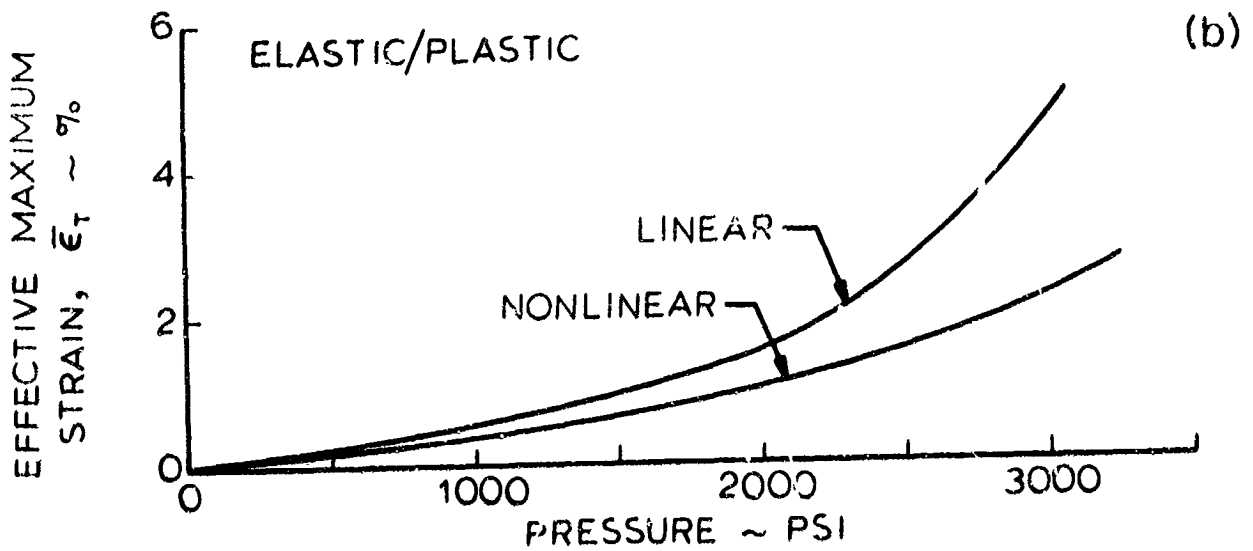


Fig. 3-3 Elastic/Plastic Analysis of Sphere with Weld Sinkage

effective stress is plotted versus surface coordinates and compared with the nonlinear elastic analysis. As expected a large stress reduction occurs at the point of maximum stress, and a minor stress redistribution occurs in adjacent areas. In order to evaluate the total effect of the nonlinear terms appearing in the elastic part of the analysis, these terms were removed and the analysis carried out without them. Results of this analysis, compared with results from the analysis with retained elastic nonlinear terms, are shown in Fig. 3-3b, where maximum effective strains are plotted versus applied pressure. The difference between the two curves is quite large: the collapse pressure would have been underestimated by a substantial amount had the nonlinear elastic terms not been included. The reason for this is, of course, that the elastic nonlinear terms, which essentially relate to changes in the shell geometry during loading, are retained in the plastic part of the analysis where, due to the change of slope in the stress-strain curve, the geometrical changes are accelerated.

3.3 Details of Plasticity Effects - Cylinders and Spheres

It may be remembered that the elastic analysis (Section 2) showed no fundamental difference between the behavior of cylinders and spheres with weld sinkage; the similarity of the two shell types is so close that the same design graphs (Section 5) can be used both for spheres and cylinders. Based on this fact the thought occurred that the plasticity effects also would be similar for the two shell types. Accordingly, spheres and cylinders with similar reduced stress factors α (i.e., with similar elastic behavior) were analyzed and compared. The comparison included plasticity effects during repeated loading, and residual stresses and strains. Figs. 3-4 through 3-10 show some of the results of this work, all of which was carried out by using the EPSOR program [2].

In Fig. 3-4 are shown the meridional (σ_ϕ) and hoop (σ_θ) stresses at the outer shell surface at the crease (center) of the weld sinkage. As the pressure is increased the σ_ϕ vs. σ_θ curve approaches the final yield surface (assumed to be an ellipse, Eq. 2.3), curves around and follows it. In the example shown in Fig. 3-4 the pressure 2400 psi has resulted in an effective

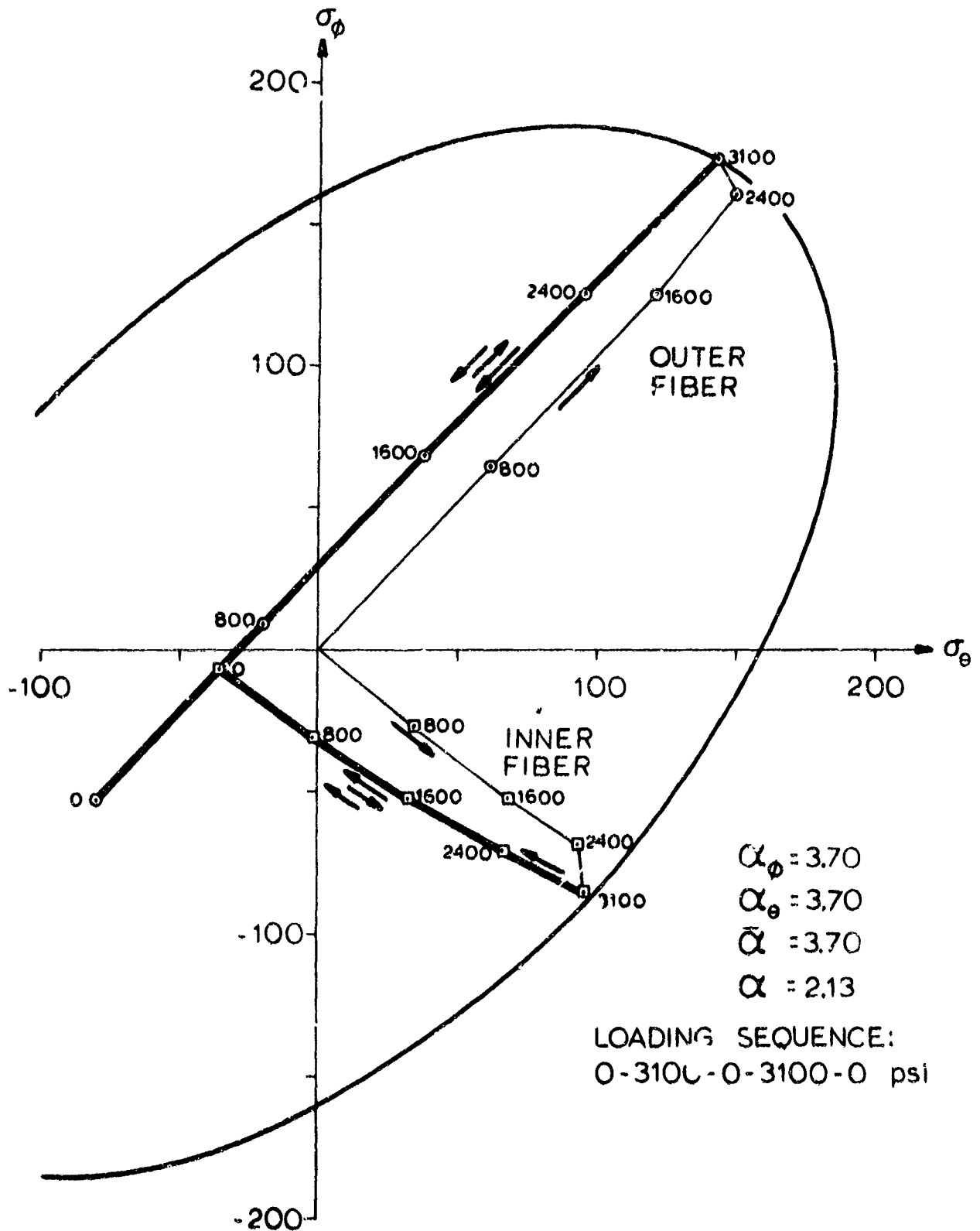


Fig. 3-4 Repeated Loading on Cylinder with Weld Sinkage

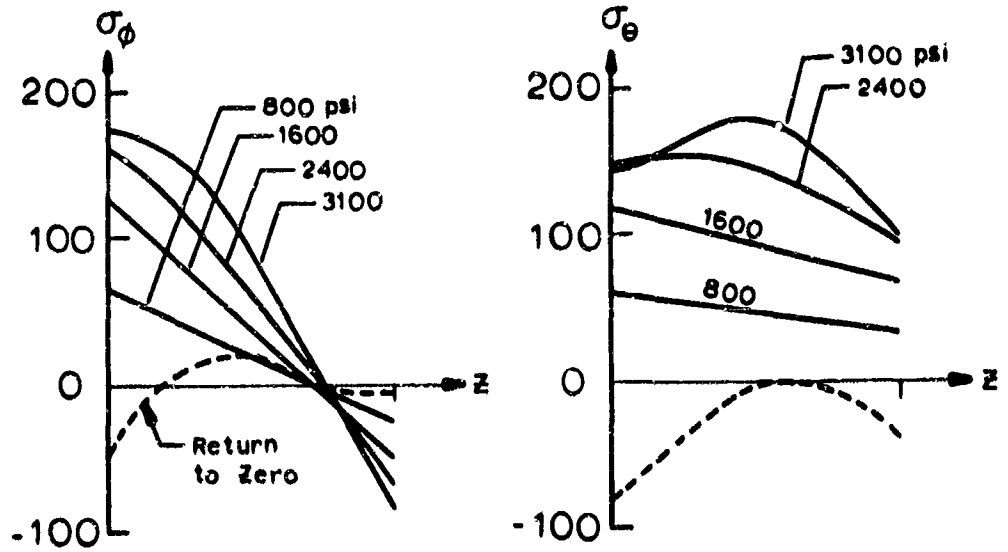
stress which is close to the ultimate, or maximum stress ($F_{tu} = 160$ ksi). Increasing the pressure to 3100 psi develops the full maximum possible stress, both at the outer and inner shell surface. Upon unloading from this point to zero pressure the shell will retain a plastic deformation resulting in the residual stresses indicated by the point "O" in the figure. Repeated loading and unloading from this point to the maximum pressure (3100 psi) will take place elastically, with no plastic strains or residual stress being added to the ones developed during the first load application. Had the residual stress at 0 psi been in the nonlinear part of the stress-strain curve, there would be a continual development of plastic strain during each successive load cycle. The development of plastic residual stresses is, however, a very remote possibility in this type of problem, requiring either an extremely severe geometrical stress riser outside of the range dealt with in the present work, or very large pressures producing strains beyond the ultimate capability of the material (see also the design graph for residual stress, Fig. 5-30 in Section 5).

Fig. 3-5 shows calculated stress variations through the thickness for the same cylinder as in Fig. 3-4. The curves are defined by five points through the thickness. The top part of the figure shows conditions during the first loading cycle; the bottom shows conditions during subsequent cycles. Note the residual stress variation (the dashed curve) is unaffected by the repeated loading.

Fig. 3-6, finally, shows applied pressure versus strain at the outer surface during the repeated loading. This figure is included because it is suitable for comparison with results from the experimental program (see Section 7).

Figures 3-7 through 3-9 show an analysis similar to the one made for the cylinder just described, but made for a sphere with a similar reduced stress factor ($\alpha = 1.975$, which is close to the value 2.13 used in the cylinder analysis). Comparing Fig. 3-7 with its cylinder counterpart, Fig. 3-4, it is immediately clear that the details of the stress variation are rather different (during loading the sphere is stressed in tension throughout the thickness, while the inner surface of the cylinder is in compression). However, the general behavior is similar: After loadings into the plastic

FIRST CYCLE :



SUBSEQUENT CYCLES :

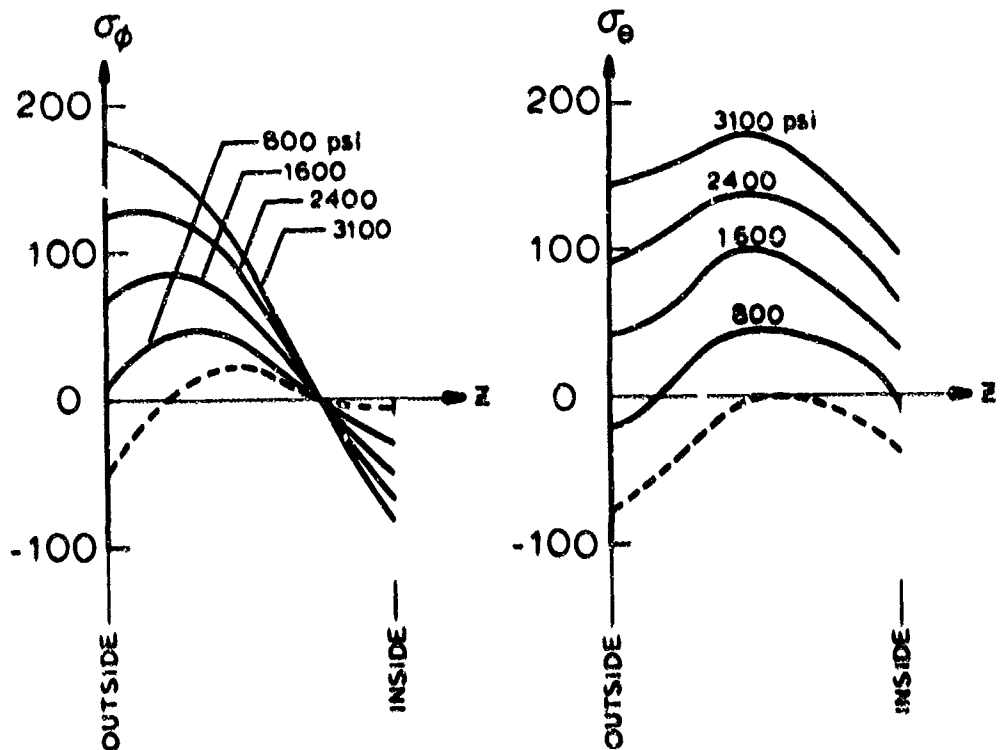


Fig. 3-5 Repeated Loading on Cylinder with Weld Sinkage;
Stress Variation through Thickness

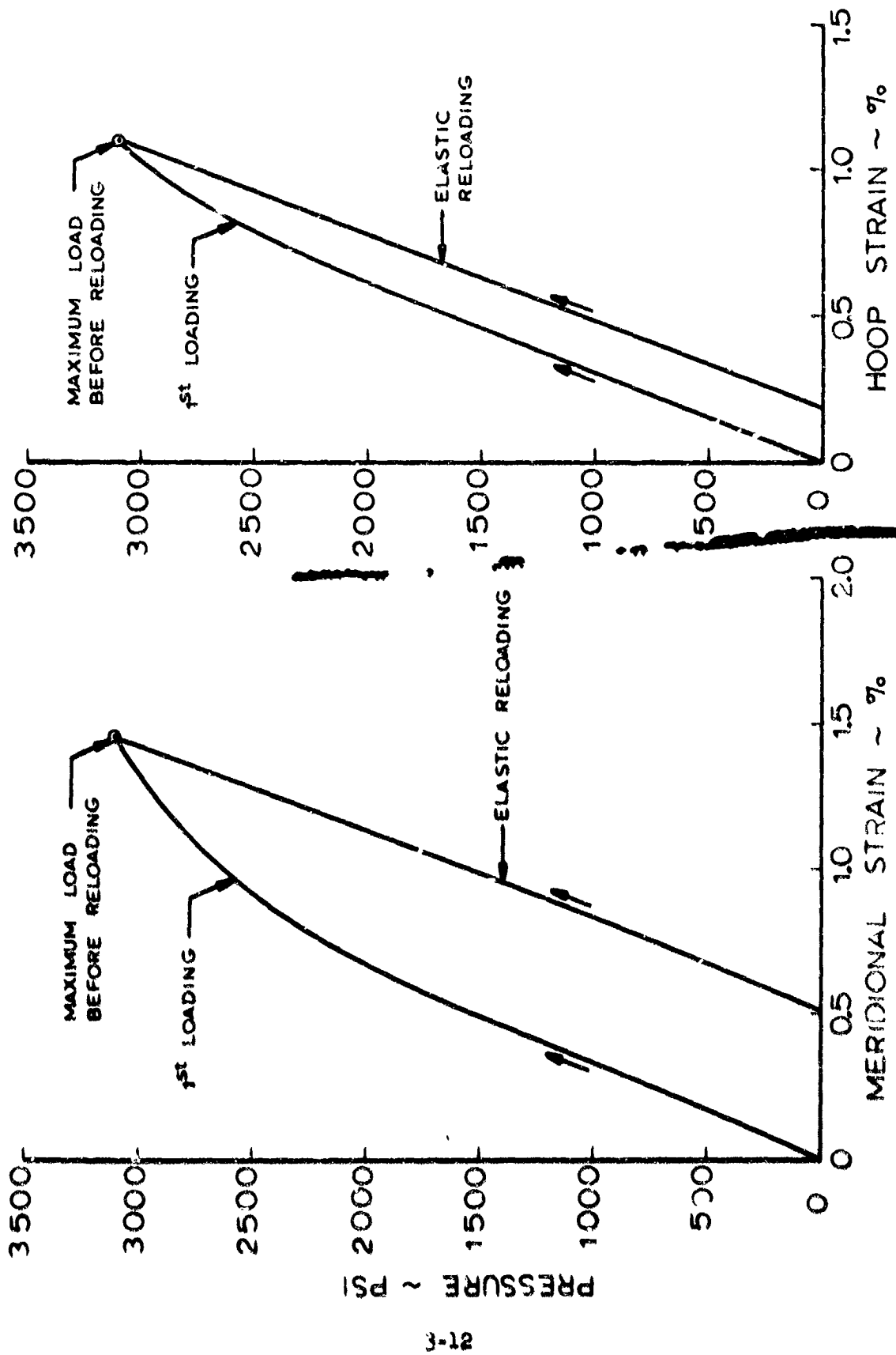


Fig. 3-6 Repeated Loading on Cylinder with Weld Sinkage

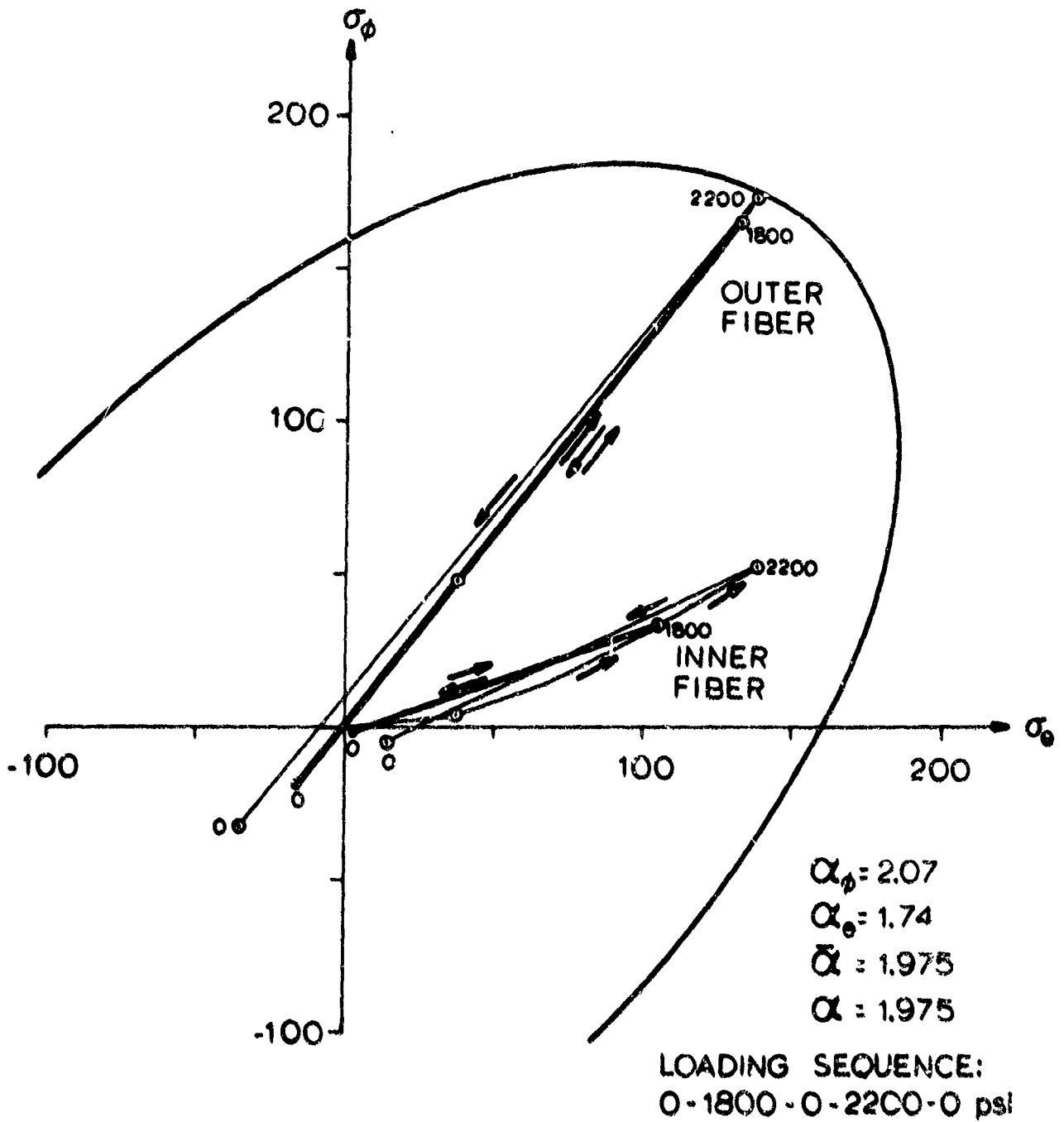


Fig. 3-7 Repeated Loading on Sphere with Weld Sinkage

region the sphere responds elastically upon renewed loading to the previous high loading. The through-the-thickness stress variations in Fig. 3-8 are quite similar to the ones for the cylinder in Fig. 3-5. Note, however, that the reloadings on the sphere are made to successively higher maximum loads, and that therefore the residual stresses are increasing with each cycle. Fig. 3-9 shows the same general behavior as the corresponding figure for the cylinder (3-6).

The above discussion has been concerned with the individual stress components σ_{ϕ} and σ_{θ} . The analysis is, however, based on the equivalent, or effective, uniaxial stress $\bar{\sigma}$ and the effective strain $\bar{\epsilon}$ (see definitions in Section 3.1), which quantities are assumed to be the sole measure of the behavior (including failure) of the shell. A comparison on the basis of effective stress and strain is shown in Fig. 3-10 between spheres and cylinders with exactly the same reduced stress factor α^* . The figure shows, in normalized form, that the shell response in the elastic region is identical for the two shells, but that the plastic region exhibits differences, which for the smaller stress factors are not great, but increases with the larger stress factors. Similar results are obtained for the residual stress, as shown in Section 5.

* σ^* curves are taken from the design graphs of Section 5.

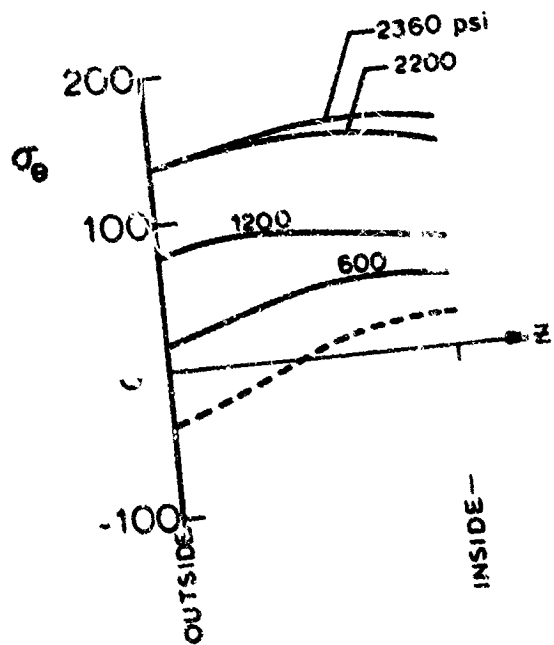
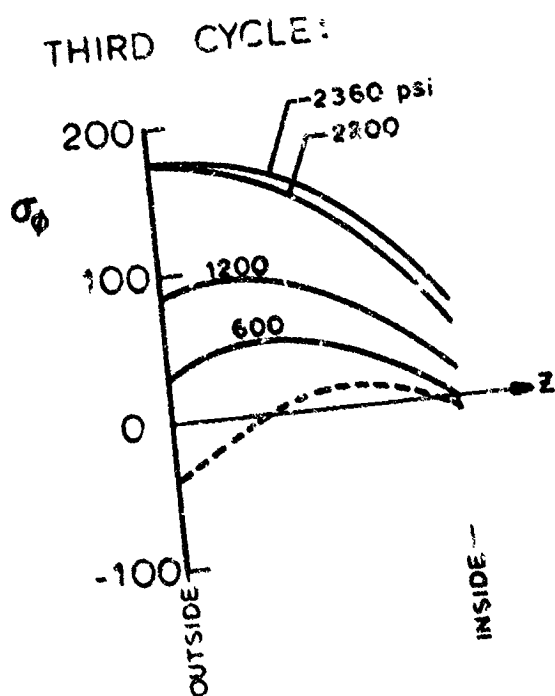
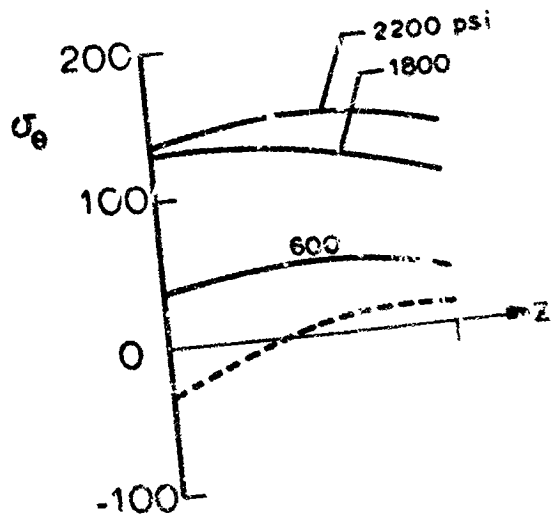
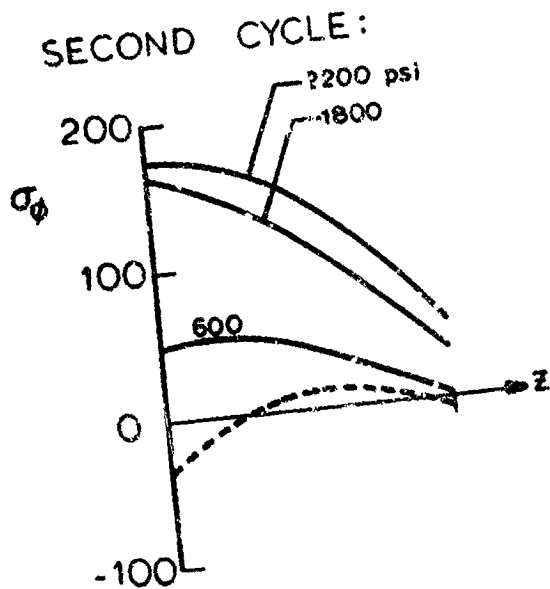
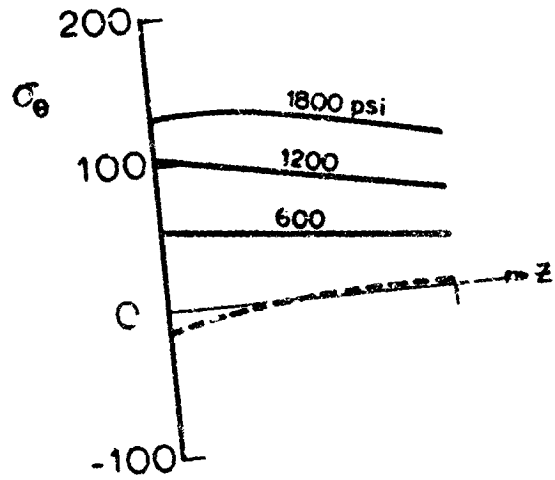
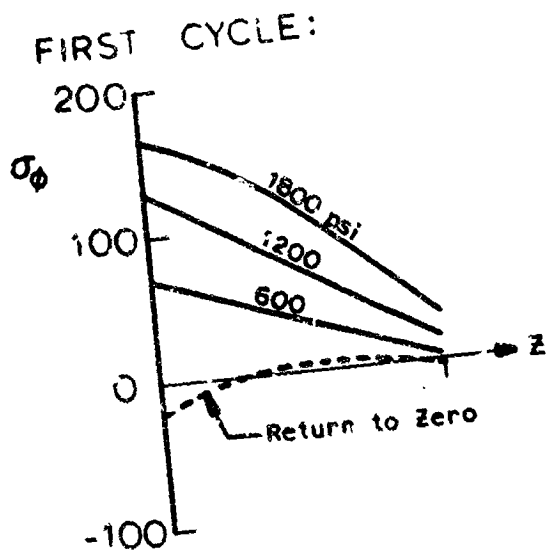


Fig. 3-8 Repeated Loading on Sphere with Weld Sinkage:
Stress Variation through Thickness

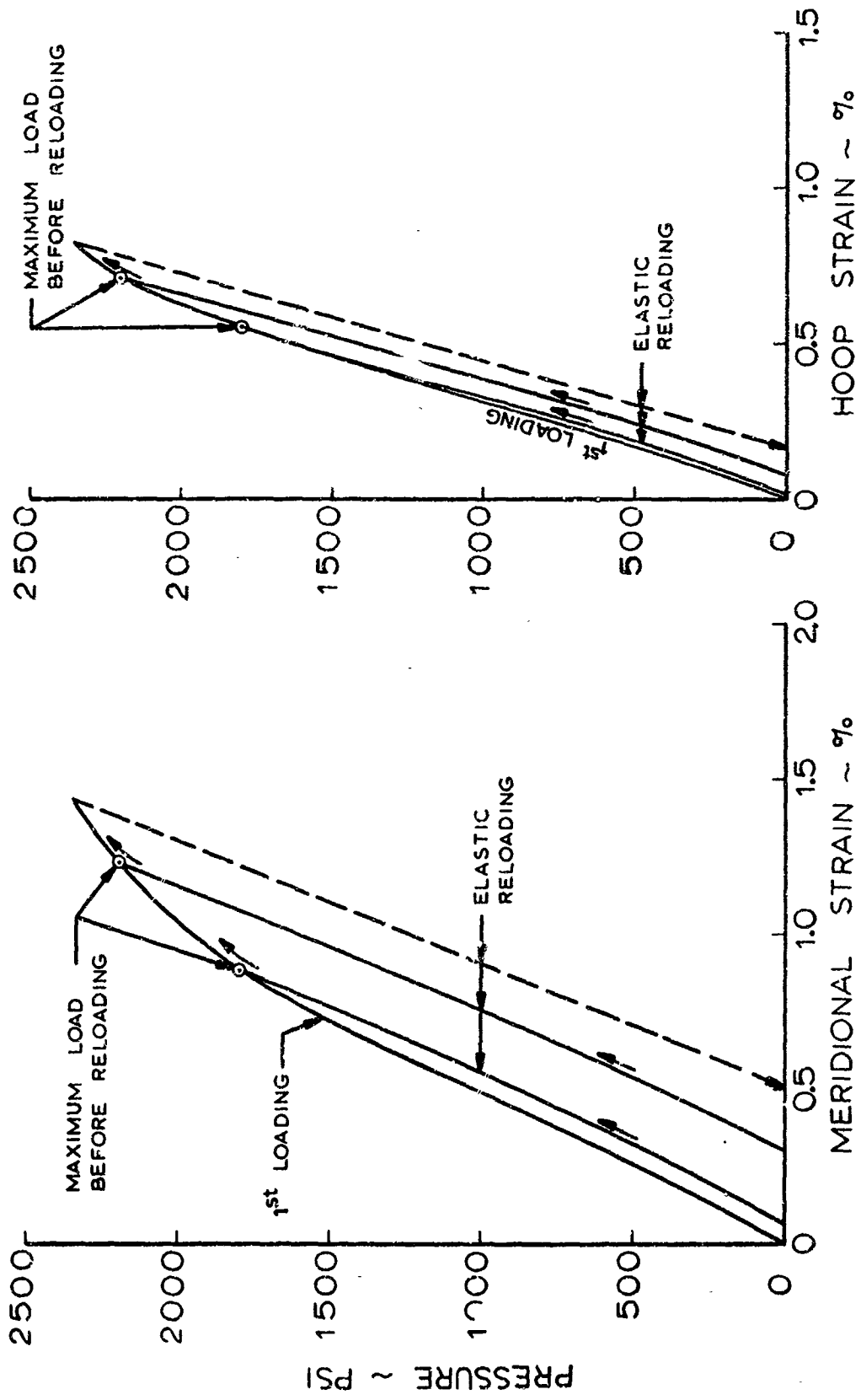


Fig. 3-9 Repeated Loadings on Sphere with Weld Sinkage

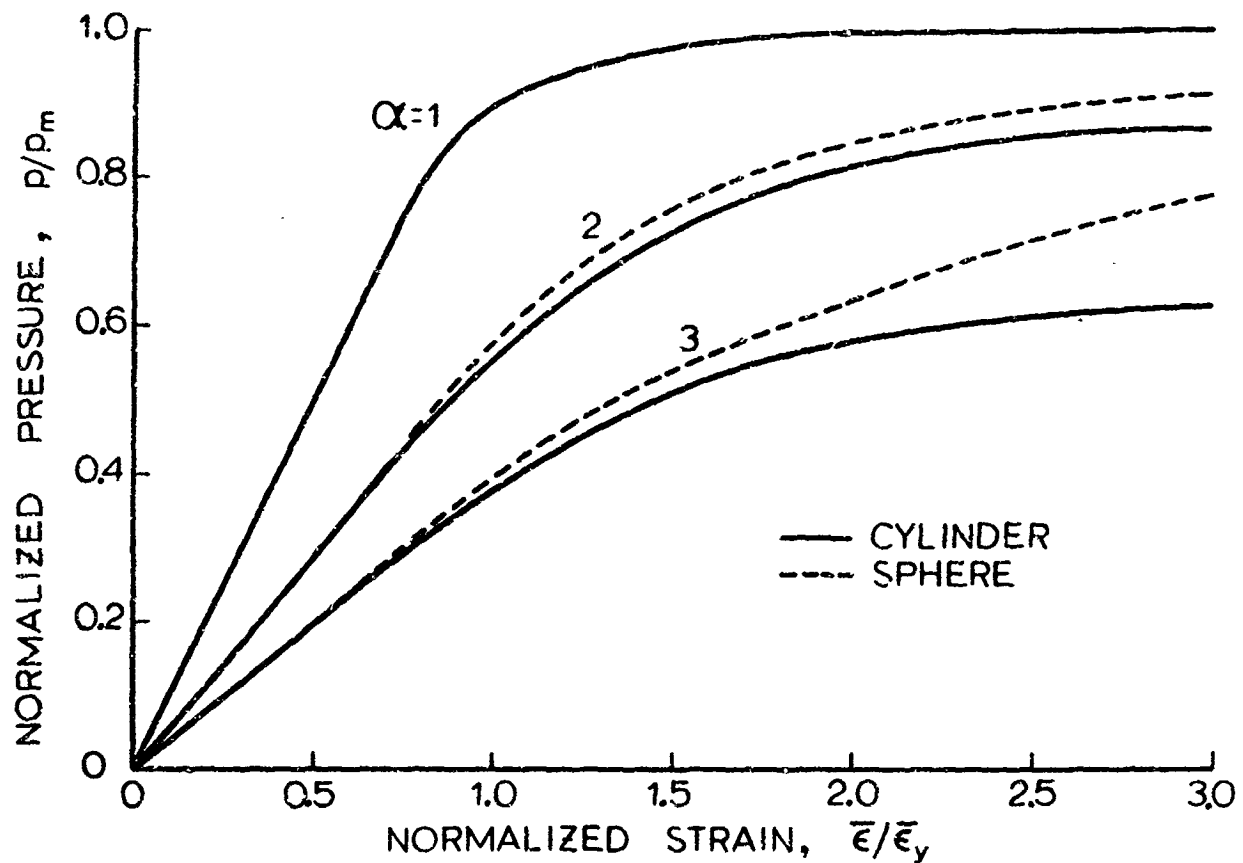


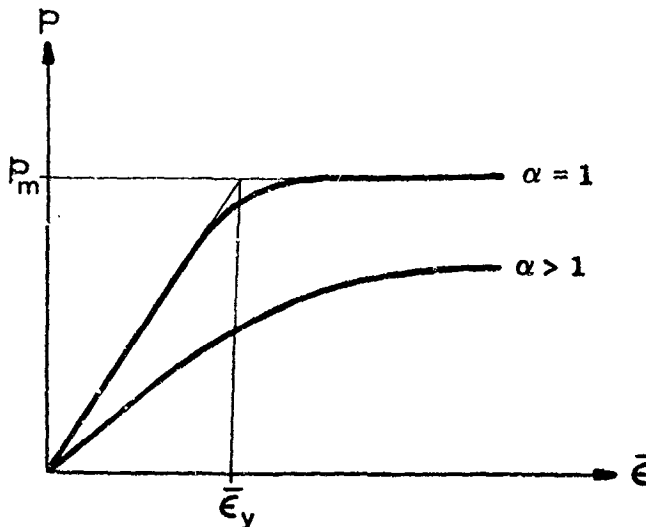
Fig. 3-10 Comparison of Cylinders and Spheres with Weld Sinkage

3.4 Design Graphs for Cylinders and Spheres

The design graphs shown in Section 5 were derived from a series of EPSOR computer runs made for the weld sinkage configuration shown in Fig. 3-1 with material properties as in Fig. 3-2. The development of these graphs is based on the observation that for both the spheres and the cylinders the shape of the stress distribution curve in the vicinity of the discontinuity is roughly triangular, both in the elastic and the plastic regions (see Fig. 3-3a). Thus, there appears to be a high degree of similarity (and continuity) in both the elastic and the plastic regions.

The height of the triangular spike in the stress distribution is proportional to $\bar{\alpha} - 1$, and the width at the base is somewhat dependent on the characteristic shell length, $3\sqrt{Rt}$. Thus, it would be expected that the main parameter of the problem is $\bar{\alpha}$, and that $3\sqrt{Rt}$ might be a secondary parameter. Accordingly, the parametric computer runs were made for a series of $\bar{\alpha}$ values by varying the radius R_T . The radius-to-thickness ratio used in generating the design graphs was 100. Spot checks on other thickness ratios were made; no deviations from the design graphs was found for R/t values as low as 10. No analysis for R/t values larger than 150 was made, but it seems unlikely that for moderately thin shells, say up to $R/t = 500$, any significant deviations should occur.

The quantities used to normalize the design graphs are the ultimate pressure for a pressure vessel without a discontinuity, p_m , and the corresponding strain, $\bar{\epsilon}_y$, as illustrated in the sketch below



The normalizing parameters are calculated as follows:

$$P_m = 2 \frac{t}{R} F_{tu} \quad (\text{Sphere}) \quad (3.6)$$

$$P_m = \frac{2}{\sqrt{3}} \frac{t}{R} F_{tu} \quad (\text{Cylinder}) \quad (3.7)$$

$$\bar{\epsilon}_y = \frac{2}{3} (1 + \nu) \frac{F_{tu}}{E} \quad (\text{General}) \quad (3.8)$$

The design graphs are derived for the following values pertaining to the titanium 6Al-4V STA stress-strain curve (see also Fig. 3-2, curve marked NASA):

$$F_{ty} = 120000 \text{ psi}$$

$$F_{tu} = 160000 \text{ psi}$$

$$E = 17 \times 10^6 \text{ psi}$$

However, through the use of the normalizing parameters other materials with stress-strain curves resembling the one used may be used, at least for an approximate analysis.

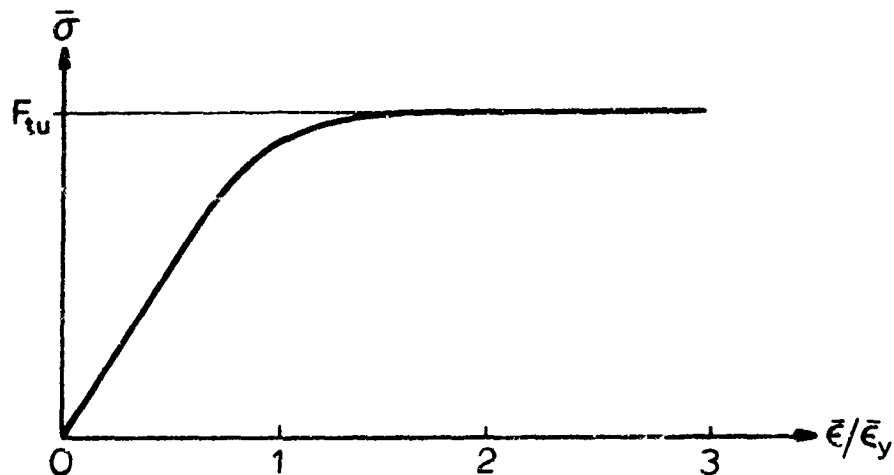
Section 4

FAILURE CRITERIA

A proper development of failure criteria for shells with discontinuities requires a testing program where a number of pressure vessels would be taken to failure. This is particularly true for repeated loadings. Such a testing program is beyond the scope of the present work, but, nevertheless, an attempt at recommending suitable criteria, based on the analytical and experimental results presented here, will be made.

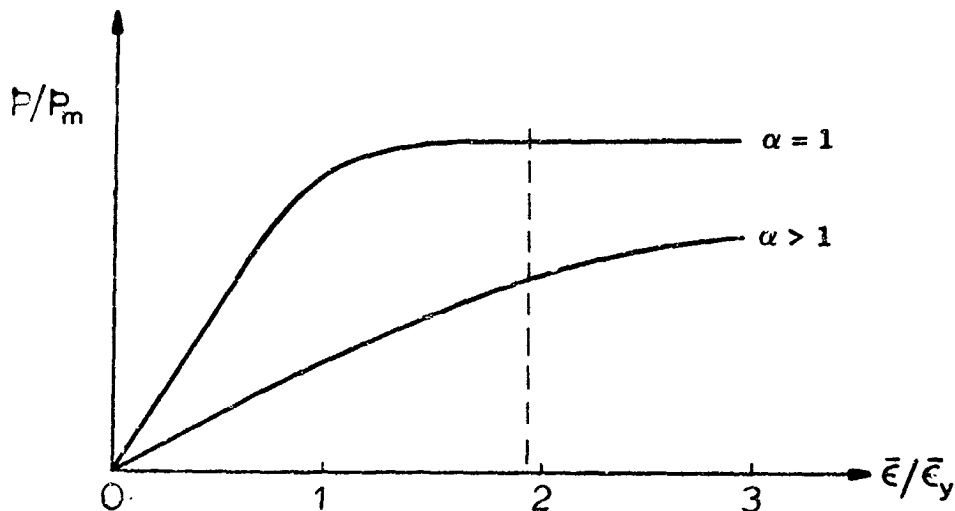
4.1 Static Failure

Consider the stress-strain curve of the material used here, titanium 6Al-4V. Whether in the annealed or the heat treated (STA) condition, this material has a practically horizontal progression after the relatively low strain $\bar{\epsilon}/\bar{\epsilon}_y \approx 2$ has been reached:



At this point the material is rather unstable and a very slight increase in pressure will cause a large increase in strain and the shell will collapse.

Consider now the pressure versus strain curves for the weld sinkage problem:



The curve marked $\alpha = 1$ pertains to a shell without discontinuity, while the curve marked $\alpha > 1$ is for a shell with discontinuity. The main difference between the two curves (from the point of view of the current discussion) is that in the $\alpha = 1$ case no additional pressure can be sustained after a strain of $\bar{\epsilon}/\bar{\epsilon}_y \approx 2$ has developed, while in the $\alpha > 1$ case the pressure can increase beyond this particular strain level. However, the material cannot withstand more than a particular measure of strain. From coupon tests (see Section 6) on titanium 6Al-4V the uniaxial ultimate strain is of the order 3 to 4 percent.

Using Eq. (3.3) and (3.8) the normalized strain may be expressed as

$$\frac{\bar{\epsilon}}{\bar{\epsilon}_y} = \epsilon_1 \frac{E}{F_{tu}} \quad (4.1)$$

where ϵ_1 is the uniaxial (coupon) strain. Taking the ultimate value of ϵ_1 equal to 0.03*, $E = 16 \times 10^6$ psi*, and $F_{tu} = 185,000$ psi*, the ultimate value of the normalized strain is, for this material

*The values are selected to give a conservative value for the ultimate strain.

$$\left(\frac{\sigma}{\sigma_y} \right)_{ult} = 2.6$$

Thus, this value may be used as an approximate failure criterion for a shell with a weld sinkage. Using this value, and taking points from the design graphs in Section 5, this criterion can be illustrated as in Fig. 4-1. In the figure the closed form solution for the cylinder, as described in Appendix D, is also shown.

4.2 Repeated Loading

The repeated loading to be considered here consists of an internal pressure which cycles between zero and some maximum pressure. For loadings in the elastic region the stress will then fluctuate between zero and some value proportional to the maximum pressure. For loadings into the plastic region, however, residual stresses will develop so that the stresses fluctuate between negative (compressive) and positive (tensile) values. As is shown in Sections 3 and 5, the residual stresses are not large enough to cause a hysteresis loop during repeated loadings into the plastic range, so that cycling subsequent to an initial load into the plastic range ("shake down") will be entirely elastic, at least for the geometries and materials considered here. (It seems, however, possible to develop sufficiently large residual stresses for repetitive plastic strains if the material is sufficiently ductile.) Thus, the cyclic loading for the weld sinkage problem is characterized by a relatively large plastic prestrain followed by cyclic elastic straining with a mean stress which is not zero.

In the book "Thermal Stress and Low Cycle Fatigue", [13], Manson discusses in detail the behavior of materials in stress and strain cycling. Manson relates the number of cycles to failure N_f to plastic strain per cycle ϵ_p by the simple equation

$$\epsilon_p^a N_f = C_p \tag{4.2}$$

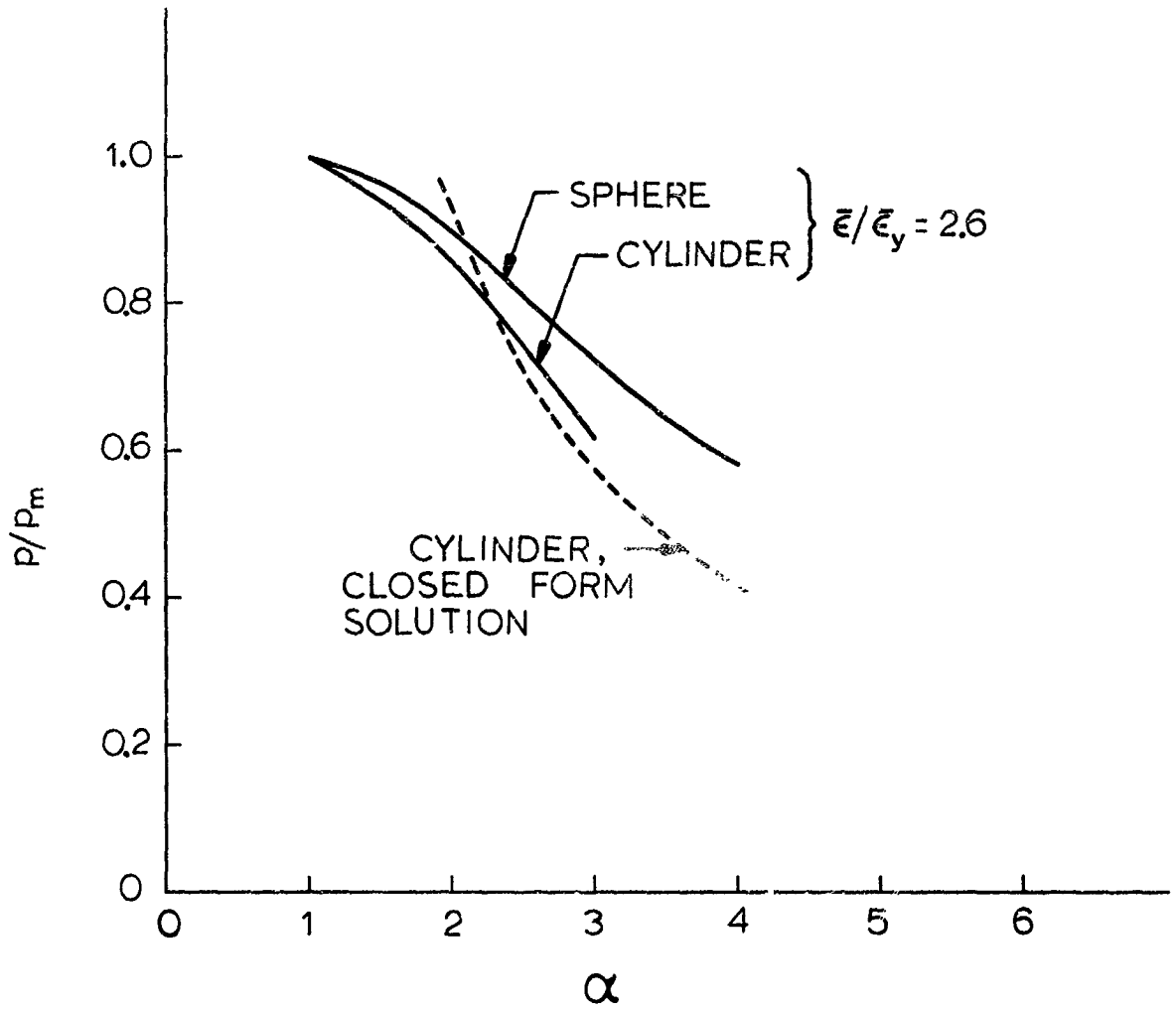


Fig. 4-1 Static Failure Criteria for Pressure Vessels with Weld Sinkage

where a and C_p are constants. A similar equation governs the elastic strain-to-life dependency:

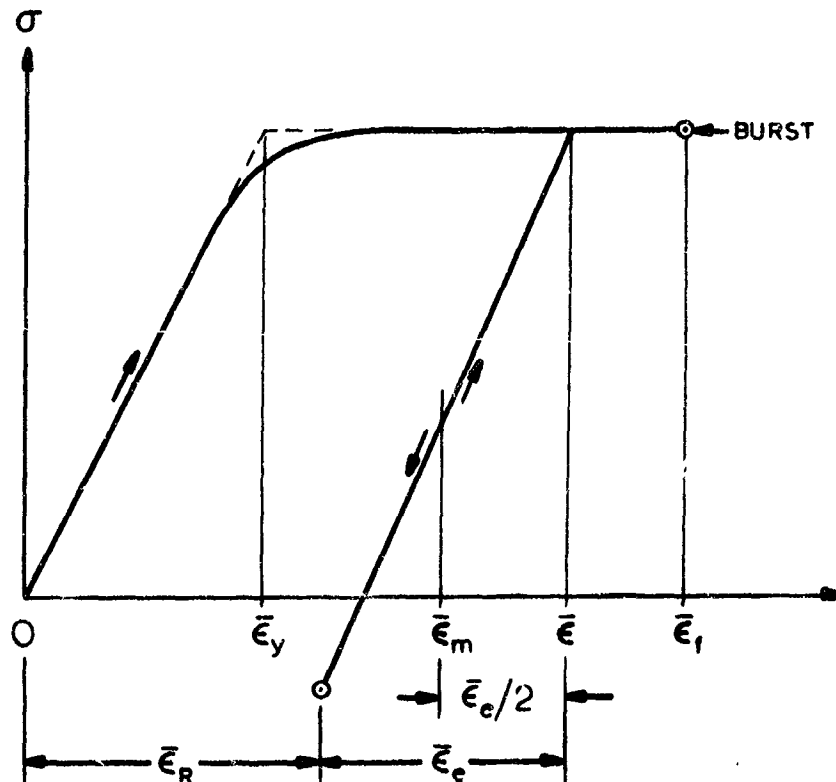
$$\bar{\epsilon}_e^b N_f = C_e \quad (4.3)$$

where b and C_e are constants. Both equations refer to completely reversed, uniaxial loadings.

Employing Equations (4.2) and (4.3) Mattavi, [14], suggests the following form of the strain versus life equation for biaxial strain distributions

$$\bar{\epsilon}_e^b N_f = (2\bar{\epsilon}_f - 2\bar{\epsilon}_m)^a / 4 \quad (4.4)$$

where the strains are "effective" strains as defined in Eq. (3.3). $\bar{\epsilon}_f$ is the fracture strain and $\bar{\epsilon}_m$ is the mean strain as indicated in the sketch below



Tests performed by Mattavi on strain cycling involving an initial strain into the plastic zone followed by elastic cycling, as shown in the figure above, indicate that the exponential relationship expressed by Eq. (4.4) does, indeed, represent actual behavior. The constants a and b are similar to Manson's values for the complete stress reversal cycling:

	a	b
Manson	2	8
Mattavi	3.2	9.2

Manson's values are recommended for a general material (including titanium); Mattavi's values are for SAE 4340 steel. Manson's curves for stress reversal cycling show very similar behavior for titanium and SAE 4340 steel (Figures 4.16, 4.20, 4.21 of Ref. 13).

On the basis of the foregoing it is suggested that Eq. (4.4) be used for an approximate evaluation of cyclic loading on shells with weld sinkage in the following form

$$\bar{\epsilon}_e^9 N_f = (\bar{\epsilon}_f - \epsilon_m)^3 K_f \quad (4.5)$$

where K_f is a material constant. Making use of the following relations

$$\bar{\epsilon}_m = \bar{\epsilon} - \frac{\bar{\epsilon}_e}{\bar{\epsilon}_R}$$

$$\bar{\epsilon}_e = \bar{\epsilon} - \bar{\epsilon}_R$$

this equation may be written

$$N_f = \frac{\left[\frac{\bar{\epsilon}_f}{\bar{\epsilon}_y} - \frac{1}{\bar{\epsilon}_R} \left(\frac{\bar{\epsilon}}{\bar{\epsilon}_y} + \frac{\bar{\epsilon}_R}{\bar{\epsilon}_y} \right) \right]^3}{\left(\frac{\bar{\epsilon}_e}{\bar{\epsilon}_y} \right)^9} (\bar{\epsilon}_y^{-6} K_f) \quad (4.6)$$

where the constant $(\bar{\epsilon}_y^{-6} K_f)$ is found from the condition that $N_f = 1$ when $\bar{\epsilon} = \bar{\epsilon}_f$:

$$\left(\bar{\epsilon}^{-6} K_f\right) = 8 \left(\frac{\bar{\epsilon}_f}{\bar{\epsilon}_y} - \frac{\bar{\epsilon}_R}{\bar{\epsilon}_y}\right)^6 \quad (4.7)$$

$\bar{\epsilon} = \bar{\epsilon}_f$

Using the stress-strain curve of titanium 6Al-4V STA (see Fig. 5-31), Eq. (4.6) was evaluated, resulting in the curve labeled "Best Estimate" in Fig. 4-2. The curve marked "Probable Lower Limit" was evaluated in a similar way, but using the Manson values of the coefficients a and b. Obviously, the life sensitivity to these values is rather high, so Fig. 4-2 should be used with caution, as long as no reliable test data exist.

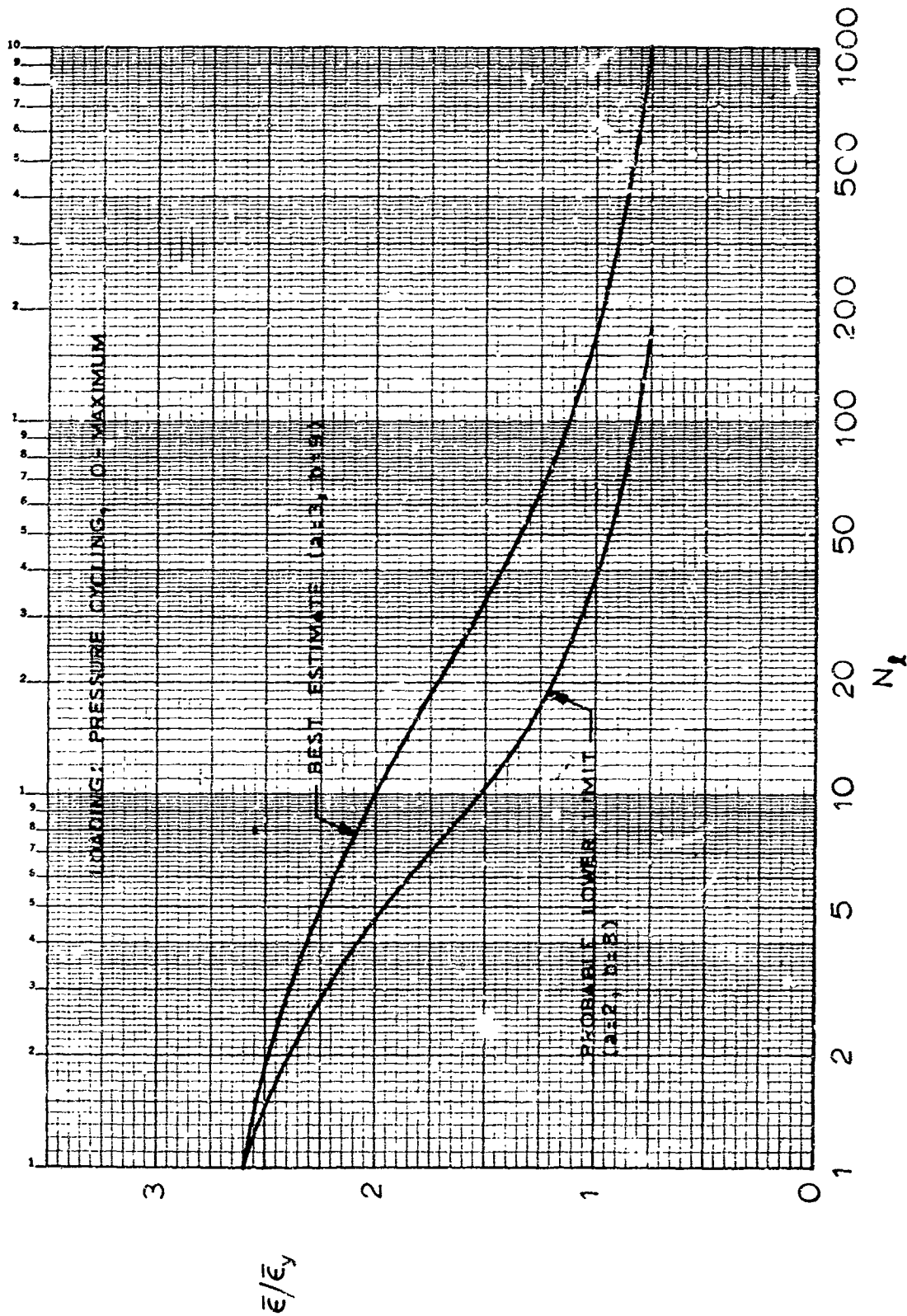


Fig. 4-2 Failure Criteria for Repeated Loadings

Section 5

APPLICATION

This section has been prepared for the practicing engineer. It contains solutions in graphical form for the following types of geometric discontinuities:

- o Elastic Stresses
 - o Mismatch and/or Thickness Change
(Example Problems: pages 5-7 and 5-11)
 - o Weld Sinkage
(Example Problem: page 5-35)
- o Plastic Stresses in Weld Sinkage
(Example Problem: page 5-41)

The information given is sufficient for accurate solution of these problems in cylinders and spheres, and may be used for other forms of shells to provide approximate results, as indicated.

5.1 Design Graphs: Elastic Stresses

5.1.1 Mismatch and Abrupt Thickness Change

Most pressure vessels are fabricated from segments of shells and then joined to form the complete structure.

The segments are sometimes of different thickness, and mismatch is often introduced during the joining process. A typical example is shown in Fig.5-1.

This section provides information to calculate stresses arising from these geometric discontinuities when the vessel is subjected to uniform internal pressure.

The method is based on the nonlinear elastic theory which incorporates pressure coupling effects (see Section 2). Stresses include membrane and bending effects

but exclude stress concentrations due to sharp corners. The information is applicable only to axisymmetric discontinuities involving long shells.

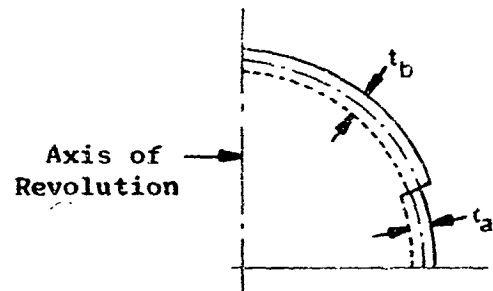


Fig.5-1 Mismatch and Thickness Change in Shells of Revolution

A shell element is considered long when there is no coupling between the discontinuity effects at A and B (see Fig.5-2).

This condition is satisfied when the meridional length L is approximately equal or greater than the characteristic length L_c of the shell. L_c is defined as the decay distance of discontinuity stresses. Linear theory predicts this distance to be approximately equal to $3\sqrt{R_2 t}$. However the results obtained by nonlinear theory [10] indicate that the characteristic lengths of shells vary with the amount of pressure. This relation is shown in Fig.5-3. The

pressure effect is a function of nonlinearity parameter which is expressed as

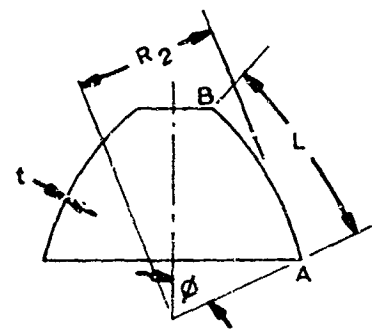


Fig.5-2 Shell of Revolution Geometry

$$\rho = \frac{P}{1.2 E \left(\frac{t}{R_2}\right)^2} \quad (\text{for } \nu = 0.3)$$

where

p = pressure (lb/in²)
 (negative pressure indicates external pressure)

E = modulus of elasticity (lb/in²)

Observe that at $\rho = 0$, $L_c = 3\sqrt{R_2 t}$ which corresponds to the linear theory solution.

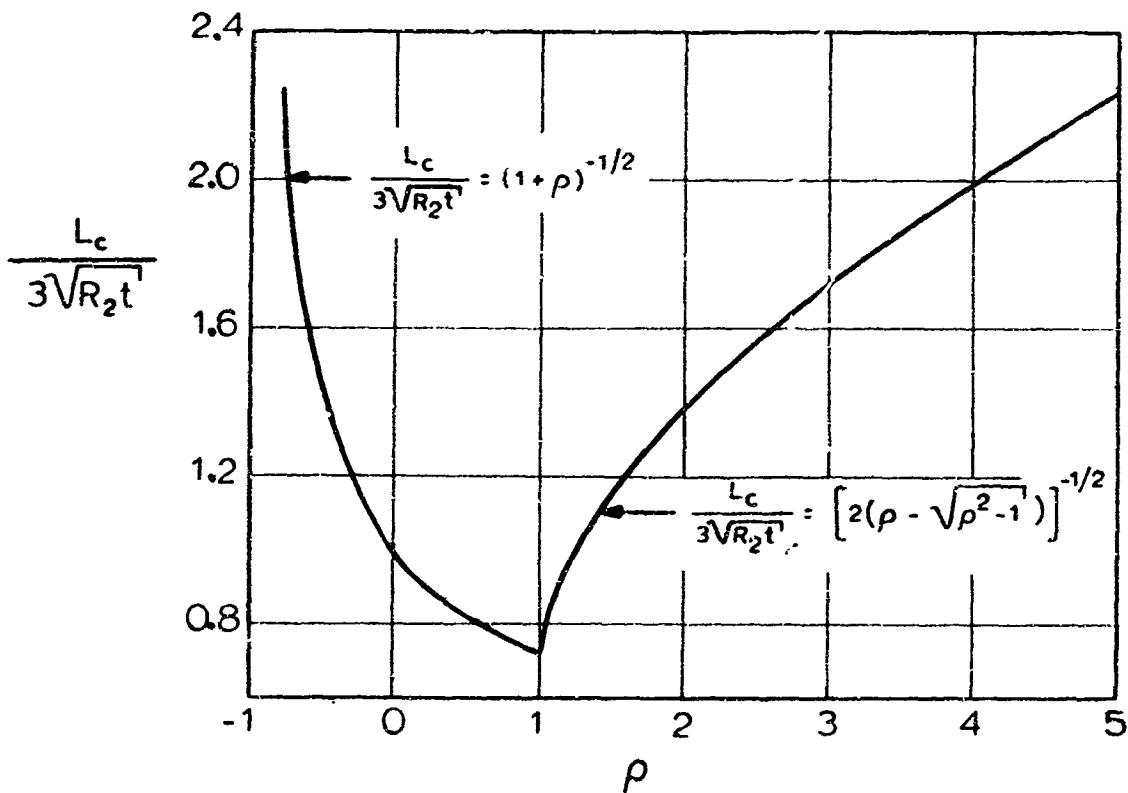


Fig.5-3 Characteristic Lengths of Shells of Revolution

The present work is based on the further assumptions that the shell segments are thin and steep. A shell is sufficiently thin when the quantity

$$1.8 \sqrt{R_2/t} \geq 10$$

and sufficiently steep when the quantity

(Ref.15)

$$1.8 \sin \phi \sqrt{R_2/t} \geq 10$$

While the information given here is based on axisymmetric discontinuities, it can also be used for discontinuities extending only partially around the circumference, provided that this length is more than about five times the characteristic length L_c . For shorter distances, the present results are usually conservative, but sometimes slight underestimation may occur (see Ref. 47, Appendix A).

5.1.1.1 Cylindrical Shell Junctions

Stresses at the juncture region of two cylindrical segments (see Fig. 5-4) can be found by the use of Figs. 5-5 through 5-21 provided that the loading is internal pressure and the geometry satisfies the requirements given in the previous section. The stresses are given in terms of stress factors which are defined as follows:

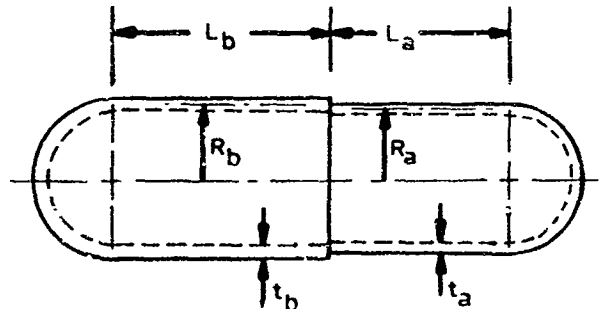


Fig. 5-4 Junction of Two Cylindrical Shells

Meridional Stress Factor

$$\alpha_{\varphi} = \frac{\sigma_{\varphi}}{\sigma_{\varphi n}} = \frac{\sigma_{\varphi}}{\frac{pR_a}{2t_a}}$$

Circumferential Stress Factor

$$\alpha_{\theta} = \frac{\sigma_{\theta}}{\sigma_{\theta n}} = \frac{\sigma_{\theta}}{\frac{pR_a}{2t_a}}$$

Effective Stress Factor

$$\bar{\alpha} = \frac{\bar{\sigma}}{\sigma_{\varphi n}} = \frac{\bar{\sigma}}{\frac{pR_a}{2t_a}}$$

where

$$\sigma_{\varphi} = \text{total meridional stress (lb/in}^2\text{)}$$

$$\sigma_{\theta} = \text{total circumferential stress (lb/in}^2\text{)}$$

$$\bar{\sigma} = \text{total effective stress (lb/in}^2\text{)}$$

The total stress is composed of membrane and discontinuity stresses. All stresses correspond to the thinner shell where the stresses are largest. The total effective stress is defined as

$$\bar{\sigma} = \sqrt{(\sigma_{\phi}^2 + \sigma_{\theta}^2 - \sigma_{\phi}\sigma_{\theta})}$$

This relationship is based on the energy of distortion theory which is used to predict the limit of elastic behavior. The theory states that yielding in a biaxial field will occur when the effective stress becomes equal to the uniaxial yield stress of the material.

Note that Figs. 5-5 through 5-21 also include stress information away from the discontinuity when stresses are not maximum at the discontinuity. For such cases, the effective stress $\bar{\sigma}$ should be obtained directly from the figures. Usage of the expression $\bar{\sigma} = \sqrt{(\sigma_{\phi}^2 + \sigma_{\theta}^2 - \sigma_{\phi}\sigma_{\theta})}$ could yield erroneous results since for a given problem the maximum value of σ_{ϕ} and σ_{θ} may occur at different locations on the cylinder.

PROCEDURE TO OBTAIN STRESS FACTORS

1. Obtain parameters required for the solution. These include the following:

- Internal pressure - p (lb/in²)
- Dimensions of shell segments in inches - R_a, R_b, t_a, t_b, L_a and L_b .
Note that subscript "a" should correspond to the thinner shell.
- Modulus of Elasticity - E (lb/in²)

(Other material properties such as F_{tu} and F_{ty} and weld properties are required for stress analysis).

2. Determine nonlinearity parameter ρ for each shell

$$\rho = \frac{p}{1.2E\left(\frac{t}{R}\right)_{a,b}^2}$$

3. Check of applicability of curves

The cylindrical shell segments must satisfy the following criteria:

Thin shell:

$$\left(1.8 \sqrt{R/t} \right)_{a,b} \geq 10$$

Steep shell:

$$\left(1.8 \sin \varphi \sqrt{R/t} \right)_{a,b} \geq 10$$

($\varphi = 90^\circ$ for cylinders)

Long shell:

$$L \geq L_c$$

L_c is obtained from Fig.5-3

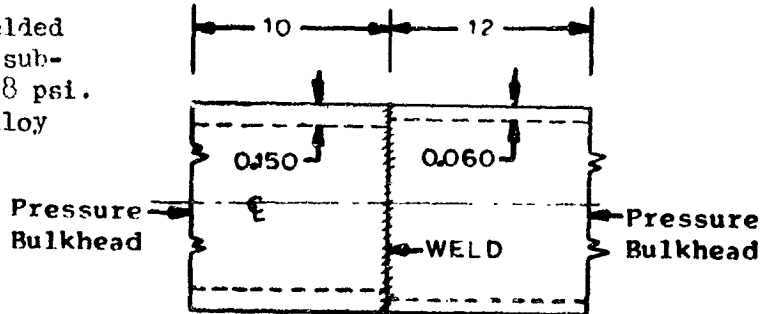
4. Determine mismatch factor m

$$m = \frac{2(R_b - R_a)}{t_a + t_b}$$

5. Determine thickness ratio t_a/t_b and select the appropriate figure. Stress factors α_φ , α_θ and $\bar{\alpha}$ are found by entering the figures with m found in step 4 and reading the value of α for the particular nonlinearity parameter ρ found in step 2.

EXAMPLE PROBLEM

Two cylindrical shell segments are welded together as shown. The structure is subjected to an internal pressure of 40.8 psi. Both segments are made of Titanium alloy Ti-6Al-4V.



Determine:

- o Stresses at the weld
- o Maximum stresses in the thinner shell.

Solution:

1. Parameters required for the solution:

p (psi)	R _a (in)	R _b (in)	t _a (in)	t _b (in)	L _a (in)	L _b (in)	E (lb/in ²)	F _{tu} (lb/in ²)	F _{ty} (lb/in ²)
40.8	59.985	59.925	0.060	0.150	12	10	17x10 ⁶	160,000	120,000

2. Determine nonlinearity parameter ρ for each shell:

$$\rho_a = \frac{40.8}{(1.2)(17.0 \times 10^6) \left(\frac{0.060}{59.985} \right)^2} = 2.0 \quad \rho_b = \frac{40.8}{(1.2)(17.0 \times 10^6) \left(\frac{0.15}{59.925} \right)^2} = 0.32$$

3. Check applicability of curves

Requirements	Segment a	Segment b
Thin & Steep Shell	1.8 (59.985/0.06) ^{1/2} = 56.9	1.8 (59.925/0.15) ^{1/2} = 36.0
Long Shell	From Fig. 5-3, L _c /3√R ₂ t = 1.38 L _c = (1.38)(3)(59.985x0.06) ^{1/2} = 7.85	From Fig. 5-3, L _c /3√R ₂ t = 0.87 L _c = (0.87)(3)(59.925x0.15) ^{1/2} = 7.85

Results indicate that curves are applicable for this case.

4. Determine mismatch factor m

$$m = \frac{(2)(59.925-59.985)}{0.060 + 0.150} = -0.571$$

5. Determine t_a/t_b , α_φ , α_θ and $\bar{\alpha}$

$$\frac{t_a}{t_b} = \frac{0.06}{0.15} = 0.4$$

	α_φ weld	α_φ max	α_θ weld	α_θ max	$\bar{\alpha}$ weld	$\bar{\alpha}$ max
Value	2.64	2.64	1.71	2.00	2.32	2.32
Fig. No.	5-12	5-12	5-13	5-13	5-14	5-14

6. Stresses at the weld

$$\sigma_\varphi = \frac{(2.64)(40.8)(59.985)}{(2)(0.06)} = 53,840 \text{ lb/in}^2$$

$$\sigma_\theta = \frac{(1.71)(40.8)(59.985)}{(2)(0.06)} = 34,880 \text{ lb/in}^2$$

$$\bar{\sigma} = \frac{(2.32)(40.8)(59.985)}{(2)(0.06)} = 47,320 \text{ lb/in}^2$$

7. Maximum stresses

$$\sigma_{\varphi\text{max}} = 53,840 \text{ lb/in}^2$$

$$\sigma_{\theta\text{max}} = \frac{(2.0)(40.8)(59.985)}{(2)(0.06)} = 40,790 \text{ lb/in}^2$$

$$\bar{\sigma} = 47,320 \text{ lb/in}^2$$

5.1.1.2 Juncture of Other Shells

The stress factor curves for cylinders (Figs. 5-5 through 5-21) may also be used for other shells of revolution to determine the stress factors α_{φ} and α_{θ} at the discontinuity. Conversion formulas are given below:

Formulas for any Shell of Revolution (at discontinuity)

$$(\alpha_{\varphi})_{SR} = (\alpha_{\varphi})_{CYL} - \left(1 - \frac{\delta_{SR}}{\delta_{CYL}}\right) (\alpha_{\varphi 0} - 1)$$

$$(\alpha_{\theta})_{SR} = 1 + (\alpha_{\theta})_{CYL} - (\alpha_{\theta 0}) \left(1 - \frac{\delta_{SR}}{\delta_{CYL}}\right) - 2 \left(\frac{\delta_{SR}}{\delta_{CYL}}\right)$$

where

δ = membrane deflection of shell in inches at the discontinuity due to internal pressure (measured normal to the shell meridian)

$$\frac{\delta_{SR}}{\delta_{CYL}} = \frac{N_{\theta m} - \nu N_{\varphi m}}{pR \left(1 - \frac{\nu}{2}\right)}$$

R = radius in inches at the discontinuity measured normal to the shell meridian (hoop radius) - see Fig. 5-2

$N_{\theta m}$ = circumferential membrane stress resultant (lb/in)

$N_{\varphi m}$ = meridional membrane stress resultant (lb/in)

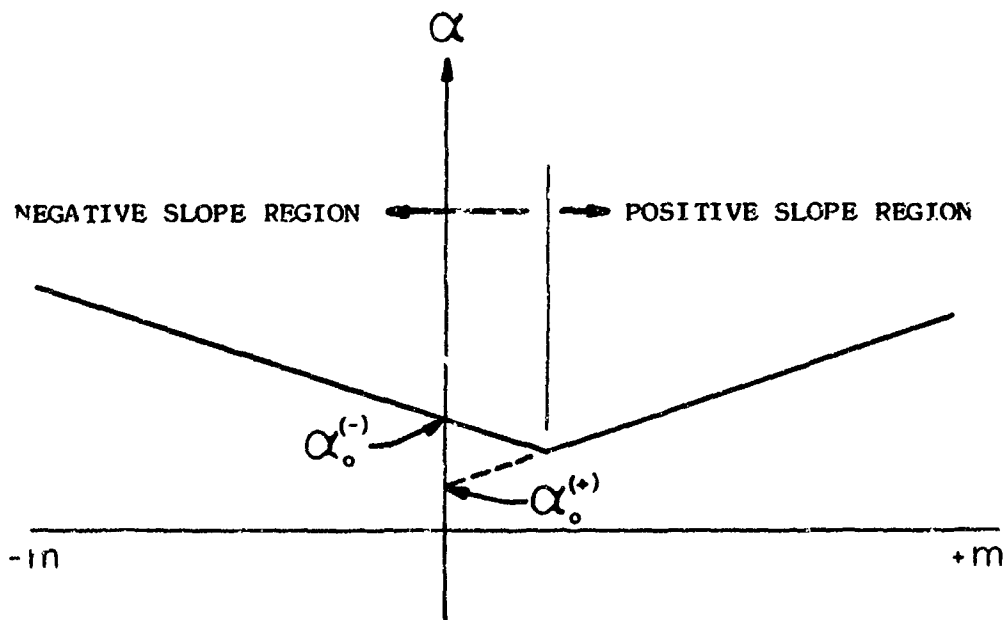
ν = Poisson's ratio

Subscripts: SR = Shell of Revolution

CYL = Cylinder

$\alpha_{\varphi 0}$, $\alpha_{\theta 0}$ = Intercepts at $m = 0$ (cylinder)

The intercepts $\alpha_{\varphi 0}$ and $\alpha_{\theta 0}$ are taken from the appropriate curves. Note that in the cases where curves have the following shape,



there are two intercepts, one for the branch of the curve with negative slope ($\alpha_0^{(-)}$), and one for the branch of the curve with positive slope ($\alpha_0^{(+)}$). For convenience both intercepts are given on the charts.

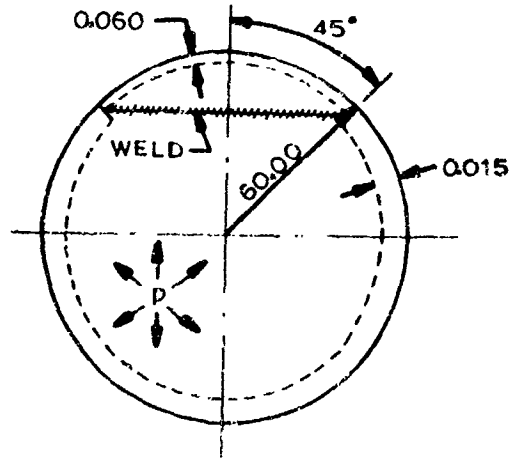
The relationship between the stress factors and stresses are given in section 5.1.1.1 .

Formulas for Spherical Shells (at discontinuity)

$(\alpha_{\varphi})_{\text{SPHERE}} = (\alpha_{\varphi})_{\text{CYL}} - 0.588 (\alpha_{\varphi} - 1)$	for $\nu = 0.3$
$(\alpha_{\theta})_{\text{SPHERE}} = (\alpha_{\theta})_{\text{CYL}} - 0.588 \alpha_{\theta} + 0.177$	

EXAMPLE PROBLEM

Two spherical shell segments are welded together as shown. The structure is subjected to an internal pressure of 81.6 psi. Both segments are made of Titanium Alloy Ti-6Al-4V.



Determine:

- o Stresses at the weld

Solution:

1. Parameters required for the solution

P (psi)	R _a (in)	R _b (in)	t _a (in)	t _b (in)	L _a (in)	L _b (in)	E lb/in ²	F _{tu} lb/in ²	F _{ty} lb/in ²
81.6	59.985	59.963	0.060	0.075	94.2	282.7	17x10 ⁶	160,000	120,000

2. Determine nonlinearity parameter ρ for each shell

$$\rho_a = \frac{81.6}{(1.2)(17.0 \times 10^6) \left(\frac{0.06}{59.985} \right)^2} = 4.0 \quad \rho_b = \frac{81.6}{(1.2)(17.0 \times 10^6) \left(\frac{0.075}{59.963} \right)^2} = 2.6$$

3. Check applicability of curves

Requirements	Segment a	Segment b
Thin Shell	$1.8(59.985/0.06)^{1/2} = 56.9$	$1.8(59.963/0.075)^{1/2} = 50.9$
Steep Shell	$(1.8)(\sin 45^\circ)(59.985/0.06)^{1/2} = 40.2$	$(1.8)(\sin 135^\circ)(59.963/0.075)^{1/2} = 35.9$
Long Shell	From Fig. 5-3, $L_c/3\sqrt{R_2 t} = 1.98$ $L_c = (1.98)(3)(59.985 \times 0.06)^{1/2} = 11.3$	From Fig. 5-3, $L_c/3\sqrt{R_2 t} = 1.6$ $L_c = (1.6)(3)(59.963 \times 0.075)^{1/2} = 10.2$

Results indicate that curves are applicable for this case.

4. Determine mismatch factor m

$$m = \frac{(2)(59.963 - 59.985)}{0.060 + 0.075} = -0.33$$

5. Determine t_a/t_b , α_φ and α_θ

$$\frac{t_a}{t_b} = \frac{0.060}{0.075} = 0.8$$

	α_φ	α_θ
Value	1.96	2.08
Fig. No.	5-18	5-19

6. Stresses at the weld

$$\sigma_\varphi = \frac{(1.96)(81.6)(59.985)}{(2)(0.06)} = 79,950 \text{ lb/in}^2 \text{ (max)}$$

$$\sigma_\theta = \frac{(2.08)(81.6)(59.985)}{(2)(0.06)} = 84,840 \text{ lb/in}^2 \text{ (max)}$$

$$\bar{\sigma} = \left[79.95^2 + 84.84^2 - 79.95 \times 84.84 \right]^{1/2} \times 10^3 = 82,500 \text{ lb/in}^2$$

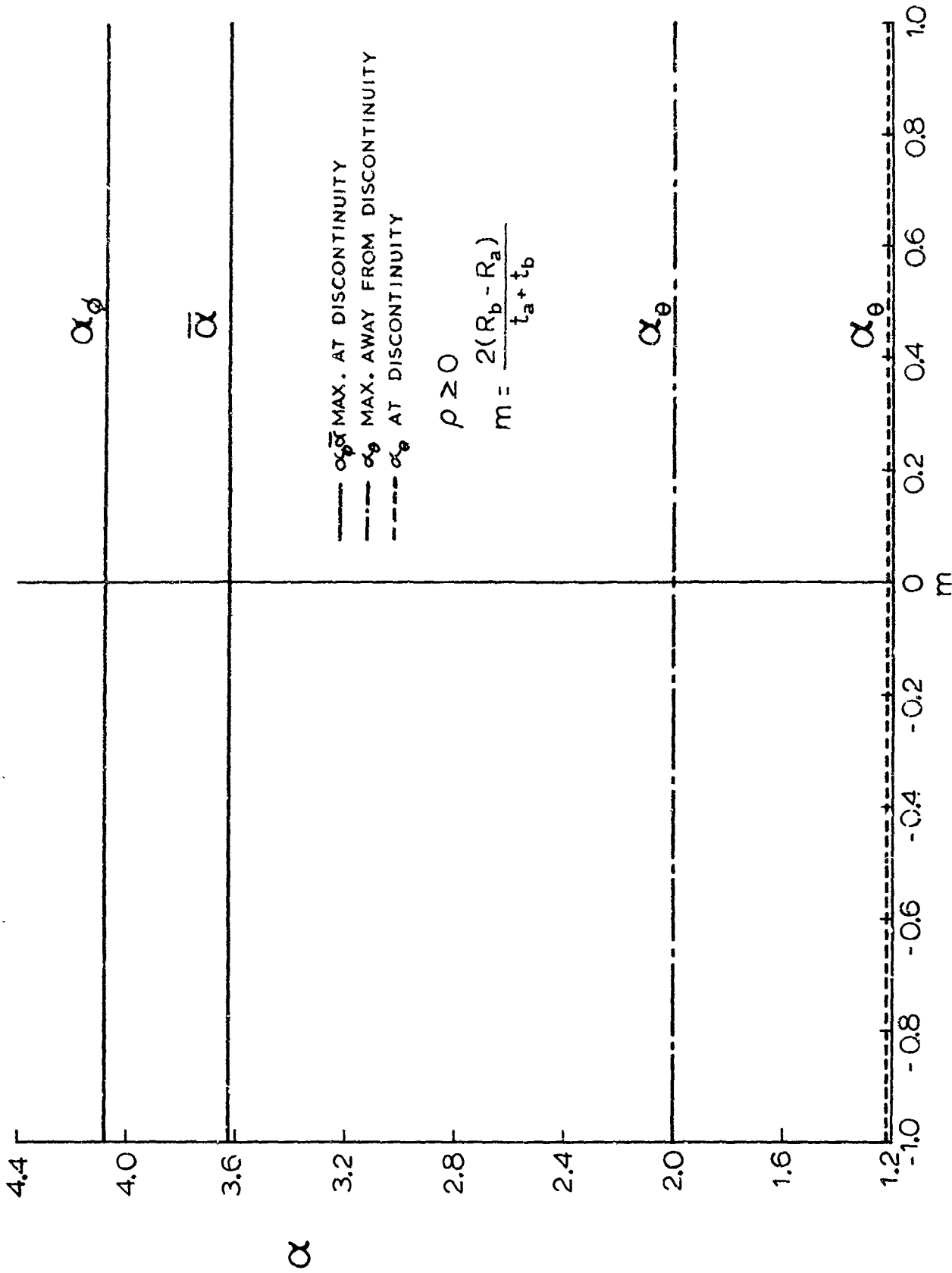


Fig. 5-5 Stress factors α , α_ϕ and $\bar{\alpha}$ at the junction region of two cylindrical shells ($t_a/t_b = 0$)

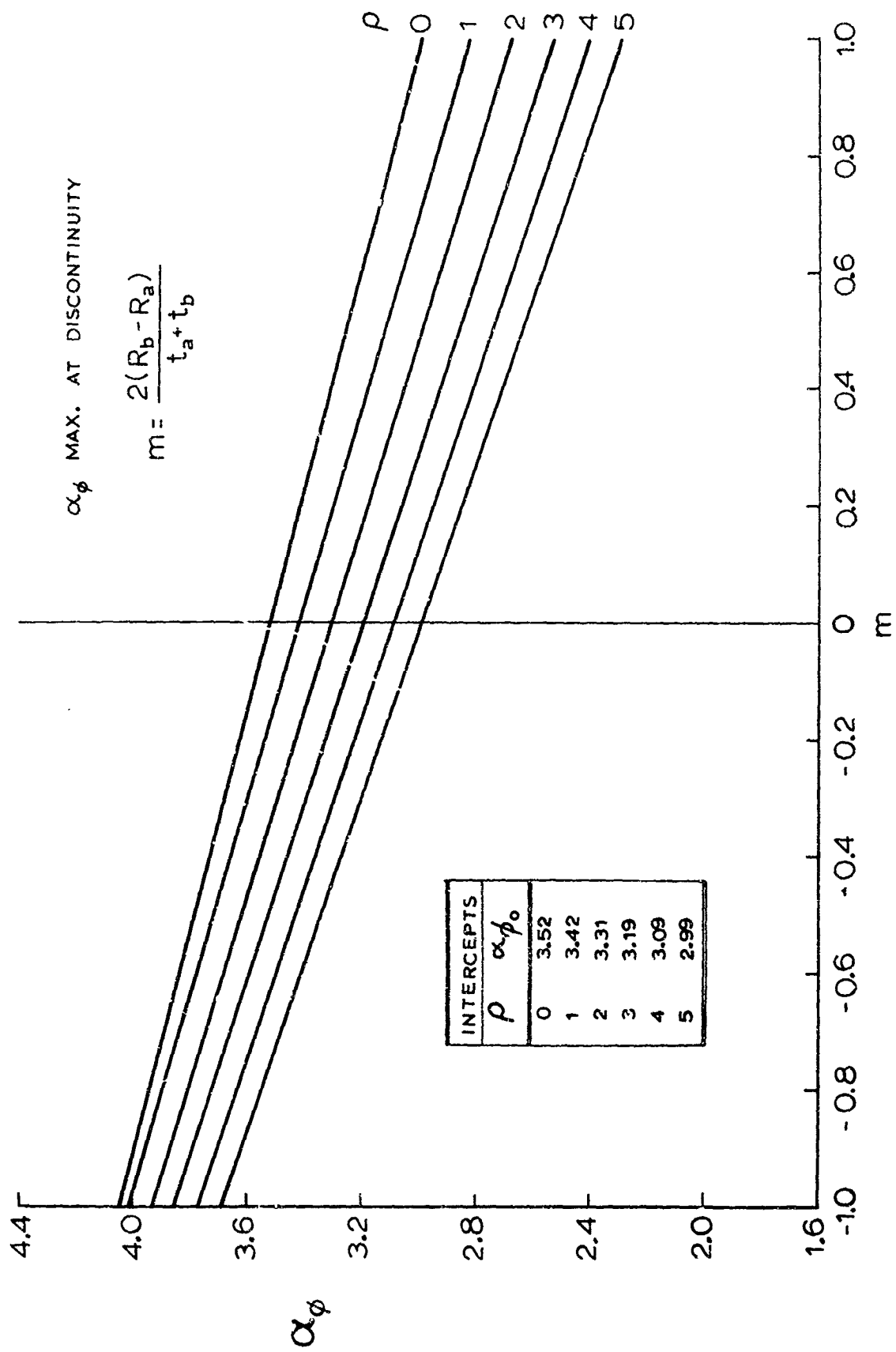


Fig. 5-6 Stress factor α_ϕ at the junction region of two cylindrical shells ($t_a/t_b = 0.1$)

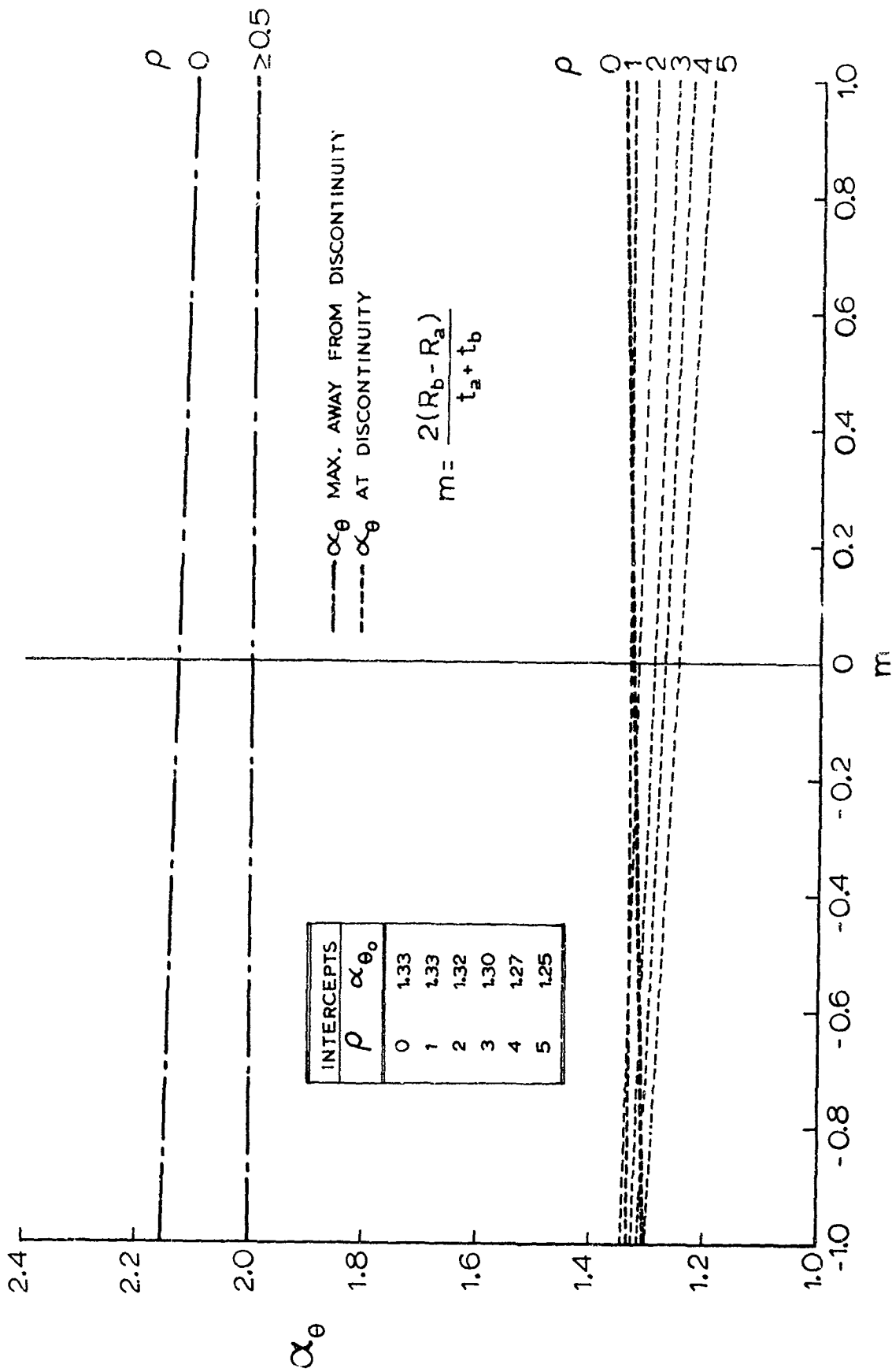


Fig. 5-7 Stress factor α_θ at the junction region of two cylindrical shells ($t_a/t_b = 0.1$)

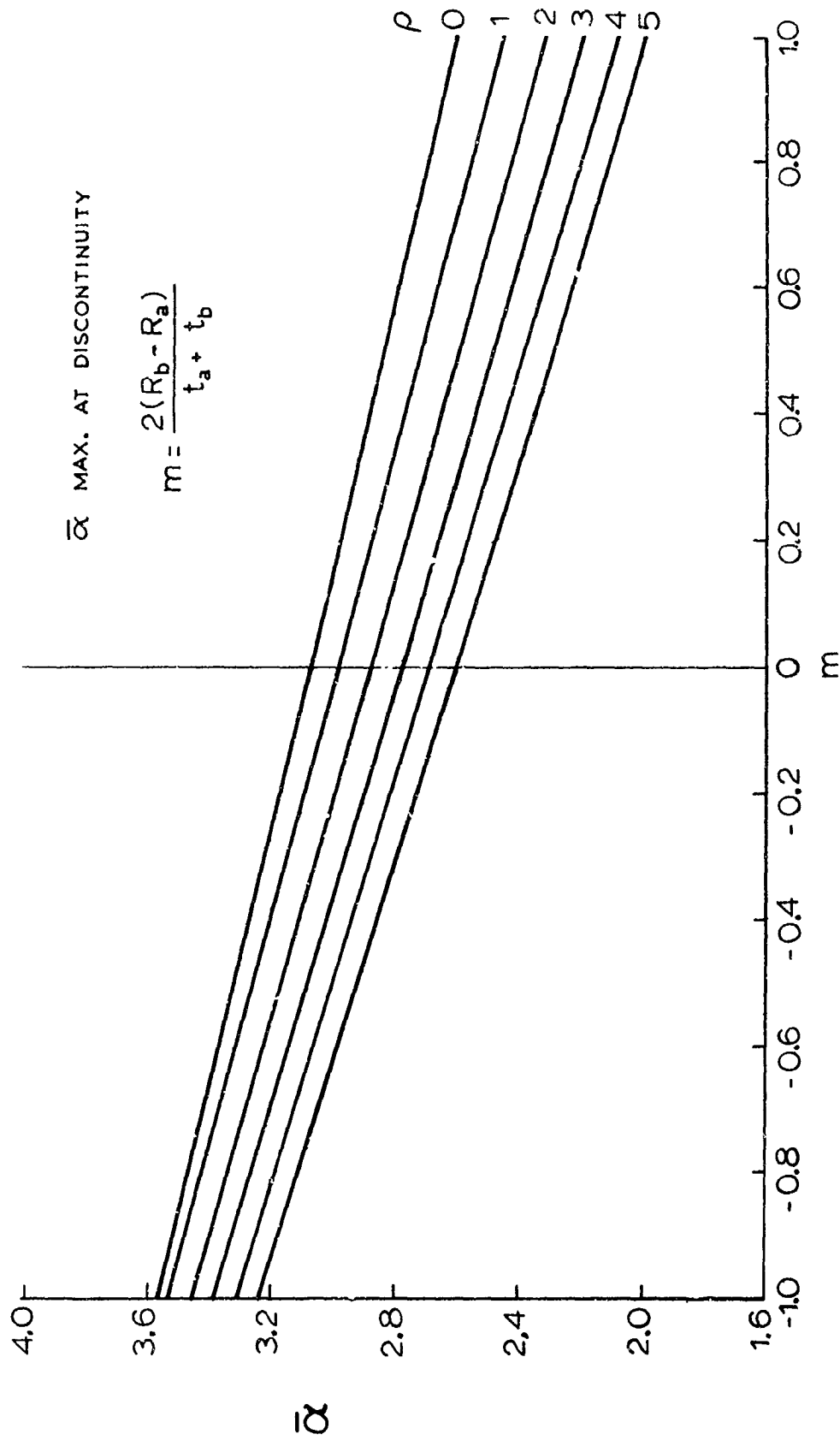


Fig. 5-8 Stress factor $\bar{\alpha}$ at the junction region of two cylindrical shells ($t_a/t_b = 0.1$)

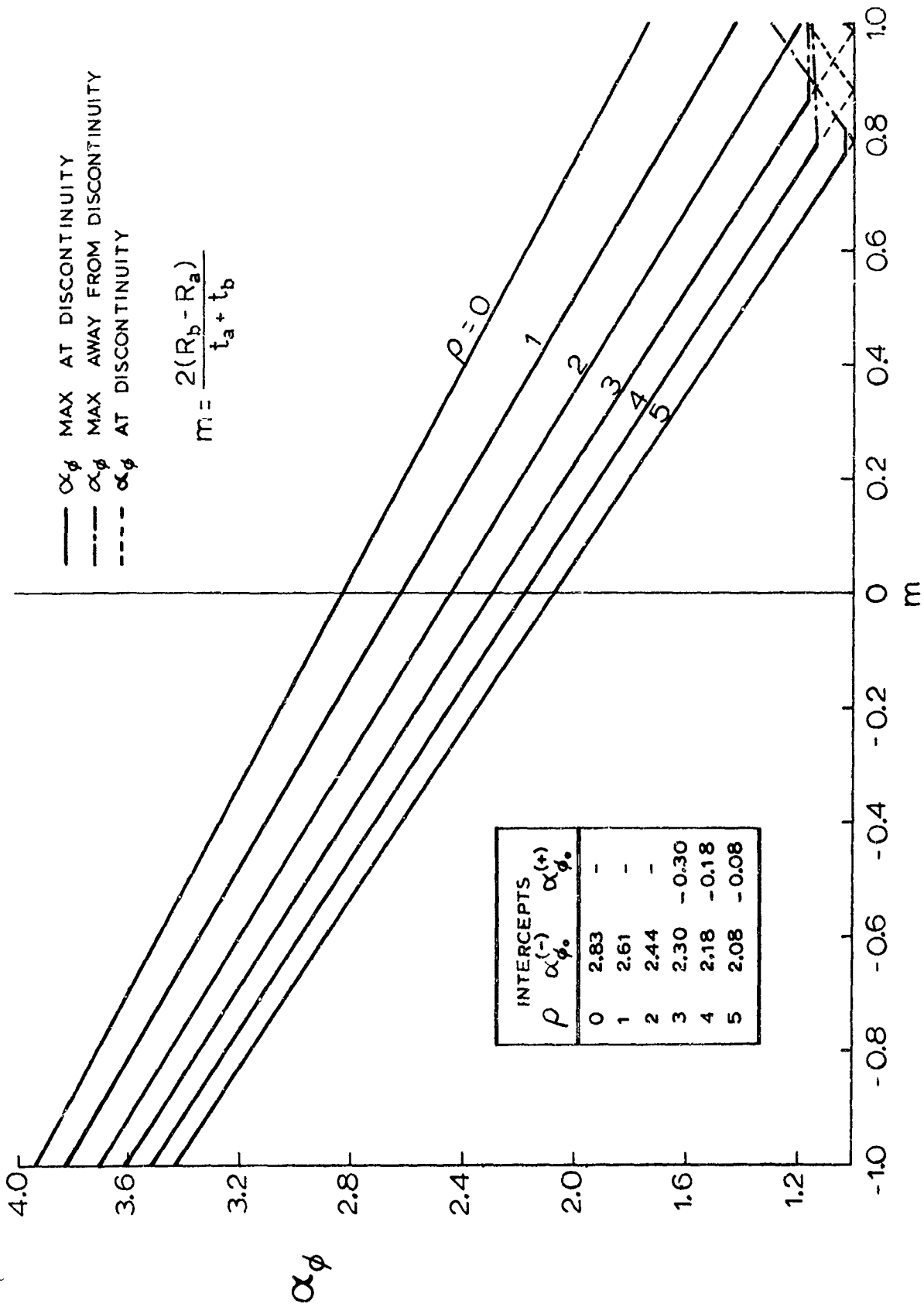


Fig. 5-9 Stress factor α_ϕ at the junction region of two cylindrical shells ($t_a/t_b = 0.2$)

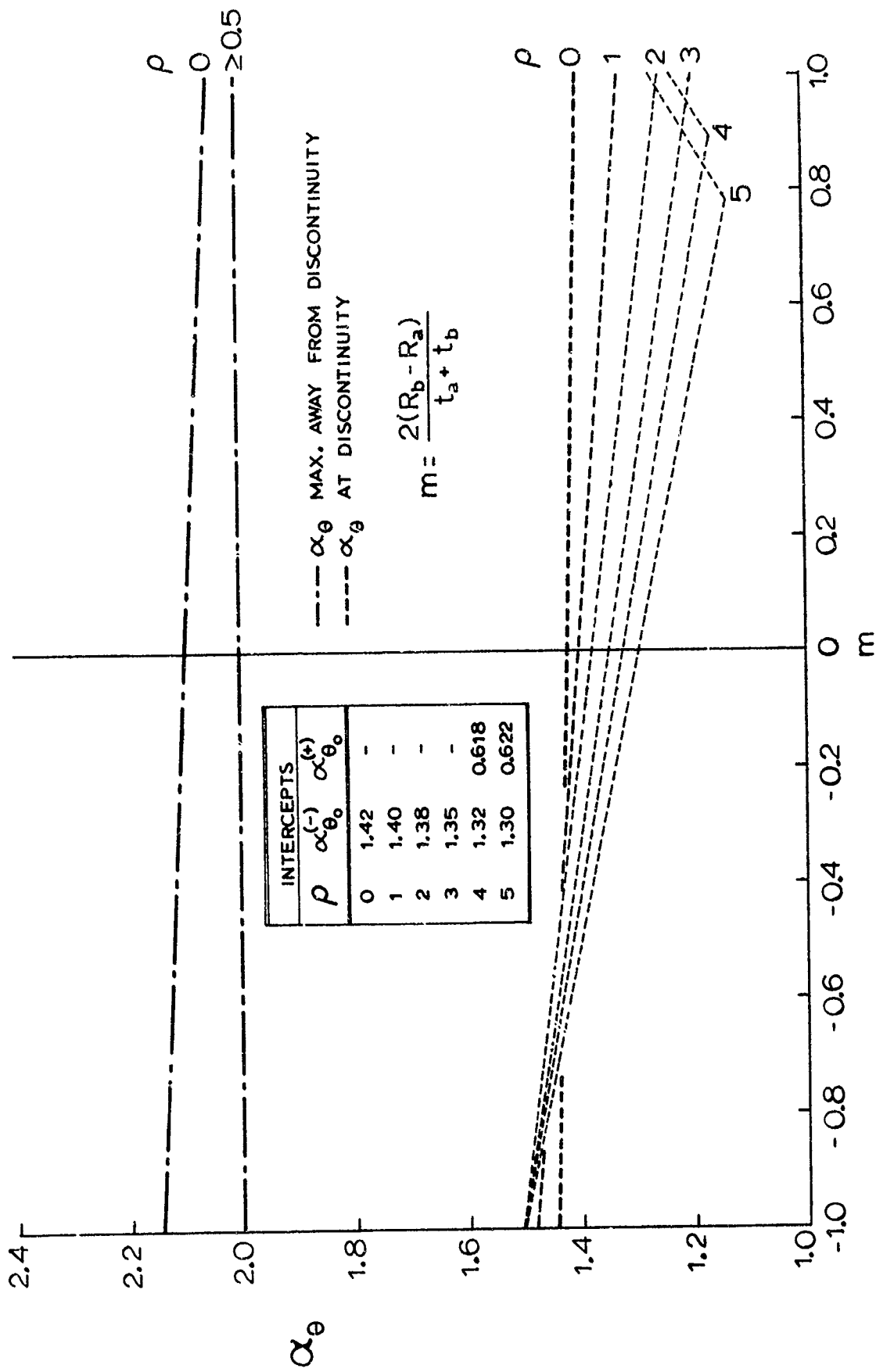


Fig. 5-10 Stress factor α_θ at the junction region of two cylindrical shells ($t_a/t_b = 0.2$)

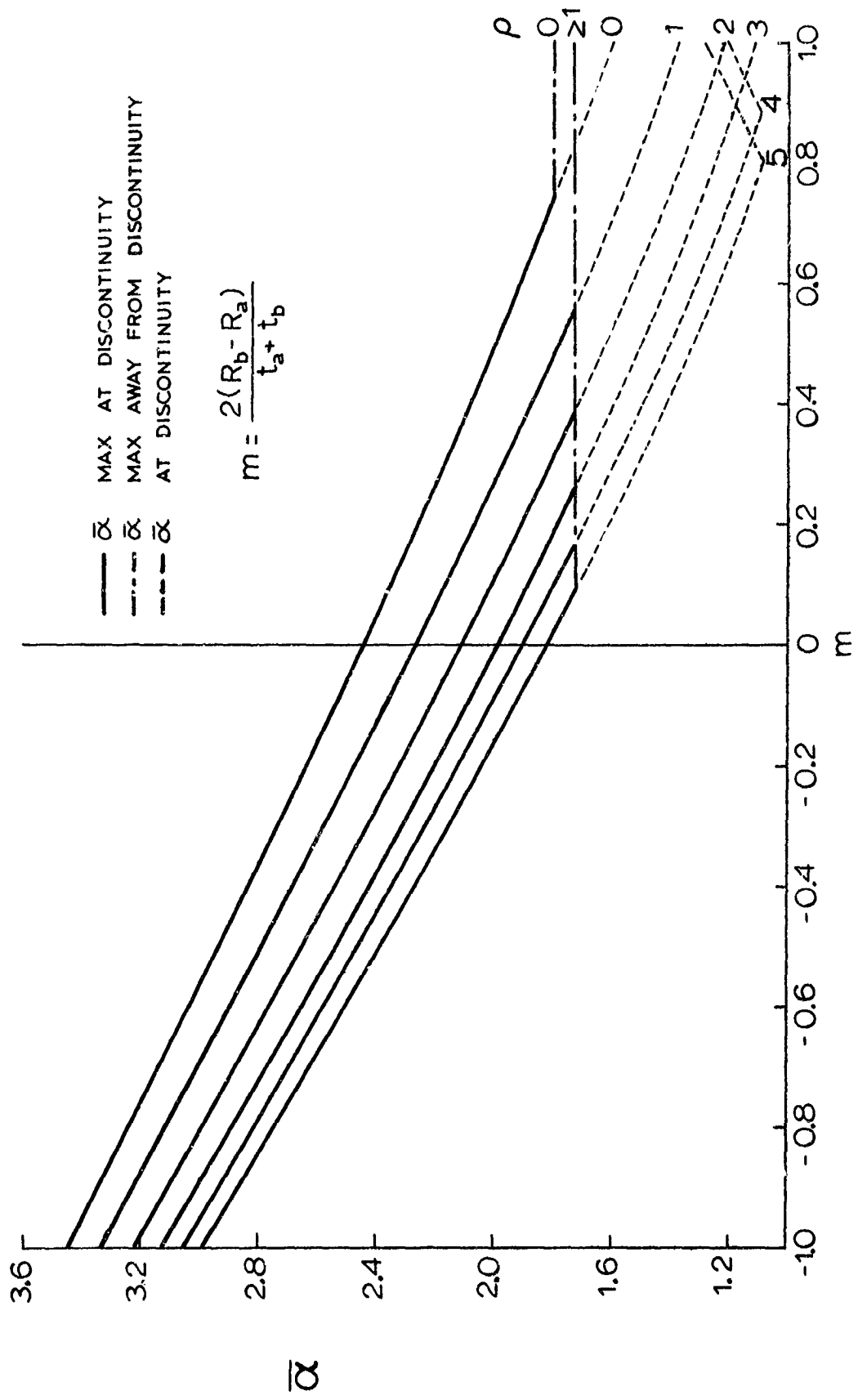


Fig. 5-11 Stress factor $\bar{\alpha}$ at the junction region of two cylindrical shells ($t_a/t_b = 0.2$)

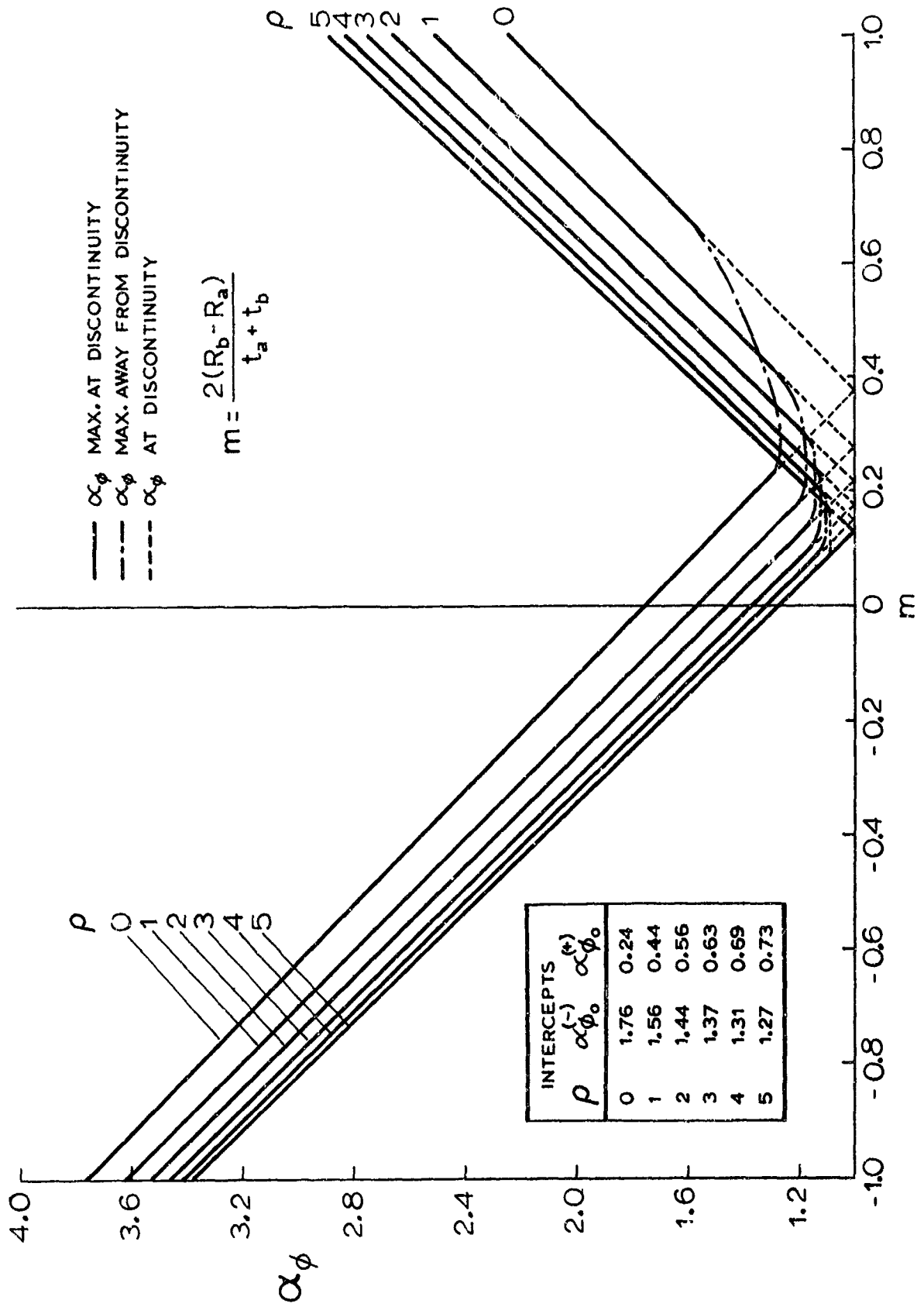


Fig. 5-12 Stress factor α_ϕ at the junction region of two cylindrical shells ($t_a/t_b = 0.4$)

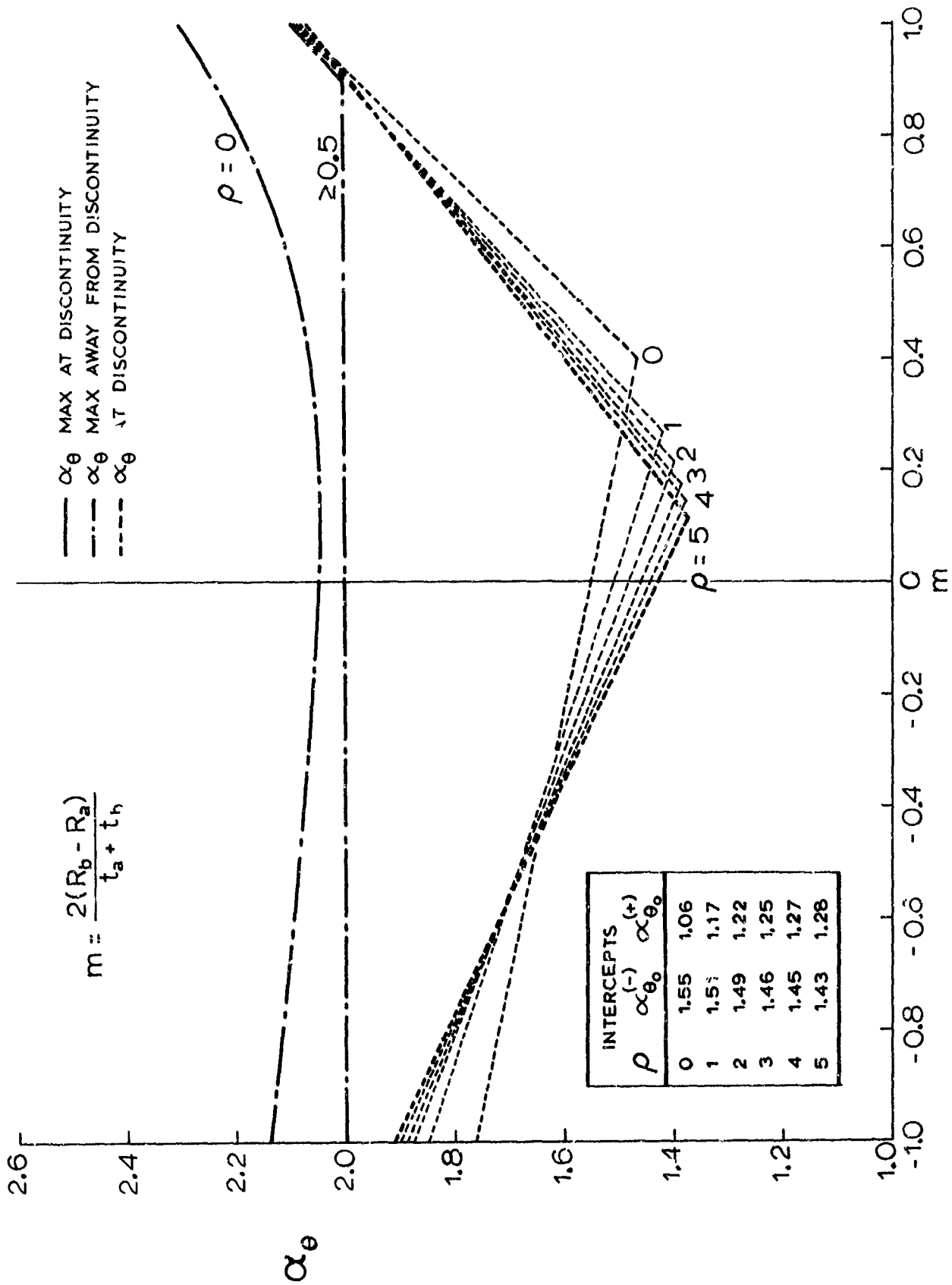


Fig. 5-13 Stress factor α_{θ} at the junction region of two cylindrical shells ($t_a/t_b = 0.4$)

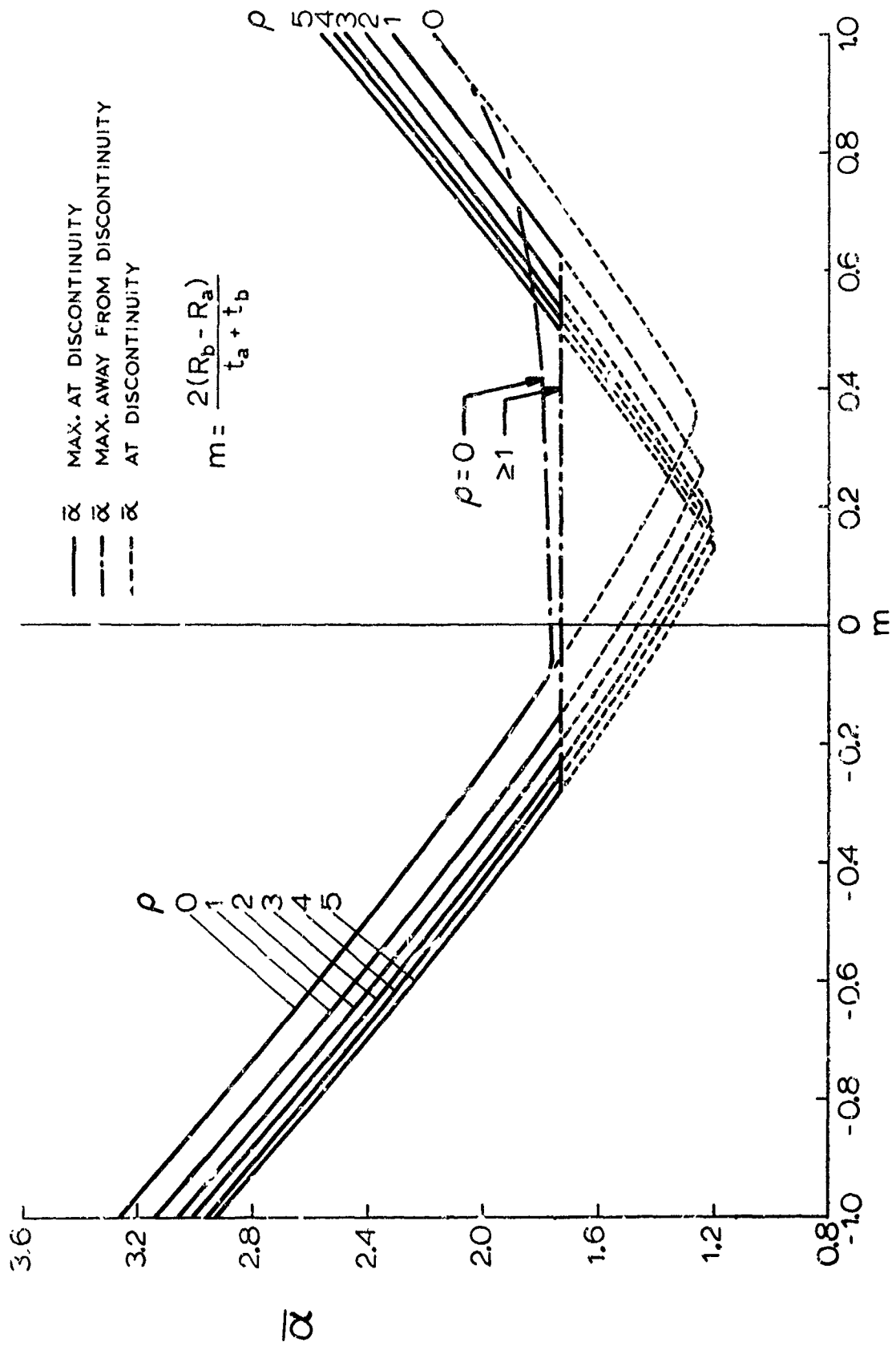


Fig. 5-14 Stress factor $\bar{\alpha}$ at the junction region of two cylindrical shells ($t_a/t_b = 0.4$)

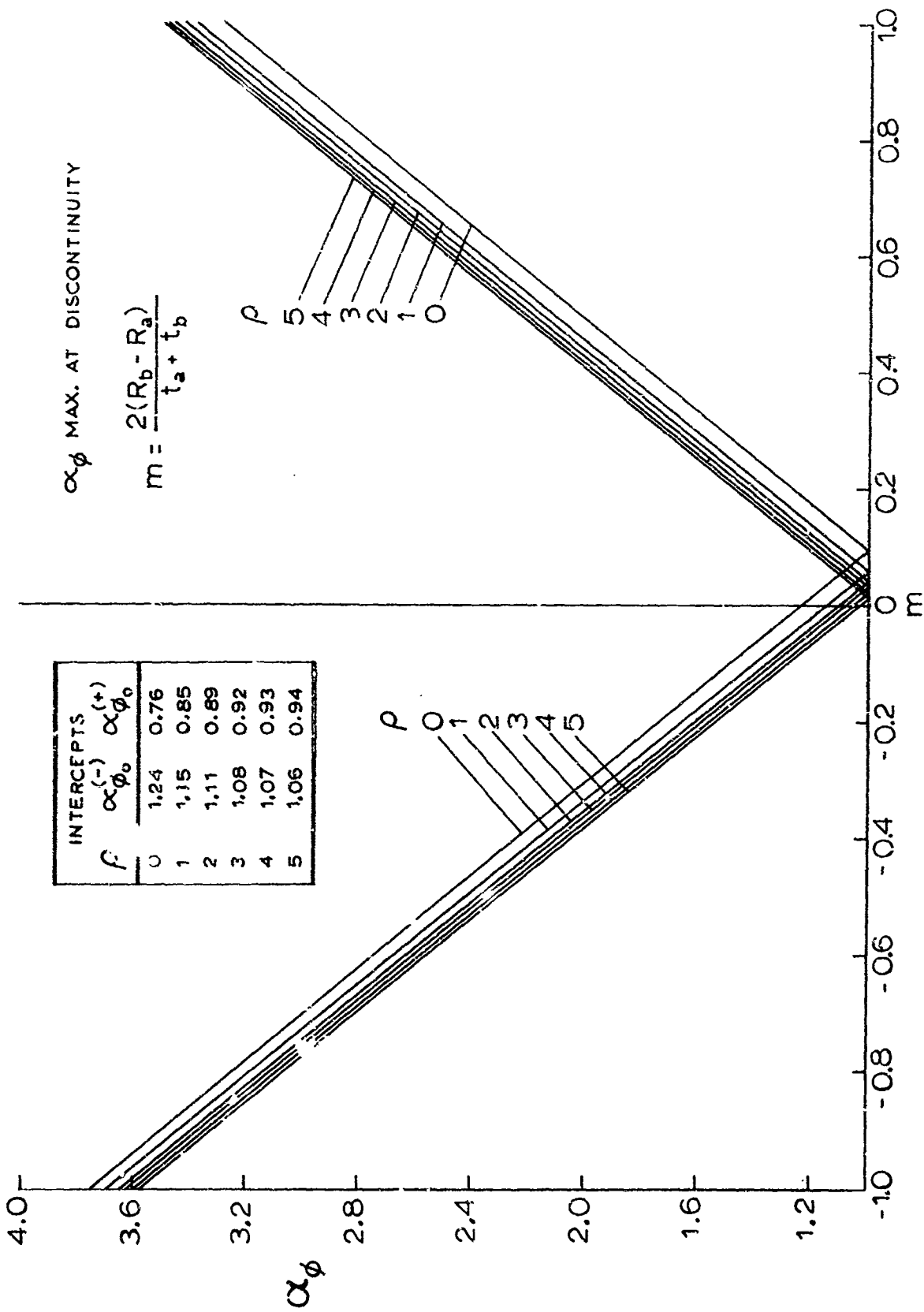


Fig. 5-15 Stress factor α_ϕ at the junction region of two cylindrical shells ($t_a/t_b = 0.6$)

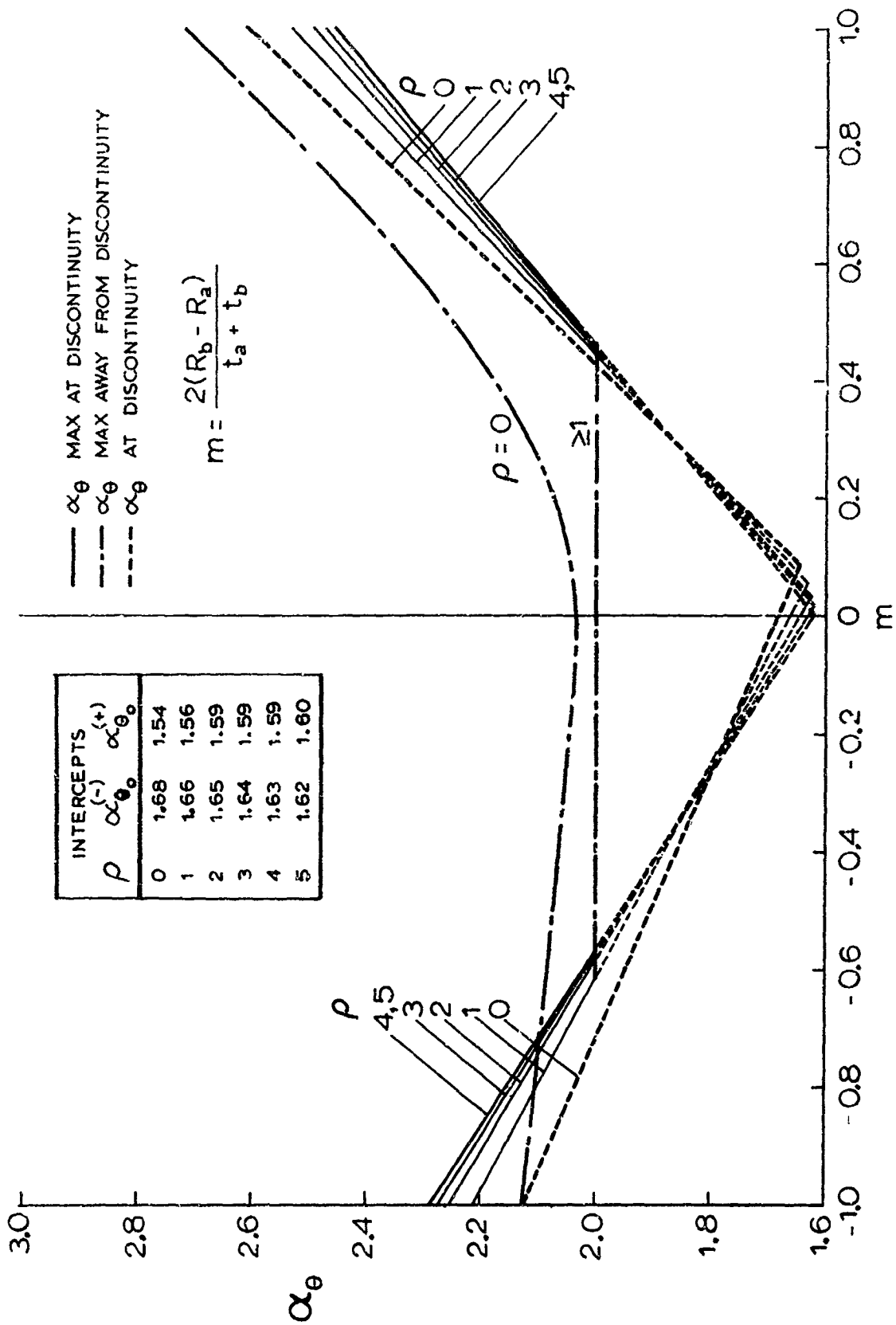


Fig. 5-16 Stress factor α_θ at the junction region of two cylindrical shells ($t_a/t_b = 0.6$)

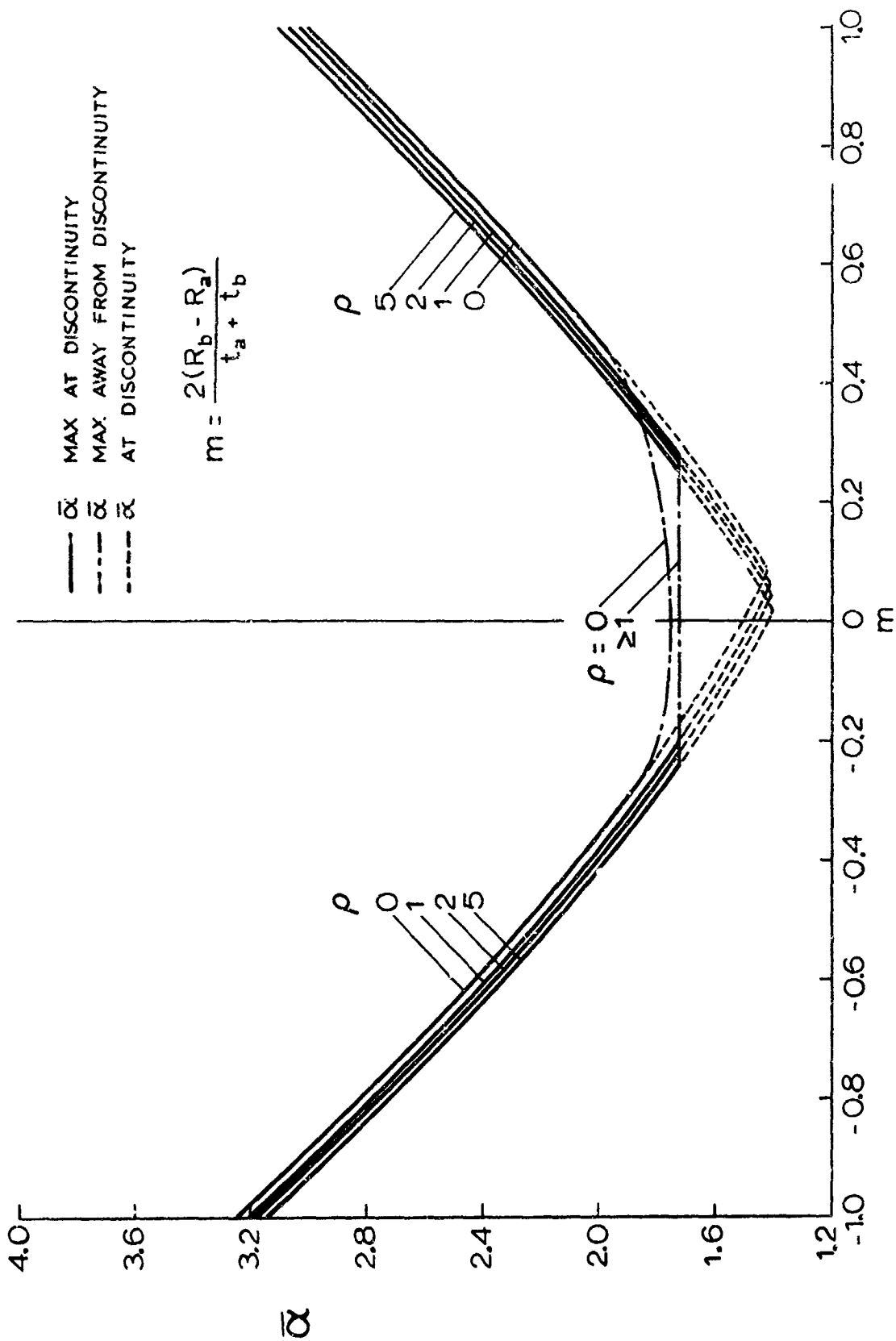


Fig. 5-17 Stress factor $\bar{\alpha}$ at the junction region of two cylindrical shells ($t_a/t_b = 0.6$)

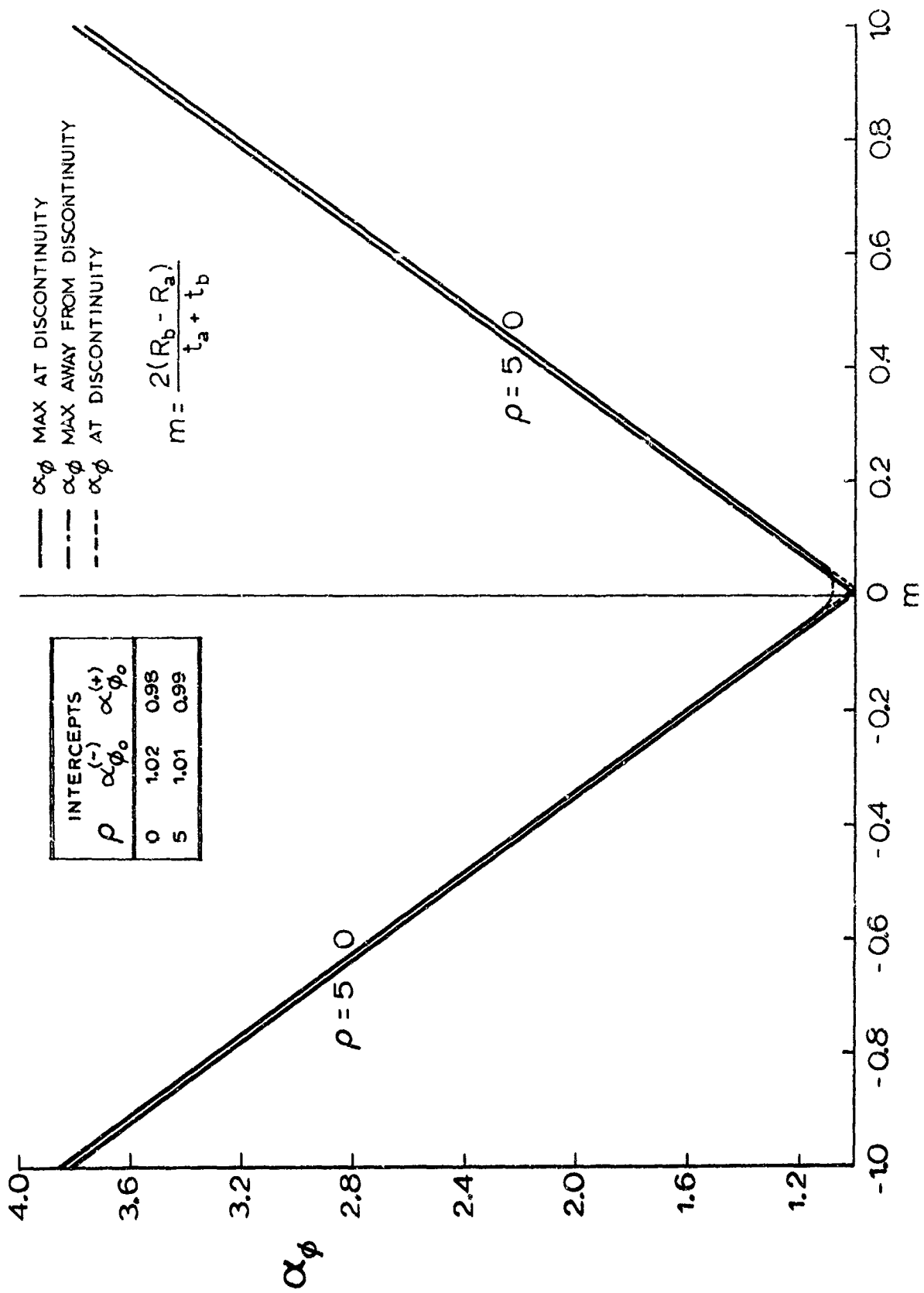


Fig. 5-18 Stress factor α_ϕ at the junction region of two cylindrical shells ($t_a/t_b = 0.8$)

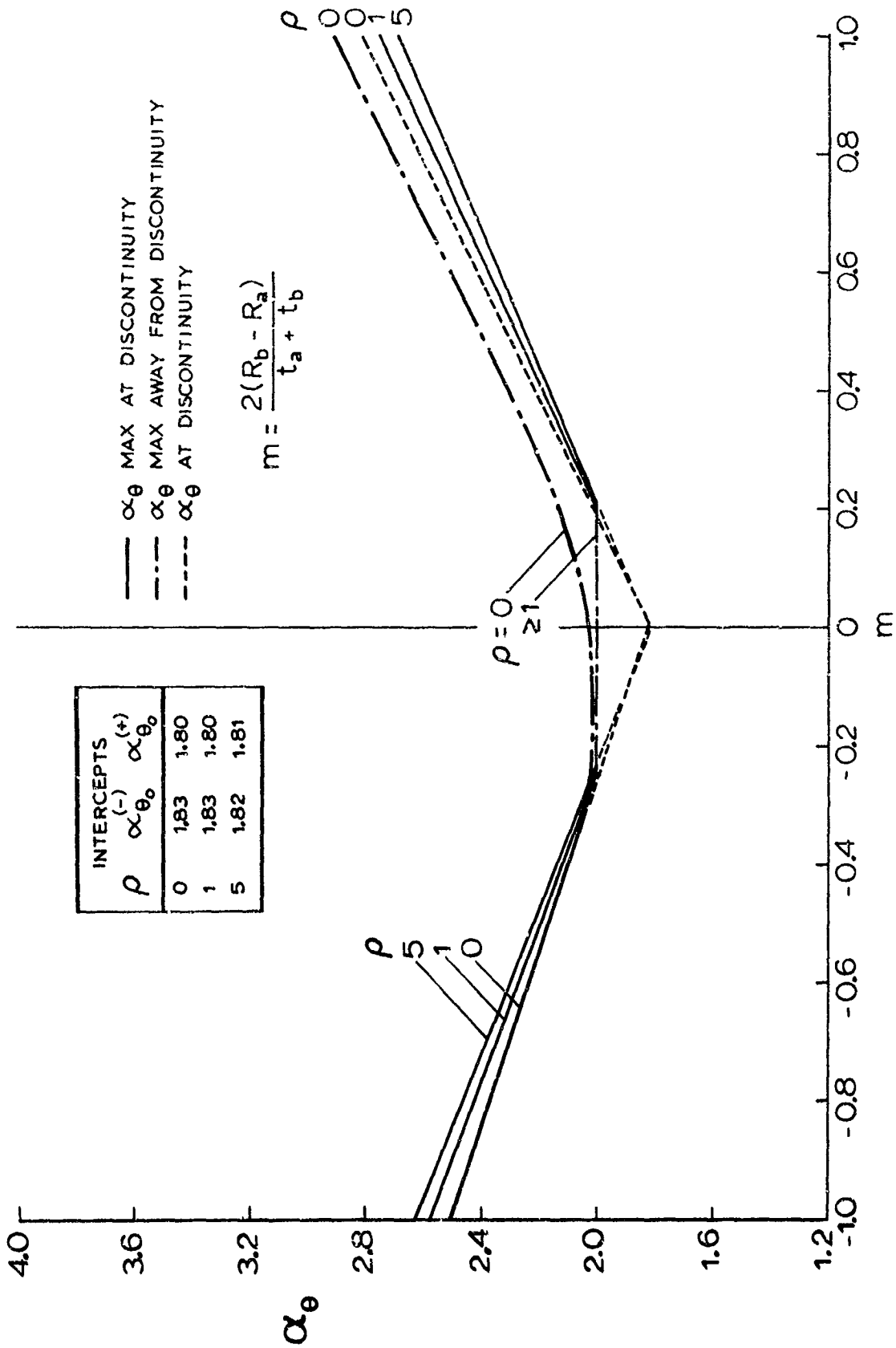


Fig. 5-19 Stress factor α_{θ} at the junction region of two cylindrical shells ($t_a/t_b = 0.8$)

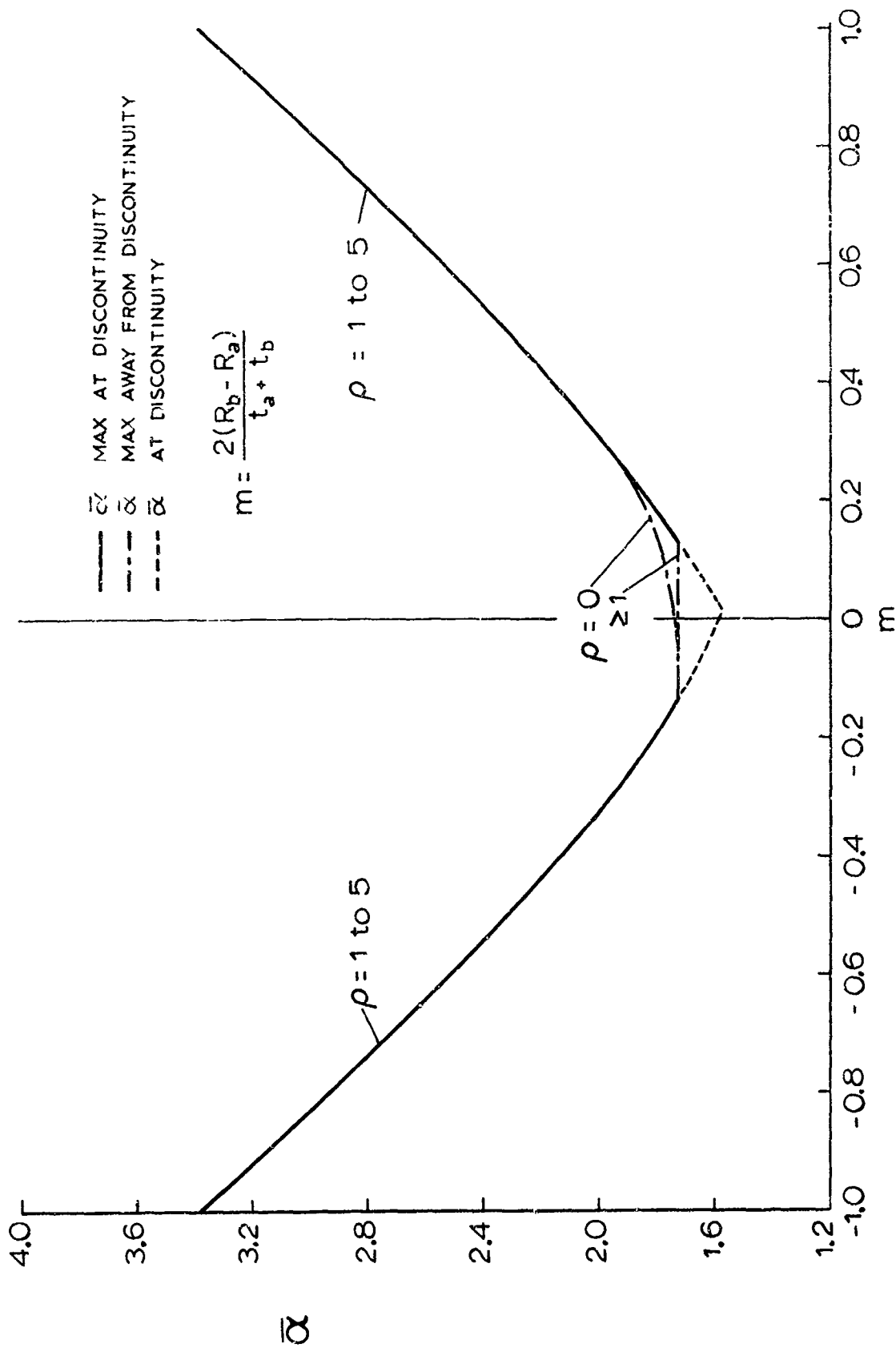


Fig. 5-20 Stress factor $\bar{\alpha}$ at the junction region of two cylindrical shells ($t_a/t_b = 0.8$)

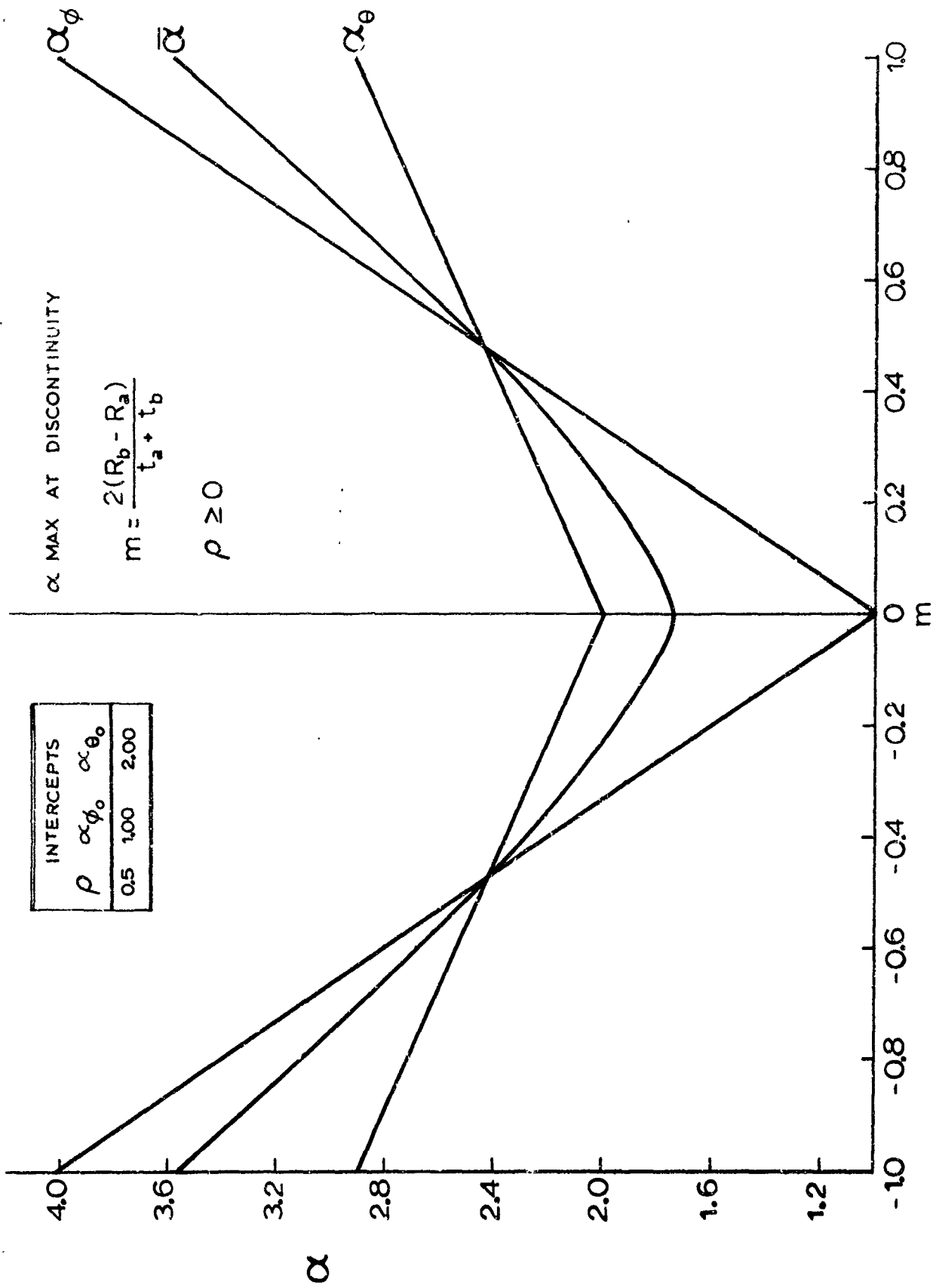


Fig. 5-21 Stress factors α_{ϕ} , α_{θ} and $\bar{\alpha}$ at the junction region of two cylindrical shells ($t_a/t_b = 1$)

5.1.2 Weld Sinkage

Weld sinkage is another form of geometric discontinuity which may occur during the fabrication of pressure vessels. A typical example is shown in Fig. 5-22.

This section provides information to calculate maximum stresses arising from this type of geometric discontinuity in cylindrical and spherical pressure vessels subjected to internal pressure. Similar to mismatch and abrupt thickness change problems the method is based on the nonlinear elastic theory which incorporates pressure coupling effects (see Section 2). Stresses include membrane and bending effects but exclude stress concentrations due to sharp corners. The information is applicable only to axisymmetric discontinuities. The shells are assumed to be thin, steep and long. The limiting conditions to these assumptions as well as exceptions are discussed in section 5.1.1.

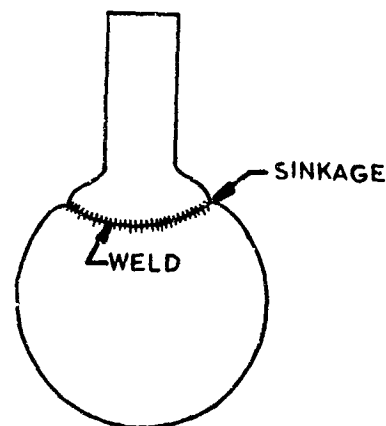


Fig. 5-22 Weld Sinkage in Pressure Vessels

Elastic stresses due to weld sinkage may be obtained from Figures 5-24 and 5-25, provided that the loading is internal pressure and the shells fall within the bounds of the theoretical assumptions. The curves are applicable to both cylindrical and spherical shells. Details of shell geometry are shown in Fig. 5-23.

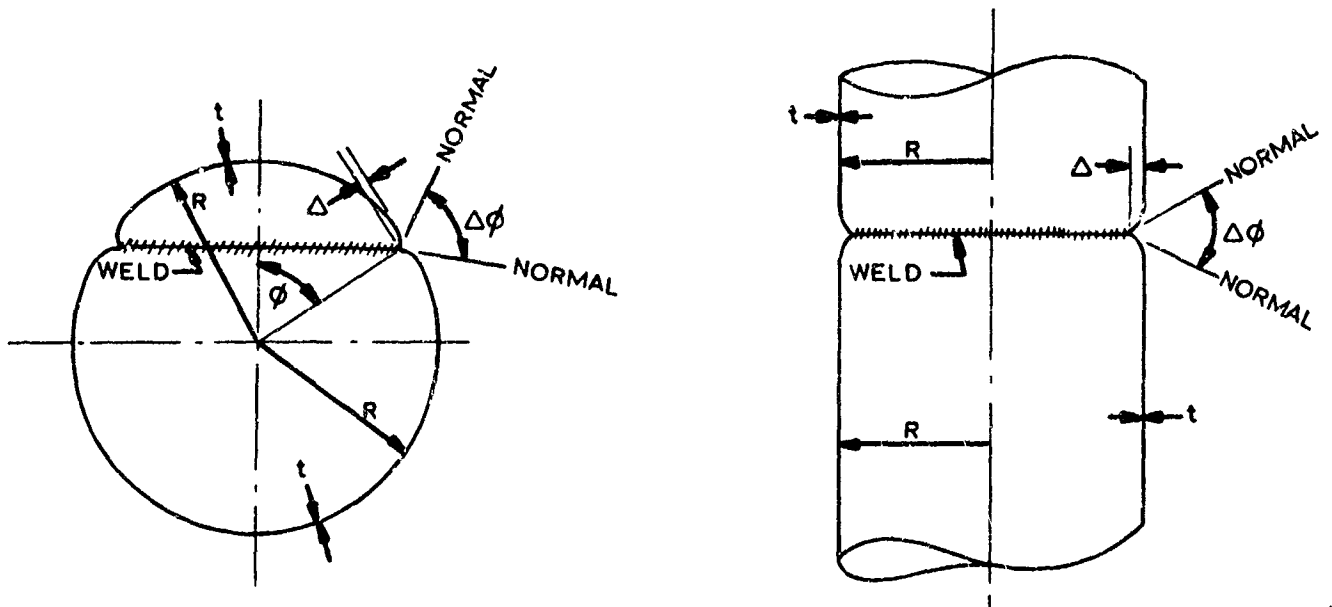


Fig. 5-23 Weld Sinkage Geometry in Spheres and Cylinders

Observe that the discontinuity in both cases are represented only by two geometric parameters, the angle ($\Delta\phi$) and the sinkage (Δ). These parameters are found to be the dominant factors affecting the stress distribution. The shape of the sinkage is relatively unimportant.

Figures 5-24 and 5-25 reflect this simplification. The sinkage parameter is represented by

$$\mu = \frac{0.55}{\Delta} \left(\sin \frac{\Delta\phi}{2} \right) \sqrt{Rt}$$

This is an approximate expression which involves only the basic shell parameters and the sinkage geometry as described above. The curves however are based on mathematical models of typical weld sinkage geometry in cylindrical and spherical pressure vessels. If the exact geometry of the sinkage is known it is suggested that the sinkage parameter be calculated using the more exact formula:

$$\mu^2 = \frac{1}{\sqrt{12(1-\nu^2)}} \frac{t}{R} \left(\frac{R}{\rho_1 \tan \frac{\Delta\phi}{2}} \right)^2$$

or, with $\nu = 0.3$

$$\mu = 0.55 \sqrt{\frac{t}{R}} \frac{R}{\rho_1 \tan \frac{\Delta\phi}{2}}$$

where

$$\frac{1}{\rho_1} = \frac{1}{R_{1D}} - \frac{1}{R_{1S}}$$

R_{1D} = Meridional radius of curvature at the discontinuity

R_{1S} = Meridional radius of curvature of the basic shell

$R_{1S} = \infty$ for cylinders

$R_{1S} = R$ for sphere

The stresses are given in terms of stress factors α_ϕ and α_θ which are defined as follows:

Meridional Stress Factor $\alpha_\phi = \frac{\sigma_\phi}{\sigma_{\phi m}} = \frac{\sigma_\phi}{\frac{pR}{2t}}$

Circumferential Stress Factor $\alpha_\theta = \frac{\sigma_\theta}{\sigma_{\phi m}} = \frac{\sigma_\theta}{\frac{pR}{2t}}$

where

σ_{φ} = total maximum meridional stress (lb/in²)

σ_{θ} = total maximum circumferential stress (lb/in²)

p = uniform internal pressure (lb/in²)

All stresses are given at the point of discontinuity (crease) where the stresses are maximum. The total stress is composed of membrane and discontinuity stresses.

The effective stress $\bar{\sigma}$ may be found by the expression

$$\bar{\sigma} = \sqrt{(\sigma_{\varphi}^2 + \sigma_{\theta}^2 - \sigma_{\varphi}\sigma_{\theta})}$$

as explained in the previous section.

PROCEDURE TO OBTAIN STRESS FACTORS

1. Obtain parameters required for the solution. These include the following:

- o Internal pressure p - lb/in²
- o Dimensions in inches R, t, Δ
- o Angles in degrees $\varphi, \Delta\varphi$
- o Modulus of elasticity E - lb/in²

(Other material properties such as F_{tu} and F_{ty} and weld properties are required for stress analysis).

2. Determine nonlinearity parameter ρ

$$\rho = \frac{p}{1.2E \left(\frac{t}{R}\right)^2}$$

3. Check of applicability of curves

The shells must satisfy the following requirements:

Thin Shell:

$$1.8 R/t \geq 10$$

Steep Shell:

$$1.8 \sin \varphi R/t \geq 10$$

($\varphi = 90^\circ$ for cylinders)

Long Shell:

$$L \geq L_c$$

L_c is obtained from Fig. 5-3

4. Determine μ

$$\mu = \frac{0.55}{\Delta} \left(\sin \frac{\Delta\varphi}{2} \right) \sqrt{R/t}$$

Enter Fig. 5-24 with μ (step 4) and read δ_φ using the proper ρ (step 2).

The meridional stress factor α_φ is found from the following expression:

$$\alpha_\varphi = 1 + 2.33 \delta_\varphi \left(\sin \frac{\Delta\varphi}{2} \right) \sqrt{R/t}$$

The circumferential stress factor α_θ is obtained from Fig. 5-25.

Using Fig. 5-25, read δ_θ . Then,

$$\alpha_\theta = \alpha_{\theta 0} + 1.29 \delta_\theta \left(\sin \frac{\Delta\varphi}{2} \right) \sqrt{R/t}$$

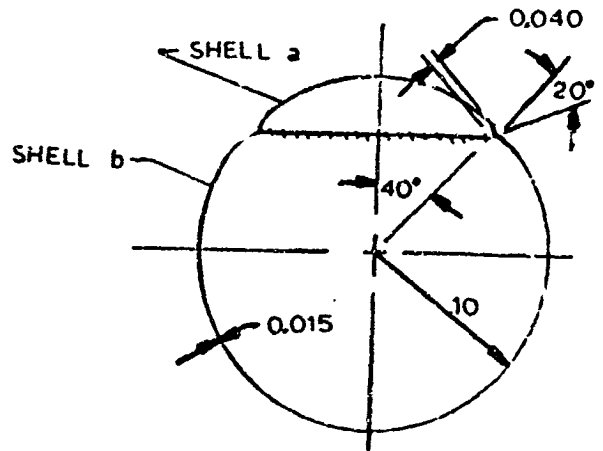
where

$$\alpha_{\theta 0} = 1 \text{ for spheres}$$

$$\alpha_{\theta 0} = 2 \text{ for cylinders}$$

EXAMPLE PROBLEM

Two spherical shell segments are welded together and at the joint sinkage formed as shown. The structure is subjected to an internal pressure of 400 psi. Both segments are made of Titanium Alloy Ti-6Al-4V.



Determine:

- o Maximum stresses

Solution:

1. Parameters required for the solution

p (psi)	R (in)	t (in)	Δ (in)	L _a (in)	L _b (in)	E (lb/in ²)	φ (deg)	Δφ (deg)	F _{tu} (lb/in ²)	F _{ty} (lb/in ²)
400	10	0.05	0.040	14	49	17.0x10 ⁶	40	20°	160,000	120,000

2. Determine nonlinearity parameter ρ

$$\rho = \frac{400}{(1.2)(17.0 \times 10^6) \left(\frac{0.05}{10}\right)^2} = 0.785$$

3. Check applicability of curves

Requirements	Segment a	Segment b
Thin Shell	$1.8(10/0.05)^{1/2} = 25.4$	Same as Segment a
Steep Shell	$1.8 \times \sin 40^\circ (10/0.05)^{1/2} = 16.3$	Same as Segment a
Long Shell	From Fig. 5-3, $L_c/3 \sqrt{Rt} = 0.71$ $L_c = (0.71)(3)(10 \times 0.05)^{1/2} = 1.51$	Same as Segment a

Results indicate that curves are applicable for this case.

4. Determine

$$\mu = \frac{0.55}{0.04} \left(\sin \frac{20}{2} \right) \sqrt{(10)(0.05)} = 1.69$$

5. Determine α_{φ} and α_{θ}

$$\text{from Fig. 5-24, } \delta_{\varphi} = 0.475, \alpha_{\varphi} = 1 + (2.33)(0.475) \left(\sin \frac{20}{2} \right) \sqrt{10/0.05} = 3.69$$

$$\text{from Fig. 5-25, } \delta_{\theta} = 0.365, \alpha_{\theta} = (1.29)(0.365) \left(\sin \frac{20}{2} \right) \sqrt{10/0.05} + 1 = 2.16$$

6. Determine maximum stresses

$$\sigma_{\varphi} = \frac{(3.69)(400)(10)}{(2)(0.05)} = 147,600 \text{ lb/in}^2 \quad \sigma_{\theta} = \frac{(2.16)(400)(10)}{(2)(0.05)} = 86,400 \text{ lb/in}^2$$

$$\bar{\sigma} = \left[147.6^2 + 86.4^2 - 147.6 \times 86.4 \right]^{1/2} \times 10^3 = 128,400 \text{ lb/in}^2$$

Since $\bar{\sigma}$ is greater than F_{ty} , the material will yield.

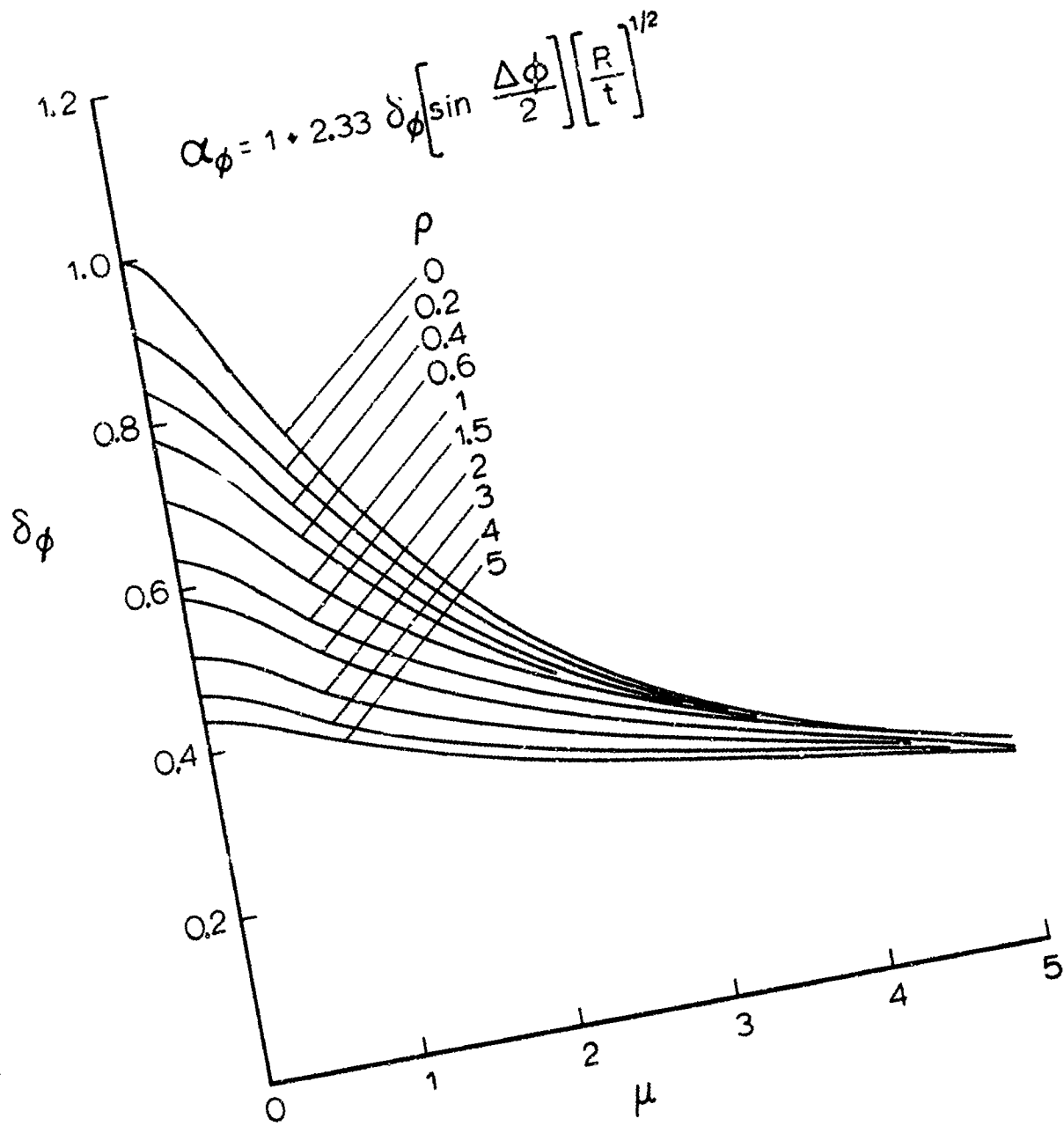


Fig. 5-24 Stress factor α_ϕ for spherical and cylindrical shells with weld sinkage

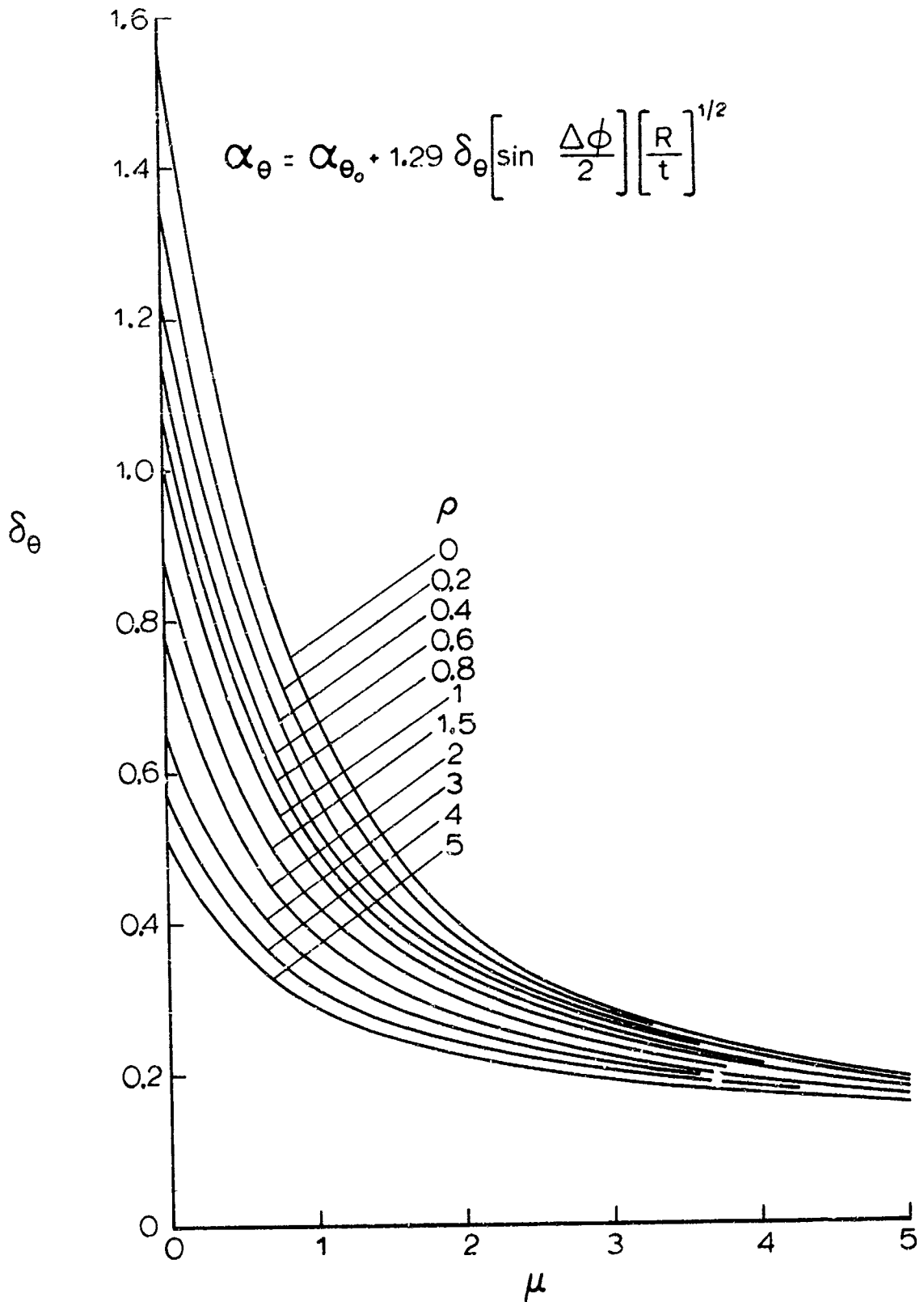


Fig. 5-25 Stress factor α_{θ} for spherical and cylindrical shells with weld sinkage

5.2 Design Graphs: Plastic Stresses

5.2.1 Weld Sinkage

This section provides information to calculate plastic stresses and strains for cylindrical and spherical with a weld sinkage as described in Section 5.1.2. The material is assumed to be titanium 6Al-4V, but any material with a similar stress-strain curve, i.e., with a smooth transition between the elastic and plastic regions, and with a practically horizontal plastic region, can be used.

Total strain and collapse pressures may be obtained from Fig. 5-26 (cylinders) and Fig. 5-29 (spheres), residual stresses from Fig. 5-27 (cylinders) and Fig. 5-30 (spheres), and maximum stress and residual strain from Fig. 5-28 (all shells).

PROCEDURE TO OBTAIN PLASTICITY SOLUTIONS

1. Obtain parameters required for the solution. These are identical to the ones needed for the elastic solution (see Section 5.1.2). Note: Plasticity curves are probably not applicable for $R/t > 500$.
2. Determine the stress factors α_φ and α_θ , for zero pressure ($p = 0$), as outlined in Section 5.1.2.
3. Determine the effective stress factor

$$\bar{\alpha} = \sqrt{\alpha_\varphi^2 + \alpha_\theta^2 - \alpha_\varphi \alpha_\theta}$$

4. Determine the reduced stress factor

$$\alpha = \bar{\alpha} / \sqrt{3} \quad (\text{Cylinder})$$

$$\alpha = \bar{\alpha} \quad (\text{Sphere})$$

5. Determine collapse pressure for shells with no weld sinkage

$$p_m = \frac{2}{\sqrt{3}} \frac{t}{R} F_{tu} \quad (\text{Cylinder})$$

$$p_m = 2 \frac{t}{R} F_{tu} \quad (\text{Sphere})$$

6. Determine normalizing strain

$$\bar{\epsilon}_y = \frac{2}{3} (1 + \nu) \frac{F_{tu}}{E}$$

7. Enter Fig. 5-26 (cylinder) or Fig. 5-29 (sphere) with p/p_m and α , and read strain $\bar{\epsilon}/\bar{\epsilon}_y$. (Or enter with strain and α , and read pressure p/p_m .)
8. Enter Fig. 5-28 with strain $\bar{\epsilon}/\bar{\epsilon}_y$ and read stress $\bar{\sigma}/F_{tu}$ and residual strain $\bar{\epsilon}_R/\bar{\epsilon}_y$.
9. Enter Fig. 5-27 (cylinder) or Fig. 5-30 (sphere) with α and $\bar{\epsilon}_R/\bar{\epsilon}_y$ and read residual stress $\bar{\sigma}_R/F_{tu}$.

EXAMPLE PROBLEM

The spherical shell in the Example Problem of Section 5.1.2 (page 5-35) was accidentally subjected to an internal pressure of 800 psi.

Determine:

- o Residual stress
- o Collapse pressure

Solution:

1. Parameters required for solution: See page 5-35.

$$R/t = 200$$

2. Determine α_φ and α_θ for $\rho = 0$

$$\text{from Fig. 5-24, } \delta_\varphi = 0.550, \alpha_\varphi = 1 + (2.33)(0.550) \left(\sin \frac{20}{2} \right) \sqrt{10/0.05} = 4.11$$

$$\text{from Fig. 5-25, } \delta_\theta = 0.455, \alpha_\theta = 1 + (1.29)(0.455) \left(\sin \frac{20}{2} \right) \sqrt{10/0.05} = 2.45$$

$$3. \bar{\alpha} = \left[4.11^2 + 2.45^2 - 4.11 + 2.45 \right]^{1/2} = 3.59$$

4. $\alpha = 3.59$

$$5. p_m = (2) \left(\frac{0.05}{10} \right) (160,000) = 1600 \text{ psi}$$

$$p/p_m = 800/1600 = 0.5$$

$$6. \bar{\epsilon}_y = \frac{2}{3} (1 + 0.3) \frac{160,000}{17 \times 10^6} = 0.00817$$

7. From Fig. 5-29, with $p/p_m = 0.5$, $\alpha = 3.59$: $\bar{\epsilon}/\bar{\epsilon}_y = 1.76$

Assuming collapse at $\bar{\epsilon}/\bar{\epsilon}_y = 2.6$ (see Section 4), Fig. 5-29 gives $(p/p_m)_{\text{collapse}}$

$$= (0.63) (1600) = 1010 \text{ psi}$$

8. From Fig. 5-28, with $\bar{\epsilon}/\bar{\epsilon}_y = 1.76$:

$$\bar{\sigma}/F_{tu} = 0.99, \quad \bar{\sigma} = (0.99)(160,000) = 158,400 \text{ psi.}$$

$$\bar{\epsilon}_R/\bar{\epsilon}_y = 0.78.$$

9. From Fig. 5-30, with $\bar{\epsilon}_R/\bar{\epsilon}_y = 0.78$, $\alpha = 3.59$:

$$\bar{\sigma}_R/F_{tu} = 0.35,$$

$$\bar{\sigma}_R = (0.35)(160,000) = 56,000 \text{ psi.}$$

Thus, after a pressure of 800 psi, the weld zone has developed a residual compressive stress of 56,000 psi.

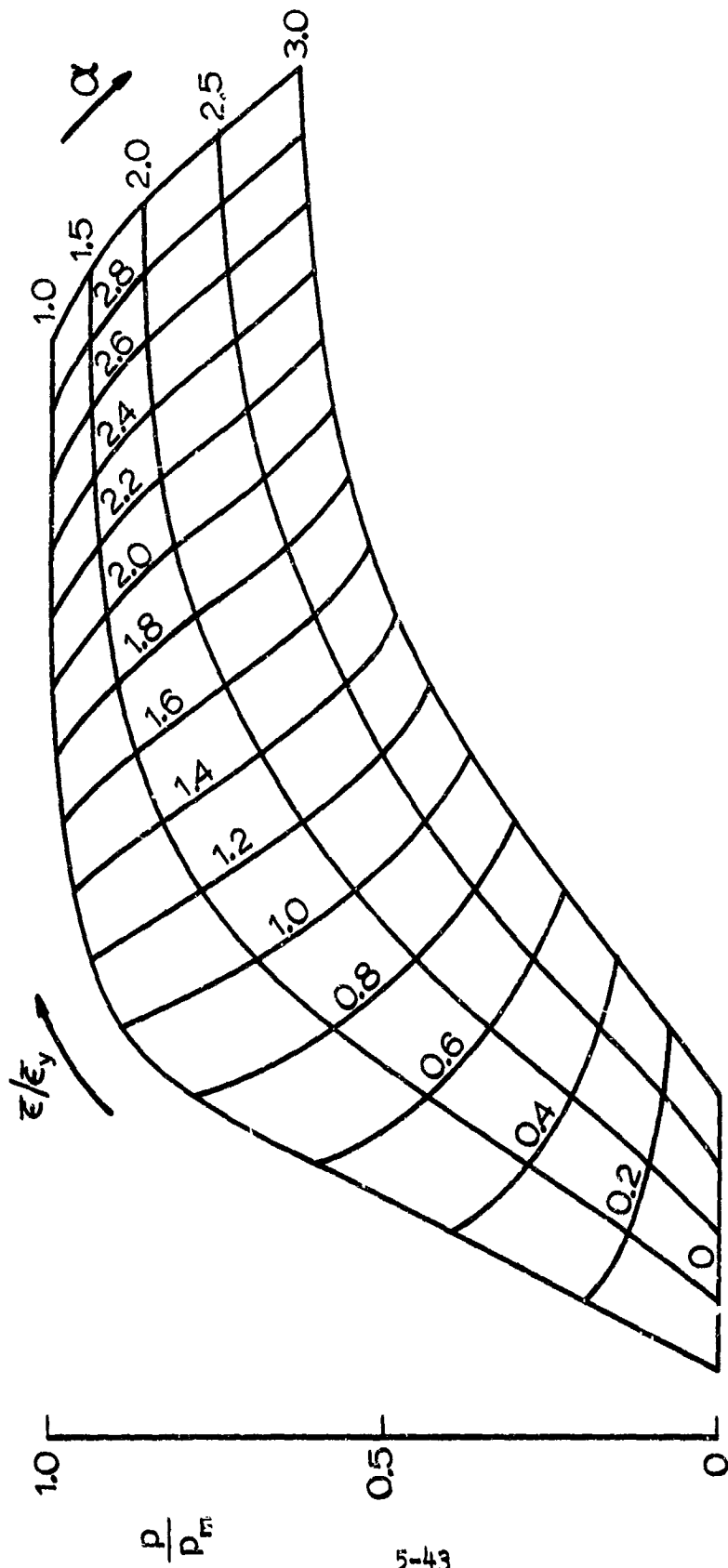


Fig. 5-26 Plasticity effects in cylinders with weld sinkage

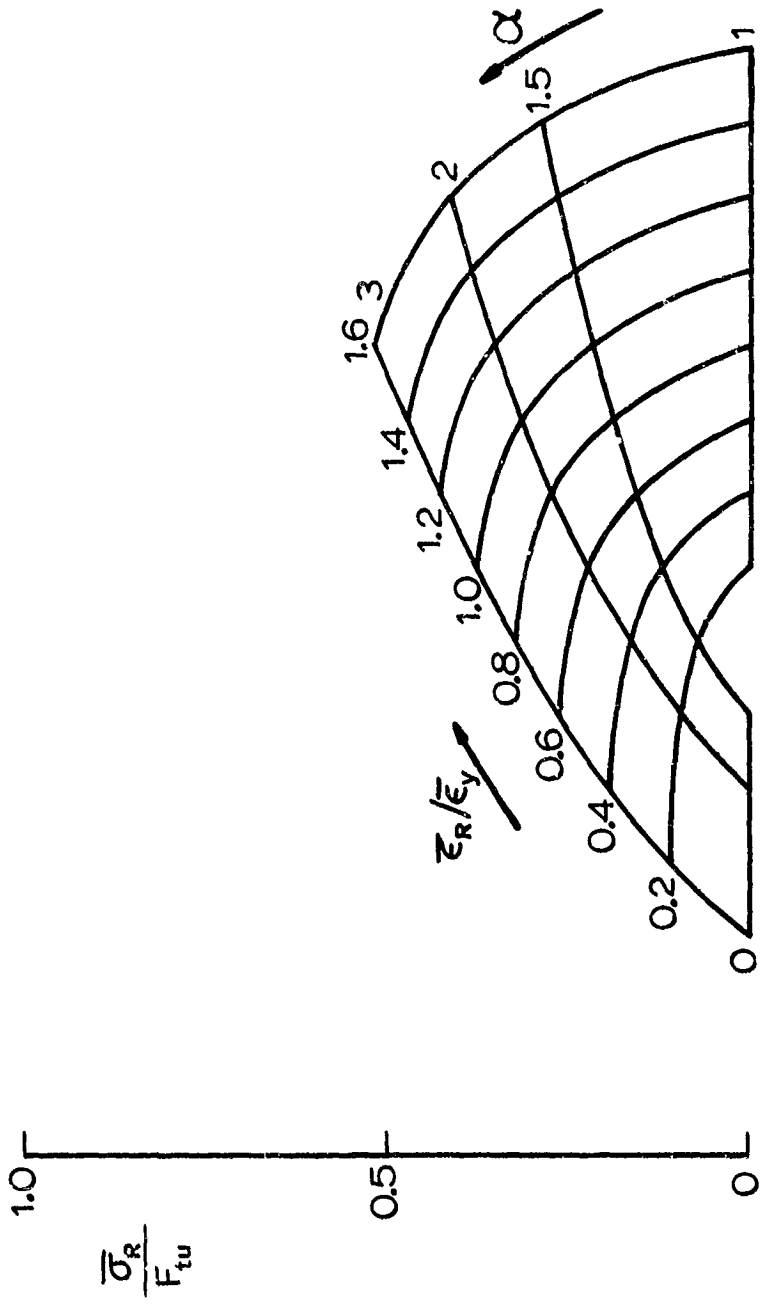


Fig. 5-27 Residual stresses in cylinders with weld sinkage

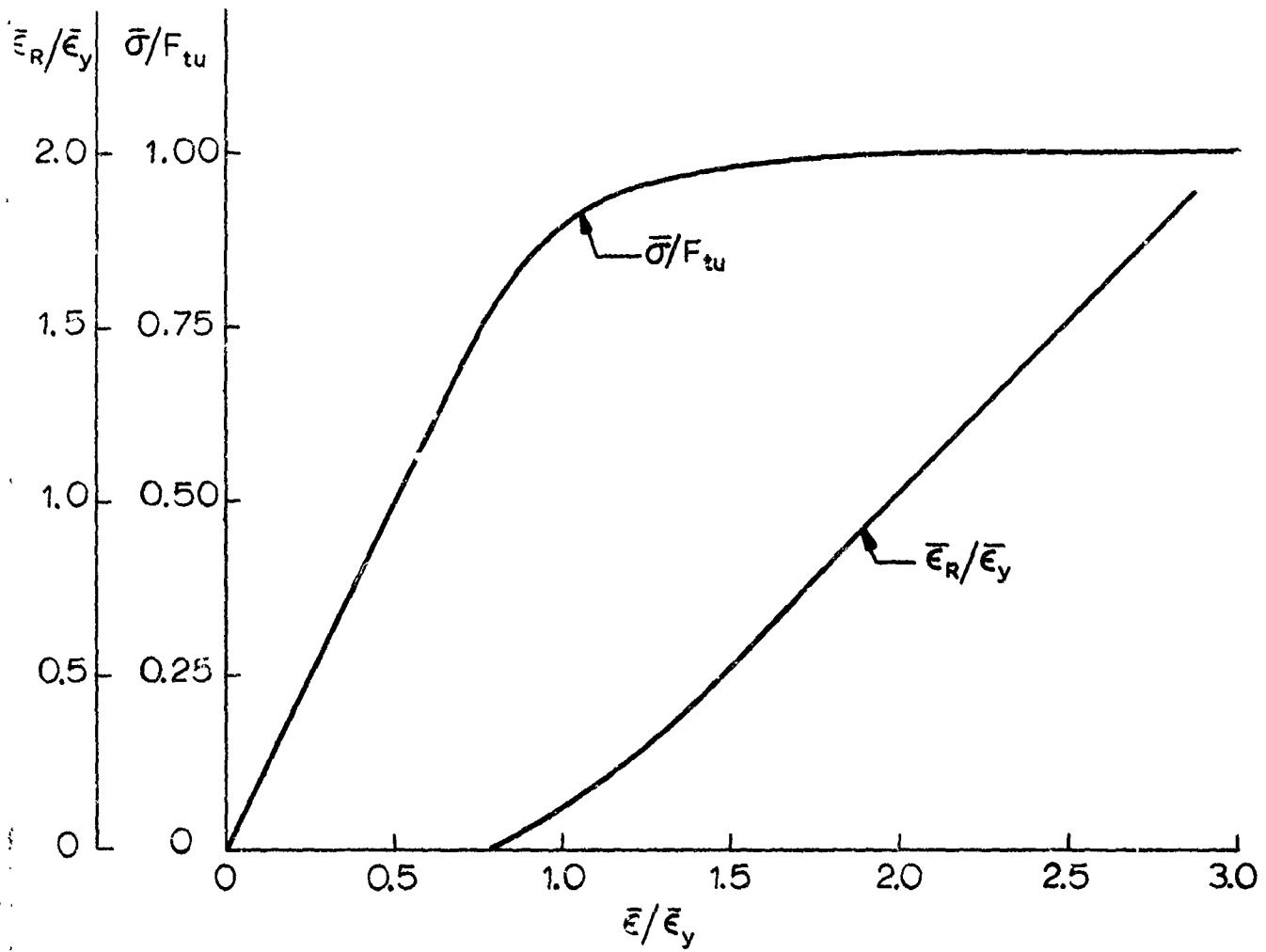


Fig. 5-28 Stress-strain relations, Ti Al6-4V

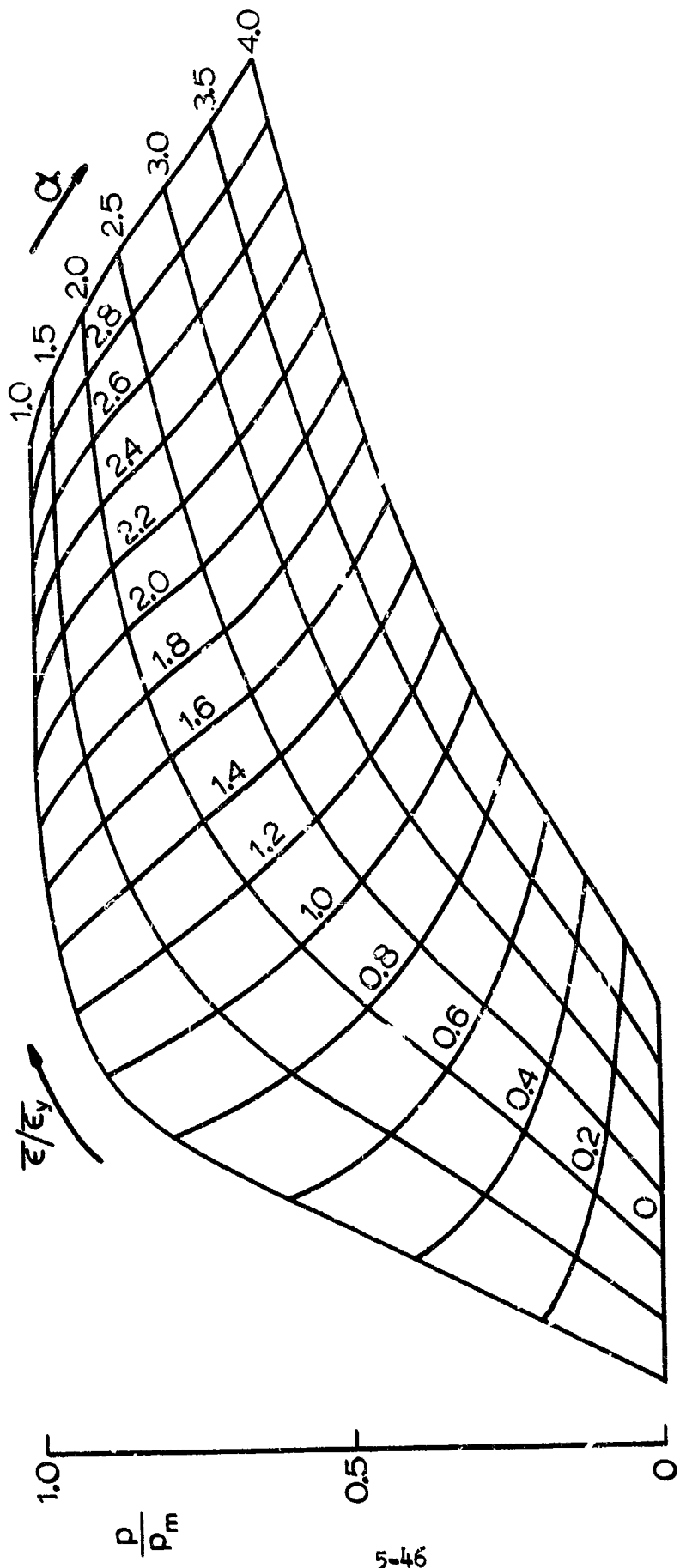


Fig. 5-29 Plasticity effects in spheres with weld sillage

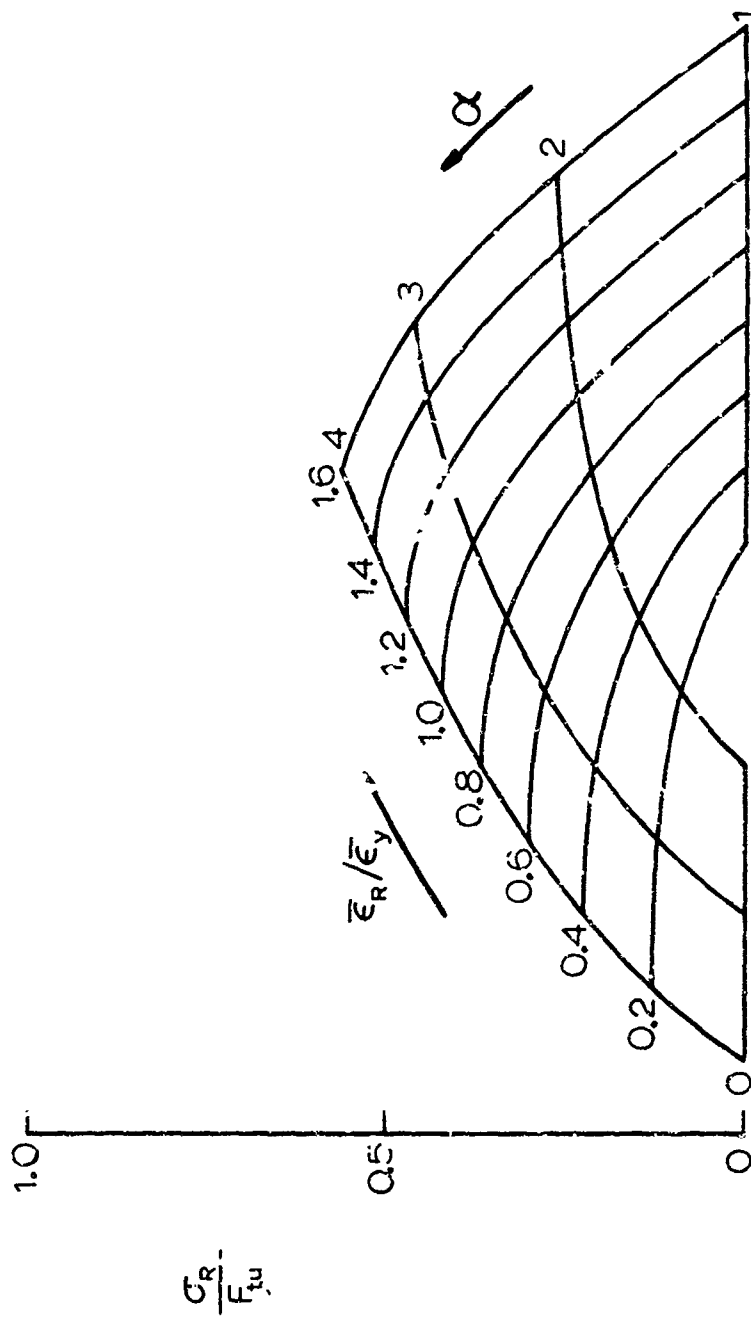


Fig. 5-30 Residual stresses in spheres with weld sinkage

Section 6
EXPERIMENTAL PROGRAM

6.1 Introduction

Five titanium specimens having simulated weld sinkages were instrumented and then pressurized to determine how closely the theory predicted the pressure-strain relationships.

The stress gradients in the vicinity of weld sinkages are very steep, so it was understood from the outset that exact numerical correlation at any given strain gage site would be impossible. But an array of gages along a meridian would show the characteristic peaks and oscillations of stress near the sinkage. Furthermore, it was imperative that the geometry of the sinkage should be clean and well defined, or correlation between theory and experiment would be difficult. For this reason, the sinkage was simulated by careful machining rather than by actual welding.

Table 6.1 summarizes the salient aspects of the five tests. Three specimens were spheres, and two were cylinders. Some were annealed titanium (6Al-4V), others were in the Solution Treated and Aged ("STA") condition.

Fourteen strain gages were installed on each specimen, and a special computer program was set up for processing the data in a way that would make it easy to determine the onset of plastic (i.e., permanent) strain by inspection of the tabulated data.

Section 6 is divided into the following subsections:

- 6.2 Description of Specimens and Their Manufacture
- 6.3 Instrumentation and Test Details
- 6.4 Data Processing

TABLE 6.1

SUMMARY OF TEST CHARACTERISTICS

	Tita #2	Tita #4	Tita #6	Tita #7	Tita #8
Type	Hemisphere	Hemisphere	Hemisphere	Cylinder	Cylinder
STA Condition	No	Yes	Yes	Yes	Yes
Weld bead	Yes	No	Yes	No	No
Failure pressure (psi)	--	805	--	1550	--
Max Press. at last strain reading (psi)	1050	800	1000	1500	1200

6.2 Description of the Specimens and Their Manufacture

6.2.1 Material

All five specimens were made of 6Al-4V titanium. Cylinders were machined from forged rings. Hemispheres were machined from drawn blanks. The titanium rings were forged by Coulter Steel and Forge Company, Emeryville, California, and received ultrasonic inspection to a 3/64" standard flat bottom hole. The hemispheres were drawn by Brooks and Perkins, Inc., Detroit, Mich. and were not inspected by ultrasonic methods. The hemispherical blanks were drawn from flat plate stock and had a pronounced oval condition (the major diameter being perpendicular to the rolling direction of the original plate, and .060 larger than the minor diameter, as received from Brooks and Perkins). This oval condition increased to about a quarter inch (discrepancy between the two diameters) upon heat treating. Fortunately, the .200-inch thick wall was thick enough to allow machining of a true sphere of .040 thickness despite the initial oval of the blank. These problems did not arise in the case of the forged cylinders.

The blank for the hemisphere called "Tita 2" was found to have a bump or outward spherical protrusion which resulted in a thin spot in the finish machined hemi. This thin spot (.015 inches thick vs. the required .040 membrane thickness) was successfully reinforced by a tapered steel disc, machined to conform to the internal concavity of the bump, and bonded in place with epoxy. The location of this patch was more than one inch from the test zone and it was deemed to have no adverse effect on the latter.

6.2.2 Solution Treatment and Aging

The STA procedure was done before final machining, after it was found* that the STA procedure could not be performed on thin machined shells without producing excessive distortion. The STA procedure consisted of soaking at 1700°F for one hour, followed by a water quench (solution treatment), then aging at 950°F for four hours

* on Tita #1, which was discarded due to bad equatorial warping

Tita #2, which did not receive STA, was stress relieved at 1400°F for one hour prior to machining (it was this process which increased the diameter discrepancy from .060 inches to 0.25 inches).

6.2.3 Weld Beads

As shown in Table 6.1, specimens #2 and #6 received a weld bead at the site of the sinkage, before machining. The intent of this was to produce the heat affected zone in the vicinity of the sinkage. In each case, the electron beam welder was set to produce a .050 inch high weld ridge on the back surface of the piece receiving the weld (see Fig. 6-1 and 6-2). This flash, along with the bead on the near (outer) surface was completely removed in the machining, though nugget material (in an "annealed" condition) remained at the center of the machined sinkage. Fig. 6-2 shows the appearance of the weld bead on the outer surface of Tita #2. The fixture visible in this picture was used to measure the unmachined specimens.

6.2.4 Closures

Two hemispheres, designated Tita #3 and #5, served as closures and were left in their "as received" condition except for a narrow width of machining required at their equator to bring them to the correct inner and outer diameter for welding onto the various test pieces. This machining included a short (.200 inch) length of cylindrical section beyond the closure hemisphere's equator to allow for the cut-off and remachining required on each subsequent test, see Fig. 6-2.

6.2.5 Cylinder Machining

In the case of the cylindrical specimens, machining to the final contour was first done on the inner surface (after the STA treatment). Two close-fitting mandrels were then introduced from each end (and joined by through bolting). The outer surfaces were then machined to their final desired contours. The contours shown in Fig. 6-4 were obtained on a lathe equipped with a cam follower. It should be added that the dimensions and tolerances given in this figure (and others in this report) were the desired rather than the achieved dimensions. Thickness on the cylinders

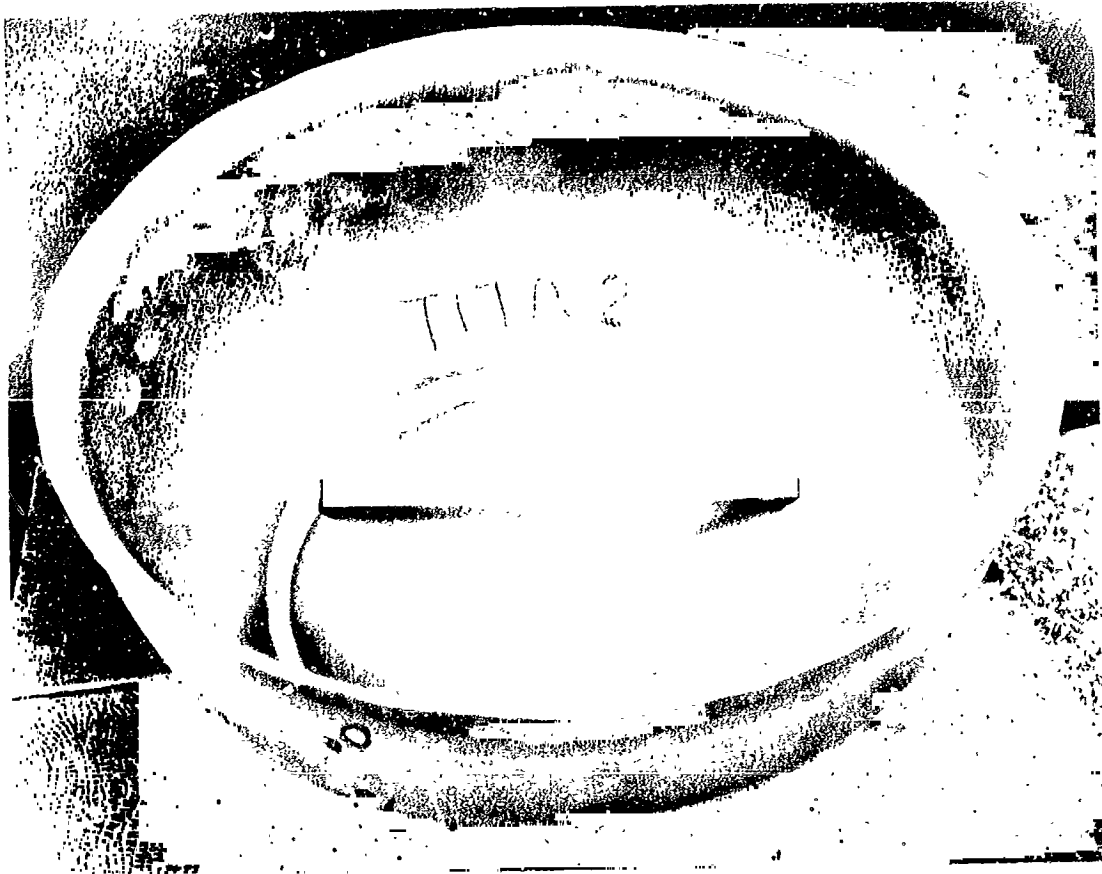


Fig. 6-1

Weld bead on inside surface of Titan #2



varied over a six mil range, with a mean that was 3 mils below the desired .050 thickness (on both cylinders, Tita #7 and #8).

6.2.6 Hemisphere Machining

In the case of the hemispheres, the outer surface was machined first, and then fitted into a close fitting "pot" (or outer mandrel) for the final inner surface machining on the cam follower controlled lathe. On Tita #2, which was machined (and tested) in the annealed and stress relieved condition, the mean thickness was .041 versus the desired .040, and the range of thickness variation was only three mils. On Tita #4, the same values as Tita #2 apply in the immediate test zone (within a half inch of the center of the sinkage) but the thickness dropped to .032 inches on a circle .60 inches from the center of the test zone, giving a range of thickness variation of ten mils. Tita #6, like Tita #4, a hemisphere in STA condition at the time of machining, the mean thickness in the test zone was .033 inches (vs. the desired .040) with a total variation of five mils, and a drop to .026 inch thickness at a circle .60 inches from the sinkage centerline.

The machinist described the titanium in STA condition as "having a tendency to walk", meaning that the material's toughness caused it to bulge slightly ahead of the cutting tool, rather than remain a close fit on the mandrel. It is believed that this condition resulted in the poorer thickness tolerances on the two hemispheres in STA condition.

All three hemispheres tested (Tita #2, #4 and #6) had nominally the same outline as shown in Fig. 6-5.

6.2.7 Closure Welding

After machining the cylinders or hemispheres and taking thickness measurements, the closures were welded on by an electron beam welder. For this operation, the test piece was bonded to a jig which made it possible to rotate the piece about its axis inside the electron beam welding chamber. This jig permitted alignment and concentricity with the rotating axis to about .005 inches T.I.R. precision. The mating piece was held on by a large stainless steel hose clamp drawn up tightly over the junction of the two

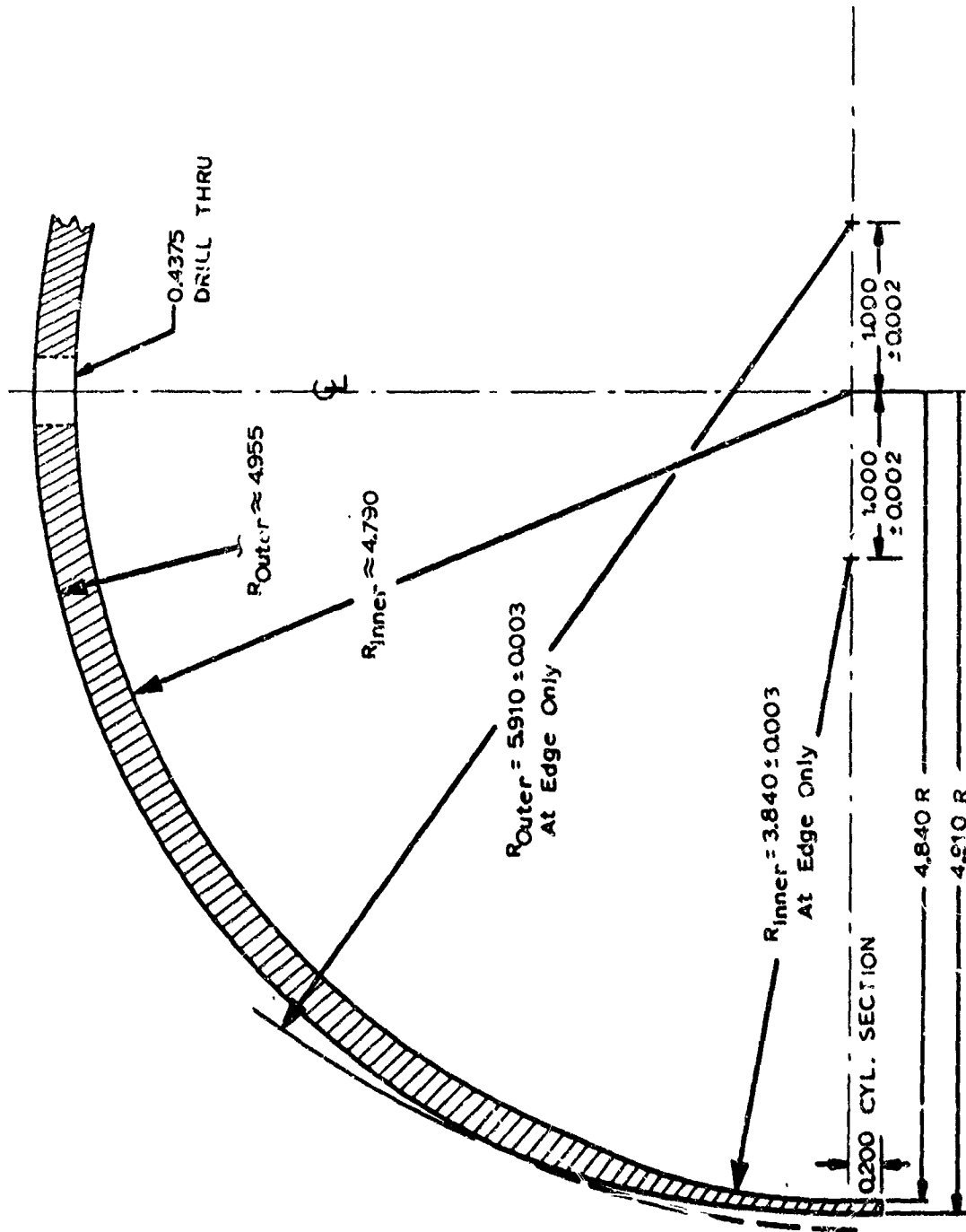


Fig. 6-3 Closure outline

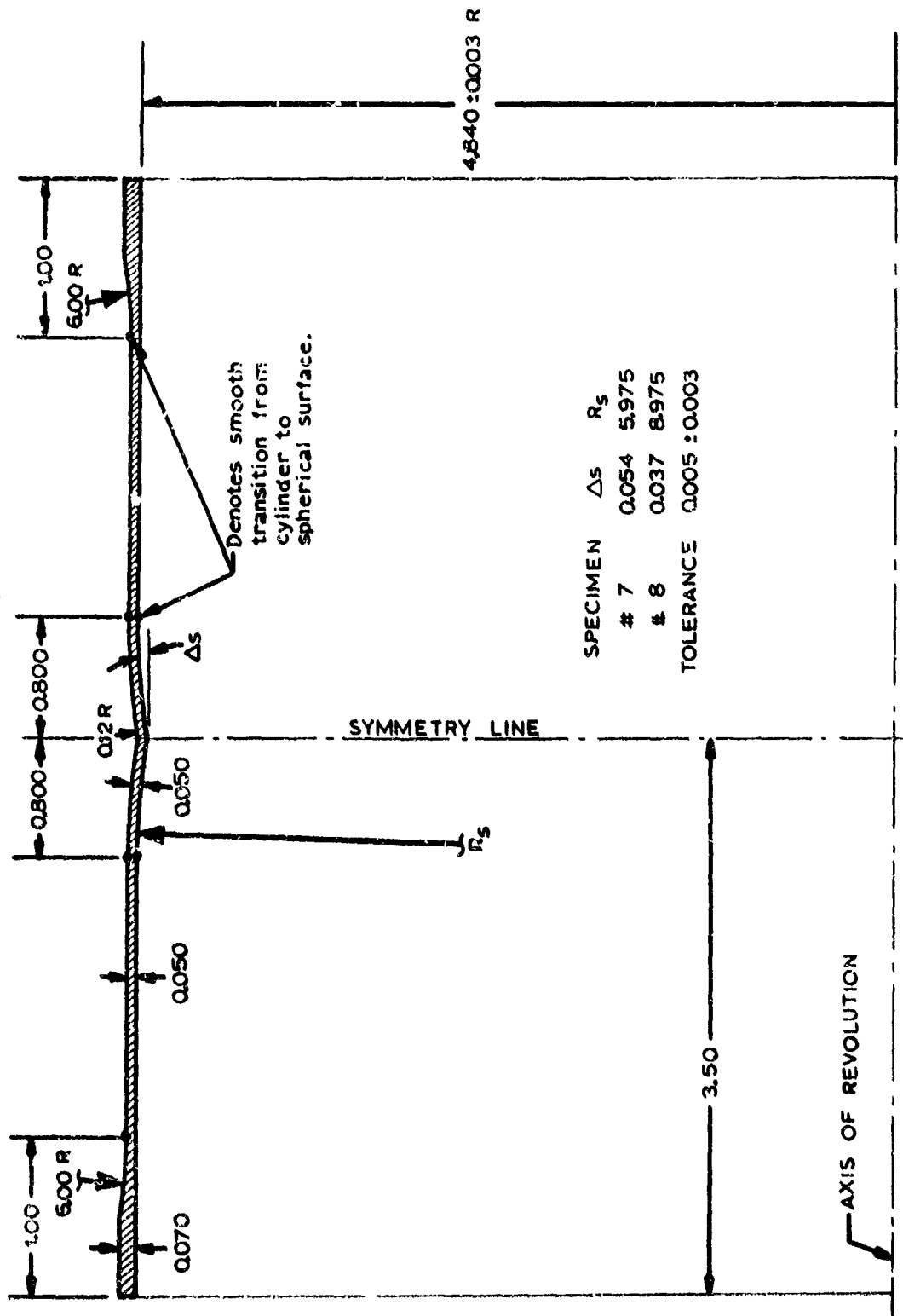


Fig. 6-4 Cylinder outlines

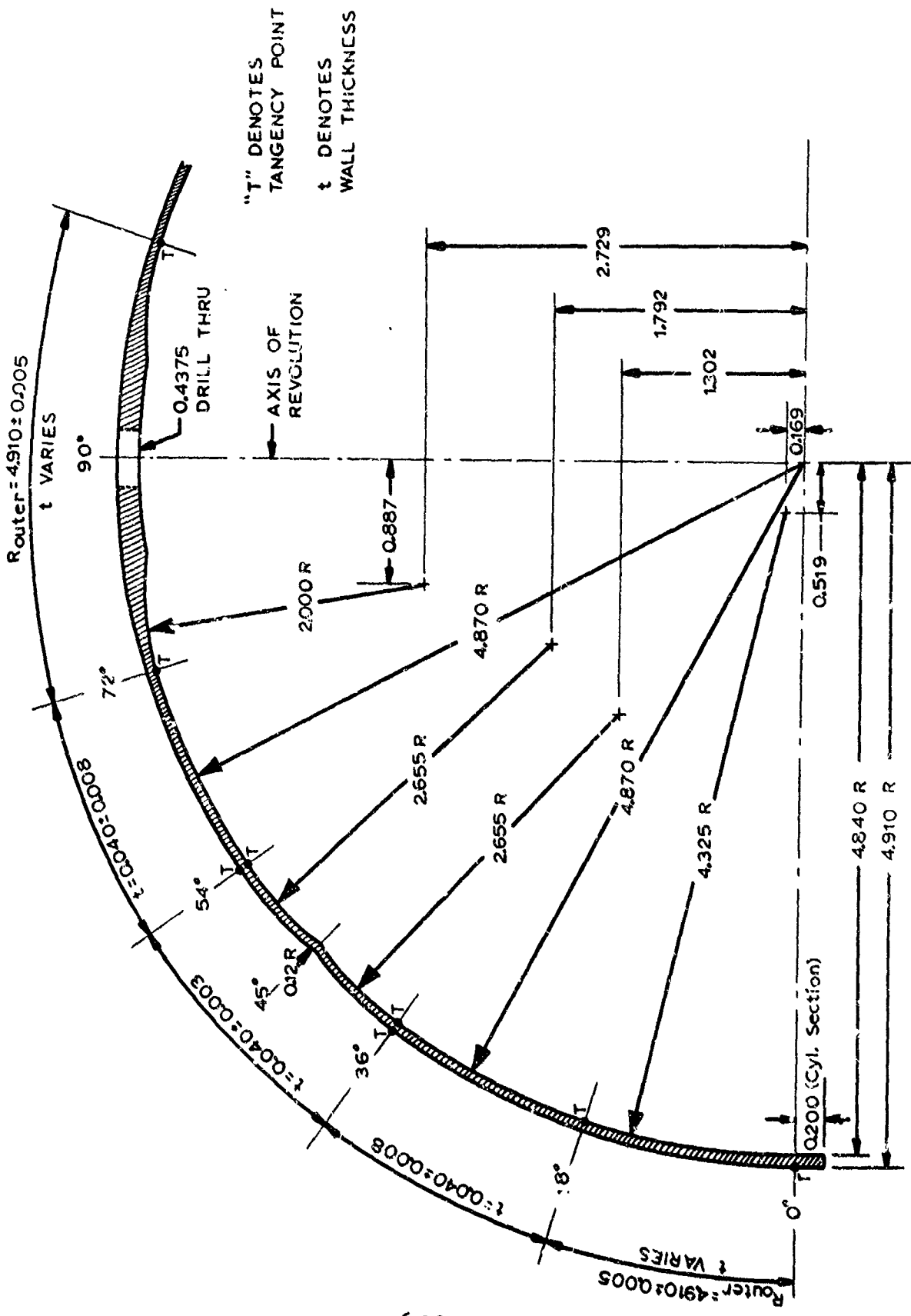


Fig. 6-5 Hemispherical mitline

pieces. A second hose clamp roughly perpendicular to the first one, kept the two pieces pressed firmly together. The first hose clamp (or steel band) had half-inch diameter holes at about four inches on centers along its length, permitting the two test pieces to be tack welded together (at the hole sites) by T.I.G. welding. The hose clamps were then removed and the weld joint completed by the electron beam welder.

Considerable difficulty was experienced in establishing the correct setting for the welder, since there was no reliable method of determining the weld penetration. Two hydraulic fittings (at each "pole") were installed prior to welding, one for pressurizing, the other for strain gage leads, but their .125 inch diameter apertures were useless for visual inspection. While the ultrasonic inspection method could have given a weld penetration measurement, such measurements are only reliable after an elaborate set of control (i.e., calibration) specimens have been made available, and this was obviously out of question. X-rays were tried and found inconclusive (as to depth of weld penetration). Adding to the problem was the material thickness (.070 inches) which made it very easy for a weld "blow-through". As a result of these welding difficulties, two pressure tests ended prematurely and had to be re-run (on Tita #4 and Tita #6) because of insufficient weld penetration at the closure joint. "Blow-through" occurred on Tita #7 (see Fig. 6-6), and the whole weld zone had to be re-machined and rewelded. In each of these cases, the weld failure (or blow-through) resulted in no damage to the test zone (which was at least three inches from the source of trouble).

6.2.8 Machining Repair on Tita #4

In the last stages of machining, the machinist accidentally allowed the cutting tool to travel beyond the range of its controlling cam, resulting in a concentric hole being cut in the crown of Tita #4. A disc matching the hole was cut from the crown of Tita #1 (which had been discarded due to bad warping at its equator), and welded into the crown of Tita #4. The weld in this repair was more than two inches from the center of the test zone, and it was therefore clear that a normal test could be run. Also, being in a region thickened for the hydraulic fitting, the repair would cause no difficulties. Such, however, was not the case. As mentioned before, Tita #4

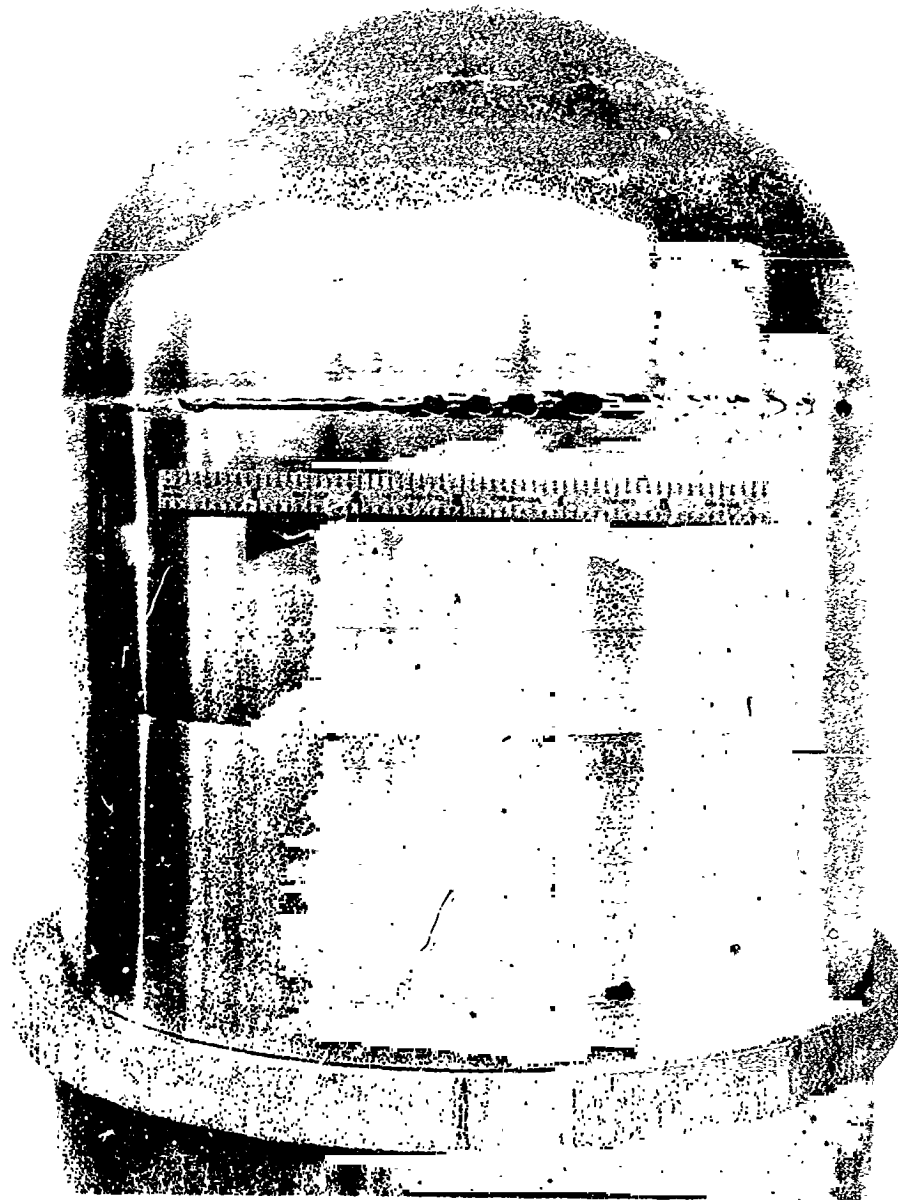


Fig. 6-6
"Blow-through" on Tita #7

failed prematurely at the closure weld (just below 500 psi). Upon repairing the closure weld, and repressurization, a crack and slow leak developed at 805 psi -- at the site of the site of the crown repair weld. The failure was diagnosed by the metallurgical staff, as due to hydrogen embrittlement and as such, was not considered repairable. The data (up to 800 psi) had shown no inelastic behavior (as contrasted with Tita #2 which had marked inelastic behavior at 700 psi) and is included in this report as being valid and pertinent.

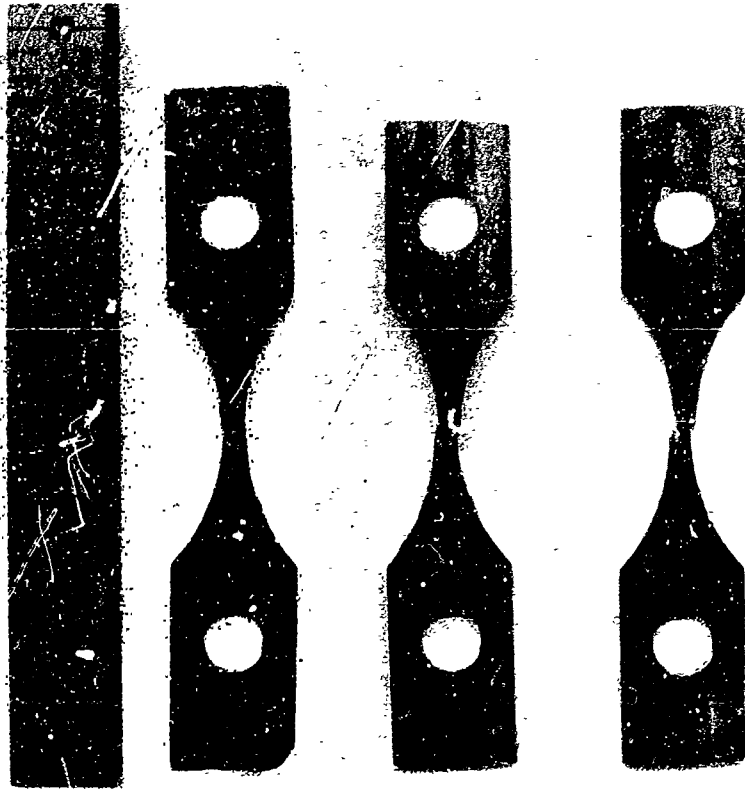
6.2.9 Test Coupons

Test coupons were milled from the ends of the cylinder and from the "flash" on the open ends of the drawn hemispherical blanks. In each case, the coupon cutting was not performed until the part had received its final heat treatment, so that coupon heat treatment coincides with that of the test article from which it was cut.

In each case, it was possible to cut a small plate 2.6 inches long by 0.50 inches wide. The thickness of the finished plate ranged from .017 to .060 inches, depending upon the availability of material. These plates were then milled to a "dog-bone" outline as shown in Fig. 6-7.

The radius leading to the narrowed section was 1.00 inches in all cases. The holes used to attach the specimens to the testing machine (by clevises) were 0.250 in diameter and great care was taken to have these holes fall on the centerline through the narrowed section. The narrowed section was .060 inches wide which permitted the use of 1/32 inch (square) strain gages.

Strain gages were installed in back-to-back pairs to read the average strain at the minimum cross section. These strain gages recorded strain up to about two percent. The approximate maximum elongation was calculated by correlating testing machine platen motion with strain measured by the strain gage in the plastic range. The coupon was too small and did not possess a constant cross section of sufficient length to permit the installation of an extensometer (which could have given a more accurate



TITA: #2 - A - B - C

Fig. 6-7

Tensile coupons for Tita #2

maximum elongation measurement). And of course, the coupon was as large as could be, and still be taken from the same blank as final hemispherical or cylindrical specimen.

The stress-strain curves obtained for coupons taken from Tita #2, #4, #6 and #7 are shown in Figs. 6-8 through 6-10.

6.3 Instrumentation and Test Details

6.3.1 Strain Gages

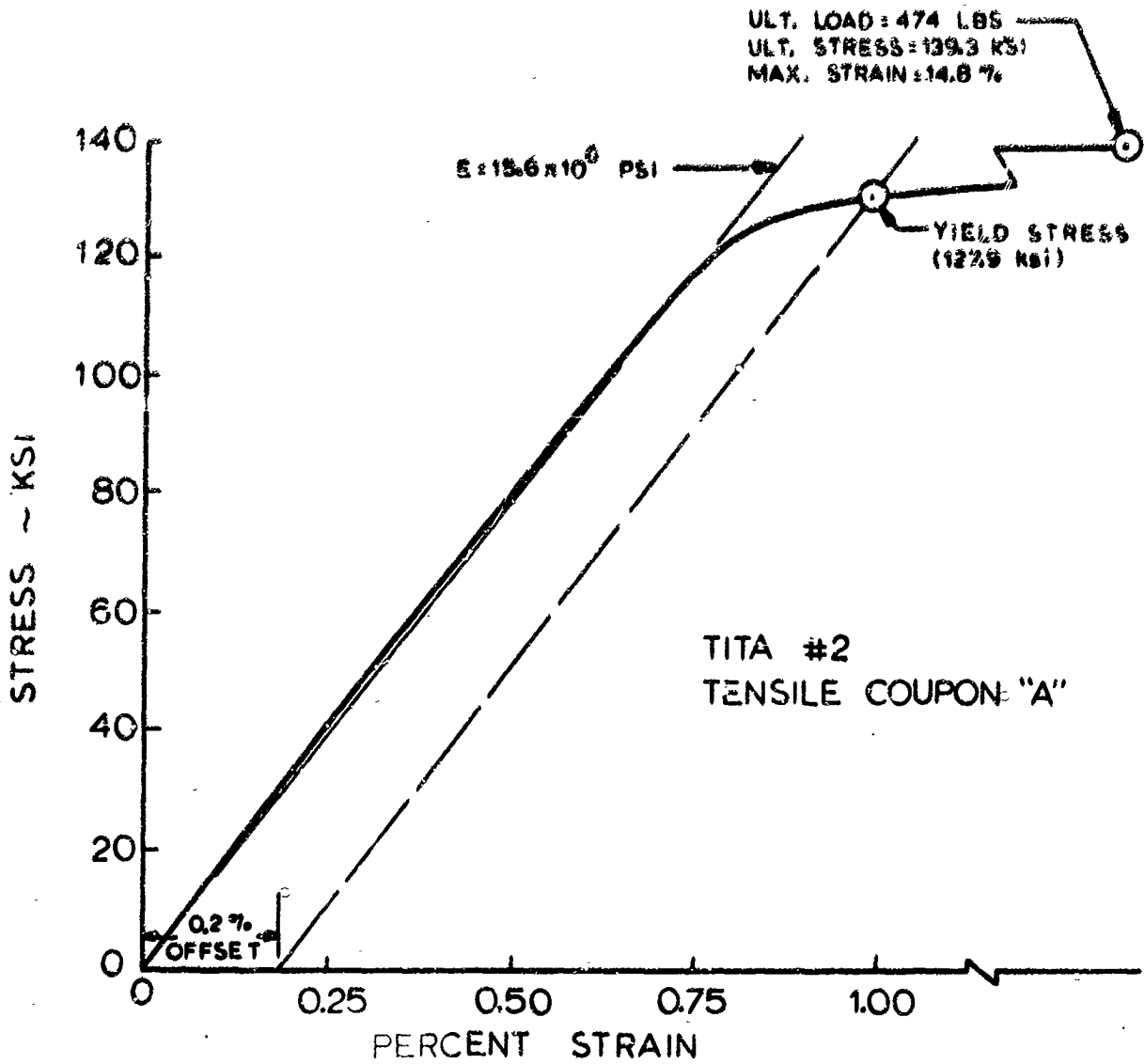
Fourteen strain gages were installed on each specimen tested. Three of these were installed on the inner surface prior to welding on the closure.

On Tita #2, #4 and #7, the numbering system and locations of the gages (relative to the center of the sinkage) were identical. These locations are shown in Fig. 6-11 and Table 6.2, and for Tita #6 and #8, in Fig. 6-12 and Table 6.3 and 6.4, respectively.

Gages used were epoxy-backed constantan foil, having six parts per million per degree F temperature compensation and 1/16 inch gage length, whether rosette or single element. The surface of the titanium was first degreased with successive acetone swabbings. A quick wipe with a dilute etchant (1.5% HF, 30% HNO₃, 68.5% H₂O) was followed by swabbing with an ammoniated neutralizer. The cement used for bonding the gages was William T. Bean's epoxy "RTC Fix-Mix" which requires an hour's cure at 140°F.

The gages were shunt calibrated, with the usual corrections applied for lead resistance and for any shunt resistors needed to balance the bridge.

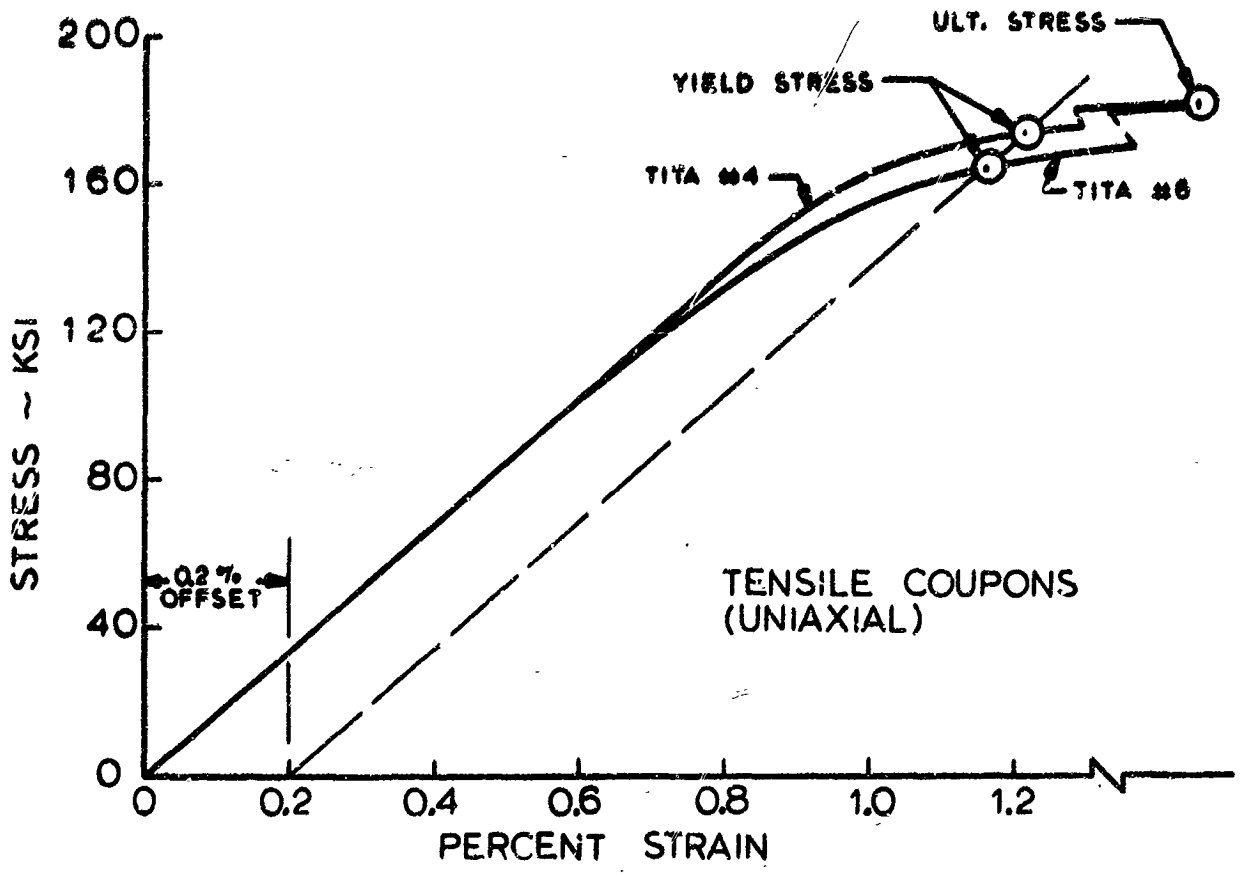
The strain gage signals, along with that of the pressure transducer, were measured and recorded by a Hewlett Packard 2445 Series Data Acquisition System (DAS). The DAS consists of a cross-bar scanner which selects the gage to be read, an integrating digital voltmeter (reading to one microvolt accuracy), and two recording devices in parallel: One, a printer which puts



	Coupon "B"	Coupon "C"
Elastic Modulus	17.9×10^6 psi	15.9×10^6 psi
Yield Stress	143.2 ksi	136.3 ksi
Ultimate Stress	149.3 ksi	145.8 ksi
Max. Elong	Not Obtained	Not Obtained

*Strain gage probably not at min. section

Fig. 6-8 Stress-strain curve for coupon



	<u>Tita #4</u>	<u>Tita #6</u>
Elastic Modulus (psi)	17.3 X 10 ⁶	16.9 X 10 ⁶
.2% Yield (psi)	174,000	164,000
Ultimate Strength (psi)	182,000	181,000
Max. Elong (approx.)	4.0%	3.5%

Fig. 6-9 Stress-strain curve for coupons

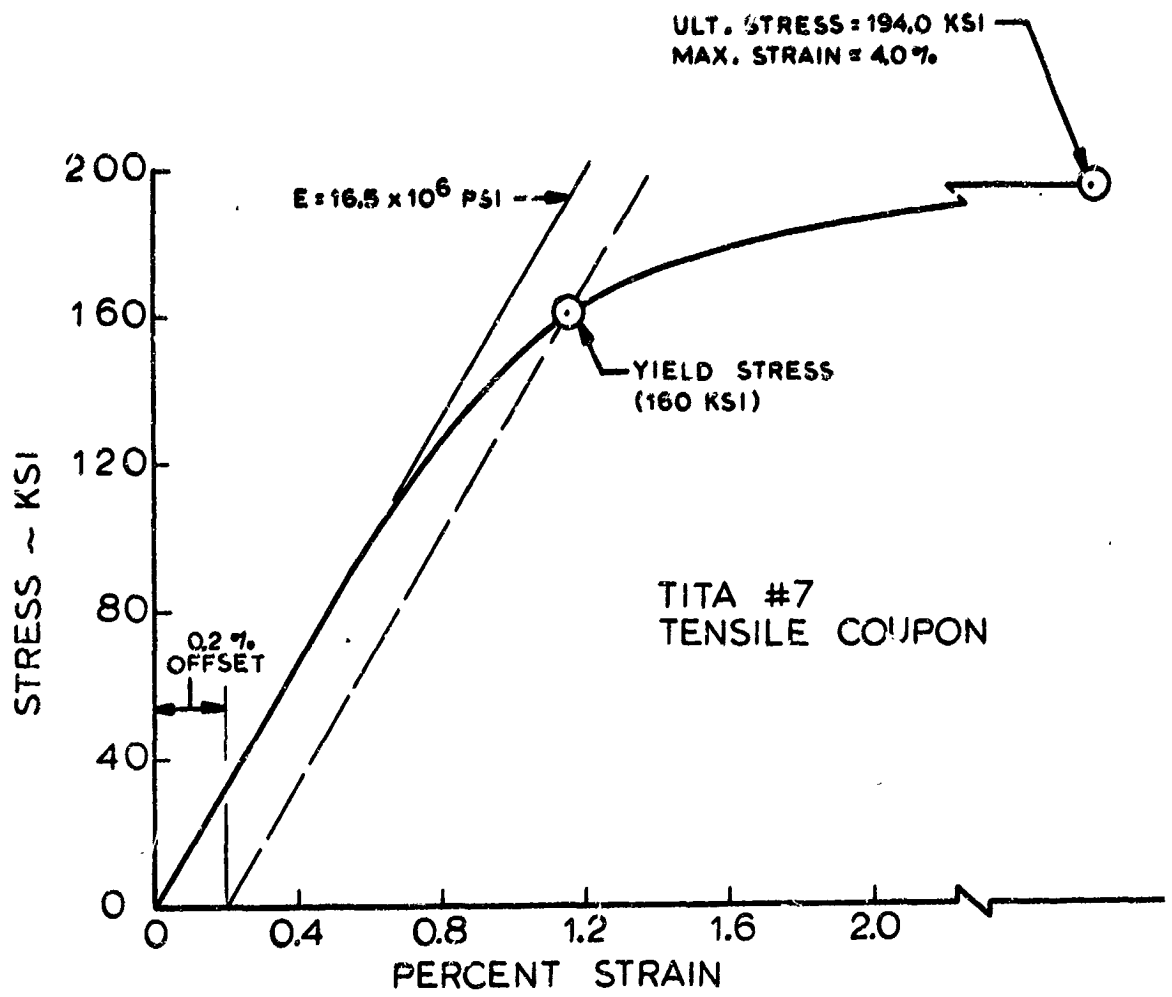


Fig. 6-10 Stress-Strain curve for coupon

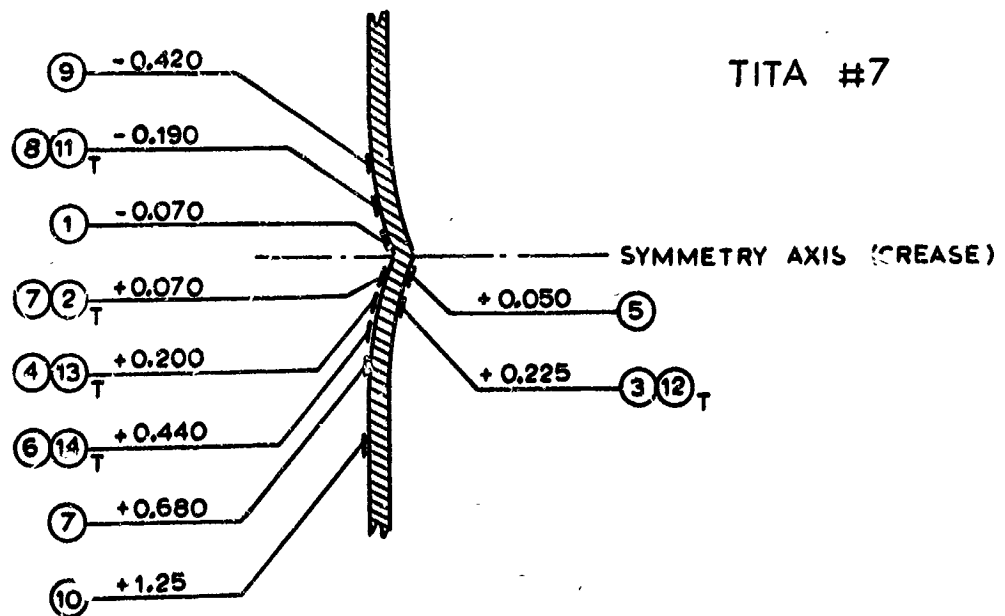
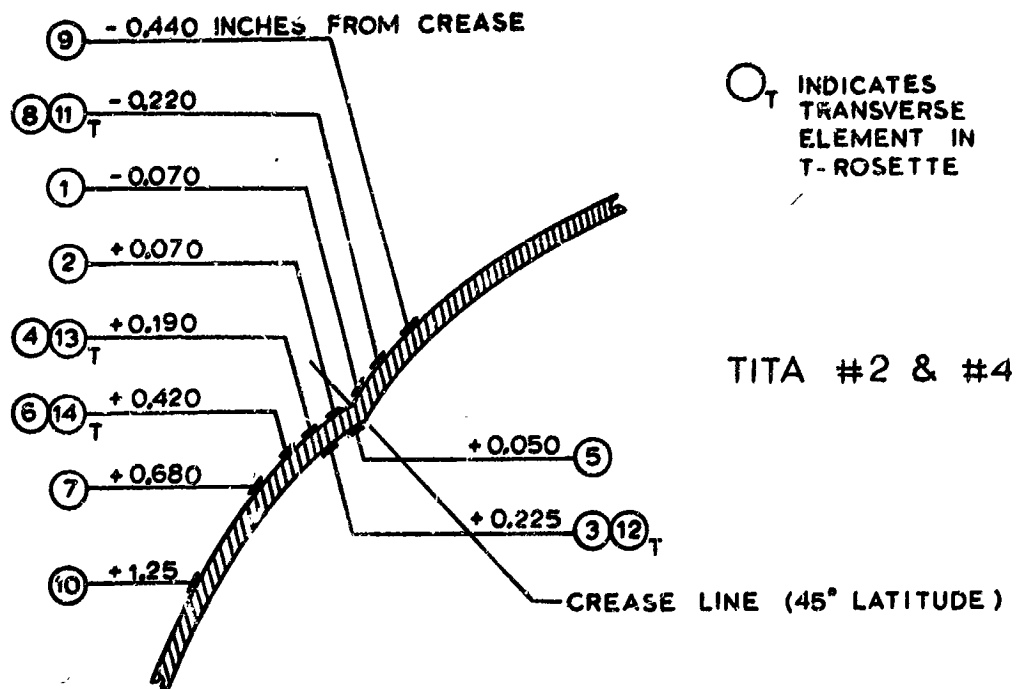


Fig. 6-11 Strain gage locations

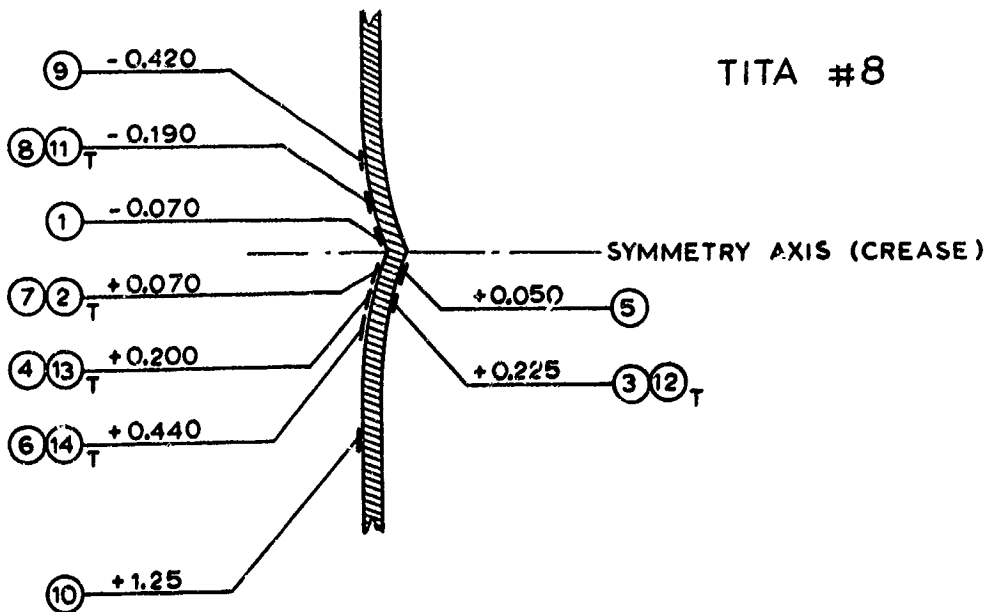
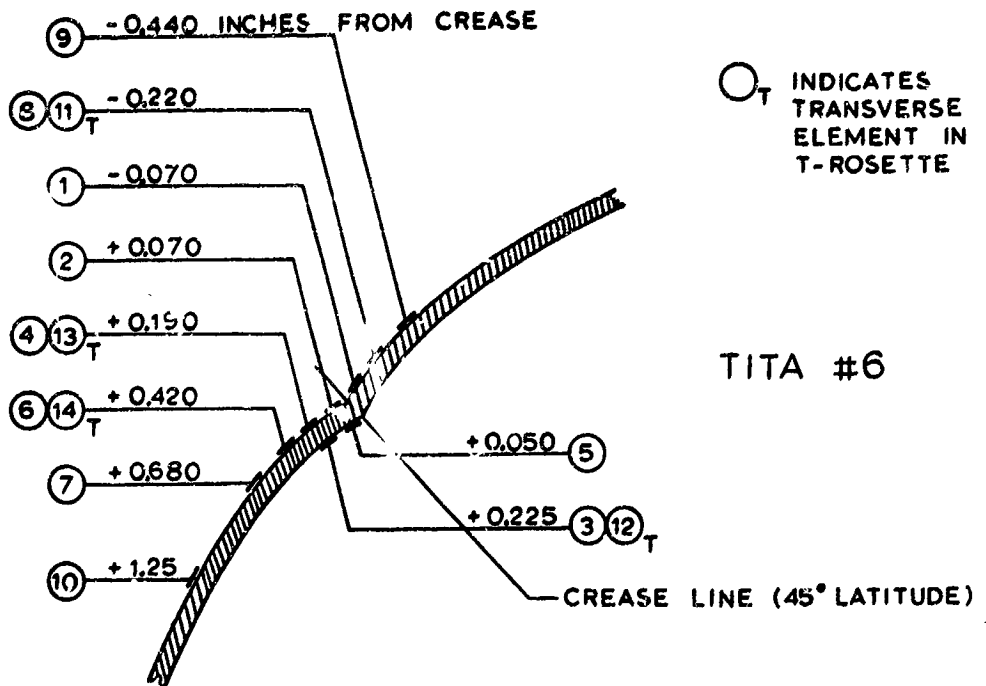


Fig. 6-12 Strain gage locations

TABLE 6.2

TITA #2, #4 & #7

STRAIN GAGE DIRECTORY

Gage Number	Rosette Mate (if any)	Orientation Longi/Transv.	Surface Inside/Outside	Distance from Crease Inches	Tita #2 Thickness at Gage Inches	Tita #4 Thickness at Gage Inches	Tita #7 Thickness at Gage Inches
1		L	Outside	- .070	.040	.040	.046
2		L	Outside	+ .070	.041	.042	.049
3		L	Insi	+ .050	.041	.042	.049
4	R-13	L	Outside	+ .190	.041	.041	.049
5	R-12	L	Inside	+ .225	.041	.042	.046
6	R-14	L	Outside	+ .420	.041	.040	.047
7		L	Outside	+ .680	.038	.032	.046
8	R-11	L	Outside	- .200	.041	.040	.046
9		L	Outside	- .440	.042	.040	.046
10		L	Outside	+1.25	.041	.032	.047
11	R-8	T	Outside	- .200	.041	.040	.046
12	R-5	T	Inside	+ .225	.041	.042	.046
13	R-4	T	Outside	+ .190	.041	.041	.049
14	R-6	T	Outside	+ .420	.041	.040	.047

TABLE 6.3

TITA #6

STRAIN GAGE DIRECTORY

Gage Number	Rosette Mate (if any)	Orientation Longi/Transv.	Surface Inside/Outside	Distance from Crease Inches	Tita #6 Thickness at Gage Inches
1		L	Outside	- .070	.031
2		L	Outside	+ .070	.036
3*	R-12	L	Inside	+ .225	.035
4	R-13	L	Outside	+ .190	.035
5*		L	Inside	+ .050	.036
6	R-14	L	Outside	+ .420	.033
7		L	Outside	+ .680	.026
8	R-11	L	Outside	- .200	.033
9		L	Outside	- .440	.037
10		L	Outside	+1.25	.027
11	R-8	T	Outside	- .200	.033
12	R-3	T	Inside	+ .225	.035
13	R-4	T	Outside	+ .190	.035
14	R-6	T	Outside	+ .420	.033

*Difference between Tables 6.3 & 6.4 is that Gages 3 & 5 are interchanged (and thicknesses)

TABLE 6.4

TITA #8
STRAIN GAGE DIRECTORY

Gage Number	Rosette Mate (if any)	Orientation Longl/Transv.	Surface Inside/Outside	Distance from Crease Inches	Tita #8 Thickness at Gage Inches
1		L	Outside	- .070	.045
2	R-7	L	Outside	+ .070	.048
3	R-12	L	Inside	+ .225	.045
4	R-13	L	Outside	+ .200	.045
5		L	Inside	+ .050	.045
6	R-14	L	Outside	+ .440	.045
7*	R-2	T	Outside	+ .070	.045
8	R-11	L	Outside	- .190	.048
9			Outside	- .420	.047
10		L	Outside	+1.25	.045
11	R-8	T	Outside	- .190	.048
12	R-3	T	Inside	+ .225	.045
13	R-4	T	Outside	+ .220	.045
14	R-6	T	Outside	+ .440	.045

6-23

*Extra rosette element added
Several gages shifted rel. to sinkage

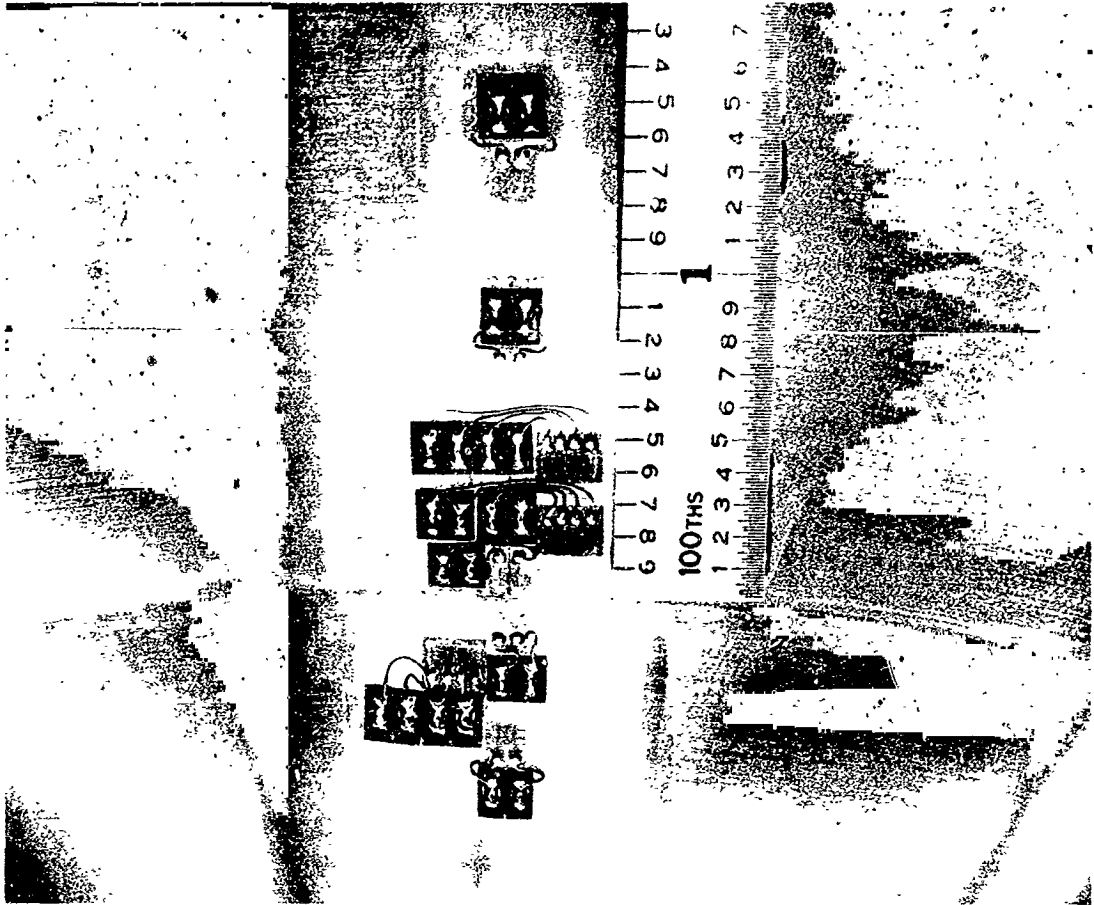


Fig. 6-13
Detail of strain gage installation

the data in digital form on a tape for test monitoring purposes, and two, a perforated tape punch so that the data can be processed on a computer.

To obtain strain data in engineering units, the DC bridge voltage is set at approximately two. The exact voltage is set with a finely adjustable control to produce the desired number of digital counts upon application of a precision calibration shunt to the gage.

The largest source of inaccuracy in the system is the manufacturer's stated precision of the gage factor (plus/minus half a percent). The resolution and repeatability of the system is one microstrain. This fact is made amply evident from the strain tables which are discussed further on.

A close-up of the strain gages installed on Tita #2 is shown in Fig. 6-13. The larger (main) leads to the gages are not yet connected, but a light film of Gagekote 2 has been applied, partially obscuring the gages. The line across the top of the scale is the center of the crease.

6.3.2 Pressure Measurement

Pressure was measured by two independent devices in parallel with the pressure line into the specimen. One of these was a Teledyne Model 206-SA strain gage bridge pressure transducer with a range from zero to 2000 psi, and the other was a Heise precision dial gage with the same range and a resolution of 2.5 psi. The Teledyne gage was connected to the above mentioned DAS, and the bridge excitation was adjusted to produce one count per psi of pressure. This transducer was also connected to a strip chart recorder for recording peak values and the time-pressure history of the test (in case needed for diagnosis).

6.3.3 Pressurization Device

Hydraulic pressure was obtained from an electrically driven hydraulic power supply, and controlled by a Research Inc. "Servac" unit which in turn controlled a Moog Series 73 servovalve with a two gpm capacity.

A ramp voltage generator also capable of holding a constant voltage at any desired level, was used to supply a command voltage to the Servac, thus

assuring smooth pressure increase with no overshoot at the pressure plateaus.

6.3.4 Test Procedure

Prior to welding the closure, the specimen thickness was uniformly mapped (in the vicinity of the test region). Gages were installed in a cluster in the thinnest region located. Thicknesses were measured using a sheet metal micrometer with a resolution of .0005 inches, at approximately two-inch intervals circumferentially and at 0.20 inch intervals longitudinally for three intervals on either side of the crease centerline. Circumferential measurements at one inch intervals were added on either side of the longitudinal section determined to be the thinnest, and destined to be the location of the strain gage cluster. The thicknesses were recorded directly on the specimen as shown in Fig. 6-14.

After closure welding, strain gage installation, and connection to the hydraulic power supply, all air was bled from the system through a T-fitting right at the specimen connection, and the specimen was installed inside a section of thick-walled pipe for personnel protection. Tita #2, fully gaged and ready for test (but not yet enclosed) is shown in Fig. 6-15.

Pressure was applied in a series of steps, with the pressure increase between the plateaus being smooth and gradual (about 100 psi per minute). The plateaus (on the pressure vs. time record) were set at nominally 100 psi increments (50 psi for Tita #2 and #4). Strain and pressure readings were taken at these plateaus while the pressure was being held constant. After reaching the third (ascending) plateau and taking readings at this level, the pressure was returned to zero, at which time a full data scan was again taken. On the next cycle, the first (lowest) plateau was set at the level of the second plateau of the previous cycle, so that the highest plateau of each cycle was one pressure increment higher than the highest pressure of the previous cycle. Each cycle thus consisted of taking strain readings at three pressures, followed by a return to zero. The pressure increments between each reading (on each cycle) were nominally equal. The reason for this loading pattern was to identify the onset of yielding and will be more apparent after reading the section on Data Processing (Section 6.4).



Fig. 6-14
Typical thickness mapping (Tita #7)



Fig. 6-15
Tita #2 ready for test

The cycling was continued until the peak pressure indicated in Table 6.1 was reached. Real failure occurred on only one specimen, Tita #7, which failed at 1550 psi. The failure is shown in Fig. 6-16. There was strong evidence that in this case the failure originated in one of the closure welds at the site of a small inclusion in the weld. The sinkage zone in this specimen (which had intentionally been taken well into the plastic stress range), showed considerable "straightening out". Tita #4 failed gradually (800 psi) at a cap closure weld. The hairline crack which formed was too fine to photograph, and is not really pertinent test information.

Since the analysis made for the test specimens does not consider local variations in thickness, and must operate on the assumption of a mean thickness, it was at first considered appropriate to supply only the mean thicknesses in the vicinity of the strain gage clusters. It was then decided that in case more elaborate analyses should some day make it desirable to review these test results, the actual thicknesses at each gage site are furnished in Tables 6.2 through 6.4.

6.4 Data Processing and Presentation

6.4.1 Data Normalization

The data was processed in the same way on all tests except the first test on Tita #2, and here the variation is slight. The general procedure will be described, then the departures from this (on Tita #2) will be pointed out.

The basic purpose of the loading sequence and data processing was to recognize and emphasize the onset of yielding, and to make it possible to differentiate between nonlinear elastic behavior and nonlinearity due to plastic stress. The key to this lies in being able to measure strain at exactly the same pressures on successive loading cycles, where each cycle progresses to some pressure level higher than the preceding cycle. The problem was to take measurements at exactly the same pressure, for purposes

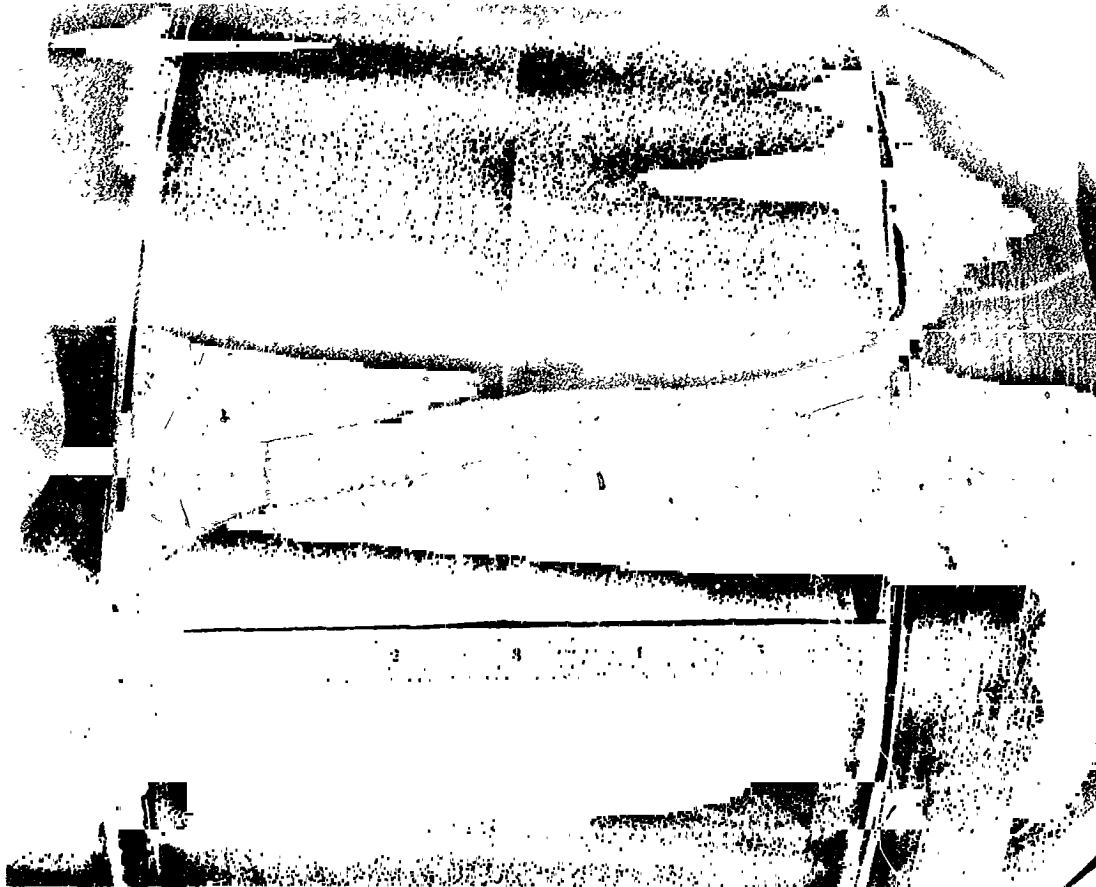


Fig. 6-16
Tita #7 after failure at 1550 psi

of comparing strain. The solution was to take strain readings at several pressures on each cycle, and to set these pressures so that their values overlapped and gradually increased from one cycle to the next. If the increment of pressure between successive strain measurements (on the same cycle) were not too large, it would then be possible to interpolate to some "exact" pressure value for each cycle. Because of the overlapping of actual pressures in the data taking on successive cycles, there could be overlapping, or more correctly, coincidence, of the interpolated "exact" pressure values from one cycle to the next.

For example, on the first test on Tita #4, full scans of strain data were taken at 194.1, 245.3, and 298.3 psi on the first cycle of the test. On the second cycle, data scans were made at 248.3, 298.7 and 350.2 psi. By interpolation it is possible to obtain the strains that would have been measured at 200, 250 and 300 psi on the first cycle, and at 250, 300 and 350 psi on the second cycle. After doing this it is then possible to compare strains at 250 and 300 psi pressures for cycles #1 and #2. The pattern can be continued throughout the test to the failure pressure. It should be added that it was sometimes necessary to extrapolate instead of interpolate. Also, that upon return to "zero" pressure at the end of each cycle, the pressure was not quite at zero, and so it was necessary to extrapolate the strain that would have been measured at zero pressure. In this case, the strain/pressure slope used to extrapolate to zero was that measured to the first pressure station on the first cycle, for the strain gage in question.

This interpolation process must of course be performed for each strain gage. The process, which was set up for handling by Tymshare computer was incorrectly called "Data Normalization", but the name was retained since it appeared on numerous printout sheets. A more correct name would be "Data Interpolation". This has the drawback of not sounding so impressive or "accepted".

That the technique leads to usefully accurate results is amply evident from the strain tables which are found in Appendix E. At the lower pressure readings (where plastic flow is unlikely) there are several gages where strain is repeated on successive cycles to within one microstrain (a "micro-strain" is one micro-inch per inch strain). On most gages, the repeatability

at low pressures is within plus/minus three microstrain. The few cases where repeatability is outside this range are believed to be gages where some plastic behavior was present even at low pressures.

The data is presented in three separate tables explained in the following sections.

6.4.2 Summary of First and Last Readings

Towards the end of a test, usually on the last cycle (when it was known to be such), readings were taken at every nominal pressure level used in previous cycles, the idea being that a strain vs. pressure relationship for the "initial pressurization" could be obtained by listing the strains corresponding to the peak pressure of each cycle. This can then be compared to the strains obtained at the corresponding same pressures on the last cycle (where readings are taken at every pressure station instead of only three). The columns of "First Strain" were used extensively in comparisons with the analytical work. While the "Last Strain" columns were not used, they may be of value in comparisons with future analytical work dealing with plastic behavior. The data in the "First and Last Readings" is normalized data as explained in the previous subsection. All values are listed in microstrain, with positive values representing tension.

On Tita #4, which was tested twice, once to 495 psi (with the highest strain readings at 450 psi), and again to 810 psi (with the highest readings at 800 psi), the two tests are included on the same sheet and marked as such. Note that Test #2 starts at 400 psi so that there is an overlap of data at 400 and 450 psi (on "First" readings). The column of "Last" readings are not continuous because in both tests (on Tita #4) the failures were not anticipated; it was not known that any given cycle was the last cycle, and so readings were not taken at each pressure increment as needed for a full column of "Last" readings.

6.4.3 "Normalized Strain on Successive Cycles"

The data in these tables is the basic normalized strain data, each column representing a pressure, each row a given cycle. The tabulated values

are microstrain, with positive values being tensile.

The "zero" pressure column lists the strain upon return to zero pressure after the previous cycle. For cycle #1 this strain should obviously be zero. This is not the case for Tita #2 which was "pre-cycled" to 200 psi before taking the cycle #1 readings, (see 6.4.6).

6.4.4 Zeros and Other Aspects of the Strain Tables

The single zeros in all experimental data tables of this report signify that no data was taken at that pressure on that cycle. The only exception to this is in the case of the zero pressure column where a zero does in fact indicate zero strain (readings were taken at zero pressure after each cycle except the last).

The gaps in the diagonal patterns of these tables where strain readings appear to be missing are where they were inadvertently not taken. The procedure is unforgiving in this respect, since any attempt to correct such an oversight would be meaningless. But the overlapping of three cycles provides a redundancy which makes an occasional oversight only a minor shortcoming.

It will be noted that when the pressure increment was 50 (or 100) psi, the first pressure listed in any table is not 50 (or 100) psi, but some multiple of this value higher. Readings were not taken at very low pressures because they would not have added useful data to an already voluminous listing. The reason is then strictly economic.

In general, the computer program was set up to operate with any one preselected pressure increment, and then to perform interpolations (or extrapolations) whenever two succeeding data scans fell within a pressure interval twice the size of the preselected pressure increment. Interpolations were then made to pressures which were integral multiples of the preselected pressure increment.

6.4.5 The Effective Strain Tables

It was originally felt that it would be helpful to calculate the effective strain for each "First" and "Last" reading and for each Tee-rosette.

(See 6.4.2 for "First" and "Last" reading explanation, and Section 3.1 for definition and explanation of "effective strain".) This data was subsequently found to be not as useful as originally anticipated, and was not used in comparisons with analysis. Since others may feel differently, and since the work of calculation is done, it is included.

6.4.6 Procedure on Tita #2

The classical load-strain test procedure usually calls for some cycling at very low loads to "break-in" the structure, the strain gages and their cement layer. In the case of the structure this was a veiled reference to yielding of the high spots, tight fits, etc., so that concentrated loads become distributed properly. In the case of strain gages and cements it is probably more superstition than fact, and possibly the older wire gages and Duco cement had some initial creep or ratcheting problems that were improved with a little "cold working", or some such effect. Be it as it may, the procedure was followed in the case of Tita #2, which was "precycled" to 200 psi before cycling began in earnest. Since the strains, even after this low a pressure, did not return to zero, some yielding was occurring (at some point in the structure if not at the gage site). It was then realized that strains on this precycle would not have been the same as on the subsequent "first" cycle. The precycling procedure was therefore deleted on subsequent tests. The strain reported for zero pressure, cycle #1, (Tita #2 only) is then the residual strain following a preliminary pressure excursion to 200 psi.

6.4.7 Onset of Yielding

There are two ways to recognize the onset of yielding from the "Successive Cycles" table. The first is non-repeatability of strain at any given pressure. The writer feels that plus/minus five microstrain non-repeatability is a suitable criterion because it is distinctly greater than the resolution of the instrumentation system and the subsequent processing procedure. If most gages will repeat to within a total span of four microstrain at three different pressurizations, it is reasonable to claim a resolution of plus/minus two microstrain. This claim can, of course, only be made with the knowledge that the system is inherently

very stable and the test set-up basically free from typical disturbances such as fluctuating "ambient" temperature, large sources of electrical noise, etc. In addition, the integrating voltmeter is a very stable device, electrical shielding was used on all leads and a "guard system" is incorporated in the scanner. The absolute strain readings may not be accurate to plus/minus two microstrain, but certainly the relative measurements (on any one gage) have this accuracy on repeatability. This accuracy begins to deteriorate after very large strain excursions (over 2500 microstrain or 0.25 percent strain), but the resolution allowance is multiplied by 2.5 for the criterion, and the criterion is usually applied before 2500 microstrain is attained.

The second sign of plastic strain is the build-up residual strain upon return to zero pressure (after each cycle). Here, the writer feels the discrepancy or resolution allowance should be increased to plus/minus ten microstrain. The reason for the larger allowance is two-fold: First, the extrapolation to zero operation uses a less reliable "correction slope" than those used at the higher pressure increments. Secondly, strains upon return to zero pressure have been found (on other testing programs) to be less repeatable than strains at some well defined load. This may be because the stresses that induce a given strain at the higher loads are large enough to overcome certain friction mechanisms that play a role in the strain magnitude, whereas at zero load/pressure levels the stress drops below a threshold level, and friction prevents the last deformations to from being "cleanly terminated". The gravity supports of the specimen itself may be significant in this respect. At high pressures, the force of the specimen's own weight at its support points is negligible compared to the force sustained by any comparable cross-section area under tension due to the pressure.

It should also be emphasized (for the benefit of the reader who may feel he is only concerned with the experimental aspects of this report), that a nonlinear pressure-strain relation at any gage is not necessarily an indication of plastic stress. The structure is inherently nonlinear in the elastic range. This is discussed more fully in the analytical portion of this report.

Another caution which should be mentioned is that a strain gage can give the indication of plastic strain (as defined above) even though plastic stress has not occurred at the site of the gage itself. If plastic strain has occurred in the vicinity of a gage (but not at the gage), it will cause stress redistributions which break the normal pressure-strain pattern for the gage (and thus have the appearance of plastic strain). Furthermore, the plastically strained region will not return to its zero strain datum (upon return to zero pressure), so that adjacent regions must "balance" out the resulting geometrical anomaly. Any gage in the zone where the anomaly is "being balanced" will then show a residual strain. This explains why some "plastic strain occurrence" is evident at relatively low strain levels in some gages. The extent to which this occurs at a gage is of course a function of how near it is to a region under plastic strain and how severe the plastic strain is in that region.

6.4.8 Tita #6, Strain-Pressure Anomaly

In reviewing the summary of "First and Last" readings for this specimen, one observes a drop off in strain for gages 1, 2 and 5 as the pressure goes from 900 to 1000 psi. Although not apparent in the "First and Last" table, a similar anomaly exists for gages 4, 6, 7, 8, 9 and 10, and can be seen in the "Successive Strain" tables for those gages.

For gages 1 and 2 the center of anomaly is in cycle 7 where the strain cascades dramatically downward as the pressure rises from 800 to 1000 psi, but on cycle 8 (the last one), the values although diminished by the drop of cycle 7, resume an upward trend with increasing pressure. For gage 5, the downward trend (with increasing pressure) was evident (only slightly) even in cycle 6, and continues, though less dramatically, in cycle 8. In gages 4, 5, 7, 8, 9 and 10, the strains never decrease with increasing pressure (within each cycle) but do show a lower range of values on succeeding cycles after cycle 6. For gage 10 this is an almost negligible trend, but since this gage is 1.25 inches from the anomaly and is virtually a "membrane" gage, this is fully understandable.

The anomaly just pointed out is a vivid example of stress redistribution resulting from plastic flow in a region near the gage cluster. In effect, the structure is being altered, slightly in cycle 6, drastically in cycle 7, completely in cycle 8 except for some minor tapering off of the alteration process in cycle 8. But in cycle 8, the majority of the gages are "on a new structure" and behaving according to new rules. Gage 5, probably the closest to the disturbance is still in a region of change.

As discussed earlier, the gage cluster was placed on the thinnest region along the crease line. It is then highly probable that the yielding made evident by the above described anomaly is confined to a small zone along the circumferential crease. Under these circumstances, the membrane forces are being channeled around the yielded zone, and gages on either side would most likely have registered upward surges on cycle 7.

Section 7
CORRELATION BETWEEN THEORY AND TEST

A series of analyses using the elastic/plastic shell analysis program EP3OR was carried out for each one of the five test specimens used in the experimental program. These analyses were made using the appropriate stress-strain curve for each of the specimens, as developed from the coupon tests. The geometry was held as close to the measured data as possible, but in all cases a constant equivalent thickness was used, rather than the randomly variable one measured on some of the specimens.

Some data for the test specimens which are pertinent to this discussion are given in the table below. (For a more detailed description of the tests and the test specimens, see Section 6.)

Specimen	Geometry	Material (1)	Thickness (2)	Discontinuity Data		
				α_{ϕ}	α_{θ}	$\Delta\phi$
Tita #2	Sphere	A	0.040	4.15	3.15	14.9°
Tita #4	Sphere	STA	0.040	4.15	3.15	14.9°
Tita #6	Sphere	A/STA	0.034	4.43	3.38	14.9°
Tita #7	Cyl.	STA	0.050	2.89	3.28	10.2°
Tita #8	Cyl.	STA	0.050	3.86	3.93	15.3°

- (1) A = Annealed, STA = Solution Treated & Aged
(2) Used in the analysis

Note: The analysis of Tita #6 was made using material data for the annealed (A) condition.

The analyses made for the test specimens have been compared to strain gage readings, and plotted in the figures of this section. When making the

comparison between theory and test the following points should be remembered:

- o The strain gages could not be positioned at the point of maximum strain, i.e., at the center of the crease.
- o In the area of interest the strains are varying very rapidly (sometimes doubling in 0.1 inch of surface length) making the accurate determination of the position of the strain gage relative to the crease critical. However, the center of the crease is somewhat undeterminable due to the fact that the profile is not a sharp V, but rather a smooth U caused by the small finite radius required by the machine tool (see machine drawings in Section 6).
- o The analysis used points (stations) spaced about .05 inch in the discontinuity area. Thus, in general no exact correspondence between analysis stations and strain gage stations exist. Rather than interpolate between analysis stations, analysis stations on either side of the strain gage stations have been plotted in the comparison figures.

As is evident from the figures of this section, there exists a high degree of correlation between the tests and the analysis. This correlation is both qualitative and quantitative and includes both the elastic and the plastic regions. The rather pronounced elastic nonlinear effects in some parts of the shell are very nicely reproduced in the tests. The comparison between residual strains will have to be considered good, remembering that these strains are rather small compared to the total strains and that they therefore cannot be determined with as high a precision as the total strains, numerically and experimentally.

It is thought that a study of the accompanying figures will be more fruitful than a lengthy discussion. Therefore, only a few comments will be made on these figures.

Tita #2 (Figures 7-1 through 7-4)

Fig. 7-1 shows strains for the relatively low pressure of 400 psi, where the entire shell is in the elastic region. Both meridional and hoop microstrains*, inside and outside surfaces, are plotted as a function of the meridional surface coordinates. The center of the discontinuity (the crease) is at $s = 3.84$ inch.

Fig. 7-2 shows strain versus pressure plots for a number of strain gage locations. Note that gage 2, located at $s = 3.47$ inch, very accurately depicts the elastic nonlinearity followed by the plastic strain increase at higher pressures, resulting in an s-shaped curve. The hoop gages (the lower part of the figure) show a very close agreement with the analytical results, even without making allowance for the possibility of inaccuracies in the location of the strain gages.

Fig. 7-3 shows residual strains after 1000 psi pressure. Due to the very narrow zone of plasticity the correlation is not very conclusive. However, taken in the context of other tests (Tita #6, 7 and 8) where higher (and therefore more accurate) residual strains were encountered, Fig. 7-3 does, indeed, back up the theoretical analysis.

Fig. 7-4 shows the effects of repeated loadings into the plastic region. The reloadings are definitely elastic, though nonlinear, as predicted by the analysis (compare Fig. 3-9).

Tita #4 (Figures 7-5 and 7-6)

These figures are similar to the Tita #2 ones and the same comments apply. This test did not go into the plastic region.

Tita #6 (Figures 7-7 through 7-9)

Fig. 7-7 shows strains at the low pressure 400 psi, which does not

* 10000 microstrains = 1 percent strain

produce any plastic strains.

Fig. 7-8 shows strains as a function of pressure. Note the extreme nonlinearity at the gage 5 location which agrees very well with the predicted behavior: The strain first increases, while after having reached a maximum at about 600 psi it decreases with higher pressures.

Fig. 7-9 shows residual strains after loading to 1000 psi. The agreement between theory and test is almost exact.

The analysis for Tita #6 was carried out by using material properties for the annealed condition, even though only the area in the weld zone is in the annealed condition (the shell outside this zone is in the STA condition). The reason for using these properties throughout the shell is that only a very narrow zone will be in the plastic region, and that the surrounding area will be elastic. Since both the annealed and the STA stress-strain curves are practically identical in the elastic region the way in which the analysis was made is both justifiable and desirable. The accuracy is well borne out by the test results.

Tita #7 (Figures 7-10 through 7-13)

Tita #7 is a cylinder and has the mildest discontinuity of all tests.

The elastic behavior shown in Fig. 7-10 is very similar to the spheres, as predicted by the analytical results, as are the nonlinear, s-shaped curves of Fig. 7-11. Figures 7-12 and 7-13 show the progression of residual strains development as the pressure is increased. (Note the change in scales between the two figures.)

Tita #8 (Figures 7-14 through 7-16)

This test - a cylinder with a relatively large stress factor - shows excellent agreement between analysis and test. Particularly the residual strains, Fig. 7-16 show a high degree of correlation.

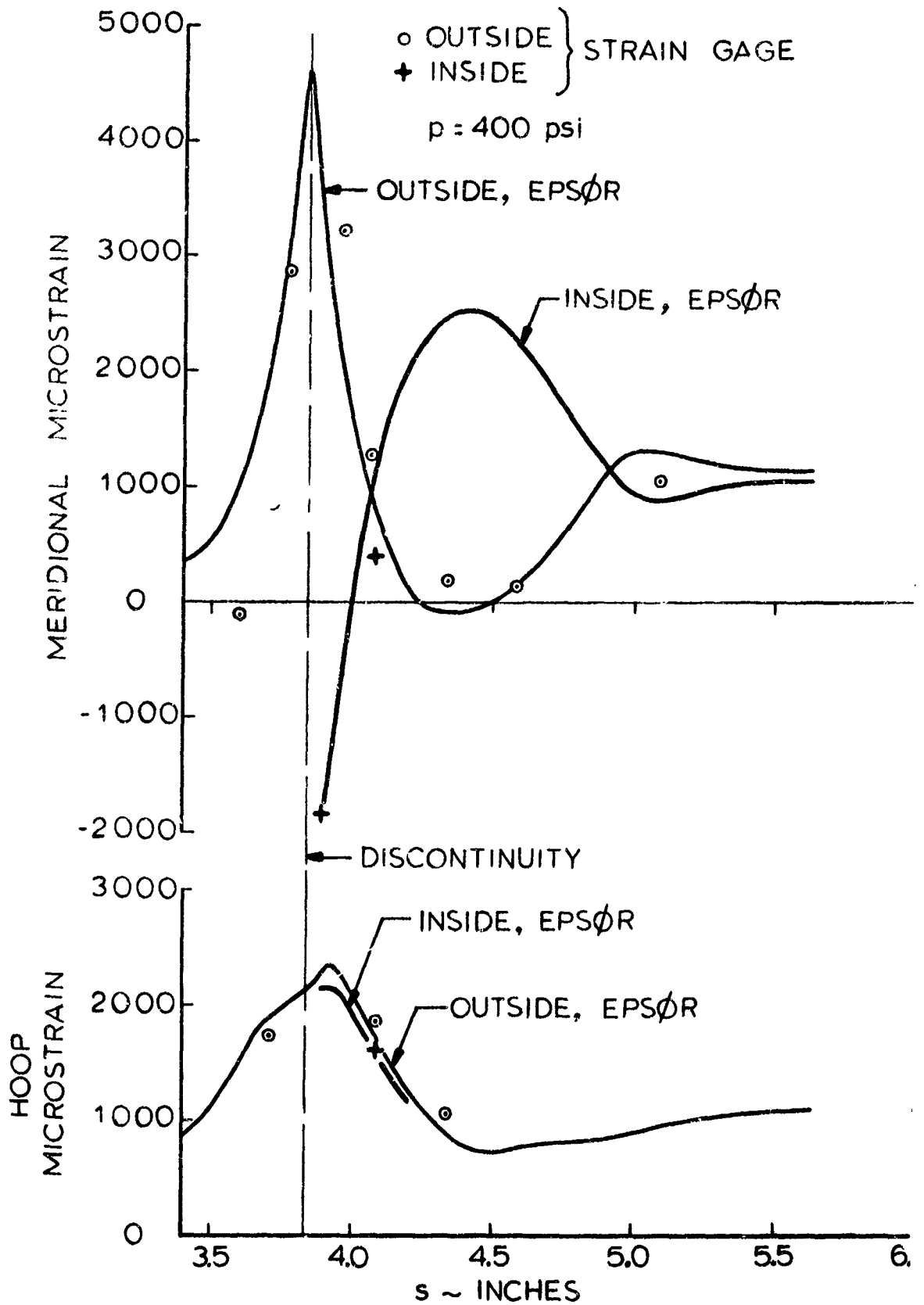


Fig. 7-1 Tita #2. Strains in the Elastic Region

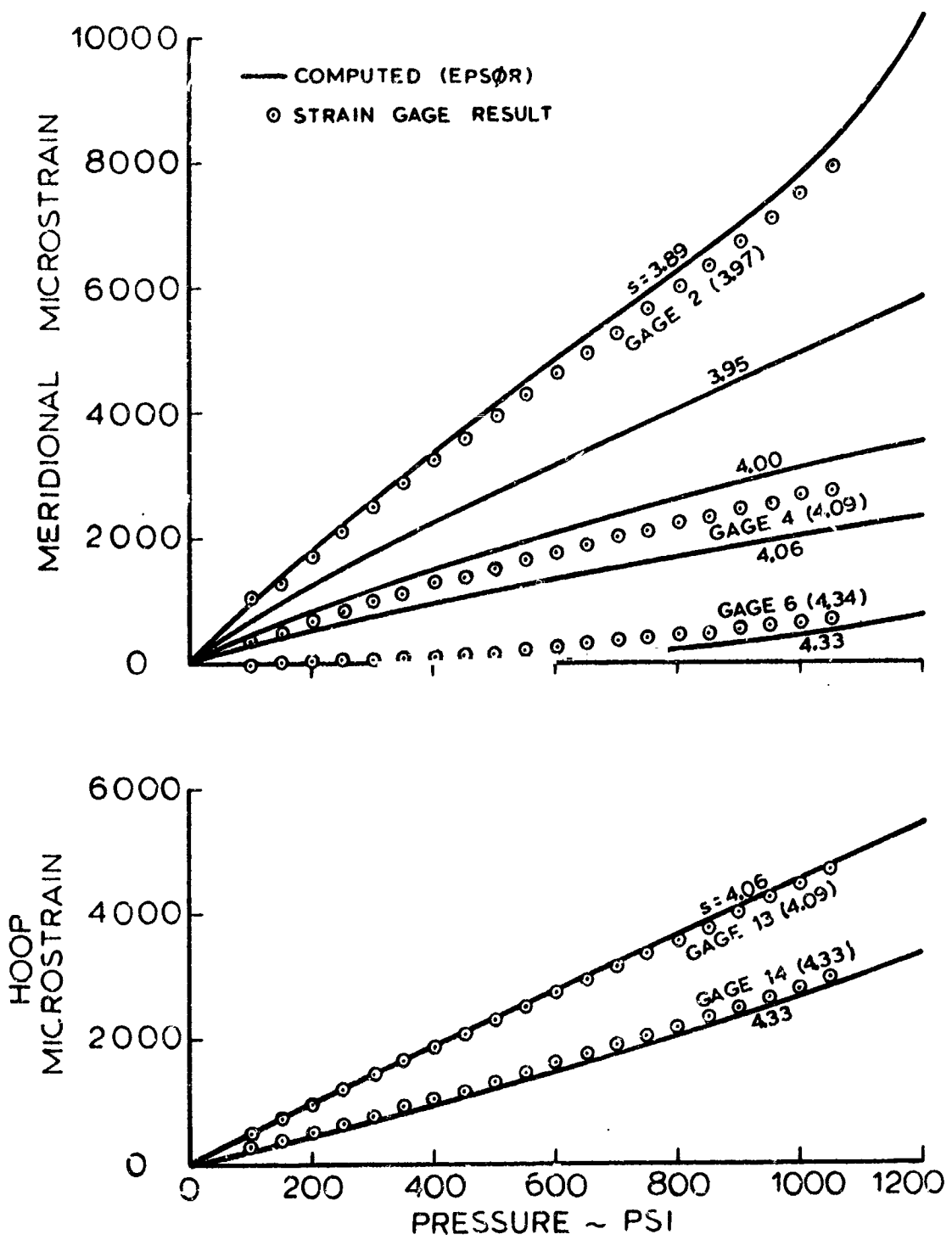


Fig. 7-2 Tita #2. Strains vs Pressure Plots

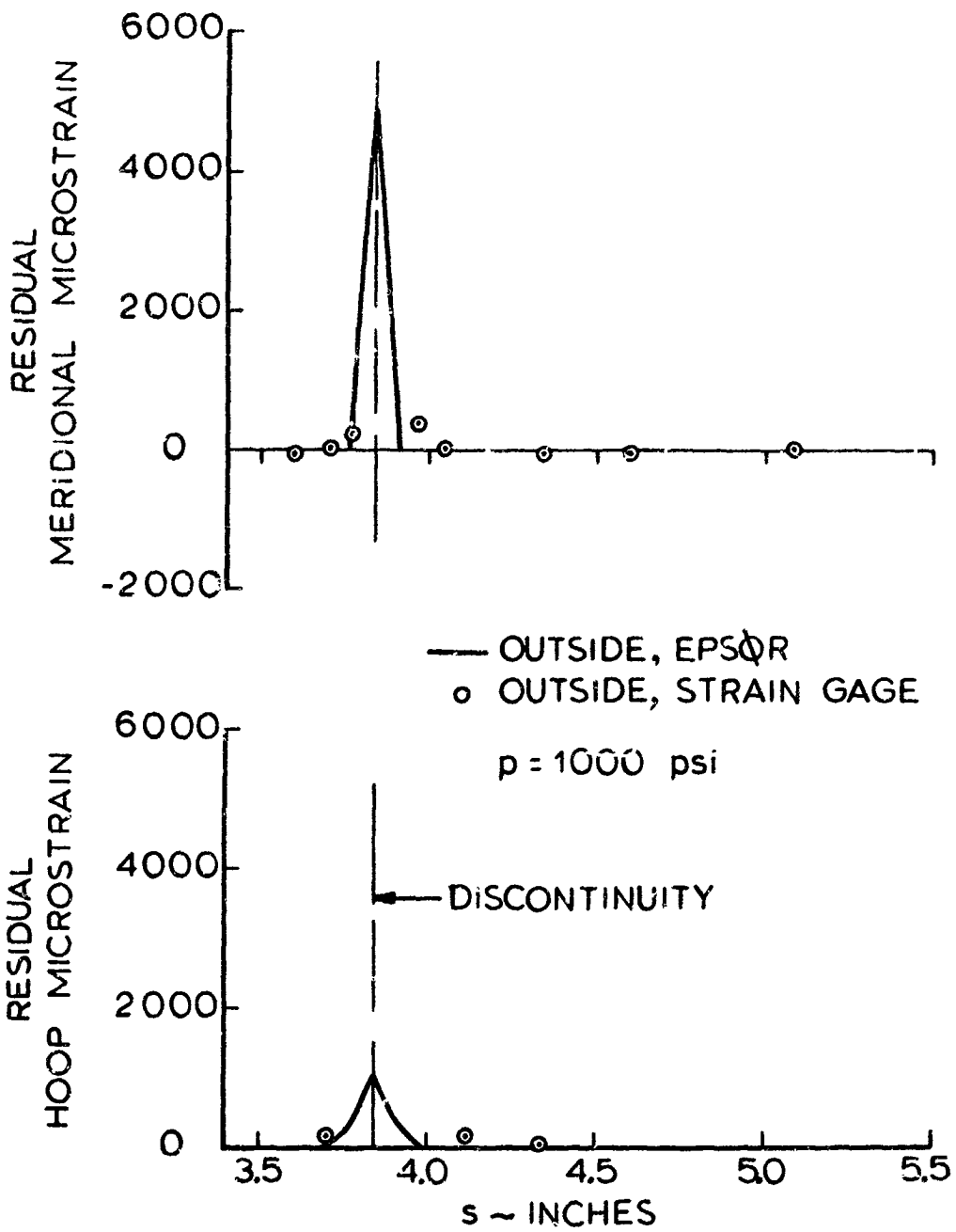


Fig. 7-3 Tita #2. Residual Strains

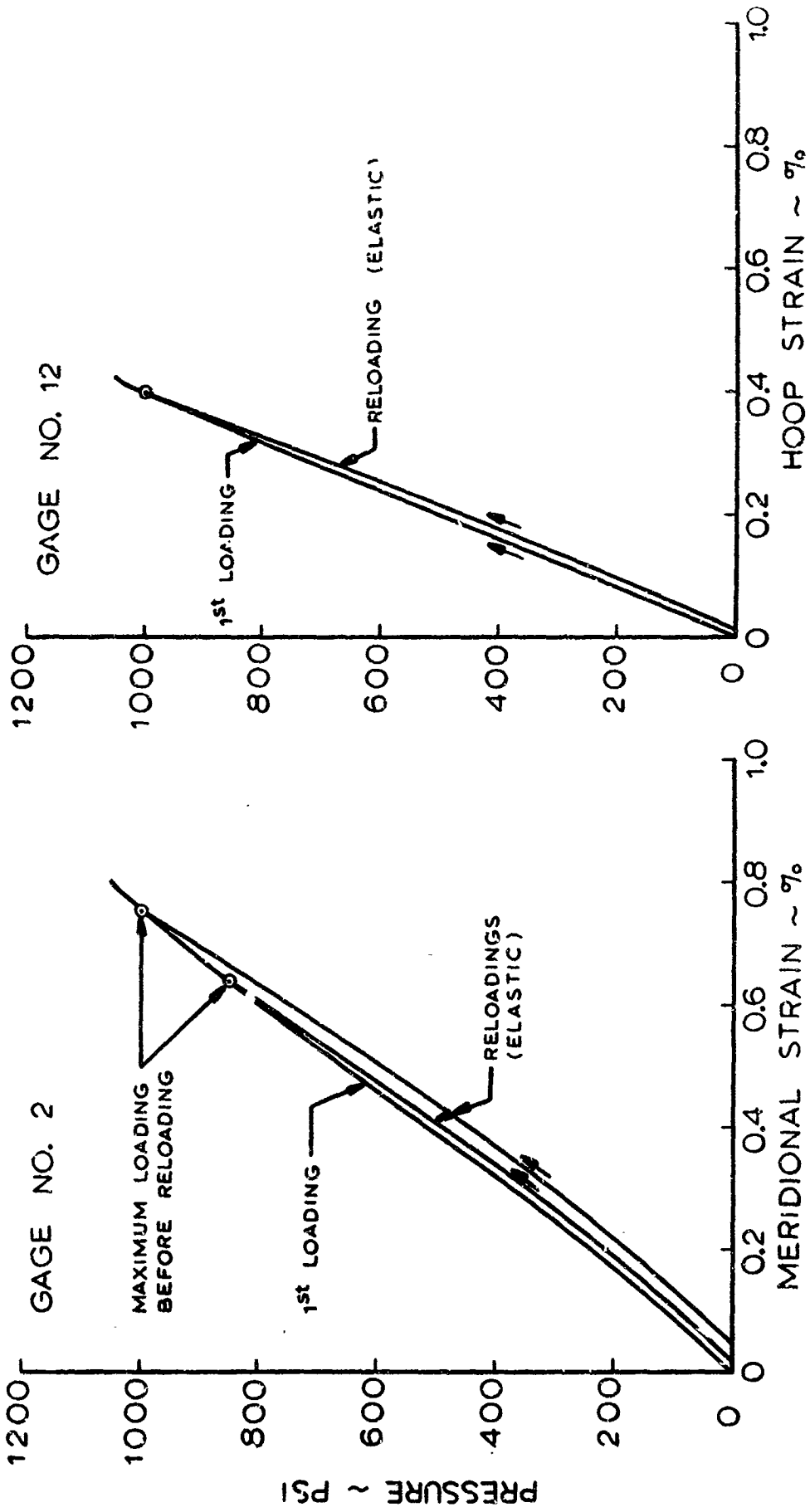


Fig. 7-4 Tita #2. Repeated Loading

NATIONAL BUREAU OF STANDARDS - DIVISION OF PHYSICS
 PHOTOGRAPHED BY THE NATIONAL BUREAU OF STANDARDS - DIVISION OF PHYSICS
 FROM THE ORIGINAL PHOTOGRAPH BY THE NATIONAL BUREAU OF STANDARDS - DIVISION OF PHYSICS

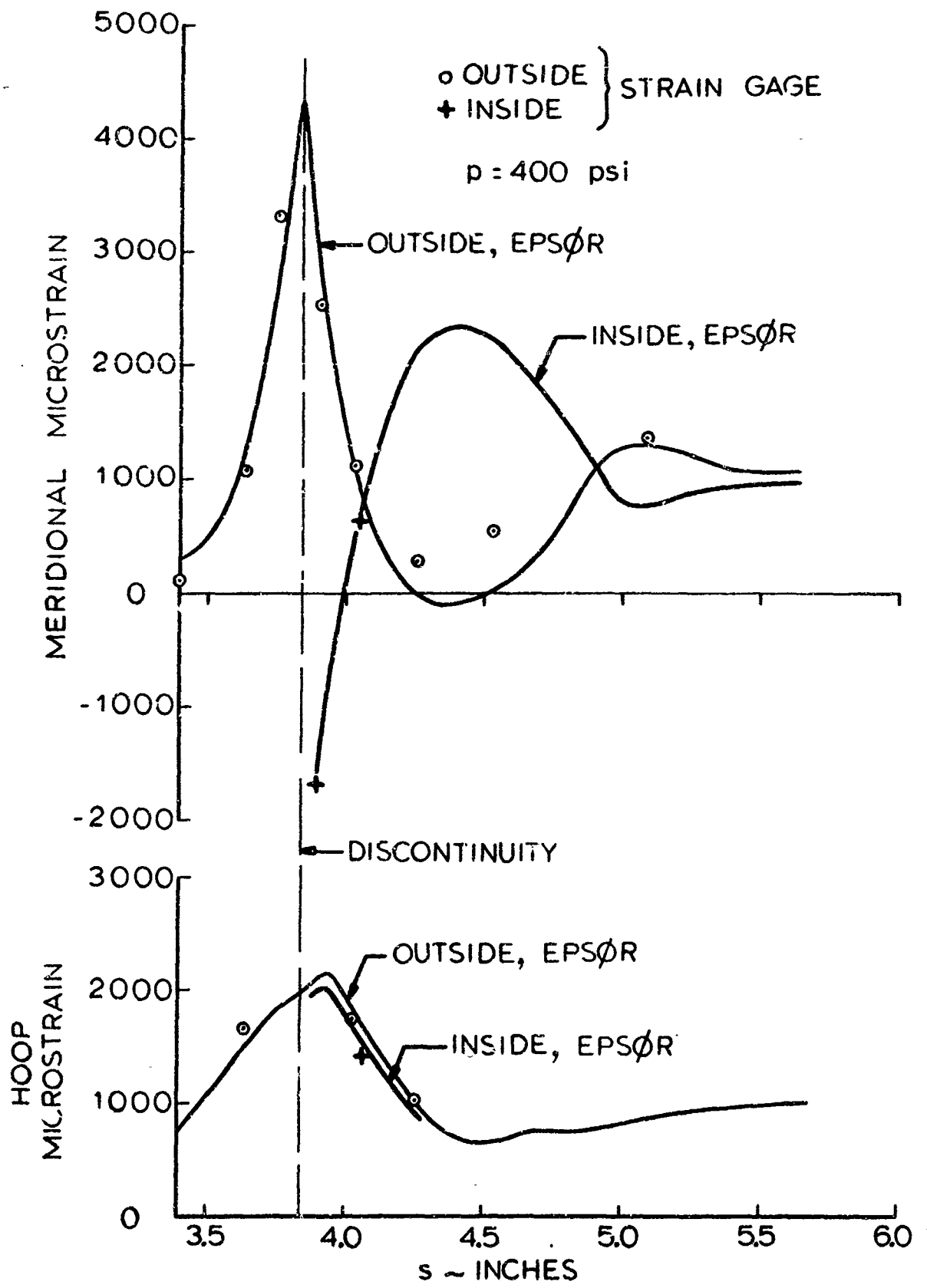


Fig. 7-5 Tita #4. Strains in the Elastic Region

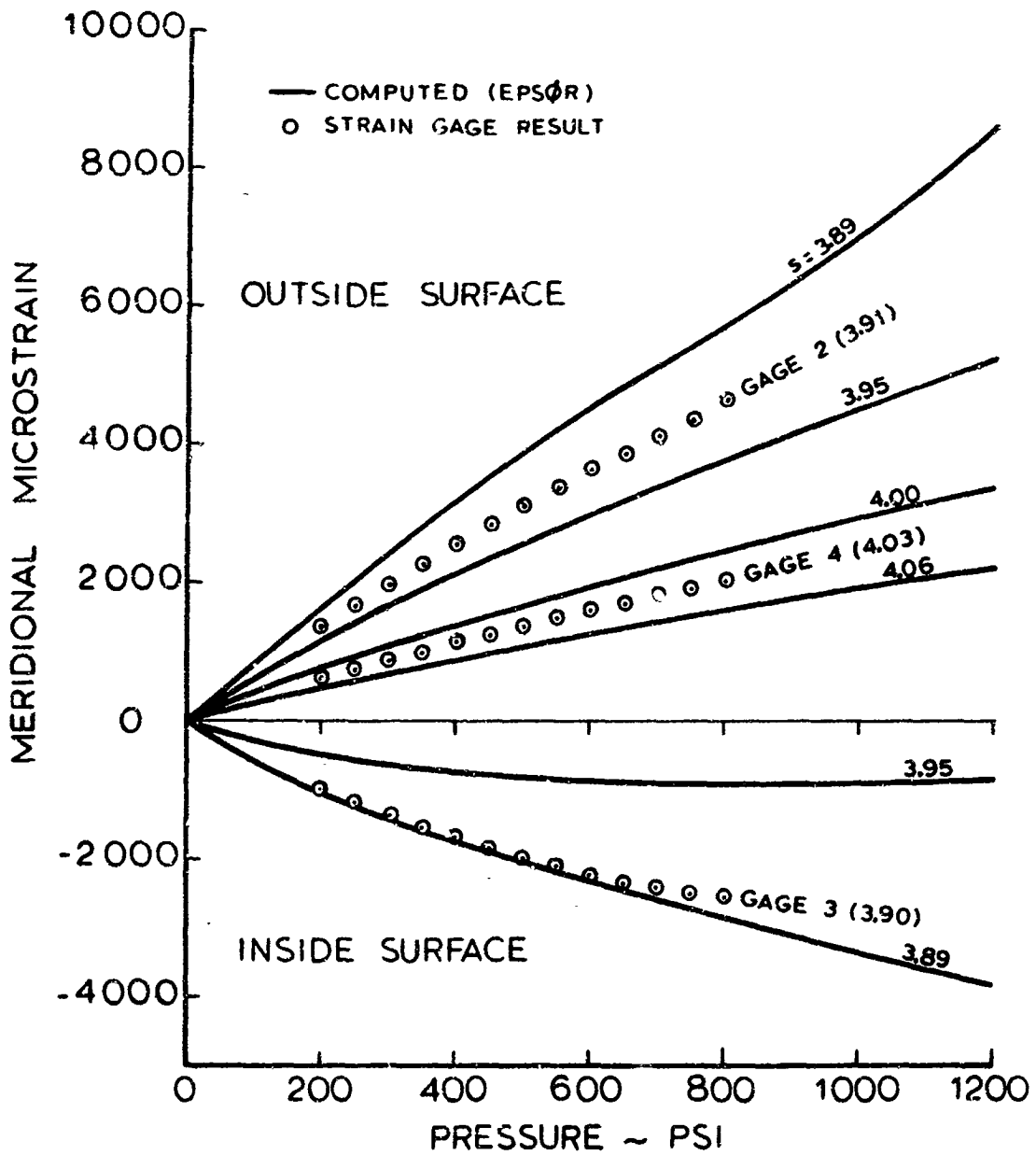


Fig. 7-6 Tita #4. Strain vs Pressure Plots

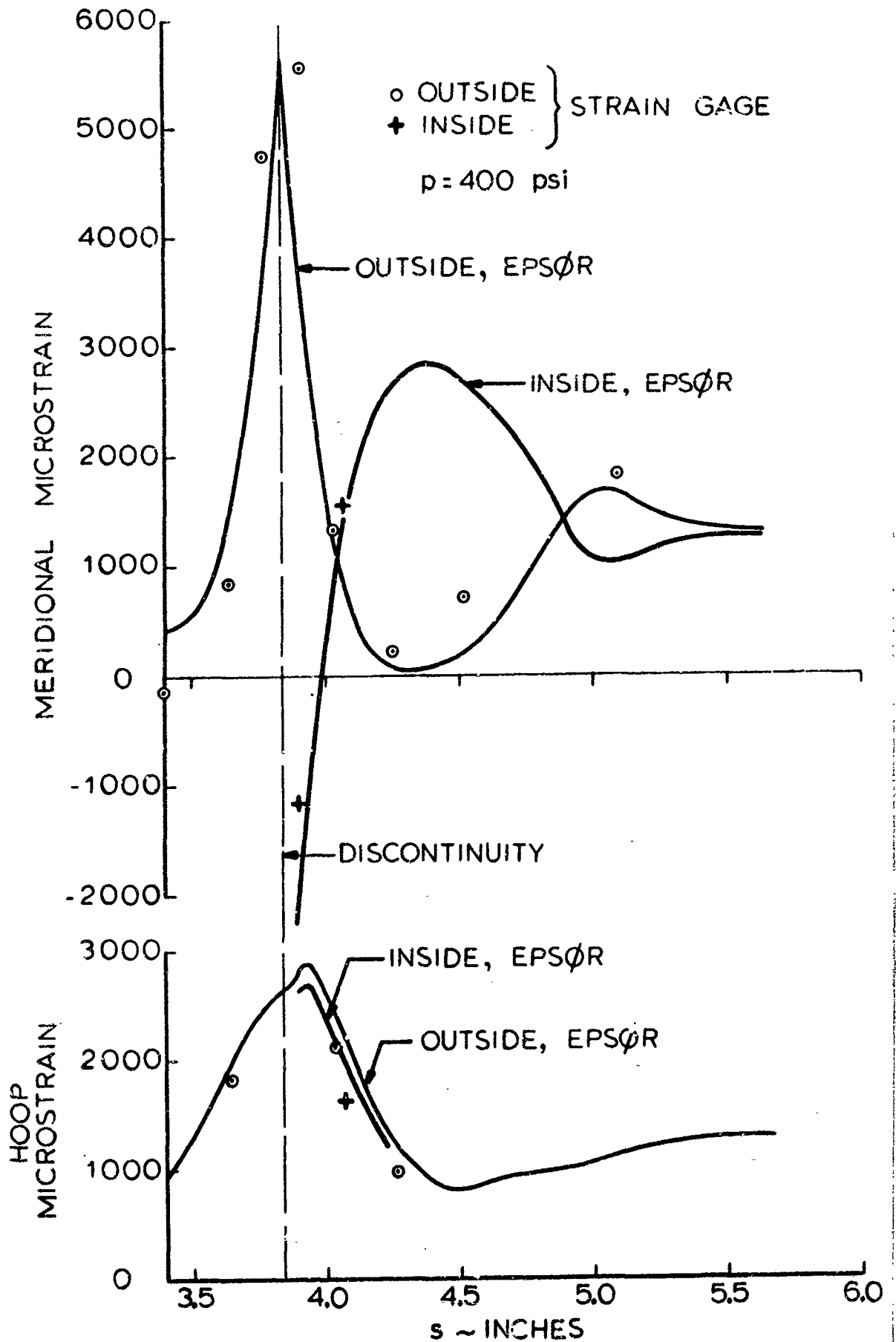


Fig. 7-7 Tita #6. Strains in the Elastic Region

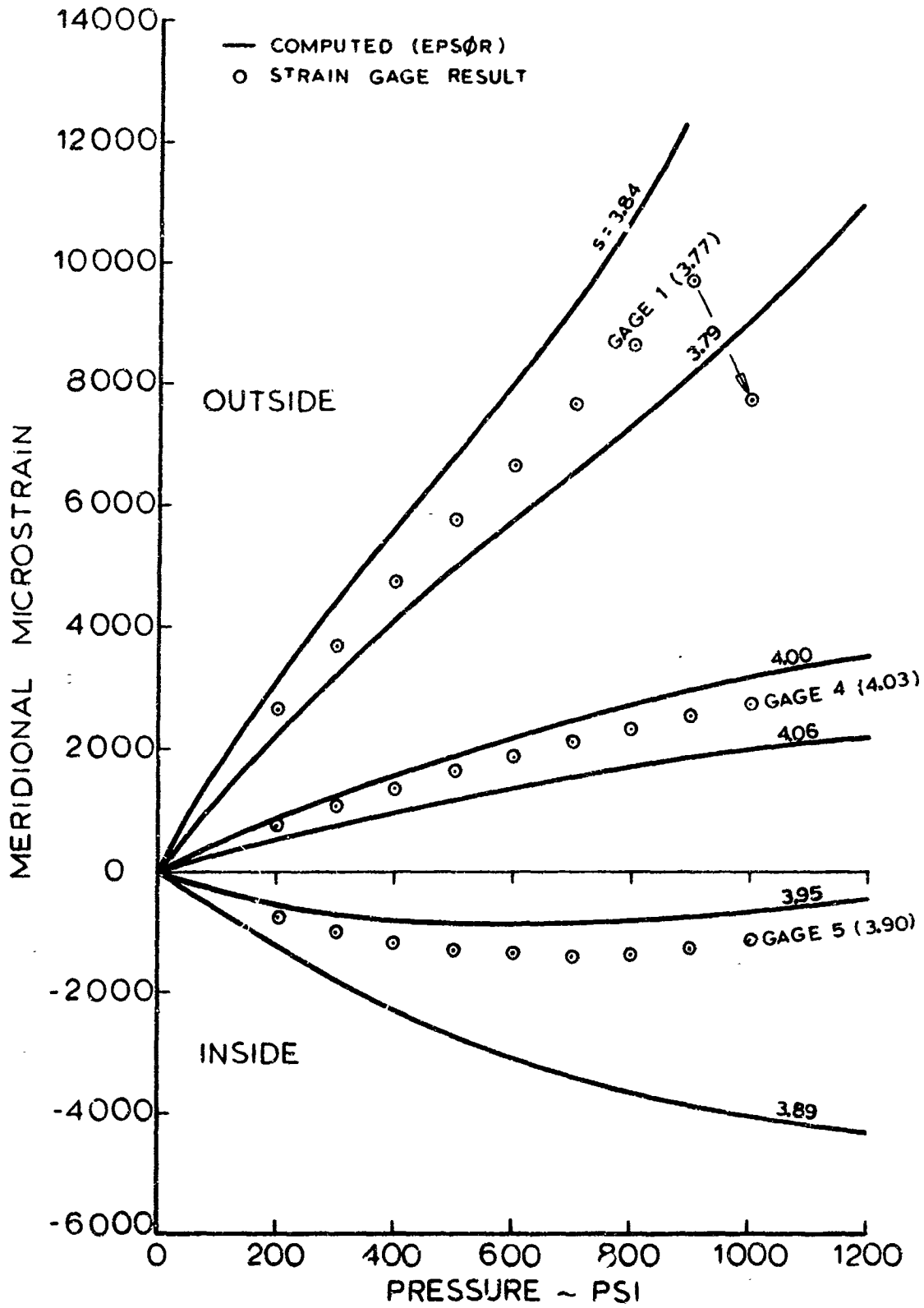


Fig. 7-8 Tita #6. Strain vs Pressure Plots

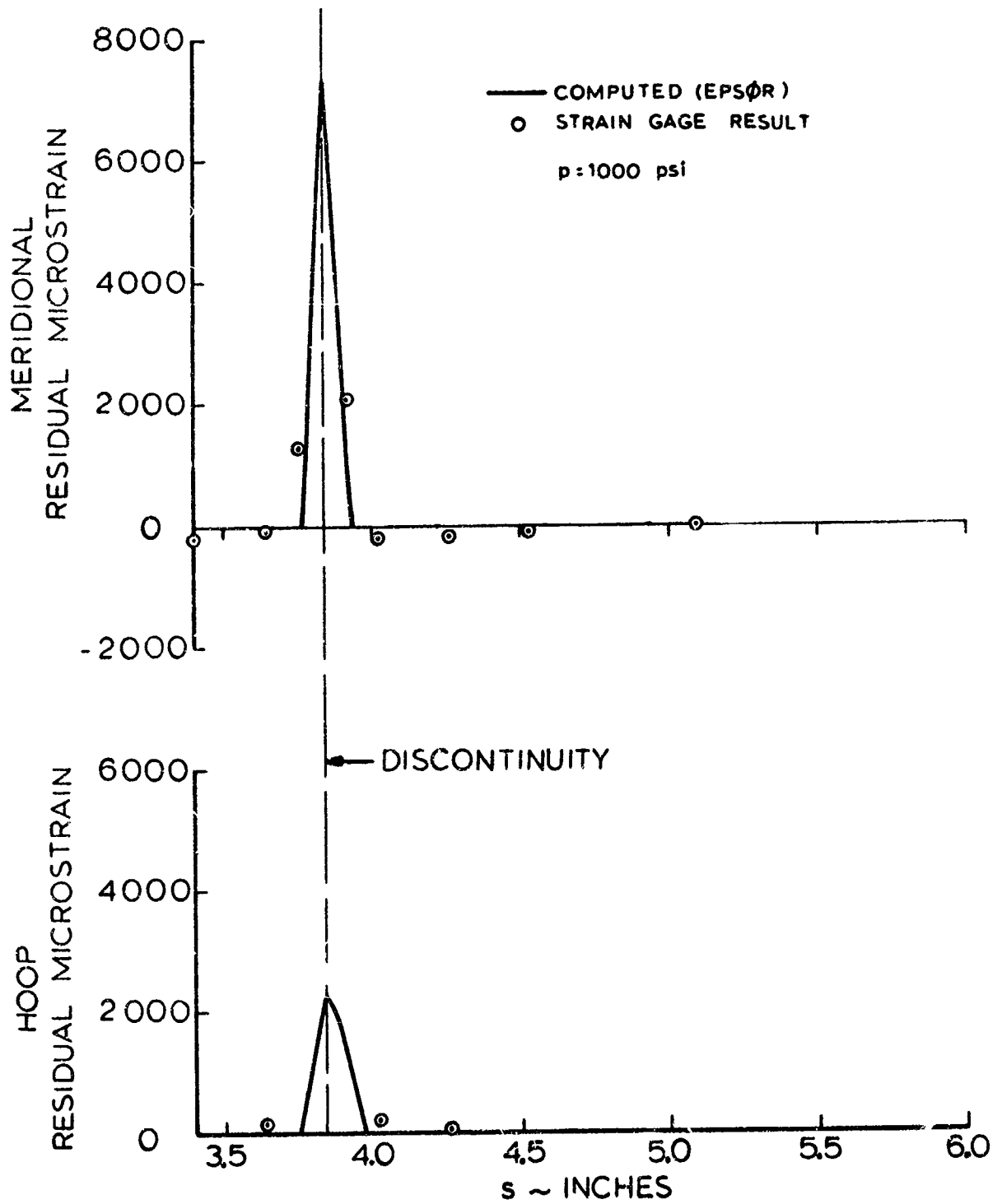


Fig. 7-9 Tita #6. Residual Strains

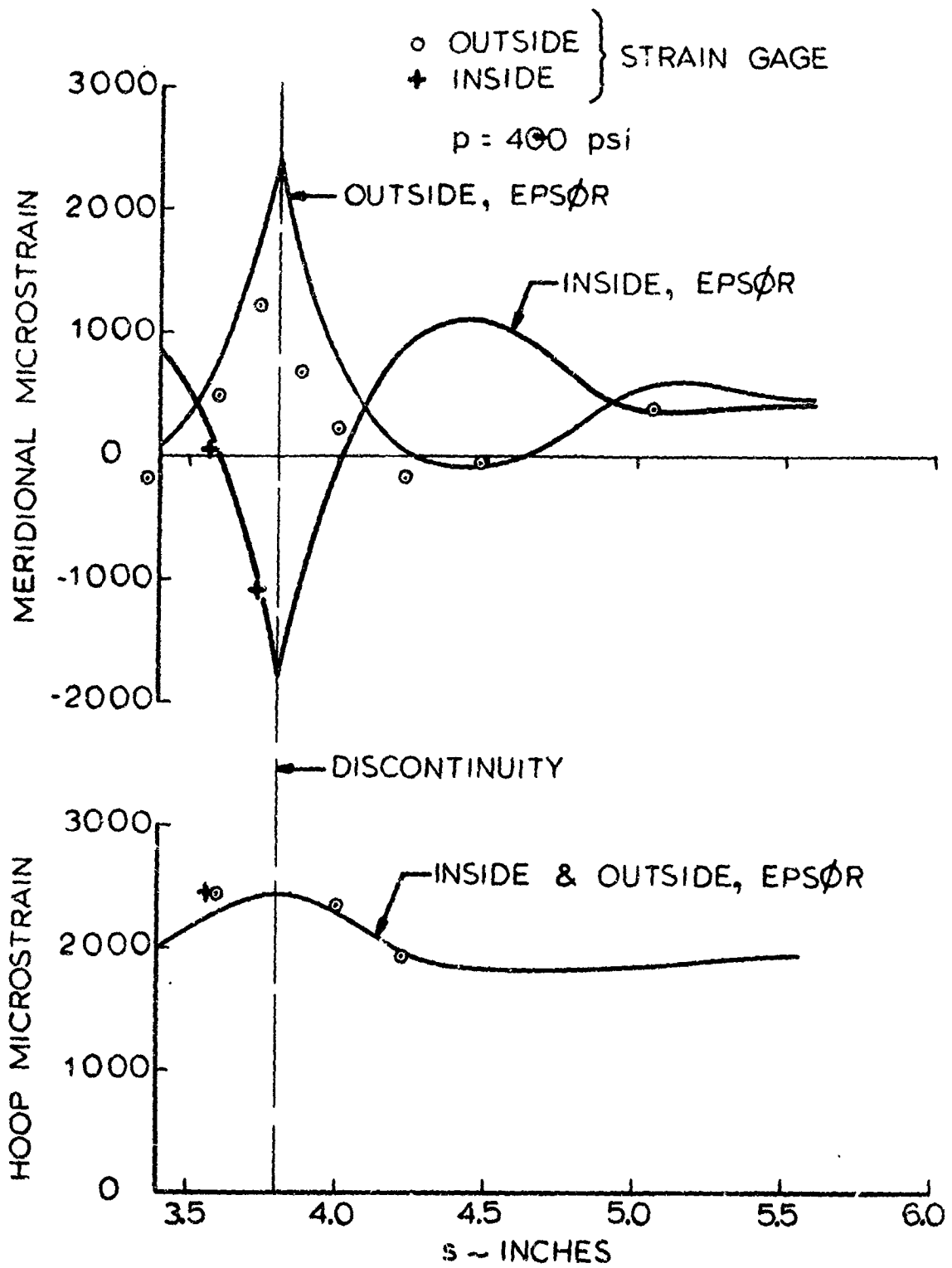


Fig. 7-10 Tita #7. Strains in the Elastic Region

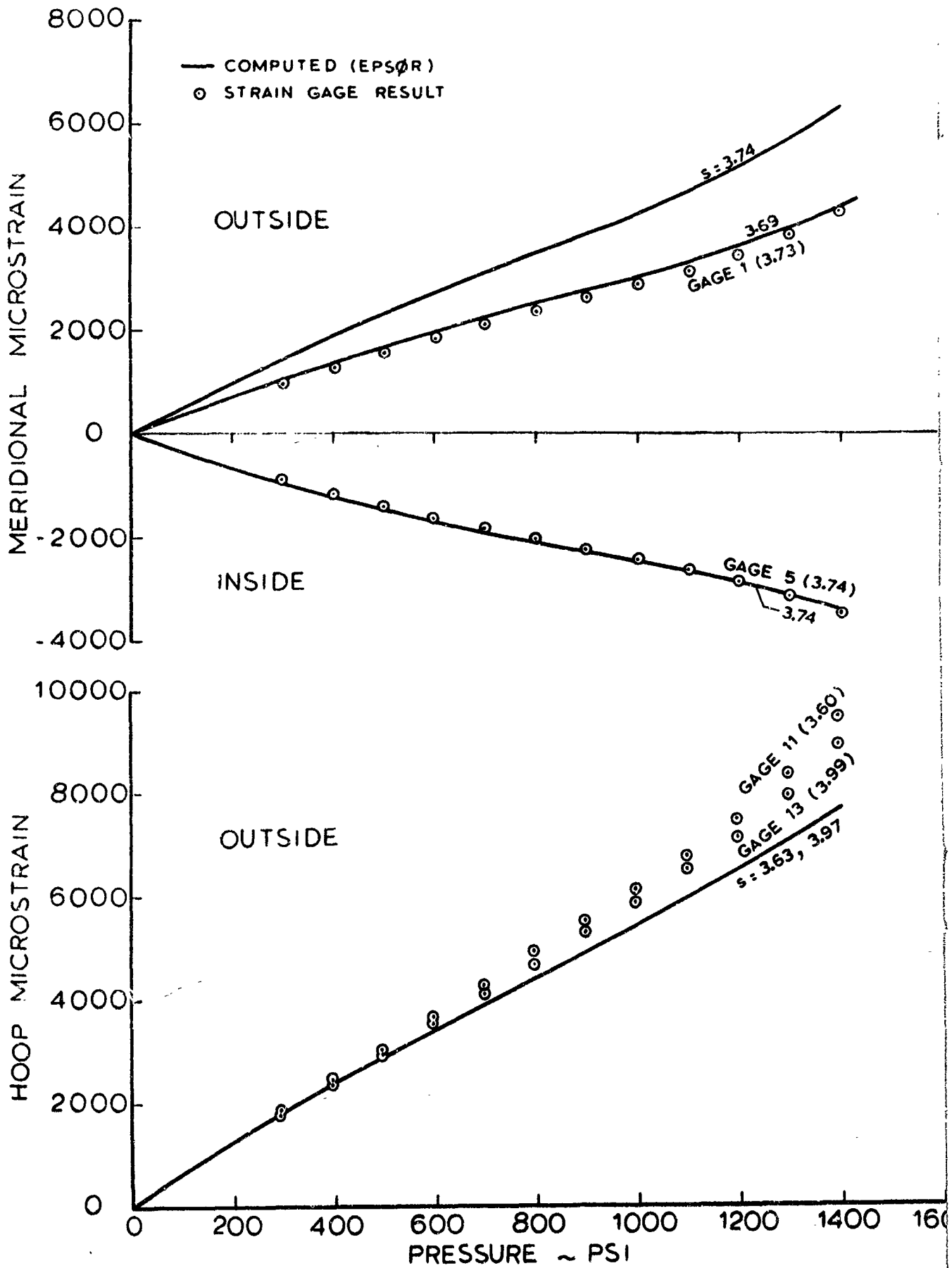


Fig. 7-11 Tita #7. Strain vs Pressure Plots

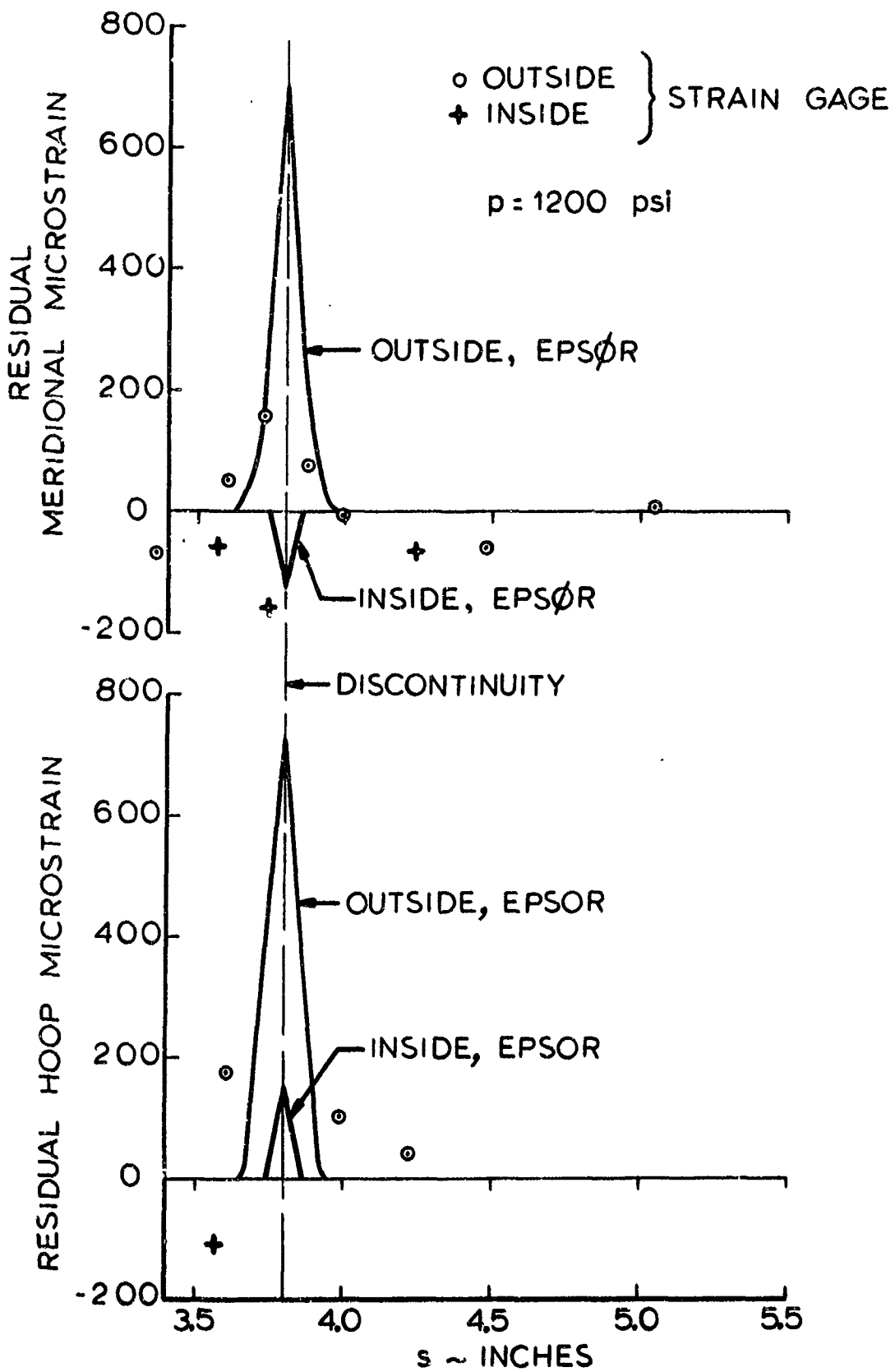


Fig. 7-12 Tita #7. Residual Strains After 1200 psi Pressure

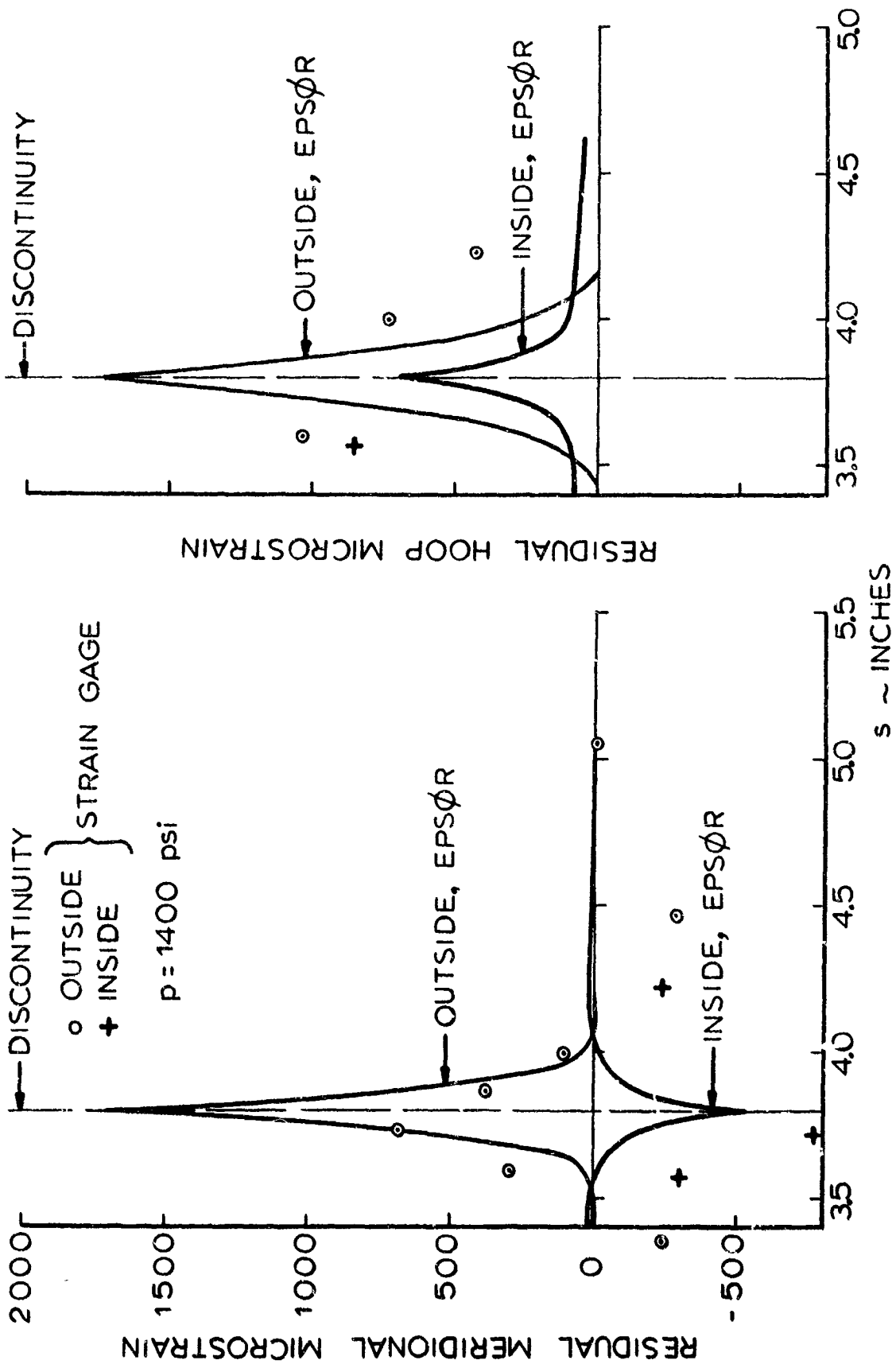


Fig. 7-13 Tita #7. Residual Strains After 1400 psi Pressure

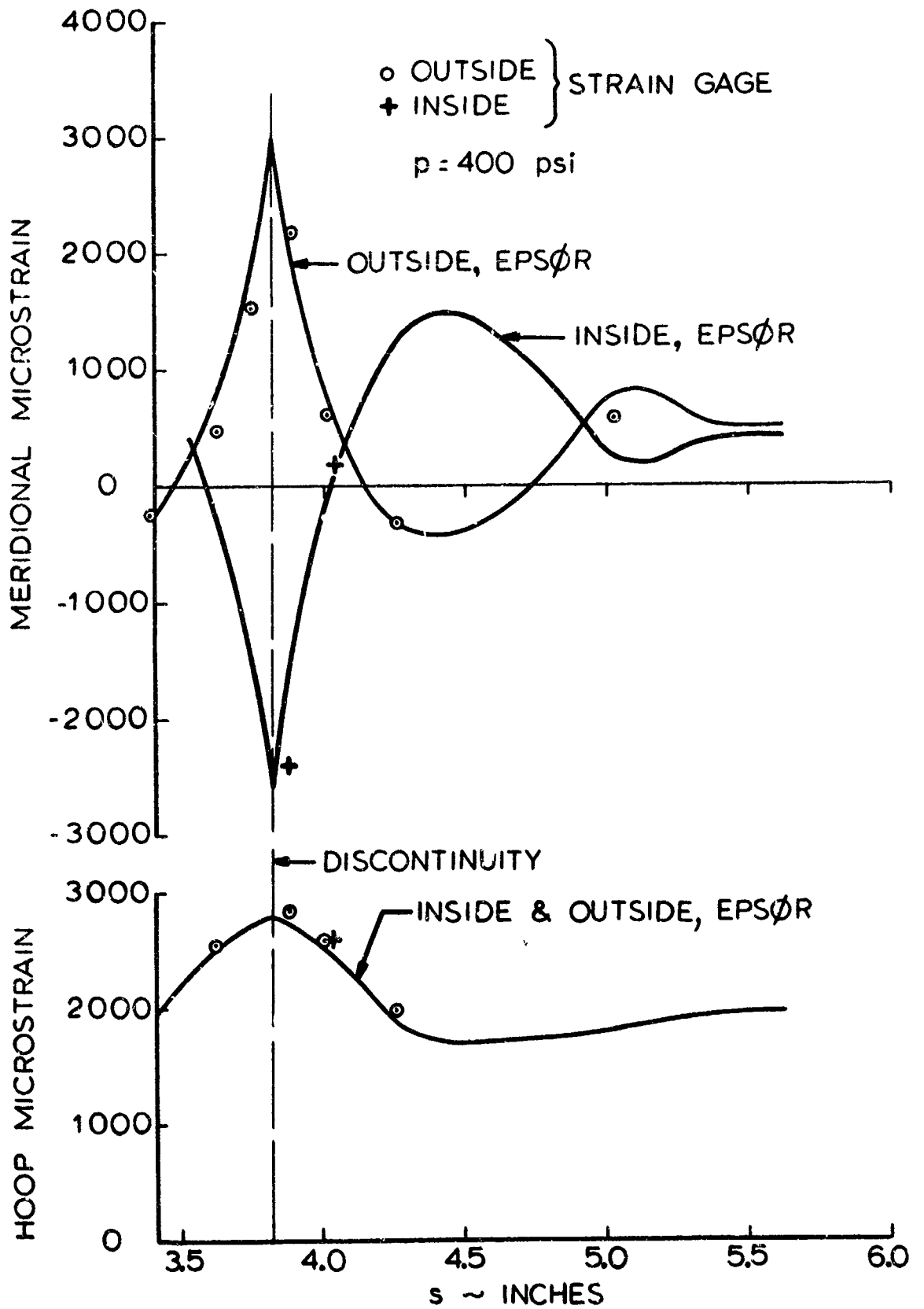


Fig. 7-14 Titc. #8. Strains in the Elastic Region

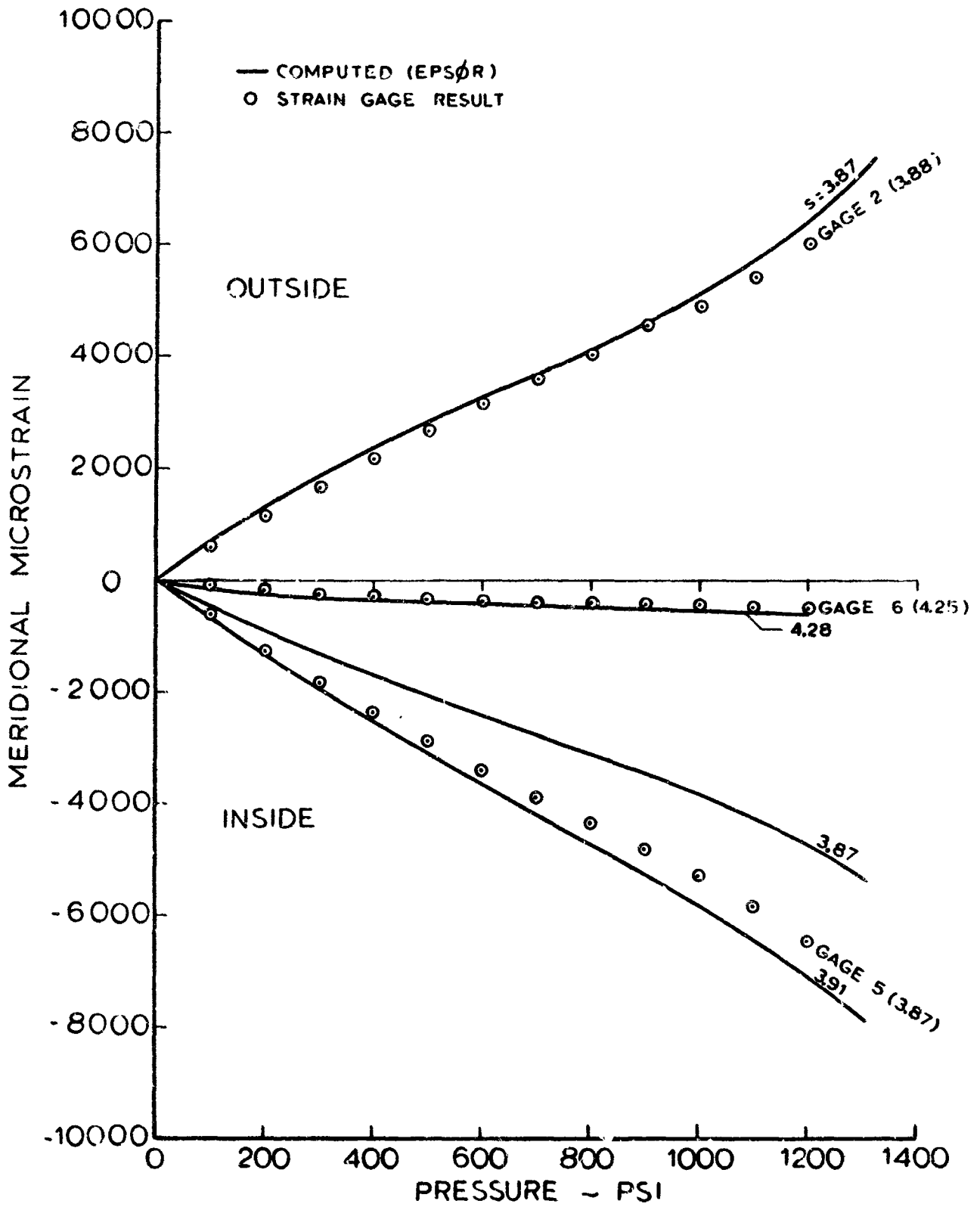


Fig. 7-15 Tita #8. Strains vs Pressure Plots

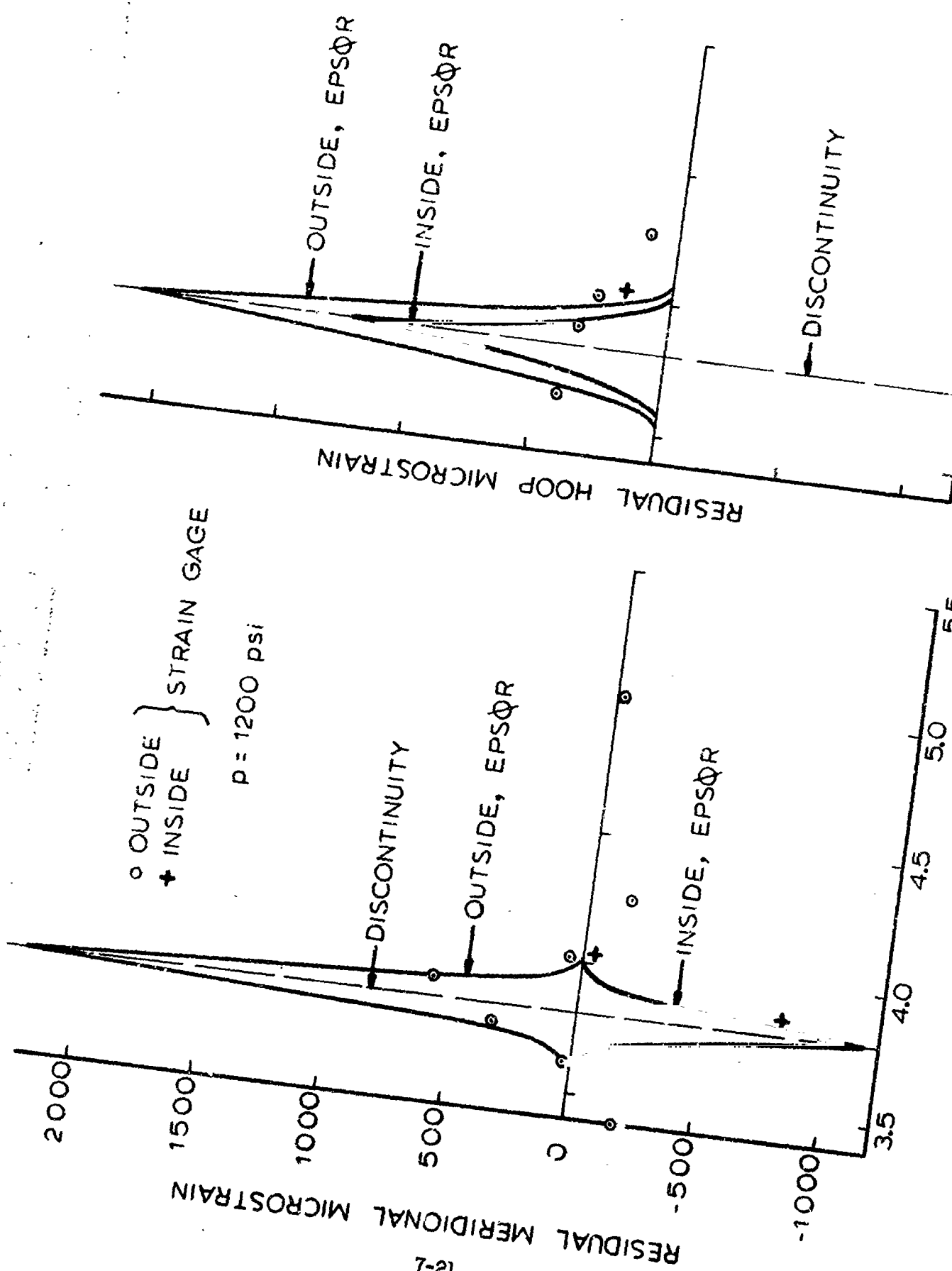


Fig. 7-16 Tita #8. Residual Strains After 1200 psi Pressure

Section 8

REFERENCES

(See also Appendix A for a systematic list of references for specified discontinuities.)

1. D. Bushnell, "Nonlinear Analysis for Axisymmetric Elastic Stresses in Ring-Stiffened, Segmented Shells of Revolution," Collection of Technical Papers on Structures and Materials, AIAA/ASME 10th Structures, Structural Dynamics and Materials Conference (published by the American Society of Mechanical Engineers, April 1969) pp 104-113
2. P. Stern, "Stresses and Displacements in Elastic/Plastic Shells of Revolution with Temperature-Dependent Properties," Report IMSC 6-90-62-123, January 1963
3. S. Timoshenko, S. Woinowsky-Krieger, Theory of Plates and Shells, Mc-Graw-Hill, New York, 1959
4. W. Flügge, Stresses in Shells, Springer-Verlag, Berlin, 1962
5. V. V. Novozhilov, The Theory of Thin Shells, P. Noordhoff Ltd., Groningen, 1959
6. E. Y. W. Tsui, "Handbook of Influence Coefficients for Axisymmetric Shells," IMSC Report 6-77-67-46, November 1967
7. C. R. Steele, "Nonsymmetric Deformation of Dome-Shaped Shells of Revolution," Transactions of the ASME, Paper No. 61-APMW-19, August 1961
8. C. R. Steele, "Shells with Edge Loads of Rapid Variation II," IMSC Report 6-90-63-84, November 1963
9. W. Nachbar, "Discontinuity Stresses in Pressurized Thin Shells of Revolution," Report LMSD-48483, March 1959

10. E. Reissner, "On Axisymmetrical Deformation of Thin Shells of Revolution," Proceedings of Symposia in Applied Mathematics, Vol. III, Mc-Graw-Hill, 1950, pp 27-52
11. P. T. Bizon, "Elastic Stresses at a Mismatched Circumferential Joint in a Pressurized Cylinder Including Thickness Changes and Meridional Load Coupling," NASA TN D-609, September 1966
12. Alf Pflüger, "Elementary Statics of Shells," F. W. Dodge Corporation, New York, 1961
13. S. S. Manson, "Thermal Stress and Low-Cycle Fatigue", McGraw-Hill, New York, 1966
14. J. L. Mattavi, "Low-Cycle Fatigue Behavior under Biaxial Strain Distribution", Journal of Basic Engineering, March 1969, pp 23-31
15. C. R. Steele, "Juncture of Shells of Revolution", Journal of Spacecraft and Rockets, Vol. 3, No. 6, June 1966


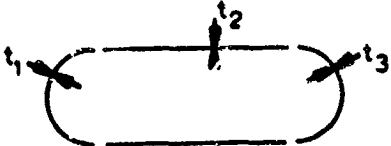

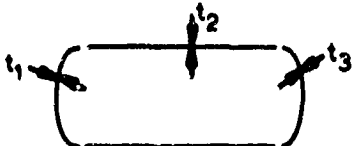
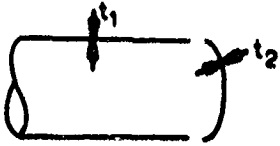
APPENDIX A

SYSTEMATIC CLASSIFICATION OF SOLUTIONS TO
DISCONTINUITY PROBLEMS IN PRESSURE VESSELS

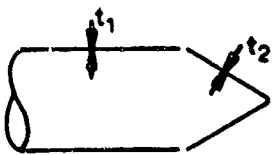
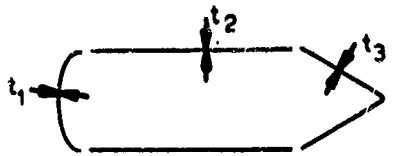
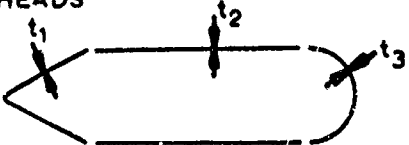
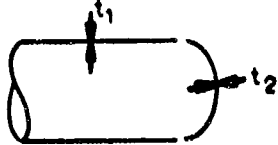
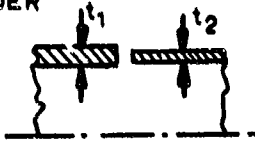
This appendix lists a number of references which are recommended for the solution of various discontinuity problems. The listing is arranged in the following manner:

	<u>Page</u>
Part 1: Common Middle Surface Discontinuities	A-1
Part 2: Eccentric Middle Surface Discontinuities	A-4
Part 3: Intersecting Shapes	A-6
References	





PART 1 - COMMON MIDDLE SURFACE DISCONTINUITIES

DESCRIPTION	LINEAR ELASTIC SOLUTION (REF.)	NONLINEAR ELASTIC SOLUTION (REF.)	ELASTIC-PLASTIC SOLUTION (REF.)
1. LONG CYLINDER - HEMISPHERICAL HEAD 	(39)	(20), (40)	(41), (42)
2. SHORT CYLINDER - HEMISPHERICAL HEAD 	(39)		(41)
3. LONG CYLINDER - ELLIPSOIDAL HEAD 	(39)		
4. SHORT CYLINDER - ELLIPSOIDAL HEAD 	(39)		
5. LONG CYLINDER - TORICONICAL AND/OR TORISPHERICAL HEAD 			(43)
NOTE: Blank space indicates no recommendation.			

PART 1 - COMMON MIDDLE SURFACE DISCONTINUITIES (Continued)




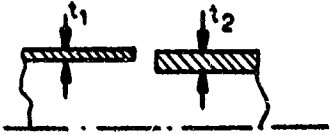
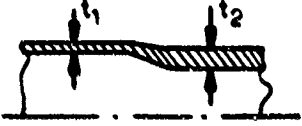
DESCRIPTION	LINEAR ELASTIC SOLUTION (REF.)	NONLINEAR ELASTIC SOLUTION (REF.)	ELASTIC-PLASTIC SOLUTION (REF.)
<p>6. LONG CYLINDER - CONICAL AND ELLIPSOIDAL HEADS</p> 	(39)		
<p>7. SHORT CYLINDER - CONICAL AND ELLIPSOIDAL HEADS</p> 	(39)		
<p>8. SHORT CYLINDER - HEMISPHERICAL AND CONICAL HEADS</p> 	(39)		
<p>9. LONG CYLINDER - SPHERE</p> 	(44)		
<p>10. CHANGE IN THICKNESS - CYLINDER</p> 	(39)	(20)	
<p>NOTE: Blank space indicates no recommendation.</p>			

PART 1 - COMMON MIDDLE SURFACE DISCONTINUITIES (Continued)

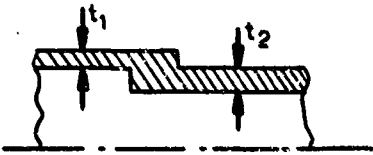

DESCRIPTION	LINEAR ELASTIC SOLUTION (REF.)	NONLINEAR ELASTIC SOLUTION (REF.)	ELASTIC - PLASTIC SOLUTION (REF.)
<p>11. CHANGE IN THICKNESS - SPHERE</p> 	(44)	(40)	
<p>12. CHANGE IN THICKNESS - CONE</p> 	(44)		
<p>13. CONE SPHERE</p> 	(44)		
<p>14. JUNCTION OF MULTIPLE SHELLS</p> 	(45)		(46)

NOTE: Blank space indicates no recommendation.






PART 2 - ECCENTRIC MIDDLE SURFACE DISCONTINUITIES

DESCRIPTION	LINEAR ELASTIC SOLUTION (REF.)	NONLINEAR ELASTIC SOLUTION (REF.)	ELASTIC - PLASTIC SOLUTION (REF.)
<p>1. CYLINDER - HEMISPHERICAL HEAD</p> 	<p>(15) Axisymmetric Mismatch (Method); (18) Method</p>	<p>(20), (40)</p>	
<p>2. CYLINDER - ELLIPSOIDAL HEAD</p> 	<p>(18) Method</p>		
<p>3. CYLINDER - CONICAL HEAD</p> 	<p>(18) Method</p>		
<p>4. MISMATCH - CYLINDER UNFILLETTED BUTT JOINT</p> 	<p>(39) Axisymmetric Mismatch; (47) Local Mismatch</p>	<p>(20) Axisymmetric Mismatch; (48) Experimental; (49) Local Mismatch</p>	
<p>5. MISMATCH - CYLINDER FILLETED BUTT JOINT</p> 		<p>(20) Axisymmetric Mismatch; (48) Experimental</p>	
<p>NOTE: Blank space indicates no recommendation.</p>			



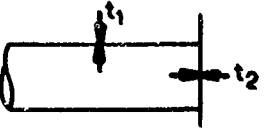
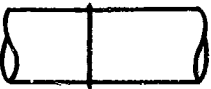

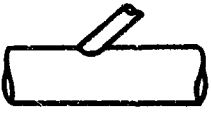
PART 2 - ECCENTRIC MIDDLE SURFACE DISCONTINUITIES (Continued)

DESCRIPTION	LINEAR ELASTIC SOLUTION (REF.)	NONLINEAR ELASTIC SOLUTION (REF.)	ELASTIC-PLASTIC SOLUTION (REF.)
<p>6. MISMATCH - CYLINDER LAP JOINT</p> 		<p>(20) Axisymmetric Mismatch</p>	
<p>7. MISMATCH - SPHERES</p> 	<p>(15) Axisymmetric Mismatch (Method); (18) Method</p>	<p>(40) Influence Coefficients Only</p>	
<p>NOTE: Blank space indicates no recommendation.</p>			

PART 3 - INTERSECTING SHAPES

DESCRIPTION	LINEAR ELASTIC SOLUTION (REF.)	NONLINEAR ELASTIC SOLUTION (REF.)	ELASTIC - PLASTIC SOLUTION (REF.)
<p>1. SPHERE - CYLINDER</p> 	(50)		(42), (51 to 56); (57), (58) Experimental
<p>2. NONRADIAL NOZZLE IN SPHERE</p> 			
<p>3. REINFORCED OPENING IN SPHERE</p> 			(58), (59) Experimental
<p>4. MULTIPLE HOLES IN SPHERICAL SHELLS</p> 	(60)		
<p>5. CYLINDER - CYLINDER</p> 	(61 to 64)		(65); (57), (58), (66). (67) Experimental
<p>NOTE: Blank space indicates no recommendation.</p>			

PART 3 - INTERSECTING SHAPES (Continued)

DESCRIPTION	LINEAR ELASTIC SOLUTION (REF.)	NONLINEAR ELASTIC SOLUTION (REF.)	ELASTIC - PLASTIC SOLUTION (REF.)
<p>6. LONG CYLINDER - FLAT HEAD</p> 	(39)		(68)
<p>7. SHORT CYLINDER - FLAT HEAD</p> 	(39)		
<p>8. CYLINDER - FLANGED ENDS</p> 	(69)		
<p>9. CYLINDER - RING</p> 	(39)		
<p>10. CYLINDER - EQUIDISTANT RINGS</p> 	(39)		(70)
<p>11. NONRADIAL NOZZLE IN CYLINDER</p> 	(71) Theoretical and Experimental		
<p>NOTE: Blank space indicates no recommendation.</p>			

REFERENCES

1. Johnston, G. S.: Weight of Ellipsoid of Revolution with Optimum Tapered Thickness. Aerospace Sci., vol. 29, no. 10, Oct. 1962, pp. 1269-1270.
2. Stern, M.; Wang, H.; and Worley, W. J.: A Method for Determining an Optimum Shape of a Class of Thin Shells of Revolution. Theoretical and Applied Mechanics Rept. 281, Univ. of Illinois, July 1965.
3. Steele, C. R.: Toroidal Pressure Vessels. Spacecraft, vol. 2, no. 6, Nov.-Dec. 1965, pp. 937-943.
4. Hoffman, G. A.: Proportions of Pressure-Vessel Heads Designed for Minimum Weight by the Mises Yield Criterion. Memo RM-2885, The Rand Corporation, June 1962.
5. Mills, E. J.; et al.: Design, Performance, Fabrication and Material Considerations for High-Pressure Vessels. RSIC-173, Battelle Memorial Institute, March 30, 1964.
6. Jones, M. L.: Thermal Insulation for Aerospace Applications: -423° to $+3,000^{\circ}$ F. Tech. Documentary Rept. ASD-TDR-63-699, Sept. 1963.
7. Ferguson, C. W.: Hypervelocity Impact Effects on Liquid Hydrogen Tanks. NASA CR-54852, 1966.
8. Cosby, W. A.; and Lyle, R. G.: The Meteoroid Environment and Its Effects on Materials and Equipment. NASA SP-7E, 1965, pp 84-85.
9. Anon.: Metallic Materials and Elements for Aerospace Vehicle

Structures, MIL-HDBK-5.

10. Lyman, Taylor, ed.: Metals Handbook. Volume 1.-Properties and Selection of Metals. Eighth ed., Amer. Soc. Metals, 1961.
11. Goodman, J. W.: Final Report on Pressure Vessel Design Criteria. STL/TR-60-0000-19427, Space Technology Laboratories, Inc., (Now TRW Systems), Dec. 31, 1960.
12. Tiffany, C. F.; and Masters, J. N.: Fracture Toughness and Its Applications. ASTM Spec. Tech. Publication No. 381, 1965, pp. 249-277.
13. Anon: Cryogenic Materials Data Handbook. ML-TDR-64-280 and Supplements, Aug. 1964.
14. Anon.: Research and Development on the Basic Design of Storable High Energy Systems and Components, AFPTC TR-60-61, 1960.
15. Flugge, W.: Stresses in Shells. Springer-Verlag (Berlin), 1960.
16. Baker, E. H.; Capelli, A. P.; Kovalensky, L.; Rish, F. L.; and Verette, R. M.: Shell Analysis Manual. NASA CR-912, 1968.
17. Timoshenko, S.; and Goodier, J. N.: Theory of Elasticity. Second ed., Second Impression, McGraw-Hill Book Company, Inc., 1951.
18. Tsui, E. Y. W.: Stresses in Shells of Revolution. Pacific Coast Publishers (Menlo Park, Calif.), 1968.
19. Langer, B. F.: PVRC Interpretive Report of Pressure Vessel Research. Sec 1 - Design Considerations, Welding Research Council Bull. no. 95, Apr. 1964.
20. Bizon, P. T.: Elastic Stresses at a Mismatched Circumferential

- Joint in a Pressurized Cylinder Including Thickness Changes and Meridional Load Coupling. NASA TN-D-3609, 1966.
21. Wichman, K. R.; Mershon, J. L.; and Hopper, A. G.: Local Stresses in Spherical and Cylindrical Shells Due to External Loadings. Welding Research Council Bull. no. 107, Aug. 1965.
 22. Johnson, D. E.: Stresses in a Spherical Shell with a Nonradial Nozzle, J. Appl. Mech., Trans. of ASME Series E 3rd, June 1967.
 23. Trapp, W. J.; and Forney, D. M., Jr.: Acoustical Fatigue In Aerospace Structures. Proceedings of the Second International Conference on Acoustical Fatigue, Syracuse University Press, 1965.
 24. Parker, E. R.: Application of Fracture Toughness Parameters to Structural Metals, AIME Metallurgical Society Conference, Philadelphia, 1964.
 25. Wessel, E. T.; Clark, W. G.; and Wilson, W. K.: Engineering Methods for the Design and Selection of Materials Against Fracture. U.S. Army Tank and Automotive Center Report, Contract No. DA-30-069-AMC-602(T), 1966.
 26. Glorioso, S. V.: Lunar Module Pressure Vessel Operating Criteria Specification. SE-7-0024, MSC (Houston, Tex.), Oct. 25, 1968.
 27. Glorioso, S. V.; and Ecord, G. M.: Apollo Command and Service Module Pressure Vessel Operating Criteria Specification. SE-V-0024, MSC (Houston, Tex.), Oct. 1968.
 28. Griffith, A. A.: The Phenomena of Rupture and Flow in Solids, Transactions, vol. 221, Royal Society of London, 1920.

29. Irwin, G. R.: Crack Extension Force for a Part-Through Crack in a Plate. *J. Appl. Mech.*, vol. 29, no. 4, Dec. 1962, pp. 651-661.
30. Srawley, J. E.; and Brown, W. F., Jr.: Plane Strain Crack Toughness Testing of High Strength Metallic Materials. American Society of Testing and Materials, STP 410, 1966.
31. Anon: Fracture Toughness Testing and Its Application. American Society of Testing and Materials, STP 381, 1965.
32. Anon.: Nondestructive Testing: Trends and Techniques, Proceedings of the Second Technology Status and Trends Symposium, Marshall Space Flight Center, NASA SP-5082, 1966.
33. Lemcoe, M. M.: Feasibility Studies of Stresses in Ligaments, Welding Research Council Bull. no. 65, Nov. 1960.
34. Anon.: ASME Boiler and Pressure Vessel Code. Section VIII-Pressure Vessels, The American Society of Mechanical Engineers, Division 1, 1968.
35. Anon.: Range Safety Manual. AFWTRM 127-1, Air Force Systems Command, Headquarters Air Force Western Test Range, Vandenberg Air Force Base, California, Nov. 1, 1966.
36. Anon.: Range Safety Manual. AFETRM 127-1, Air Force Systems Command, Headquarters Air Force Eastern Test Range, Patrick Air Force Base, Florida, Nov. 1, 1966.
37. Johnston, R. L., et al.: Stress Corrosion Cracking of Ti-6Al-4V Alloy in Methanol, NASA TN D-3868, 1967.
38. Barry, W. E.: Corrosion and Compatibility. DMIC Review,

- Battelle Memorial Institute, Columbus, Ohio, Sept. 13, 1968.
39. Au, Norman N.: Stresses in Thin Vessels Under Internal Pressure. SSD-TR-63-367, Rept. TDR-269(4304)-5, Aerospace Corporation, Jan. 10, 1964.
 40. Van Dyke, P.: Nonlinear Influence Coefficients for a Spherical Shell with Pressure Loading. AIAA J., vol. 4, no. 11, Nov. 1966, pp. 2054-2047.
 41. Weil, N. A.; Salmon, M. A.; and Costantino, C. J.: Approximate Burst Strength of Thin-Walled Cylinders with Hemispherical Caps. AIAA J. vol. 1, no. 9, Sept. 1963, pp. 2088-2092.
 42. Dinno, K. S.; and Gill, S. S.: The Limit Analysis of a Pressure Vessel Consisting of the Junction of A Cylindrical and Spherical Shell. International J. Mech. Sci., vol. 7, No. 1, Jan. 1965, pp. 21-42.
 43. Shield, R. T.; and Drucker, D. C.: Design of Thin-Walled Torispherical and Toriconical Pressure-Vessel Heads, ASME Trans. J. Appl. Mech., vol. 28, no. 2, June 1961, pp. 292-297.
 44. Johns, R. H.; and Orange, T. W.: Theoretical Elastic Stress Distributions Arising from Discontinuities and Edge Loads in Several Shell-Type Structures. N-62-70527, Lewis Research Center, Cleveland, Ohio (NASA Tech. Rept. R-103), 1961.
 45. Steele, C. R.: Juncture of Shells of Revolution. J. Spacecraft Rockets, vol. 3, no. 6, June 1966, pp. 881-884.
 46. Spera, D. A.: Analysis of Elastic-Plastic Shell of Revolution Containing Discontinuities. AIAA J., vol. 1, no. 11, Nov. 1963,

pp. 2583-2584.

47. Johns, R. H.: **Theoretical Elastic Mismatch Stresses.** NASA TN D-3254, 1966.
48. Morgan, W. C.; and Bizon, P. T.: **Comparison of Experimental and Theoretical Stresses at a Mismatch in a Circumferential Joint in a Cylindrical Pressure Vessel.** NASA TN D-3608, 1966.
49. Sechler, E. E.: **Stress Rise Due to Offset Welds in Tension.** Rept. EM9-18, Space Technology Laboratories, Inc. (now TRW Systems), Aug. 28, 1959.
50. Galletly, G. D.: **Analysis of Discontinuity Stresses Adjacent to a Central Circular Opening in a Hemispherical Shell.** Rept. 870, David Taylor Model Basin, May 1956.
51. Calladine, C. R.: **On the Design of Reinforcement for Openings and Nozzles in Thin Spherical Pressure Vessels.** J. Mech. Eng. Sci., vol. 8, no. 1, Mar. 1966, pp. 1-14.
52. Allman, D. J.; and Gill, S. S.: **The Effect of Change of Geometry on the Limit Pressure of a Flush Nozzle in a Spherical Pressure Vessel.** Engineering Plasticity Conference, Cambridge University (Cambridge, England), Mar. 1968, Papers (A68-25813 11-32).
53. Ellyin, F.; and Sherbourne, A. N.: **Limit Analysis of Axisymmetric Intersecting Shells of Revolution.** Nucl. Structural Eng., vol. 2, No. 1, July 1965, pp. 85-91.
54. Cloud, R. L.: **The Limit Pressure of Radial Nozzles in Spherical Shells.** Nucl. Structural Eng., vol. 1, No. 4,

Apr. 1965, pp. 403-413.

55. Duralli, A. J.; del Rio, C. J.; Parks, V. J.; and Feng, H.: Distribution of Stresses in a Pressurized Hollow Cylinder with a Circular Hole. Final Rept. N66-38180, Catholic University of America (Washington, D. C.), July 1966.
56. Dinno, K. S.; and Gill, S. S.: Limit Pressure for a Protruding Cylindrical Nozzle in a Spherical Pressure Vessel, J. Mech. Eng. Sci., vol. 7, no. 3, Sept. 1965, pp. 259-270.
57. Riley, W. F.: Experimental Determination of Stress Distributions in Thin-walled Cylindrical and Spherical Pressure Vessels with Circular Nozzles. Welding Research Council Bull.
58. Taylor, C. E.; and Lind, N. C.: Photoelastic Study of Stresses Near Openings in Pressure Vessels; Leven, M. M.: Photoelastic Determination of the Stresses in Reinforced Openings in Pressure Vessels; Mershon, J. L.: Preliminary Evaluation of PVRC Photoelastic Test Data on Reinforced Openings in Pressure Vessels. Welding Research Council Bull. no. 113, Apr. 1966.
59. Kaufman, A.; and Spera, D. A.: Investigation of the Elastic-Plastic Stress State Around a Reinforced Opening in a Spherical Shell. NASA TN D-2672, 1965.
60. Mahoney, J. B.; and Salerno, V. L.: Stress Analysis of a Circular Plate Containing a Rectangular Array of Holes; and Stress Distribution Around Periodically Spaced Holes in a

- Spherical Membrane Shell Under Uniform Internal Pressure.
Welding Research Council Bull. no. 106, July 1965.
61. Eringen, A. C.; and Suhubi, E. S.: Stress Distribution at Two Normally Intersecting Cylindrical Shells. Nucl, Structural Eng., Sept. 1965, pp. 253-270.
 62. Eringen, A. C.; Naghdi, A. K.; and Thiel, C. C.: State of Stress in a Circular Shell with a Circular Hole. Welding Research Council Bull. no. 102, Jan. 1965.
 63. Shevlyakov, Yu. A.: Stress Concentration in a Cylindrical Shell with a Round Aperture in its Side. NASA TT-F-282, 1964.
 64. Eringen, A. C., et al.: Stress Concentrations in Two Normally Intersecting Cylindrical Shells Subject to Internal Pressure. Tech. Rept. 3-9, General Technology Corporation, Jan. 1967.
 65. Coon, M. D.; Call, S. S.; and Kitching, R. A.: A Lower Bound to the Limit Pressure of a Cylindrical Pressure Vessel with an Unreinforced Hole. International J. Mech. Sci. vol. 9, no. 2, Feb. 1967, pp. 69-75.
 66. Clare, K. D.; and Gill, S. S.: Effect of Vessel Diameter/Thickness Ratio on the Behavior Beyond the Elastic Limit of Flush Nozzles in Cylindrical Pressure Vessels: Experimental Investigation. J. Mech. Eng. Sci., vol. 8, no. 4, Dec. 1966, pp. 357-362.
 67. Cottam, W. J.; and Gill, S. S.: Experimental Investigation of the Behavior Beyond the Elastic Limit of Flush Nozzles in Cylindrical Pressure Vessels. J. Mech. Eng. Sci., vol. 8,

no. 9, Sept. 1966, pp. 330-350.

68. Salmon, N. A.: Plastic Instability of Cylindrical Shells with Rigid End Closures. N65-16931, IIT Research Inst. (Chicago, Illinois), 1962.
69. Roark, R. J.: Formulas for Stress and Strain. Third ed., McGraw-Hill Book Company, Inc., 1954.
70. Higginson, G. R.: The Theoretical Strength of Band Reinforced Pressure Vessels. J. Mech. Eng. Sci., vol. 2, no. 4, Dec. 1960, pp. 298-301.
71. Corum, J. M.: A Theoretical and Experimental Investigation of the Stresses in a Circular Cylindrical Shell with an Oblique Edge. Nucl. Eng. Design, Feb/Mar. 1966, pp. 256-280.
72. Johnson, H.H.; and Paris, P.C.: Sub-Critical Flow Growth. Engineering Fracture Mechanics, vol. 4, no. 1, Pergamon Press, June 1968.

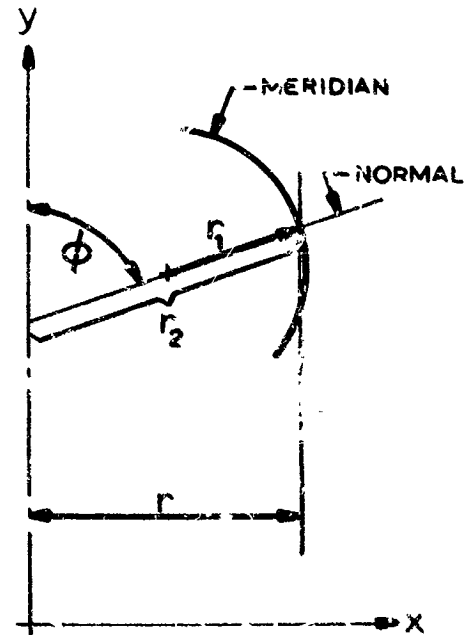
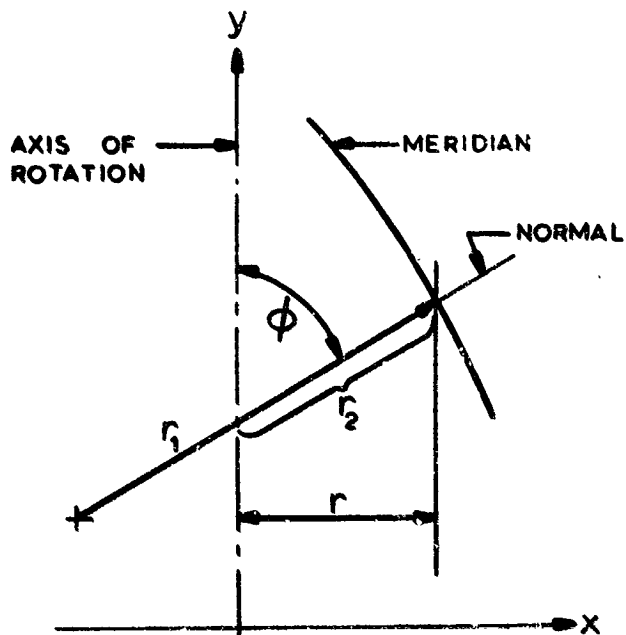
APPENDIX B

DERIVATION OF SHELL EQUATIONS IN COMPLEX FORM

CONTENTS

	<u>Page No.</u>
1. Geometrical Relationships	B-1
2. Surface Loads	B-3
3. Internal Forces	B-4
4. Equilibrium	B-6
4.1 Vertical Equilibrium	B-7
4.2 Horizontal Equilibrium	B-8
4.3 Moment Equilibrium	B-9
4.4 Summary of Equilibrium Equations	B-11
5. Deformations	B-11
6. Strain	B-13
7. Strain Compatibility	B-14
8. Stress-Strain Relations	B-15
9. Shell Equations	B-17
10. Stresses Calculated from the Solution rH	B-23
11. Membrane Solution	B-24
12. Edge Effect Solution	B-26

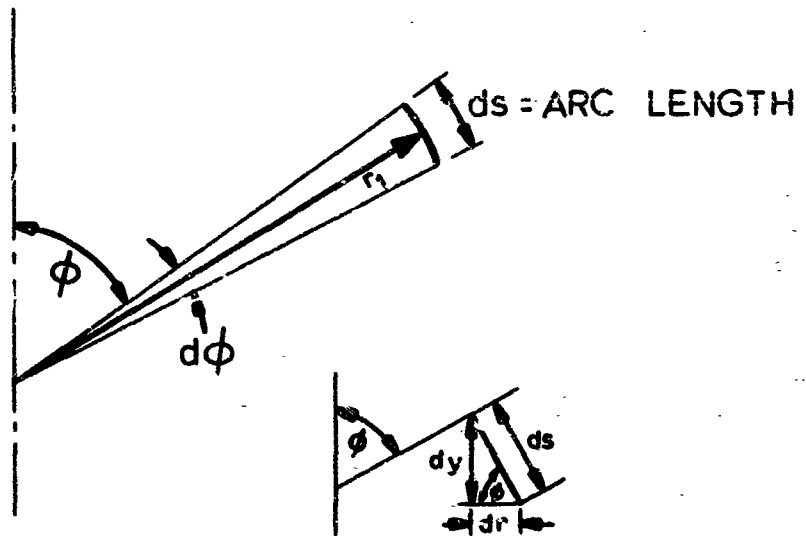
1. Geometrical Relationships



- x, y = Cartesian coordinates
- r_1 = meridional radius of curvature
- r_2 = hoop radius of curvature
- r = "horizontal" radius ($r = x$)
- ϕ = meridional angle

$$r_2 = \frac{r}{\sin \phi} \quad (B1.1)$$

SHELL ELEMENT

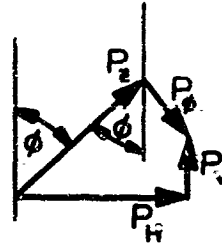
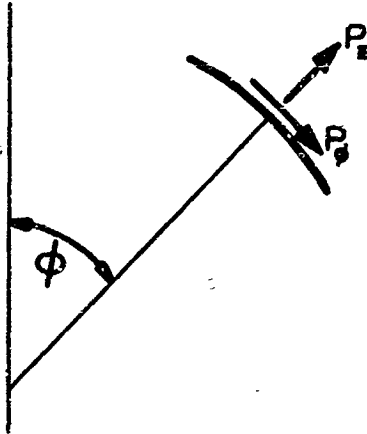


$$ds = r_1 d\phi \quad , \quad \frac{d\phi}{ds} = \frac{1}{r_1} \quad (B1.2)$$

$$dr = ds \cos \phi \quad , \quad \frac{dr}{ds} = \cos \phi \quad (B1.3)$$

$$dy = ds \sin \phi \quad , \quad \frac{dy}{ds} = \sin \phi \quad (B1.4)$$

2. Surface Loads



P_z, P_ϕ, P_H shown positive

P_V shown negative

Unit for surface loads: force/unit area

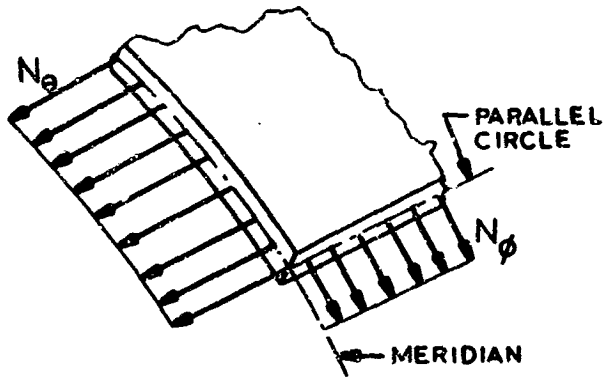
$P_z = \text{normal}$	}	$P_H = \text{horizontal}$	}	components
$P_\phi = \text{tangential}$		$P_V = \text{vertical}$		

Vertical and horizontal components:

$$P_V = P_\phi \sin \phi - P_z \cos \phi \quad (\text{B2.1})$$

$$P_H = P_\phi \cos \phi + P_z \sin \phi \quad (\text{B2.2})$$

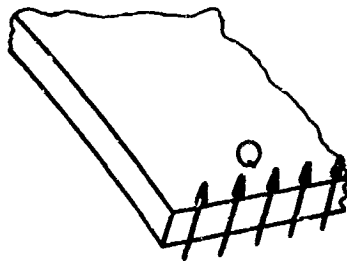
3. Internal Forces



Unit Normal Forces

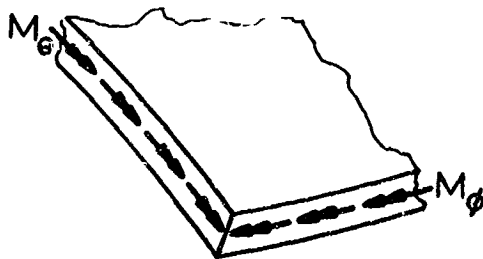
N_θ = hoop stress resultant

N_ϕ = meridional stress resultant



Unit Normal Shear

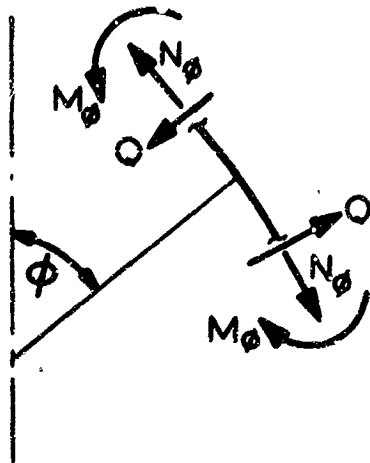
Q = shear stress resultant



Unit Bending Moments

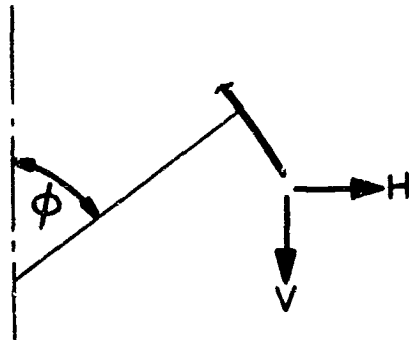
M_ϕ = meridional } stress resultants
 M_θ = hoop }

Note: The above figures refer to rotational symmetric problems, hence central shears and twisting moments are omitted.

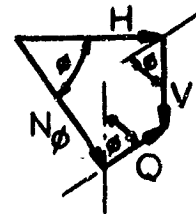


Meridional cut showing internal forces, positive sense

Resolving forces shown above into horizontal and vertical components:



All forces shown in positive directions



$$\left. \begin{aligned} Q &= H \sin \varphi - V \cos \varphi \\ N_{\varphi} &= H \cos \varphi + V \sin \varphi \end{aligned} \right\} \quad (B3.1)$$

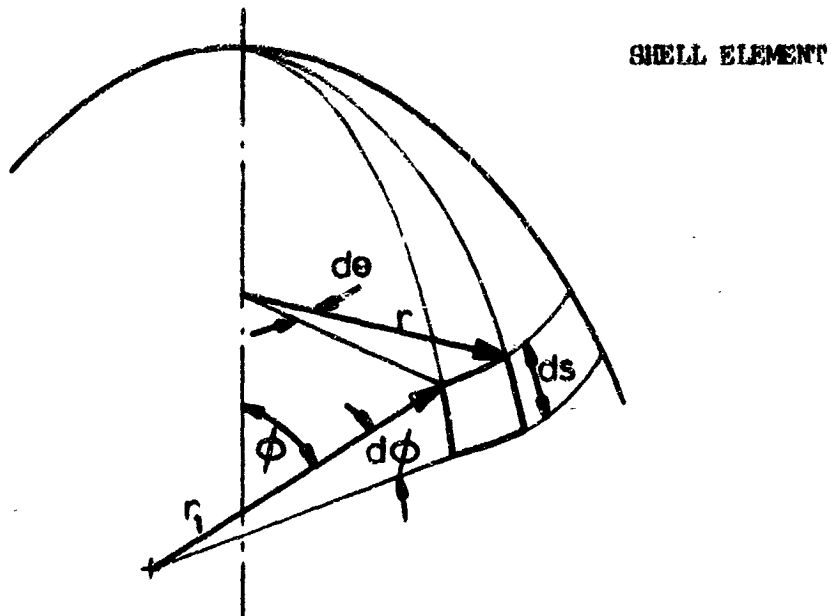
or

$$\left. \begin{aligned} V &= N_{\varphi} \sin \varphi - Q \cos \varphi \\ H &= N_{\varphi} \cos \varphi + Q \sin \varphi \end{aligned} \right\} \quad (B3.2)$$

4. Equilibrium

For the rotational symmetric problem the equilibrium conditions are as follows:

- o Vertical force equilibrium
- o Horizontal force equilibrium
- o Moment equilibrium with respect to the tangent of the parallel circle



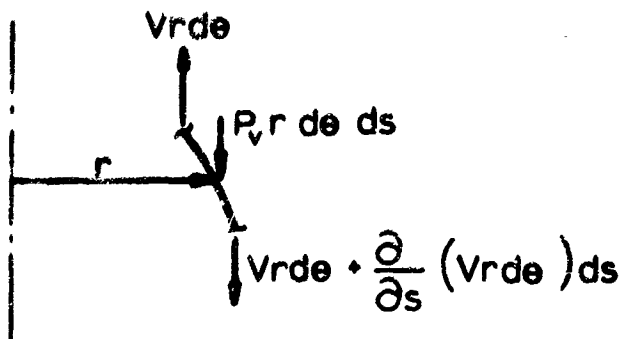
Lengths of element sides:

in hoop direction: $rd\theta$

in meridional direction: $r_1 d\phi = ds$

area of element $(rd\theta) \times ds$

4.1 Vertical Equilibrium



Vertical components
of forces on element.

Net vertical load on annulus: $P_v r d\theta ds \times \frac{2\pi}{d\theta}$

Net vertical internal force on annulus: $\frac{\partial}{\partial s} (Vr d\theta) ds \frac{2\pi}{d\theta}$

Sum of all forces is zero:

$$\frac{\partial}{\partial s} (Vr 2\pi) + P_v r ds 2\pi = 0 \quad *$$

Integrate,

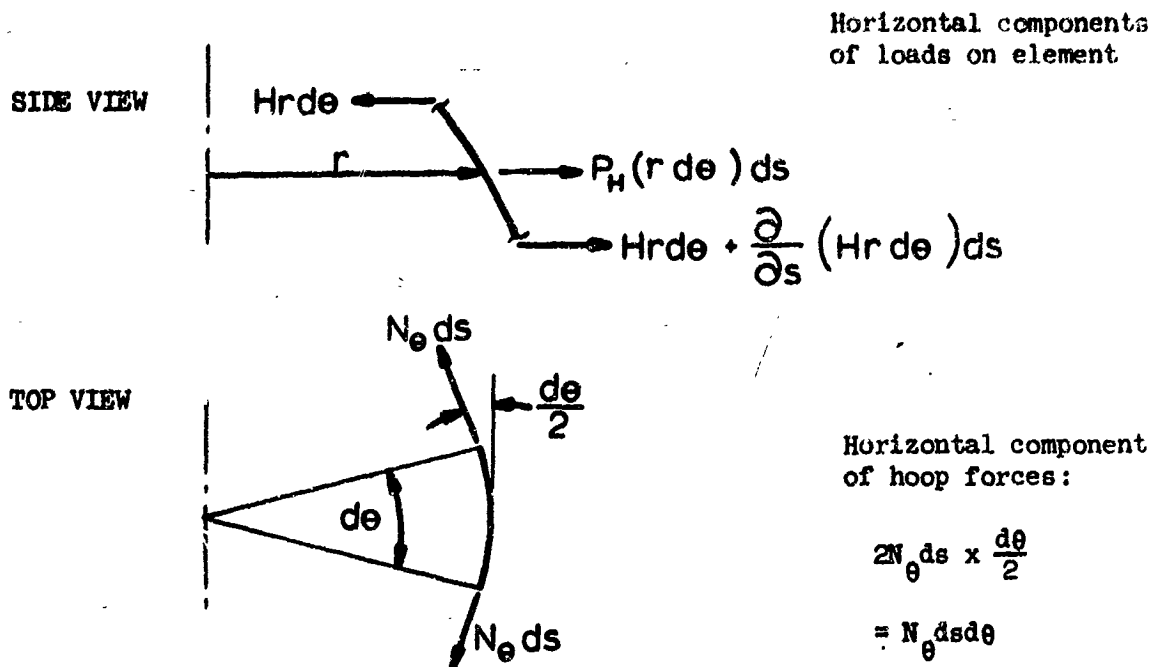
$$rV = - \int r P_v ds + C \quad (B4.1)$$

where C is constant of integration.

Thus vertical equilibrium is statically determinate.

* Sign rules for lower edge pertain

4.2 Horizontal Equilibrium



Adding all horizontal components:*

$$P_H (r d\theta) ds + \frac{\partial}{\partial s} (Hr d\theta) ds - N_{\theta} ds d\theta = 0$$

or

$$r P_H + \frac{\partial}{\partial s} (rH) - N_{\theta} = 0$$

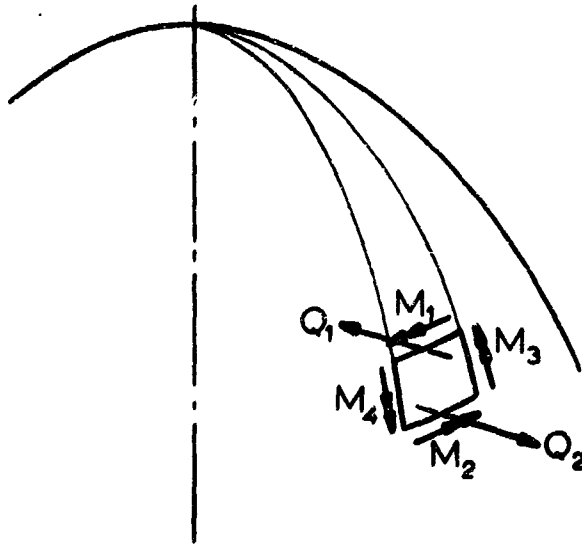
using the common symbol of differentiation

$$\frac{d}{ds} (rH) - N_{\theta} + r P_H = 0$$

(B4.2)

* Sign rules for lower edge pertain

4.3 Moment Equilibrium



Bending moments
and shears on
shell element

$$M_1 = M_\varphi r d\theta$$

$$M_2 = M_\varphi r d\theta + \frac{\partial}{\partial s} (M_\varphi r d\theta) ds$$

$$Q_1 = Q(r d\theta)$$

$$Q_2 = Q r d\theta + \frac{\partial}{\partial s} (Q r d\theta) ds$$

$$M_3 = M_\theta ds$$

$$M_4 = M_\theta ds$$

meridional
moments

shears

hoop
moments

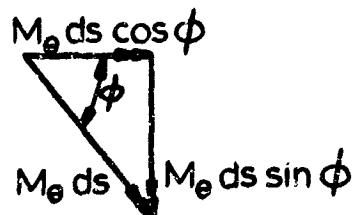
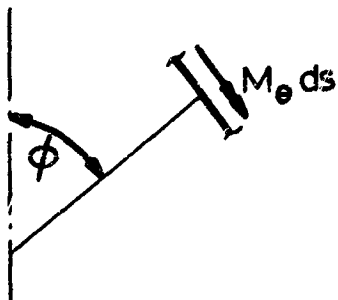
The moment caused by the shear, about the lower edge, is

$$M_Q = - Q(r d\theta) ds$$

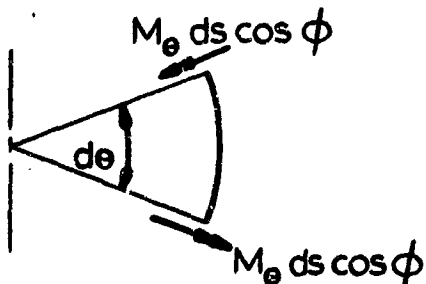
The contribution of the hoop moment to equilibrium about the lower edge is now calculated.

Resolve M_θ into axial and vertical components

SIDE VIEW



TOP VIEW



Horizontal component
of hoop moments:

$$2M_\theta ds \cos \varphi \frac{d\theta}{2}$$

(compare page B-8 for N_θ)

Adding all moments*

$$\frac{\partial}{\partial s} (M_\theta r d\theta) ds - Q r d\theta ds - M_\theta \cos \varphi ds d\theta = 0$$

Divide by $ds d\theta$ and use common differentiation symbol.

$$\frac{d}{ds} (rM_\theta) - rQ - M_\theta \cos \varphi = 0 \tag{B4.3a}$$

Replace Q by Eq. (B3.1):

$$\frac{d}{ds} (rM_\theta) - M_\theta \cos \varphi - rH \sin \varphi = -rV \cos \varphi \tag{B4.3}$$

* Sign rules for lower edge pertain

4.4 Summary of Equilibrium Equations

The equilibrium equations as derived above are*

$$\left\{ \begin{array}{l} rV = - \int rP_V ds + C \end{array} \right. \quad (B4.1)$$

$$\left\{ \begin{array}{l} \frac{d}{ds} (rH) - N_\theta + rP_H = 0 \end{array} \right. \quad (B4.2)$$

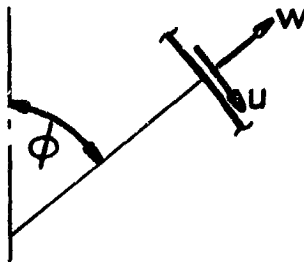
$$\left\{ \begin{array}{l} \frac{d}{ds} (rM_\varphi) - M_\theta \cos \varphi - rH \sin \varphi = -rV \cos \varphi \end{array} \right. \quad (B4.3)$$

These three equations contain the five unknown quantities V , H , N_θ , M_φ , and M_θ .

Note that the only unknown in the first equation is V , which is solved explicitly.

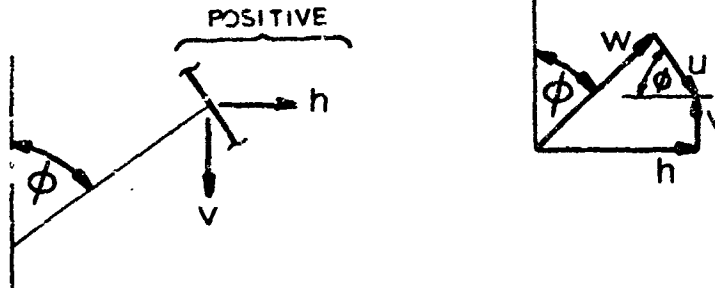
5. Deformations

The deflection of a point on the mid-surface is defined by the normal component w and the tangential component u , measured positive as shown in the figure below:



*Compare equations (312) in Timoshenko, "Theory of Plates and Shells", 2nd ed., which were derived in a similar way, but considering equilibrium in the normal and tangential directions.

Resolving into horizontal and vertical components

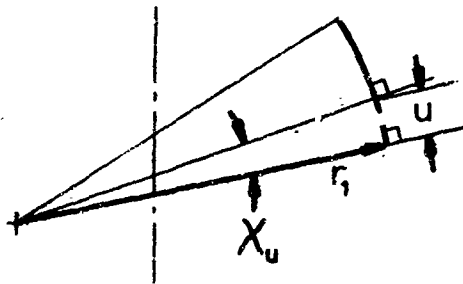


$$h = w \sin \phi + u \cos \phi$$

$$v = -w \cos \phi + u \sin \phi$$

(B5.1)

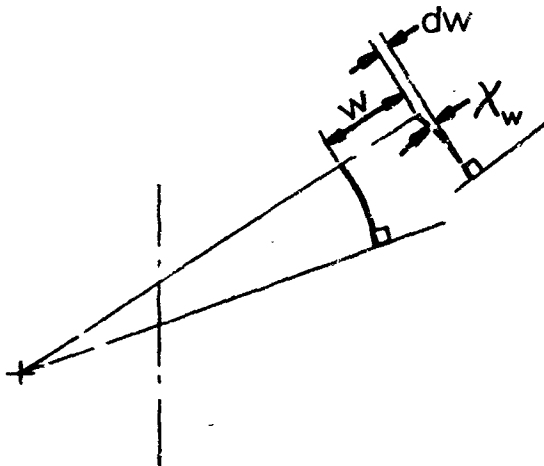
The rotation of a point on the mid-surface is χ



Element of length ds

Rotation of lower edge due to displacement u:

$$\chi_u = + \frac{u}{r_1}$$



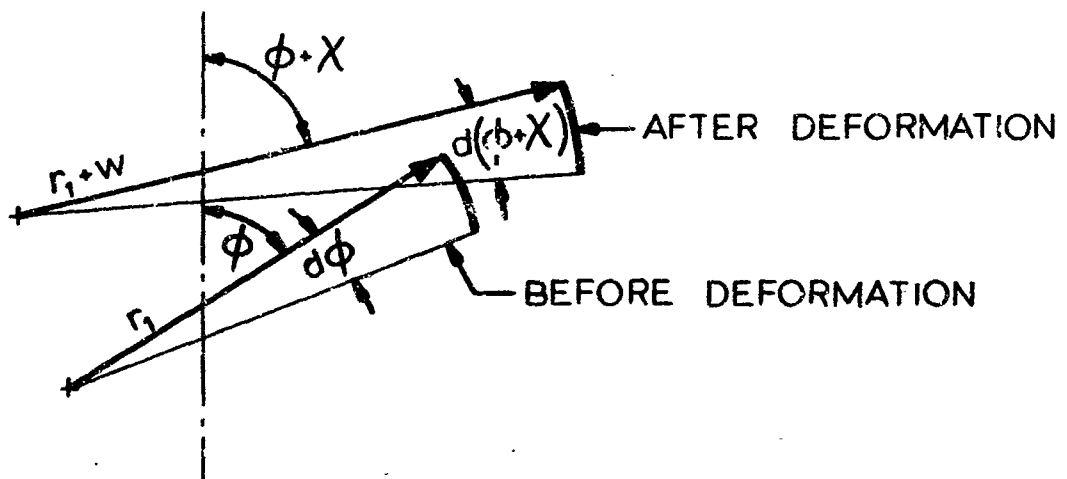
Rotation of lower edge due to displacement w:

$$\chi_w = - \frac{dw}{ds}$$

Total rotation $\chi = \chi_u + \chi_w$ due to displacements u and w :

$$\chi = \frac{u}{r_1} - \frac{dw}{ds} \quad (B5.2)$$

6. Strain



Original length $ds = r_1 d\phi$

Length after deformation: $(r_1 + w)d\phi + du$

Strain = $\frac{\text{Change in Length}}{\text{Original Length}}$

Meridional Strain

$$\begin{aligned} \epsilon_\phi &= \frac{(r_1 + w)d\phi + du - r_1 d\phi}{r_1 d\phi} \\ &= \frac{wd\phi + du}{r_1 d\phi} \end{aligned}$$

$$\epsilon_\phi = \frac{w}{r_1} + \frac{du}{ds} \quad (B6.1)$$

Hoop strain

Original length of parallel circle $2\pi r$

Length after deformation $2\pi(r + h)$

$$\epsilon_{\theta} = \frac{2\pi(r + h) - 2\pi r}{2\pi r}$$

$$\epsilon_{\theta} = \frac{h}{r} = \frac{w \sin \varphi + u \cos \varphi}{r} \quad (\text{B6.2})$$

Change in meridional curvature (definition)

$$\kappa_{\varphi} = \frac{d\chi}{ds} \quad (\text{B6.3})$$

Change in hoop curvature

$$\kappa_{\theta} = \frac{\chi \cos \varphi}{r} \quad (\text{B6.4})$$

7. Strain Compatibility

All the strains (ϵ_{φ} , ϵ_{θ} , κ_{φ} , κ_{θ}) are functions of only the two displacements w and u . It is, therefore, possible to express their interrelation in two equations.

Solve Eq. (B6.2) for the quantity $r\epsilon_{\theta}$

$$r\epsilon_{\theta} = w \sin \varphi + u \cos \varphi$$

Differentiate with respect to s :

$$\frac{d(r\epsilon_{\theta})}{ds} = \sin \varphi \left(\frac{dw}{ds} - u \frac{d\varphi}{ds} \right) + \cos \varphi \left(w \frac{d\varphi}{ds} + \frac{du}{ds} \right)$$

But $\frac{d\varphi}{ds} = \frac{1}{r_1}$ (Eq.B1.2)

$$\frac{dw}{ds} = \frac{u}{r_1} = -\chi \quad (\text{Eq.B5.2})$$

$$\frac{w}{r_1} + \frac{du}{ds} = \epsilon_{\varphi} \quad (\text{Eq.B6.1})$$

Thus

$$\frac{d(r\epsilon_{\theta})}{ds} - \epsilon_{\varphi} \cos \varphi + \chi \sin \varphi = 0 \quad (\text{B7.1})$$

Solve Eq. (B6.4) for χ

$$\frac{r\kappa_{\theta}}{\cos\varphi} = \chi \quad (\text{B7.2})$$

Differentiate with respect to s :

$$\frac{d}{ds} \left(\frac{r\kappa_{\theta}}{\cos\varphi} \right) = \frac{d\chi}{ds}$$

or (see Eq. B6.3)

$$\frac{d}{ds} \left(\frac{r\kappa_{\theta}}{\cos\varphi} \right) = \kappa_{\varphi} \quad (\text{B7.3})$$

8. Stress-Strain Relations

The following relations are given without proof:

$$\left. \begin{aligned}
 N_{\varphi} &= \frac{Et}{1-\nu^2} (\epsilon_{\varphi} + \nu\epsilon_{\theta}) \\
 N_{\theta} &= \frac{Et}{1-\nu^2} (\epsilon_{\theta} + \nu\epsilon_{\varphi}) \\
 M_{\varphi} &= \frac{Et^3}{12(1-\nu^2)} (\kappa_{\varphi} + \nu\kappa_{\theta}) \\
 M_{\theta} &= \frac{Et^3}{12(1-\nu^2)} (\kappa_{\theta} + \nu\kappa_{\varphi})
 \end{aligned} \right\} \begin{array}{l} \text{(Stress Resultants)} \\ \text{(B8.1)} \\ \text{(a-d)} \end{array}$$

$$\left. \begin{aligned}
 \sigma_{\varphi} &= \frac{N_{\varphi}}{t} \pm \frac{6M_{\varphi}}{t^2} \\
 \sigma_{\theta} &= \frac{N_{\theta}}{t} \pm \frac{6M_{\theta}}{t^2}
 \end{aligned} \right\} \begin{array}{l} \text{(Stresses)} \\ \text{(B8.2)} \end{array}$$

Solving (B8.1) for the strains:

$$\left. \begin{aligned}
 \epsilon_{\varphi} &= \frac{1}{Et} (N_{\varphi} - \nu N_{\theta}) \\
 \epsilon_{\theta} &= \frac{1}{Et} (N_{\theta} - \nu N_{\varphi}) \\
 \kappa_{\varphi} &= \frac{12}{Et^3} (M_{\varphi} - \nu M_{\theta}) \\
 \kappa_{\theta} &= \frac{12}{Et^3} (M_{\theta} - \nu M_{\varphi})
 \end{aligned} \right\} \begin{array}{l} \text{(Strains)} \\ \text{(B8.3)} \\ \text{(a-d)} \end{array}$$

In the above equations ν = Poisson's ratio
 t = shell thickness

9. Shell Equations

The three equilibrium equations (B4.1, B4.2, B4.3) and the strain compatibility equation (B7.1) are

$$\left. \begin{aligned}
 rV &= - \int rP_V ds + C \\
 \frac{d}{ds} (rH) - N_\theta + rP_H &= 0 \\
 \frac{d}{ds} (rM_\varphi) - M_\theta \cos\varphi - rH \sin\varphi &= -rV \cos\varphi \\
 \frac{d}{ds} (r\epsilon_\theta) - \epsilon_\varphi \cos\varphi + \chi \sin\varphi &= 0
 \end{aligned} \right\} \begin{array}{l} \text{(B9.1)} \\ \text{(a - d)} \end{array}$$

In this system of equations,

$$\epsilon_\theta = \epsilon_\theta (N_\varphi, N_\theta) = \epsilon_\theta (H, V, N_\theta)$$

$$\epsilon_\varphi = \epsilon_\varphi (N_\varphi, N_\theta) = \epsilon_\varphi (H, V, N_\theta)$$

also $\chi = \chi (M_\varphi, M_\theta)$

but $M_\varphi = M_\varphi (\kappa_\varphi, \kappa_\theta)$

$$\kappa_\varphi = \kappa_\varphi (\kappa_\theta) \quad (\text{Eq. B7.2})$$

thus $M_\varphi = M_\varphi (\kappa_\theta)$

Similarly $M_\theta = M_\theta (\kappa_\theta)$

Thus, the unknown in Equation (B9.1) may be expressed by the following quantities:

$$V, H, N_\theta, \kappa_\theta$$

The four equations (B9.1) are reduced by substitution to a system of two equations containing the unknowns H and χ .

Substitute the stress-strain relations (B8.3, a,b) into the compatibility equation (B9.1d)

$$\frac{1}{Et} \left(\frac{d}{ds} \left[r(N_{\theta} - \nu N_{\varphi}) \right] - (N_{\varphi} - \nu N_{\theta}) \cos \varphi \right) + \chi \sin \varphi = 0$$

Replace N_{θ} by

$$N_{\theta} = \frac{d}{ds} (rH) + rP_H \quad (\text{Eq. B9.1b})$$

and N_{φ} by

$$N_{\varphi} = H \cos \varphi + V \sin \varphi \quad (\text{Eq. B3.1})$$

$$\begin{aligned} & \frac{1}{Et} \left\{ \frac{d}{ds} \left[r \left[\frac{d}{ds} (rH) + rP_H - \nu (H \cos \varphi + V \sin \varphi) \right] \right\} - \right. \\ & \left. - \left[H \cos \varphi + V \sin \varphi - \nu \left(\frac{d}{ds} (rH) + rP_H \right) \right] \cos \varphi \right\} + \chi \sin \varphi = 0 \end{aligned}$$

Collecting terms containing H and χ on the left hand side

$$\begin{aligned} & \frac{1}{Et} \left(\frac{d}{ds} \left[r \frac{d}{ds} (rH) - \nu (rH) \cos \varphi \right] - H \cos^2 \varphi + \nu (\cos \varphi) \frac{d}{ds} (rH) \right) + \chi \sin \varphi = \\ & = \frac{1}{Et} \left(\frac{d}{ds} \left[-r^2 P_H + \nu r V \sin \varphi \right] + \cos \varphi \left[V \sin \varphi - \nu r P_H \right] \right) \end{aligned}$$

Perform the differentiation $\frac{d}{ds} (-\nu r H \cos \varphi)$

$$\frac{d}{ds} (-\nu r H \cos \varphi) = -\nu \frac{d}{ds} (rH) \cos \varphi + \nu r H (\sin \varphi) \frac{1}{r_1}$$

Thus

$$\begin{aligned} & \frac{1}{Et} \left(\frac{d}{ds} \left[r \frac{d}{ds} (rH) \right] + \left(v \frac{\sin \varphi}{r_1} - \frac{\cos \varphi}{r} \right) (rH) \right) + \chi \sin \varphi = \\ & = \frac{1}{Et} \left(- \frac{d}{ds} \left[+ r^2 P_H - v r V \sin \varphi \right] + \cos \varphi (V \sin \varphi - v r P_H) \right) \end{aligned} \quad (B9.1)$$

Substitute the stress-strain relations (B8.1c, d) in the equilibrium Equation (B9.1c)

$$\frac{Et^3}{12(1-\nu^2)} \left(\frac{d}{ds} \left[r(\kappa_\varphi + \nu \kappa_\theta) \right] - (\cos \varphi)(\kappa_\theta + \nu \kappa_\varphi) \right) - rH \sin \varphi = -rV \cos \varphi$$

Replace κ_φ by

$$\kappa_\varphi = \frac{d\chi}{ds} \quad (\text{Eq. B6.3})$$

and κ_θ by

$$\kappa_\theta = \frac{\chi \cos \varphi}{r} \quad (\text{Eq. B6.4})$$

Then

$$\frac{Et^3}{12(1-\nu^2)} \left(\frac{d}{ds} \left[r \frac{d\chi}{ds} + \nu \chi \cos \varphi \right] - \cos \varphi \left[\frac{\chi \cos \varphi}{r} + \nu \frac{d\chi}{ds} \right] \right) - rH \sin \varphi = -rV \cos \varphi$$

$$\text{But } \frac{d}{ds} (\nu \chi \cos \varphi) = \nu \frac{d}{ds} (\chi) \cos \varphi - \nu \chi (\sin \varphi) \frac{d\varphi}{ds}$$

Thus

$$\frac{Et^3}{12(1-\nu^2)} \left(\frac{d}{ds} \left[r \frac{d\chi}{ds} \right] - \left(v \frac{\sin \varphi}{r_1} + \frac{\cos^2 \varphi}{r} \right) \chi \right) - rH \sin \varphi = -rV \cos \varphi \quad (B9.2)$$

At this point, Equations (B9.1) and (B9.2) are a pair of second-order equations with the unknowns rH and χ .

Multiply Eq. (B9.2) by $-ik^{-1}$, where $k = \text{constant}$.

$$\begin{aligned} & \frac{1}{Et} \left(\frac{E^2 t^4}{12(1-v^2)} \right) \left(\frac{d}{ds} \left[r \frac{d}{ds} (-ik^{-1} \chi) \right] + ik^{-1} v \frac{\sin \varphi}{r_1} \chi + \right. \\ & \left. + ik^{-1} \frac{\cos^2 \varphi}{r} \chi + ik^{-1} rH \sin \varphi = ik^{-1} rV \cos \varphi \right) \end{aligned} \quad (\text{B9.2a})$$

Add, term by term, Equations (B9.1) and (B9.2a):

$$\begin{aligned} & \frac{1}{Et} \left(\frac{d}{ds} \left[r \frac{d}{ds} \left(rH - \frac{E^2 t^4}{12(1-v^2)} ik^{-1} \chi \right) \right] + \frac{v \sin \varphi}{r_1} \left(rH + ik^{-1} \frac{E^2 t^4}{12(1-v^2)} \chi \right) - \right. \\ & \left. - \frac{\cos^2 \varphi}{r} \left(rH - ik^{-1} \frac{E^2 t^4}{12(1-v^2)} \chi \right) + ik^{-1} (\sin \varphi) \left(rH + \frac{1}{ik^{-1}} \chi \right) = \right. \\ & \left. = ik^{-1} rV \cos \varphi + \frac{1}{Et} \left(- \frac{d}{ds} [r^2 P_H - vrV \sin \varphi] + (\cos \varphi) [V \sin \varphi - vrP_H] \right) \right) \end{aligned} \quad (\text{B9.3})$$

The constant k is chosen to be

$$k = Ect \quad (\text{B9.4})$$

where

$$c = \frac{t}{\sqrt{12(1-v^2)}} \quad (\text{B9.5})$$

giving

$$\frac{E^2 t^4}{12(1-v^2)} = k^2 \quad (\text{B9.6})$$

The last term on the left hand side of Eq. (B9.3) is

$$ik^{-1} (\sin \varphi) \left(rH + \frac{1}{ik^{-1}} \chi \right) = ik^{-1} \sin \varphi (rH - ik\chi)$$

Substituting this and Equation (B9.6) in Equation (B9.3):

$$\begin{aligned}
 & \frac{1}{Et} \left(\frac{d}{ds} \left[r \frac{d}{ds} r \left(H - ik \frac{X}{r} \right) \right] + \frac{v \sin \varphi}{r_1} r \left(H + ik \frac{X}{r} \right) - \right. \\
 & \left. - \frac{\cos^2 \varphi}{r} r \left(H - ik \frac{X}{r} \right) \right) + ik^{-1} (\sin \varphi) r \left(H - ik \frac{X}{r} \right) = \\
 & = ik^{-1} \cos \varphi r \left(V + \frac{k}{iEt r \cos \varphi} \left[- \frac{d}{ds} (r^2 P_H - v r V \sin \varphi) + \right. \right. \\
 & \left. \left. + (\cos \varphi)(V \sin \varphi - v r P_N) \right] \right) \tag{B9.7}
 \end{aligned}$$

$$\text{Set } \tilde{H} = H - ik \frac{X}{r} \tag{B9.8a}$$

$$\tilde{H}^* = H + ik \frac{X}{r} \tag{B9.8b}$$

The last factor on the right hand side of Equation (B9.7) is

$$\left(V + \frac{k}{iEt r \cos \varphi} \left[- \frac{d}{ds} \dots \right] \right) = \left(V + \frac{ic}{r} \frac{1}{\cos \varphi} \left[\frac{d}{ds} \dots \right] \right)$$

This factor is designated \tilde{V} :

$$\tilde{V} = \left(V + \frac{ic}{r} \left[\frac{1}{\cos \varphi} \frac{d}{ds} (r^2 P_H - v r V \sin \varphi) - V \sin \varphi + v r P_H \right] \right) \tag{B9.9}$$

Substitute Equations (B9.8) and (B9.9) into (B9.7):

$$\begin{aligned}
 & \frac{1}{Et} \left(\frac{d}{ds} \left[r \frac{d}{ds} (r \tilde{H}) \right] + \frac{v \sin \varphi}{r_1} r \tilde{H}^* - \frac{\cos^2 \varphi}{r} r \tilde{H} \right) + ik^{-1} (\sin \varphi) r \tilde{V} = \\
 & = ik^{-1} (\cos \varphi) r \tilde{V}
 \end{aligned}$$

Multiply both sides by $-ik$, remembering that $k =$ Etc

$$-ic \left(\frac{d}{ds} \left[r \frac{d}{ds} (r\tilde{H}) \right] + \frac{v \sin \varphi}{r_1} r\tilde{H}^* - \tilde{H} \cos^2 \varphi \right) + r\tilde{H} \sin \varphi = r\tilde{V} \cos \varphi \quad (B9.10)$$

This equation is the shell equation in complex form with the unknown H (horizontal force) associated with the real part and the variable χ (rotation) associated with the imaginary part, according to definitions (B9.8).

We note that the term $\frac{v \sin \varphi}{r_1} r\tilde{H}^*$ drops out when $r_1 \rightarrow \infty$ (cylinder or cone), or when $v \rightarrow 0$. (Even when $v \neq 0$ and $r_1 < \infty$ this term may be deleted: the equation then becomes similar to the wellknown Geckeler* approximation, when the actual shell is locally substituted by a cylinder or cone**.) We also note that, since $|\tilde{H}^*| = |\tilde{H}|$ the term $-\frac{icv}{r_1} r\tilde{H}^* \sin \varphi$ is of the relative magnitude $\frac{vc}{r_1}$ when compared to the term $r\tilde{H} \sin \varphi$ and, thus, may be deleted.

The quantity \tilde{V} (see Eq. B9.9) contains only a surface load (P_H) and the statically determinate vertical force (V). In the homogeneous solution (edge solution, bending solution) these quantities are identically zero, or $\tilde{V} \equiv 0$.

In the membrane solution (particular solution) these forces are nonzero and have to be accounted for. However, we note the following

$$\tilde{V} = V \left[1 + O \left(\frac{c}{r \cos \varphi} \right) \right], \quad \frac{c}{r} \ll 1$$

Thus, if the load distribution and geometry are smooth enough so that the differentiation does not cause an order-of-magnitude change, and if $r \cos \varphi \neq 0$, we have $\tilde{V} \approx V$. However, it is not necessary to postulate, a priori, that $\tilde{V} \approx V$ and $\tilde{H}^* = 0$.

* See Timoshenko: Theory of Plates and Shells, 2nd Ed., p. 548

** See also Pflüger: Elementary Statics of Shells, p. 72, F.W. Dodge Publishers, N.Y., 1961

A particular solution ($\tilde{V} \neq 0$) to Equation (B9.10) may be obtained by assuming the series expansion

$$r\tilde{H} = r\tilde{H}_0 + cr\tilde{H}_1 + c^2 r\tilde{H}_2 t \dots$$

If this function and its derivatives are substituted in Equation (B9.10) it is found that \tilde{H}^* and $\tilde{V}-V$ only occur in higher-order terms and that the familiar membrane formulas for a general thin shell of revolution are, indeed, obtainable by setting $\tilde{H}^* = 0$, $\tilde{V} = V$. However, the main advantage of the complex formulation of the shell equation is its use for the homogeneous solution, where $\tilde{V} = 0$.

10. Stresses calculated from the Solution $r\tilde{H}$

With the solution $r\tilde{H}$ the stress resultants are calculated as follows:

Hoop from Eq. (B4.2)

$$N_{\theta} = \frac{d}{ds} (rH) + rP_H$$

or, since H is the real part of \tilde{H}

$$N_{\theta} = \Re e \frac{d}{ds} (r\tilde{H}) + rP_H \quad (B10.1)$$

Meridional from Eq. (B3.1b)

$$N_{\varphi} = H \cos \varphi + V \sin \varphi \quad (B10.2)$$

where V is according to Eq. (B4.1)

Shear from Eq. (B3.1a)

$$Q = H \sin \varphi - V \cos \varphi \quad (B10.3)$$

Note again that $H = \Re e(\tilde{H})$

The moments are calculated using the stress-strain relationships:

Meridional from Eq. (B8.1c)

$$M_{\varphi} = \frac{Et^3}{12(1-\nu^2)} (\kappa_{\varphi} + \nu\kappa_{\theta}) \quad (\text{B10.4})$$

Hoop from Eq. (B8.1d)

$$M_{\theta} = \frac{Et^3}{12(1-\nu^2)} (\kappa_{\theta} + \nu\kappa_{\varphi}) \quad (\text{B10.5})$$

In these equations κ_{θ} and κ_{φ} are defined by equations (B7.2) and (B6.3), respectively:

$$\kappa_{\theta} = \frac{\chi \cos \varphi}{r}$$

$$\kappa_{\varphi} = \frac{d\chi}{ds}$$

where χ is associated with the imaginary part of \tilde{H} (Eq. B9.8a)

$$\chi = -\frac{1}{k} \text{Im}(r\tilde{H})$$

11. Membrane Solution

If the surface loads are "smooth" a particular solution to Eq. (B9.10) may be obtained by assuming the series expansion

$$r\tilde{H} = r\tilde{H}_0 + cr\tilde{H}_1 + c^2r\tilde{H}_2 + O(c^3)$$

Substitution into Eq. (B9.10) gives schematically

$$(\sin \varphi r\tilde{H}_0 - \cos \varphi r\tilde{V}) + c(\dots) + c^2(\dots) + c^3(\dots) = 0$$

The functions $r\tilde{H}_1$ are found by equating each coefficient to zero. They are

$$\begin{aligned}
 r\tilde{H}_0 &= \cot \varphi rV \\
 r\tilde{H}_1 &= \left[i \frac{d}{ds} \left(r \frac{d}{ds} (r\tilde{H}_0) \right) - i(\cos^2 \varphi) \tilde{H}_0 + \frac{iv}{r_1} r(\sin \varphi) \tilde{H}_0^* \right. \\
 &\quad \left. + r \cos \varphi \frac{1}{r} \left(\frac{1}{\cos \varphi} \frac{d}{ds} (r^2 p_H - vrV \sin \varphi) - V \sin \varphi + vrp_H \right) \right] (\sin \varphi)^{-1} \\
 &= i \left[\frac{d}{ds} \left(r \frac{d}{ds} (V \cot \varphi) \right) - \frac{\cos^3 \varphi}{\sin \varphi} V + v \frac{r \cos \varphi}{r_1} V \right. \\
 &\quad \left. + \frac{d}{ds} (r^2 p_H - vrV \sin \varphi) - V \sin \varphi \cos \varphi + vrp_H \cos \varphi \right] (\sin \varphi)^{-1} \\
 r\tilde{H}_2 &= \left[i \frac{d}{ds} \left(r \frac{d}{ds} (r\tilde{H}_1) \right) - i(\cos^2 \varphi) \tilde{H}_1 - \frac{iv}{r_1} (\sin \varphi) r\tilde{H}_1^* \right] (\sin \varphi)^{-1}
 \end{aligned} \tag{B11.1, a-b}$$

Using the result of Eq. (B11.1), and Section 10,

$$\begin{aligned}
 N_\varphi &= V \sin \varphi + V \cot \varphi \cos \varphi \\
 &= \frac{V}{\sin \varphi} \tag{B11.2}
 \end{aligned}$$

$$Q = V \cot \varphi \sin \varphi - V \cos \varphi = 0 \tag{B11.3}$$

$$\begin{aligned}
 N_\theta &= \frac{d}{ds} (rV \cot \varphi) + r p_H \\
 &= -\frac{r_2}{r_1} N_\varphi + r_2 p \tag{B11.4}
 \end{aligned}$$

which equations are the known results for the membrane solution to shells of revolution.

12. Edge Effect Solution

The edge effect solution is obtained from Eq. (B9.10) with $\tilde{V} \cos \varphi = 0$:

$$-ic \left[\frac{d}{ds} \left(r \frac{d}{ds} (r\tilde{H}) - \tilde{H} \cos^2 \varphi \right) + r \tilde{H} \sin \varphi \right] = 0 \quad (\text{B12.1})$$

The expansion for $r\tilde{H}$ is assumed to be

$$r \tilde{H} = \exp(c^{-1/2} \xi) \left[\psi_0 + c^{1/2} \psi_1 + c \psi_2 + \dots \right] \quad (\text{B12.2})$$

Differentiating

$$\begin{aligned} \frac{d}{ds} (r\tilde{H}) &= c^{-1/2} \exp(c^{-1/2} \xi) \frac{d\xi}{ds} \left[\psi_0 + c^{1/2} \psi_1 + \dots \right] \\ &+ \exp(c^{-1/2} \xi) \left[\psi_0' + c^{1/2} \psi_1' + \dots \right] \end{aligned}$$

etc., and inserting into Eq. (B13.1)

$$\left[-i r (\xi')^2 + \sin \varphi \right] \psi_0 + c^{1/2} (\dots) + c (\dots) + \dots = 0$$

Setting the leading coefficient equal to zero gives

$$\left(\frac{d\xi}{ds} \right)^2 = \frac{1}{ir \sin \varphi}$$

or

$$\xi' = \frac{1}{\sqrt{i r_2}} \quad (\text{B12.3a})$$

Similarly, from the coefficient for $c^{1/2}$,

$$\psi_0 = C (r \sin \varphi)^{-1/4} \quad (\text{B12.3b})$$

The next coefficient gives a value for ψ_1 , and so on.

At the edge ($s = 0$)

$$\widetilde{rH} = \psi_0$$

$$\begin{aligned} \frac{d}{ds} (\widetilde{rH}) &= c^{-1/2} \xi' \psi_0 + \psi_0' + c^{1/2} \psi_1' + c \psi_2' + \dots \\ &= c^{-1/2} \xi' \psi_0 \left[1 + \frac{c^{1/2} \psi_0'}{\xi' \psi_0} + c \frac{\psi_1'}{\xi' \psi_0} + \dots \right] \end{aligned}$$

Inserting Eq. (B12.3a, b...):

$$\frac{d}{ds} (\widetilde{rH}) = \frac{\psi_0}{\sqrt{1 - c} r_2} \left[1 - \sqrt{1 - c} \tilde{\epsilon}_1 + (1 - c) \tilde{\epsilon}_2 + \dots \right]$$

where

$$\left. \begin{aligned} \tilde{\epsilon}_1 &= \frac{1}{4} \left(\frac{c}{r_2} \right)^{1/2} \cot \varphi \left(1 + \frac{r_2}{r_1} \right) \\ \tilde{\epsilon}_2 &= \frac{1}{2} \frac{c}{r_2} \left[\cot^2 \varphi \left(1 - \frac{1}{16} \left(1 + \frac{r_2}{r_1} \right)^2 \right) + \frac{r_2}{4r_1} \left(1 + \frac{r_2}{r_1} \right) \right. \\ &\quad \left. - \frac{1}{4} r_2 \left(\frac{r_2}{r_1} \right) \cot \varphi + \dots \right] \end{aligned} \right\} \quad (\text{B12.4})$$

Rearranging,

$$\frac{d}{ds} (\widetilde{rH}) = \frac{\psi_0}{\sqrt{2 - c} r_2} \left[1 - (1 - c) \tilde{\epsilon}_1 + (1 - c)^2 \tilde{\epsilon}_2 + \dots \right] \quad (\text{B12.5})$$

where $r\tilde{H} = \psi_0 = rH - ik\chi$, as in Eq. (B9.8a). For a shell with the horizontal edge load H and rotation χ , the edge moment is obtained from Eq. (B9.10), with $k = Ect$:

$$\begin{aligned} \frac{1}{c} M_\varphi &= - \operatorname{Im} \left[\frac{d}{ds} (r\tilde{H}) + \nu \tilde{H} \cos \varphi \right] \\ &= \frac{rH}{\sqrt{2cr_2}} (1 - \epsilon_2) + \frac{k\chi}{\sqrt{2cr_2}} \left[1 - (\tilde{\epsilon}_1 - \nu(\cot \varphi) \sqrt{\frac{2c}{r_2}}) + \tilde{\epsilon}_2 \right] \quad (\text{B11.6}) \end{aligned}$$

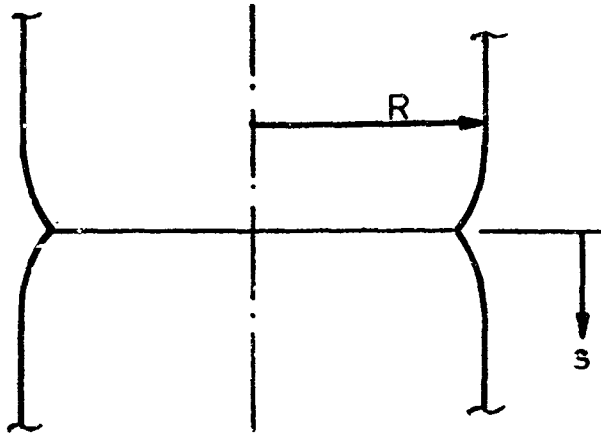
and the edge displacement from

$$\begin{aligned} \frac{Eth}{r} &= \frac{d}{ds} (rH) - \nu H \cos \varphi \\ &= \frac{rH}{\sqrt{2cr_2}} \left(1 - \left[\tilde{\epsilon}_1 + \nu(\cot \varphi) \left(\frac{2c}{r_2} \right)^{1/2} \right] + \tilde{\epsilon}_2 \right) - \frac{k\chi}{\sqrt{2cr_2}} (1 - \epsilon_2) \quad (\text{B12.7}) \end{aligned}$$

APPENDIX C
DERIVATION OF ANALYTICAL EXPRESSIONS
FOR A CYLINDER WITH WELD SINKAGE

Assume an imperfection which is described by the following equation for the meridian

$$r = R (1 - \epsilon e^{-K|s|/R}) \quad (C.1)$$



For $s < 0$ the following geometrical relationships follow:

$$\cos \varphi = \frac{dr}{ds} = -\epsilon K e^{Ks/R}$$

$$\frac{1}{r_1} = -\frac{1}{\sin \varphi} \frac{d}{ds} (\cos \varphi) = \frac{\epsilon K^2}{R \sin \varphi} e^{Ks/R}$$

$$\frac{r_2}{r_1} = \frac{\epsilon K^2}{\sin^2 \varphi} e^{Ks/R} (1 - \epsilon e^{Ks/R})$$

$$\frac{d}{ds} \left(\frac{r_2}{r_1} \right) = \frac{\epsilon K^3}{R} \frac{e^{Ks/R} (1 - 2\epsilon e^{Ks/R} + \epsilon^2 K^2 e^{2Ks/R})}{(1 - \epsilon K^2 e^{2Ks/R})^2}$$

(C.2)

For $\epsilon \ll 1$ and $K \gg 1$:

$$\left. \begin{aligned} r &\approx R \\ \cos\varphi &\approx -\epsilon K e^{Ks/R} \\ \sin\varphi &\approx 1 \\ \frac{r_2}{r_1} &\approx \epsilon K^2 e^{Ks/R} \\ \left(\frac{r_2}{r_1}\right)' &= \frac{\epsilon K^3}{R} e^{Ks/R} \end{aligned} \right\} \quad (C.)$$

With the above formulæ and $V = \frac{pr}{2}$ the membrane solution (see Appendix B, Section 11)

$$r\tilde{H}_0 = \frac{pr^2}{2} \cot\varphi = -\frac{pR^2}{2} \epsilon K e^{Ks/R}$$

$$r\tilde{H}_1 = i r (r\tilde{H}_0)'' + \dots = i \frac{K^2}{R} r\tilde{H}_0$$

$$r\tilde{H}_n \approx i \frac{K^2}{R} r\tilde{H}_{n-1} = \left(i \frac{K^2}{R}\right)^n r\tilde{H}_0$$

Thus, the variable

$$r\tilde{H} = r\tilde{H}_0 + c r\tilde{H}_1 + \dots + c^n r\tilde{H}_n$$

is a geometric series with the constant ratio $i c K^2/R$, the sum of which is, simply

$$r\tilde{H} = r\tilde{H}_0 \frac{1}{1 - i c K^2/R}$$

$$= -\frac{pR^2}{2} \epsilon K e^{Ks/R} \frac{1 + i c K^2/R}{1 + (cK^2/R)^2} \quad (C.)$$

The membrane solution, then, gives the edge values (see Appendix B)

$$H = -\frac{pR}{2} \frac{\epsilon K}{1 + (c K^2/R)^2} = (H)_m \quad (C.5)$$

$$\chi = \frac{pR^2}{2Etc} \frac{\epsilon K (c K^2/R)}{1 + (c K^2/R)^2} = (\chi)_m \quad (C.6)$$

By using Section 10 of Appendix B the membrane stress resultants are derived

$$\left. \begin{aligned} N_{\varphi_m} &= H \cos\varphi + V \sin\varphi \approx \frac{pR}{2} \\ N_{\theta_m} &= \frac{d}{ds} (rH) + rP_H \approx \frac{pR}{2} \left[2 - \frac{\epsilon K^2 e^{Ks/R}}{1 + (c K^2/R)^2} \right] \\ \frac{M_{\varphi_m}}{c} &= -Im \left[\frac{d}{ds} (rH) + \nu \tilde{H} \cos\varphi \right] \\ &\approx \frac{pR}{2} \frac{\epsilon K^2 e^{Ks/R}}{1 + (c K^2/R)^2} \left(\frac{c K^2}{R} \right) \\ M_{\theta_m} &\approx \nu M_{\varphi_m} \end{aligned} \right\} \quad (C.7)$$

To the above "membrane" solution must be added the complementary edge effect solution, which has the edge values $-(H)_m$ and $-(\chi)_m$. The edge moment is obtained from Eq. (B12.6) of Appendix B. It is found that the correction terms $\tilde{\epsilon}_1$ and $\tilde{\epsilon}_2$ are small, so that the significant terms are

$$\frac{M_{\varphi_m}}{c} = -\frac{r(H)_m}{\sqrt{2 c r_2}} - \frac{E t c}{\sqrt{2 c r_2}} (\chi)_m$$

or

$$M_{\varphi_c} = \frac{pR}{2} \epsilon K \left(\frac{R}{2c}\right)^{1/2} \frac{1 - cK^2/R}{1 + (cK^2/R)^2} \quad (C.8)$$

Adding the particular solution, Eq. (C.7), to the edge effect solution, Eq. (C.8), the total meridional edge stresses are found:

$$\frac{\sigma_{\varphi}}{\frac{pR}{2t}} = 1 + \left(\frac{3}{1-\nu^2}\right)^{1/2} \epsilon K \left(\frac{R}{2c}\right)^{1/2} \frac{1 + \sqrt{2\mu}}{1 + \mu^2 + \sqrt{2\mu}} \quad (C.9)$$

where
$$\mu^2 = \frac{cK^2}{R} \quad (C.10)$$

The complementary edge effect solution for hoop stress is somewhat more complicated than the solution for the meridional stresses, due to the fact that the horizontal force component $-(H)_m$, and the rotation $-(\chi)_m$ cause an expansion of the radius, thus affecting the size of the total hoop stress resultant.

The horizontal force is

$$-(H)_m = \frac{pR}{2} \frac{\epsilon K}{1 + (cK^2/R)^2} \quad (C.11)$$

and the rotation is

$$-(\chi)_m = -\frac{pR^2}{2Et c} \frac{\epsilon K (cK^2/R)}{1 + (cK^2/R)^2} \quad (C.12)$$

The horizontal deformation is, from Eq. (B12.7) of Appendix B, neglecting as before the small correction terms $\tilde{\epsilon}_1$ and $\tilde{\epsilon}_2$:

$$\frac{E t h}{r} = \frac{rH}{\sqrt{2cr_2}} - \frac{k \chi}{\sqrt{2cr_2}} \quad (C.13)$$

or, with $k = Ect$ and with the hoop radius $r_2 = r/\sin \varphi$:

$$\frac{E t h}{r} = \frac{r\sqrt{\sin \varphi}}{\sqrt{2cr}} \left[H - \frac{Ect}{r} \chi \right] \quad (C.14)$$

Replacing H and χ by the edge values, Eq. (C.11) and (C.12), and noting that $\frac{Eth}{r}$ is the hoop stress resultant, N_{θ_c} ,

$$N_{\theta_c} = \frac{Vr\sin\varphi}{\sqrt{2c}} \epsilon K \frac{1 + (r/R)(cK^2/R)}{1 + (cK^2/R)^2} \quad (C.14)$$

But

$$\begin{aligned} \sin \varphi &= \sin \left(\frac{\Delta\varphi}{2} + \frac{\pi}{2} \right) \\ &= \cos \frac{\Delta\varphi}{2} \\ &= \sqrt{1 - (cK)^2} \end{aligned}$$

$$\therefore \sqrt{\sin \varphi} \approx 1$$

Also $r \approx R$

Thus

$$N_{\theta_c} = \frac{\sqrt{R}}{\sqrt{2c}} \epsilon K \frac{1 + cK^2/R}{1 + (cK^2/R)^2} \quad (C.15)$$

The total stress resultant is the sum of the particular solution Eq. (C.7) and the complementary solution Eq. (C.14)

$$\begin{aligned} N_{\theta_{TOT}} &= N_{\theta} + N_{\theta_c} \\ &= pR - \frac{e K^2}{1 + (cK^2/R)^2} \frac{pR}{2} + \sqrt{\frac{R}{2c}} e K \frac{1 + cK^2/R}{1 + (cK^2/R)^2} \end{aligned} \quad (C.16)$$

but

$$e K^2 = e K \sqrt{\frac{R}{c}} \sqrt{\frac{c K^2}{R}}$$

Thus

$$\frac{N_{\theta_{TOT}}}{\left(\frac{pR}{2}\right)} = 2 + e K \sqrt{\frac{R}{2c}} \frac{1 + cK^2/R - \sqrt{2 c K^2/R}}{1 + (c K^2/R)^2} \quad (C.17)$$

Set $(c K^2/R) = \mu^2$ (Eq. C.10)

Then

$$\begin{aligned} \frac{N_{\theta_{TOT}}}{\frac{pR}{2}} &= 2 + e K \sqrt{\frac{R}{2c}} \frac{1 + \mu^2 - \sqrt{2} \mu}{1 + \mu^4} \\ &= 2 + e K \sqrt{\frac{R}{2c}} \frac{1}{1 + \mu^2 + \sqrt{2} \mu} \end{aligned} \quad (C.18)$$

The hoop bending moment is

$$M_{\theta_c} = \nu M_{r_c}$$

so that the total hoop stress is

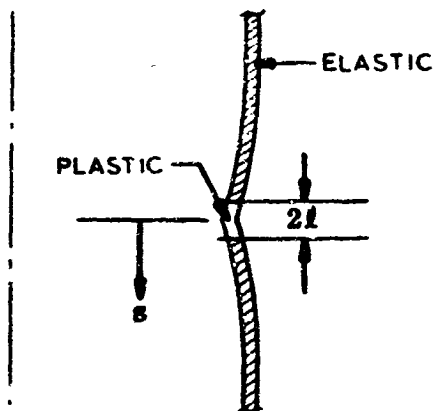
$$\frac{\sigma_{\theta}}{\frac{pR}{2t}} = 2 + \epsilon K \sqrt{\frac{R}{2c}} \frac{1}{1 + \mu^2 + \sqrt{2} \mu} + \nu \left[\frac{\sigma}{\frac{pR}{2t}} - 1 \right] \quad (C.19)$$

where $\frac{\sigma}{\frac{pR}{2t}}$ is calculated in accordance with Eq. (C.9).

Equations (C.9) and (C.19) give the total meridional and hoop stresses, respectively.

APPENDIX D
ELASTIC-PLASTIC BEHAVIOR OF CYLINDER
WITH SMALL SLOPE DISCONTINUITY

The following, simplified, derivation for the elastic-plastic behavior of a shell with a discontinuity is made for the same type of shell treated in Appendixes B and C, i.e., a cylinder with a weld-sinkage type slope discontinuity. During pressurization, this shell develops a narrow plastic region, of length $2l$, in the center of the sinkage:



At the edge of the elastic region, $s = -l$, the moment equals the yield moment, M_y . For no plastic zone, the elastic moment at $s = 0, M_e$, is defined by Eq. (C.8), Appendix C. When M_e is greater than the yield moment, there is a plastic zone and the rotation at $s = -l$ is

$$\frac{\chi_l}{\kappa_l} = -\sqrt{2rc} \left(\frac{M_e}{M_y} - 1 \right)$$

where the curvature at the edge of the elastic zone is

$$\kappa_l = \frac{M_y}{Etc^2} \quad c^2 = \frac{t^2}{12(1-\nu^2)}$$

Since the curvature is the derivative of the rotation

$$\kappa = \frac{d\chi}{ds}$$

in the plastic zone we have the condition

$$\chi_l = \int_0^{-l} \kappa ds$$

The plastic zone is assumed to be small, i.e., $l \ll \sqrt{cr}$, so that the moment is essentially linear with the arc length for $0 > s > -l$

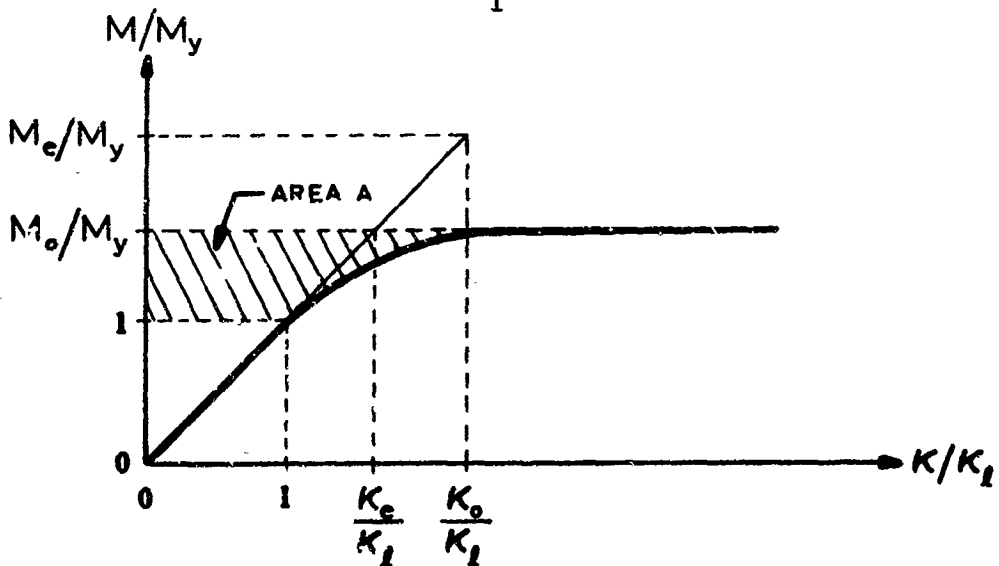
$$M \approx - \frac{pr\Delta\theta}{l} (s + l) + M_y = M_y \left[1 + \frac{M_e}{M_y} \frac{2(s+l)}{\sqrt{2cr}} \right]$$

$$M_o = M(0) \approx M_y \left[1 + \frac{M_e}{M_y} \frac{2l}{\sqrt{2cr}} \right]$$

Thus
$$\frac{d}{ds} \left(\frac{M}{M_y} \right) \approx \frac{pr|\Delta\theta|}{4M_y} = \frac{2}{\sqrt{2cr}} \frac{M_e}{M_y}$$

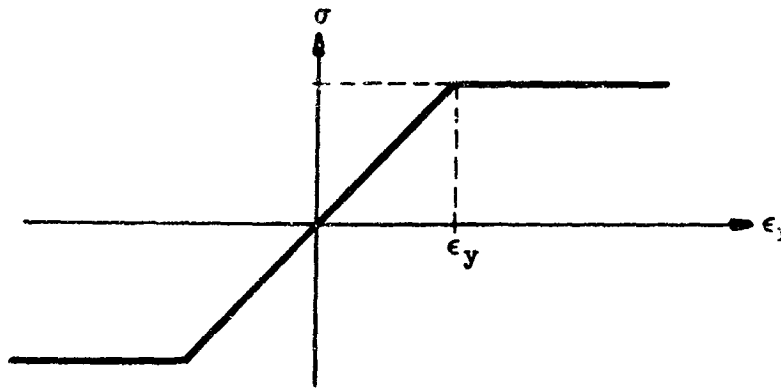
so that the condition on the rotation gives

$$2 \frac{M_e}{M_y} \left(\frac{M_o}{M_y} - 1 \right) = \int_1^{M_o/M_y} \frac{\kappa}{\kappa_l} d \frac{M}{M_y} = A$$



For a given moment-curvature relation, such as that shown in the sketch above, an integration provides the relation between the actual moment at the discontinuity, M_0 , and the moment M_e that would occur if the material were linear elastic.

The actual moment-curvature relation for a cylinder involves a complex interaction of meridional and circumferential force and moment resultants. For the present, however, we consider only uniaxial meridional effects. For an elastic-perfectly plastic material, the stress-strain curve is shown in the sketch below.



For the linear variation in strain across the shell thickness $-t/2 < z < t/2$

$$\epsilon_1 = \epsilon_0 + z\kappa$$

the stress and moment resultants

$$N = \int_{-t/2}^{t/2} \sigma dz$$

$$M = \int_{-t/2}^{t/2} \sigma z dz$$

give, for the three regions of no yielding, yielding in tension, and yielding in tension and compression, the results

$$\frac{6M}{Et^2\epsilon_y} = \bar{m} = \begin{cases} \bar{y} & 0 < \bar{y} < 1-\bar{n} \\ \bar{y} - \frac{1}{4\bar{y}^2} (\bar{y}+\bar{x}-1)^2(2\bar{y}-\bar{x}+1) & 1-\bar{n} < \bar{y} < \frac{1}{1-\bar{n}} \\ \frac{\bar{x}}{\bar{y}} & \frac{1}{1-\bar{n}} < \bar{y} \end{cases}$$

$$\frac{N}{E\epsilon_y t} = \bar{n} = \begin{cases} \bar{x} & 0 < \bar{y} < 1-\bar{n} \\ \bar{x} - \frac{(\bar{y}+\bar{x}-1)^2}{4\bar{y}} & 1-\bar{n} < \bar{y} < \frac{1}{1-\bar{n}} \\ \frac{3}{2} \left(1 - \frac{3\bar{x}^2+1}{3\bar{y}^2} \right) & \frac{1}{1-\bar{n}} < \bar{y} \end{cases}$$

where $\bar{x} = \epsilon/\epsilon_y$, $\bar{y} = t\kappa/z\epsilon_y$. Thus the ratio of maximum strain to yield strain is $\bar{x} + \bar{y}$. We assume that the axial force is constant, (i.e., $\bar{n} = \text{const} < 1$), and solve for \bar{m} as a function of \bar{y} , with \bar{n} as the parameter

$$\bar{m} = \begin{cases} \bar{y} & 0 < \bar{y} < 1-\bar{n} \\ 3(1-\bar{n}) - \frac{2(1-\bar{n})}{\bar{y}^{1/2}} & 1-\bar{n} < \bar{y} < \frac{1}{1-\bar{n}} \\ \frac{3(1-\bar{n}^2)\bar{y}^2 - 1}{2\bar{y}^2} & \frac{1}{1-\bar{n}} < \bar{y} \end{cases}$$

which provides the desired moment-curvature relation.

For the elastic-perfectly plastic material, without strain hardening, there is a maximum area A which gives the load at which the strain becomes infinite and that provides a simple upper limit on the load capacity of the shell. For the above moment-curvature relation, we have

$$\begin{aligned}
 A_{\max} &= \int_1^{(M_o/M_y)_{\max}} \frac{\kappa}{\kappa_l} d\left(\frac{M}{M_y}\right) \\
 &= \frac{1}{(1-\bar{n})^2} \int_1^{(\bar{m}_o)_{\max}} y d\bar{m} \quad \left(\begin{array}{l} \frac{M}{M_y} = \frac{\bar{m}}{1-\bar{n}} \\ \frac{\kappa}{\kappa_l} = \frac{\bar{y}}{1-\bar{n}} \end{array} \right) \\
 &= \frac{1}{1-\bar{n}^2} \int_{1-\bar{n}}^{\infty} \bar{y} \frac{d\bar{m}}{dy} dy \\
 &= -2 + \frac{3}{1-\bar{n}}
 \end{aligned}$$

Since, by definition,

$$\frac{M_e}{M_y} = \frac{\alpha \bar{n}}{1-\bar{n}}$$

$$\bar{n} = \frac{pR}{2Ete_y}$$

the equation for the maximum pressure is

$$\frac{\alpha \bar{n}}{1-\bar{n}} \left(\frac{\alpha \bar{n}}{1-\bar{n}} - 1 \right) = \frac{3}{1-\bar{n}} - 2$$

This is a difficult equation to solve if the discontinuity parameter (stress factor) α_{φ} is prescribed; however, the inverse relation is simple

$$\alpha_{\varphi} = \left[1 + \sqrt{1 + 2 \left(\frac{3}{1-\bar{n}} - 2 \right)} \right] \frac{1-\bar{n}}{2\bar{n}}$$

Using this equation the graph in the following figure was prepared. Rather than using the meridional stress factor α_{φ} , however, the equivalent, bi-axial, stress factor $\bar{\alpha}$, has been used, with the geometric parameter μ set equal to zero (see Section 2 for definitions and discussions of these quantities). Also shown in the figure are results from computer analyses where the solutions were oscillatory, indicating an unstable situation very near (above or below) collapse (pressures below collapse result in convergent solutions, pressures above collapse result in divergent solutions).

o OSCILLATORY COMPUTER SOLUTIONS

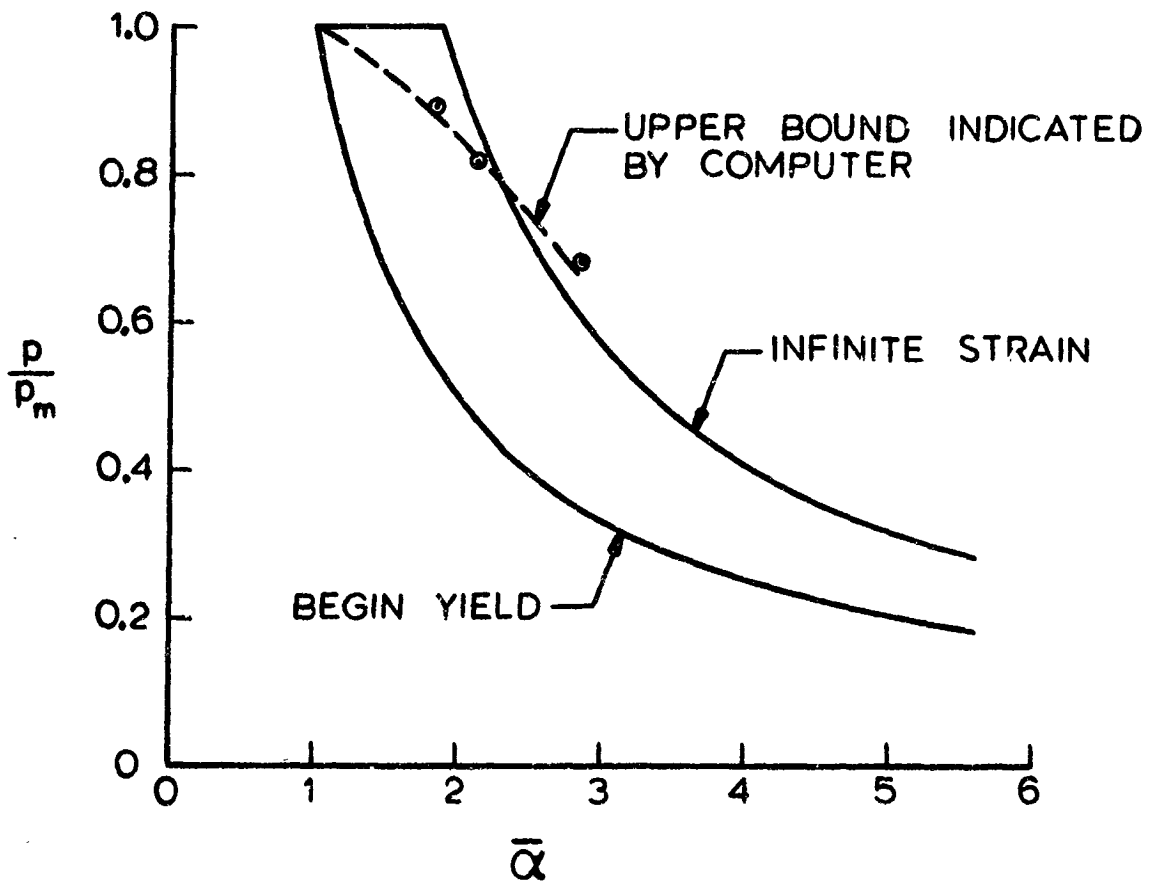


Fig. D-1 Comparison of closed form and computer solution for the elastic/plastic problem

APPENDIX E
EXPERIMENTAL RESULTS

NOTE: The data of Appendix E are bound in a separate volume
with limited distribution.